UNIVERSIDADE DE COIMBRA
FACULDADE DE CIÊNCIAS E TECNOLOGIA
Departamento de Ciências da Terra

Study of the geochemical affinities of the mercury and other trace elements in coals from the Carboniferous of the Iberian Peninsula

Helena Raquel Oliveira Moura

Mestrado em Geociências – Especialização em Recursos Geológicos

Setembro, 2016

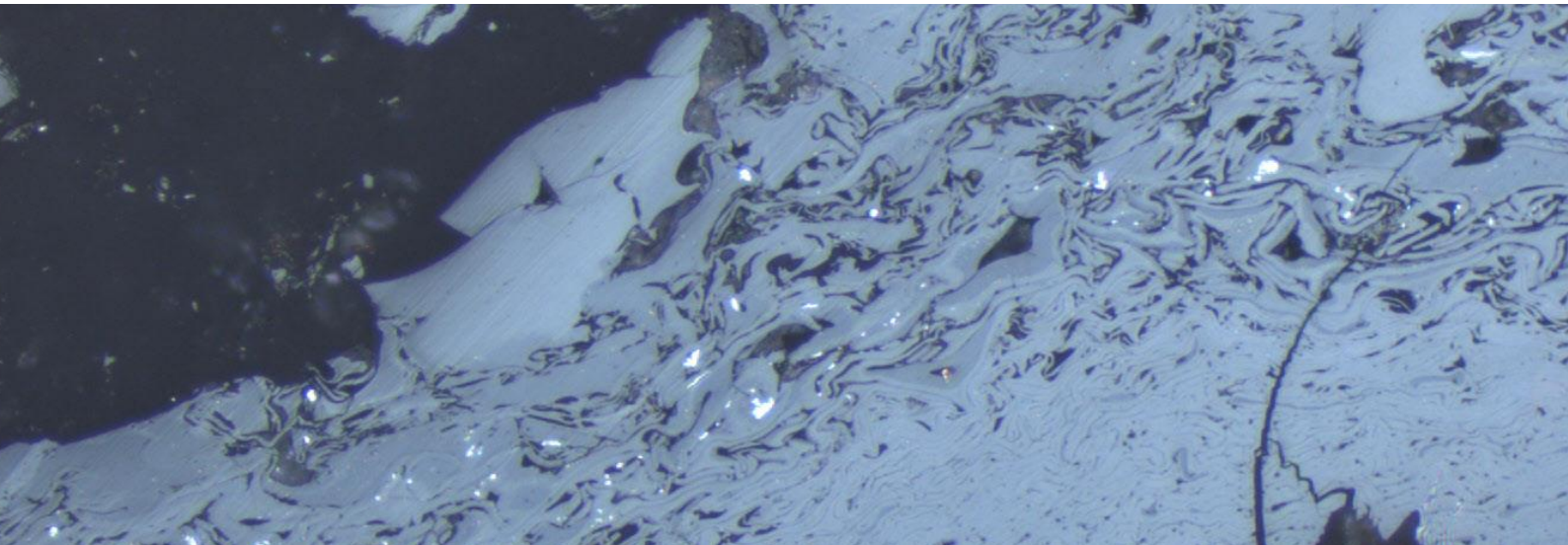

UNIVERSIDADE DE COIMBRA
FACULDADE DE CIÊNCIAS E TECNOLOGIA
Departamento de Ciências da Terra

Study of the geochemical affinities of the mercury and other trace elements in coals from the Carboniferous of the Iberian Peninsula

Helena Raquel Oliveira Moura

Mestrado em Geociências – Especialização em Recursos Geológicos

Orientadores Científicos
Professora Doutora Deolinda Maria dos Santos Flores Marcelo da Fonseca,
Faculdade de Ciências da Universidade do Porto
Professor Doutor Pedro Manuel Rodrigues Roque Proença e Cunha, Faculdade de Ciências e Tecnologia da Universidade de Coimbra

Setembro, 2016

À minha Mãe,

Acknowledgments

After this journey, it must be said that this work would not be possible without the guidance, help and support of many people. Thus, I would like to extend my thanks to all of those who helped me.

À minha orientadora, Professora Doutora Deolinda Flores, um obrigado por todas as oportunidades que me proporcionou e por tudo o que me ensinou nunca será suficiente. Obrigado por ter aceite trabalhar comigo, pelo tema proposto, por toda a orientação e paciência. Um obrigado pelo suporte de grande parte deste trabalho, pela oportunidade de passar uma semana no INCAR, e também pela oportunidade de poder participar no 9th ICCP Training Course in Organic Petrology.

Ao meu co-orientador, Professor Doutor Pedro Proença e Cunha, obrigado por todo o apoio e disponibilidade desde o primeiro dia, por todas as críticas construtivas, e por se preocupar sempre com o meu trabalho. Um obrigado também pelo apoio e suporte que me permitiu participar no 9th ICCP Training Course in Organic Petrology.

To Dr. Isabel Suárez-Ruiz from the Instituto Nacional del Cárbon (INCAR-CSIC, Oviedo, Spain), many thanks for providing the samples and data from the Central Asturian Coal Basin, and also for supporting the respective chemical analysis. I am truly grateful for receiving me at INCAR and for all the scientific guidance and advices for this research.

À Doutora Joana Ribeiro, obrigado por toda a paciência que teve comigo, por toda a ajuda que me deu, e por tudo o que me ensinou. Um obrigado também por todas as palavras de apoio, bem como pela companhia e amizade na semana que passamos no INCAR.

À Doutora Manuela Marques, o meu obrigado pela disponibilidade e amabilidade com que sempre esclareceu todas as minhas dúvidas em relação à Bacia de Peñarroya-Belmez-Espiel.

To Hilgers Technisches Büro, many thanks for the grant to attend the 9th ICCP Training Course in Organic Petrology, the course was a really asset for the realization of this research.

À Doutora Cândida Garcia Neto, responsável pelo Laboratório de Química Orgânica e Inorgânica (DGAOT-FCUP), obrigado pela disponibilidade e paciência que teve para me explicar todos os procedimentos laboratoriais, e também pela simpatia com que sempre me recebeu.

À D. Irene Lopes, funcionária do Laboratório de Preparação de Material Petrográfico (DGAOT-FCUP), um obrigado pela ajuda que me prestou quando me viu mais aflita.

Ao Instituto de Ciências da Terra - Pólo da Universidade do Porto e ao Departamento de Geociências, Ambiente e Ordenamento do Território da Faculdade de Ciências da Universidade do Porto, um agradecimento por me permitirem preparar e realizar as análises petrográficas nas instalações da Universidade do Porto.

Ao Departamento de Ciências da Terra da Faculdade de Ciências e Tecnologia da Universidade de Coimbra e a todos os meus Professores, o meu obrigado pela minha formação enquanto geóloga, pois foram também as bases que me foram dadas que me permitiram realizar este trabalho.

Um obrigado também a todos os meus amigos:

Ao meu amigo Alexandre Miguel Mateus, por todas as palavras de apoio, assim como por toda a força que me deu durante a realização deste trabalho.

Ao David Vaz, pela amizade e por todos os “Estou cheio!” deste mundo.

À Carina Carvalho, por todas as palavras de apoio e amizade ao longo destes anos.

À Carolina Flores, por todo o apoio e amizade nas situações mais difíceis. Um obrigado também pela ajuda com o inglês neste trabalho.

À Filipa Domingos, pela amizade e por todos os conselhos.

À Joana Leite, por ter acolhido “a caloira” e por ter estado sempre lá para me ajudar e ouvir. Feliz de quem viveu Coimbra como nós.

Ao João Lages, pela amizade e por algumas das melhores memórias que levo de Coimbra.

Ao Vitor Valente, pela amizade, pela paciência para me ouvir e, principalmente, por ser sempre capaz de me fazer rir.

À Raquel Freitas, pela amizade e por todo o apoio que me deu ao longo destes anos, longe ou perto.

À Marisa Santos, obrigado por ter estado sempre lá para mim, nos piores e melhores momentos, e por toda a ajuda que sempre deu. Não foram seiscentos anos juntas, mas certamente se sentem como tal.

Por último, e não menos importante, um agradecimento também, pela amizade e por todos os bons momentos que me proporcionaram em Coimbra, à Beatriz Cruz, Janete Gomes, Fábio Marques, Dan Dany, Pedro Oliveira, Hugo Correia, Bruno Teixeira, André Paiva, Marlisa Brito, João Trigo e João Tavares.

Ao João Tomás, um obrigado por tudo. Obrigado pela amizade, pelo apoio incondicional, e por toda a paciência. Obrigado pelos “verdes anos”.

À minha família, um obrigado por todo o apoio que sempre me deram, sem vocês nada disto seria possível. Um agradecimento especial às minhas tias, que sempre se preocuparam comigo e me ajudaram em tudo aquilo que podiam.

Ao Bertinho, obrigado por todas as palavras de força, e por ser a maior “claque de apoio” que alguém pode ter.

O maior agradecimento de todos à minha mãe, que sempre foi um exemplo de força para mim ao longo destes anos. Obrigado por todos os sacrifícios que fez para suportar os meus estudos. Um obrigado principalmente por, e apesar de todas as adversidades, nunca me dizer que existia algo que eu não pudesse ser ou fazer.

Abstract

This research aims an integrated study of organic and inorganic fractions in coals from the Carboniferous of the Iberian Peninsula, including three basins: the Douro Carboniferous Basin (DCB), the Central Asturian Coal Basin (CAB) and the Peñarroya-Belmez-Espiel Basin (PBEB). Therefore, this study presents the results of the petrographic composition of coals belonging to these basins, including the maceral analysis and vitrinite reflectance. Results regarding the geochemical composition of these coals are also presented, these were obtained through the proximate and ultimate analysis as well as the elements abundance and geochemical affinities. These in combination with the identification of the mineral phases allowed to infer on the mode of occurrence of some of these elements.

The results indicate that the major organic constituent across all coals is vitrinite, being telovitrinite the main subgroup. The content of mineral matter presented in the samples is variable and consists mainly of clay minerals and carbonates, even though the pyrite also displays a relevant occurrence. In DCB, where the coalification process reached a higher degree, thermal effects are also visible, such as devolatilization vacuoles. The proximate and ultimate analysis data agree with the rank and shows variable ash yields, the atomic H/C and O/C ratios data of the coal samples in the Van Krevelen diagram is not always in agreement with the petrographic data for CAB and PBEB.

The study of the trace elements abundance demonstrated that the enrichment/depletion is variable between each basin however Zn, Pb, Sb and Cs enrichment is more or less transversal to all basins, which arises as a result of magmatic fluids circulation. In DCB and PBEB trace elements show a more organic affinity with the ash yield, which can be the responsible for a slight enrichment of the heavy rare earth elements (HREEs). Whereas the aluminum-silicate affinity displayed by the light rare earth elements (LREEs) indicates that its enrichment is related to the clay minerals, particularly with the occurrence of authigenic kaolinite. Mercury has significant concentration coefficients in all the basins and presents a different mode of occurrence in each one.

Keywords: coal; Carboniferous; petrographic composition; trace elements; geochemical affinity; concentration coefficients.

Resumo

O presente trabalho tem por objectivo um estudo integrado da fração orgânica e inorgânica dos carvões do Carbonífero da Península Ibérica, nomeadamente de três das suas bacias: a Bacia Carbonífera do Douro (DCB), a Bacia Central Asturiana (CAB) e a Bacia de Peñarroya–Belmez-Espiel (PBEB). Deste modo, neste trabalho são apresentados os resultados do estudo petrográfico dos carvões pertencentes a estas bacias, nomeadamente a composição petrográfica e a refletância da vitrinite. São também apresentados os resultados relativos à composição quimica destes carvões, obtidos através das análises imediata e elementar, bem como a análise da abundância dos elementos e afinidades geoquímicas. Estas últimas, em conjunto com o estudo das fases minerais, permitiram ainda inferir acerca do modo de ocorrência de alguns desses elementos.

Os resultados revelam que o principal constituinte orgânico em todos os carvões é a vitrinite, onde o subgrupo da telovitrinite ocorre em maior percentagem. Já o conteúdo de matéria mineral presente nas amostras é variável, e consiste maioritariamente em minerais de argila e carbonatos, possuindo a pirite também uma ocorrência relevante. Na BCD, onde o processo de incarbonização atingiu um maior grau, são visiveis efeitos térmicos, como vacúolos de volatilização. Os dados das análise imediata e elementar são concordante com o grau sendo o rendimento em cinzas variável. O grau dos carvões estabelecido pelas razões atómicas H/C e O/C no diagrama de Van Krevelen nem sempre está de acordo o obtido pelos dados petrogáficos, nomeadamente para a CAB e PBEB.

O estudo da abundância dos elementos traço demonstrou que o enriquecimento/empobrecimento é variável nas bacias estudadas, no entanto o Zn, Pb, Sb e Cs apresentam um enriquecimento mais ou menos transversal em todas elas, como consequência da circulação de fluídos magmáticos. Na DCB e PBEB os elementos traço apresentam uma afinidade orgânica, o que pode estar na origem de um enriquecimento ligeiro das terras raras pesadas (HREEs). Já a afinidade alumino-silicatada exibida pelas terras raras leves (LREEs) indica que o seu enriquecimento está relacionado com os minerais argilosos, particularmente com uma ocorrência em caulinite autigénica. O mercúrio possui coeficientes de concentração relevantes em todas as bacias e apresenta um modo de ocorrência diferente em cada uma delas.

Palavras chave: carvão; Carbonífero; composição petrográfica; elementos traço; afinidade geoquímica; coeficientes de concentração.

Contents

List of figures

List of tables

Chapter 1 – Introduction

1. Introduction

The present study was developed in the scope of the dissertation to obtain the Master in Science Degree, in Earth Sciences with a branch in Geological Resources by the Faculty of Science and Technology, University of Coimbra. The research consists on the study of the geochemical affinities of the mercury and other trace elements in coals from the Carboniferous of the Iberian Peninsula.

With this research is intended to develop skills within the Geological Resources, particularly in the areas of petrography and geochemistry of coal, using techniques for the determination of the petrographic composition (including maceral analysis and vitrinite reflectance), as well as techniques for the organic and inorganic geochemical characterization by determining the proximate and ultimate analysis and composition in major and trace elements.

This research aims to increase the knowledge about the coals of the Iberian Peninsula through an integrated study of the organic/inorganic fractions and definition of the geochemical affinities of mercury and other trace elements in the bituminous and anthracite coals from the Douro Carboniferous Basin (DCB), Central Asturian Coal Basin (CAB) and Peñarroya-Belmez-Espiel Basin (PBEB). For this purpose, the main objectives were the following:

- To characterize the petrographic composition;
- To assess the rank;
- To characterize the geochemical composition through the proximate and ultimate analysis and the content on major and trace elements;
- To establish the geochemical affinities of the elements with the organic and inorganic matter;
- To define the mode of occurrence of the trace elements;
- To relate the enrichment of trace elements with the genesis and geological evolution of the coal basins.

The study aims to accomplish these objectives by using a set of 42 samples (5 from DCB, 19 from PBEB and 18 from the CAB), with the exception of the characterization of the petrographic composition and the proximate and ultimate analysis of the coals from CAB, which were performed and provided for the present study by Dr. Isabel Suárez-Ruiz.

This study is relevant for the characterization of coals from a geological point of view, mainly the concentration in trace elements and the relationship with the geological events that occurred in the basin history, as well as for the technological and industrial coal use, mainly for energy supply or for the production of metallurgical coke. Furthermore, coal may

contain trace elements with industrial significance such as U, Ge, Ga, Sc and REEs (rare earth elements). Nowadays the demand for rare earth elements and yttrium (REY) is greater than the supply and coal deposits can be an alternative to the conventional deposits. Furthermore, coal is rich in some harmful elements such as mercury, which during the technological and industrial processes are emitted to the atmosphere. In addition to the relevance of the energy and mining industries, as well as the technological market, studies like these can reveal new information about the geological conditions, namely be an indicator of mineralization.

Therefore, the present study focuses in the geochemical composition of the coals from the three Carboniferous basins in order to determine the enrichment/depletion and modes of occurrence of mercury and other trace elements, such as REY. The coals from these basins may represent an economic resource or a possible environmental impact, depending of the element enriched and taking into account its concentration and mode of occurrence in the raw coal, since it can give information for the beneficiation of coals for further technological and industrial use. The large volumetric waste piles resulting from the exploitation of the coals of these basins can also be a material to be beneficiated and recycled for further reuse

Chapter 2 – Main concepts

2. Main concepts

The theoretical framework that supports the issues addressed in this research is presented in this chapter. Topics related to coal, as its genesis and the science used in its study (organic petrography and geochemistry) are approached. Subjects as coal characterization, namely coal petrographic composition, rank and grade, and coal inorganic geochemistry, specifically the elements abundance and its modes of occurrence, are also summarized.

2.1. Coal genesis

Coal is a combustible sedimentary rock resulting from the accumulation and burial of plant remains, in different preservation states, in shallow sedimentary basins (ICCP, 1963). It is a product of biogeochemical processes, particularly of the evolution of organic materials with increasing temperature and pressure. In this sedimentary rock the organic matter content is high, though with presence of mineral matter in small quantities.

A more precise definition is provided by the Glossary of Geology of the American Geological Institute (1987), fixing quantitative limits for the composition, in which coal is a "combustible rock containing more than 50% by weight and more than 70% by volume of carbonaceous matter, including the intrinsic moisture ("moisture in the coal bed")".

These definitions exclude peat, considered as the raw material from which some coal is formed, which is in agreement with ICCP (1963) (Lemos de Sousa, 1999). Peat consists of dead remains of vegetation in bogs, marshes and lagoons, for example. The vegetation debris deposited are not consolidated, being strongly decomposed by humidification under mostly anaerobic and water saturation conditions. Thus, it presents high humidity levels (at least 75%, and often exceeding 90%) and a carbon content of about 50% to 60% (Taylor et al., 1998).

The peat formation (peatification) precedes the coalification process and includes chemical, physical and biological processes that occur almost immediately after the deposition of the plant material in the bogs. The biomass of peat is therefore gradually transformed into coals of increasing coalification rank.

2.2. Organic petrography and geochemistry

The study of the carbonaceous rocks, including coal, is based on two main subjects: organic petrology and organic geochemistry. The organic petrography studies the petrographic characteristics, namely the identification and description of the organic

constituents and the rank determination (Taylor et al., 1998). The organic geochemistry includes the definition of the chemical composition of the organic and inorganic fractions of the coal.

Nowadays, the two are practically inseparable, either by the genetic evidence or by the methodologies developed that are used in both areas. Example of this relationship is the van Krevelen diagram (van Krevelen, 1993), which relates both the rocks and other organic products based on the materials' composition, genetic affiliation and evolution.

2.3. Coal characterization

Coals are characterized based on the combined assessment of three properties: petrographic composition, rank and grade (Taylor et al., 1998):

- The petrographic composition is related with the plants remains, precursors of the carbonaceous material, as well as the depositional and burial environment. The individual components which occur in the coals are referred to as macerals (Suárez-Ruiz and Crelling, 2008);
- The rank reflects the degree of coalification that the biomass was subjected during its burial, which is related with the temperature, the pressure and the time during which it occurred (Suárez-Ruiz and Crelling, 2008);
- The grade of the coal refers to the amount of mineral matter, disregarding its degree and petrographic composition. This property is important for coal beneficiation (Suárez-Ruiz and Crelling, 2008).

2.3.1. Coal petrographic composition

The petrographic composition corresponds to the nature of the plant debris that originated coal, together with the depositional conditions. The Stopes-Heerlen (SH) nomenclature system is the international system used according the ICCP definitions (ICCP, 1998, 2001; Pickel et al., 2015).

The macerals are the microscopically recognizable organic constituents of coal. They are distinguished on the basis of their differences in reflectance, color, fluorescence, morphology, size and hardness. Macerals are grouped into maceral groups and sub-groups and can be further differentiated into maceral varieties (Table 1) (ISO 7404-1, 2016). The three maceral groups show characteristic differences in their chemical composition. The liptinite tends to be comparatively rich in hydrogen (aliphatic structure), inertinite rich in carbon (aromatic structure) and vitrinite rich in oxygen (cycloaromatic structure).

Table 1 - Maceral classifications of medium and high rank coals (ICCP, 1998, 2001; Pickel et al., 2015; ISO 7404-1, 2016).

Groups	Subgroups	Macerals
Vitrinite	Telovitrinite	Telinite Collotelinite
	Gelovitrinite	Corpogelinite Gelinite
	Detrovitrinite	Vitrodetrinite Collodetrinite
Liptinite		Sporinite Cutinite Resinite Alginite Bituminite Exsudatinite Liptodetrinite
Inertinite		Fusinite Semifusinite Macrinite Micrinite Funginite Secretinite Inertodetrinte

Vitrinite group

This group includes the most important constituents of coal, corresponding to the generally more abundant maceral group, especially in the Carboniferous coals in the Northern Hemisphere. This group has also great relevance for the industry, playing a decisive role in the coal behavior. The vitrinite is used for rank determination through its reflectance (Suárez-Ruiz and Crelling, 2008).

Vitrinite is the coalification product of a humic substance originated from lignocellulosic constituents of higher plants and is used for medium and high rank coals. For low rank coals the humic material is grouped within the Huminite maceral group (not described in this dissertation). The limit between low and medium rank coal is defined at 0.5% random vitrinite reflectance (ICCP, 1998; Sýkorová et al., 2005).

Vitrinite is a maceral group characterized by a grey color with a reflectance usually located between the darkest liptinite and the lighter inertinite and is divided into three subgroups defined by the degree of destruction (tissues, gels and detritus) and six macerals defined by morphology and/or degree of gelification.

Telovitrinite

This maceral subgroup is characterized by the presence of cellular structures, which may or may not be visible. It comprises two macerals, telinite and collotelinite, distinguishable by their degree of gelification (vitrinitization) (ICCP, 1998).

- **Telinite** is a maceral that consists of clearly recognizable gelified cell walls. The size, shape, and openness of cell lumens is variable;
- **Collotelinite** is a maceral with a more-or-less structureless homogeneous appearance.

Detrovitrinite

Detrovitrinite refers to fragments of vitrinized plant remains that may occur isolated or cemented by amorphous vitrinitic matter (ICCP, 1998). It is typically the dominant vitrinite maceral subgroup (Benner et al., 1985; Pickel and Wolf, 1989) and includes two macerals, vitrodetrinite and collodetrinite:

- **Vitrodetrinite** occurs as discrete small vitrinitic fragments;
- **Collodetrinite** refers to a mottled vitrinitic groundmass that binds other coal components.

Gelovitrinite

Gelovitrinite corresponds to infillings of vitrinic material in colloidal voids. This subgroup comprises two macerals, corpogelinite and gelinite (ICCP, 1998):

- **Corpogelinite** describes discrete bodies representing mainly the primary infillings of cell lumens occurring in situ or isolated within the coaly or mineral matrix. Corpogelinite may be spherical, ovoid or elongated;
- **Gelinite** is a maceral of secondary origin. It consists in homogeneous and structureless infillings of cracks and other voids.

Liptinite group

The liptinite group macerals correspond to different plant parts (spores, cuticles, suberin cell walls, resins and polymerized waxes, fats and oils of vegetable origin), some degradation products and can also been generated during the coalification process from products of secondary generation. During the coalification process some of the macerals can disappear due to the effect of temperature and some can develop similar characteristics to the vitrinite group (Suárez-Ruiz and Crelling, 2008).

Liptinite is distinguished from other macerals by its lower reflectance and fluorescence, although it disappears with increasing coal rank. Macerals can be identified by their morphology into (Pickel et al., 2015):

- **Sporinite** may appear oval or elongated, depending on the cross section view, arising from the outer cell walls of spores and pollens. In reflected white light sporinite displays a black color and fluoresces under blue or ultraviolet incident lights at low rank coals;
- **Cutinite** originates from the leaves' outer walls, stems or other aerial plants. It presents a narrow band form or a serrated saw blade appearance. Cutinite is characterized by a black color under reflected white light and displays fluorescence under blue or ultraviolet incident lights at low rank coals;
- **Resinite** is a maceral that presents a round or oval form and occurs occasionally as diffuse impregnations or filling cell cavities in telinite. It displays a dark color under reflected white light that will appear darker when surrounded by vitrinite, under blue or ultraviolet incident lights it will fluoresce with varying intensities in low rank coals. In the ICCP system 1994 fluorinite is included in the resinite maceral;
- **Suberinite** refers to a maceral which precursor is suberin, a fatty acid found in corkified cell walls of barks. Suberinite appears as black cell walls in reflected white light and is fluorescent under blue or ultraviolet incident lights;
- **Exsudatinite** is a secondary maceral, generated from lipid-rich materials during coalification, that infills empty cell lumens, cracks or other voids. This maceraI is a petroleum like substance with an appearance that can vary on the same coal but is usually black under reflected white light and fluoresces under blue or ultraviolet incident lights;
- **Bituminite** is a maceral without a specific. This maceral occurs as an autochthonous material in the bedding or as a groundmass for other macerals and for minerals;
- **Alginite** comprises unicellular or colonial algae of planktonic or benthic origin. It has been divided into two varieties, **telalginite** and **lamalginite**. These macerals display a dark

color under reflected white light and varying fluorescence under blue or ultraviolet incident lights according with the coal rank;

- **Liptodetrinite** consists in fragments of liptinite macerals. It is characterized by a black color under reflected white light and a fluorescence with varying intensity under blue or ultraviolet incident lights.

Inertinite Group

The inertinite group is characterized by plant derived material that underwent alteration and degradation in oxic environments before deposition. These changes may also occur through biochemical and chemical processes during the peat stage (ICCP, 2001; Suárez-Ruiz and Crelling, 2008).

The macerals from this group are more inert and, therefore, are less reactive to the carbonization process in relation to other macerals (ICCP, 2001). In reflected white light, inertinite presents a grey to white color. The reflectance is always higher than of the other groups (ICCP, 2001).

This maceral group is subdivided according to the presence (fusinite, semifusinite, funginite) or absence of cell structure (secretinite, macrinite, micrinite) or if the material is fragmented (inertodetrinite). Micrinite is a maceral of neoformation which is present only in medium and high rank coals. This macerals group comprises the following macerals (ICCP, 2001):

- **Fusinite** is a maceral derived from well preserved plant cell walls. These cell walls are thinner than those of telovitrinite and semifusinite. The fusinite has a grey color and always a relatively higher reflectance, increasing with the rank;
- **Semifusinite** consists of preserved plant cell wall structures, an intermediate reflectance and a structure between telovitrinite and fusinite in the same coal. Cell lumens are smaller than those of fusinite;
- **Funginite** is derived from either single or multi-celled fungal spores or fungal remains. Size and shape is dependent upon the cellular spores and the physical characteristics of the original fungal bodies;
- **Secretinite** consists of round, vesicled to non-vesicled, and equant to elongate bodies without obvious plant structure;
- **Macrinite** is a structureless maceral, commonly elongated, formed from dehydration and oxidation of humic materials that occurs either as an amorphous matrix or as discrete bodies;

- **Micrinite** is a secondary maceral, generated during coalification that occurs as very small rounded grains. Micrinite is separated from inertodetrinite by an upper size limit of 2 mm and differs from macrinite by their granularity;
- **Inertodetrinite** is characterized by small fragments (>2 μm and <10 μm in size) of varying shape.

2.3.2. Coal Rank

Coalification is the process from which coal is formed through the burial of plant remains under the influence of temperature, pressure and geological time. With this premise, the rank corresponds to the stage reached by the coal during the coalification process and thus it corresponds to a certain position in its scale (Suárez-Ruiz and Crelling, 2008; Ward and Suárez-Ruiz, 2008). In this process peat develops primarily into a low coal rank and then, successively, into medium and high coal rank.

The coalification process occurs in the following phases (Tissot and Welte, 1984): diagenesis, catagenesis and metagenesis. Hence, can be distinguished two coalification phases, biochemical and geochemical (Taylor et al., 1998). The first phase corresponds to the humification, having a strong influence of the biological agents. This process is influenced by the type of plant material deposited as well as other three factors that influence the bacterial activity, namely: the supply of nutrients, the acidity in the mires (higher acidity translates into a lower bacterial activity) and the temperature of the mires (high temperature favors the life and metabolism of bacteria and fungi). The second phase corresponds to the catagenesis and metagenesis and is dominated by physicochemical factors, including temperature and pressure, as well as the time of action of these two variables (Taylor et al., 1998).

During coalification a progressive decrease in moisture and volatile functional groups is noted with a consequent increase in the carbon content of the coal. According to Stach et al. (1982), four coalification jumps (more or less abrupt modifications of the fundamental properties in correlation with the fundamental transformations in coals) (Table 2), can be defined as follows:

- **1st coalification jump** - Occurs at about 0.5% Rr, coinciding with the formation of the micrinite maceral;
- **2nd coalification jump** - Takes place when vitrinite reflectance reaches about 1.3% Rr. A reduction of oxygen content takes place in the form of CO_2 and H_2O, and the early loss of hydrogen in the form of methane;

- **3rd coalification jump** - Materializes at about 2.5% Rr. It coincides with additional hydrogen losses in the form of methane, corresponding to a strong aromatization and condensation in the rings of the humic compounds;
- **4th coalification jump** - Occurs at a reflectance of about 3.7% Rr. It coincides with a further loss of hydrogen in the form of methane and with an increase in aromatization and condensation processes.

Table 2 - Physico-chemical coalification rank change (modified after Pickel, 2015).

ORIGINAL MATERIAL	PROCESS	RESULT
→		
BROWN COAL IMMATURE DISPERSED ORGANIC MATTER	COALIFICATION	HIGHER RANK COALS, ANTHRACITE, GRAPHITE MATURE DISPERSED ORGANIC MATTER
COMPOUND GROUPS		
→		
	Aromatization, loss of functional groups, loss of oxygen preferentially and then hydrogen	Rise in carbon content, loss of oxygen and then hydrogen
The main changes in humic material are the loss of O, H, N and an increase in C, the degree of aromaticity, removal of alkyl groups, functional groups, cracking of aliphatic molecules, dehydration and decarboxylation. Changes in the more aliphatic and naphthenic components (mostly found within liptinite) are small until the middle of the bituminous rank range when evolution of long chain hydrocarbons, demethylation and aromatisation occur.		

The rank can be determined through physical and/or chemical or physicochemical properties. The most common coal rank parameter is the vitrinite reflectance. However, the carbon content and the calorific value (on a moist ash-free basis) can also be used.

2.3.3. Coal Grade

The coal grade concerns the amount of impurities in coal (inorganic fraction). It is largely influenced by the environmental setting, representing an enormous importance in the mining and technological sector of the coal (Suárez-Ruiz and Crelling, 2008). The mineral matter content (in volume, %) in coal can be determined by a quantitative microscopic analysis. Table 3 includes the main identifiable mineral inclusions of coal (Mackowsky, 1968).

Table 3 - Main mineral inclusions present in coal (modified after Mackowsky, 1968).

<table>
<tr><th colspan="5">Minerals in Coal</th></tr>
<tr><th rowspan="2">Mineral Group</th><th colspan="2">Syngenetic Formation (Intimately Intergrown)</th><th colspan="2">Epigenetic formation</th></tr>
<tr><th>Transported by water or wind</th><th>Newly formed</th><th>Deposited in Fissures, Cleats and Cavities (Coarsely Intergrown)</th><th>Transformation of Syngenetic Minerals (Intimately intergrown)</th></tr>
<tr><td>Clay Minerals</td><td colspan="2">Kaolinite, ilite, sericite, clay minerals with mixed-layer structure “tonstein”</td><td></td><td>Illite, chlorite</td></tr>
<tr><td>Carbonates</td><td></td><td>Siderite-ankerite concretions, Dolomite, Calcite, Ankerite</td><td>Ankerite, calcite, dolomite</td><td></td></tr>
<tr><td></td><td></td><td colspan="2">Siderite, calcite, ankerite in fusite</td><td></td></tr>
<tr><td>Sulfide ores</td><td></td><td>Pyrite concretions, melnikowite-pyrite, coarse pyrite (marcasite), concretions of FeS_2–$CuFeS_2$–ZnS</td><td>Pyrite, marcasite, zinc sulfide (sphalerite), lead sulfide (galena), copper sulfide (chalcopyrite)</td><td>Pyrite from the transformation of syngenetic concretions of $FeCO_3$</td></tr>
<tr><td></td><td></td><td colspan="2">Pyrite in fusite</td><td></td></tr>
<tr><td>Oxide ores</td><td></td><td>Hematite</td><td>Goethite, lepidocrocite (needle iron ore)</td><td></td></tr>
<tr><td>Quartz</td><td>Quartz grains</td><td>Chalcedony and quartz from the weathering of feldspar and mica</td><td>Quartz</td><td></td></tr>
<tr><td>Phosphates</td><td>Apatite</td><td>Phosphorite</td><td></td><td></td></tr>
<tr><td>Heavy minerals and accessory minerals</td><td>Zircon, rutile, tourmaline, orthoclase, biotite</td><td></td><td>Chlorides, sulfates, nitrates</td><td></td></tr>
</table>

2.4. Coal inorganic geochemistry

Coal consists mainly in organic matter and inorganic constituents. These inorganic constituent have great importance as they often determine the coal application. Thus, with the exception of some elements (actinium, astatine, francium, polonium, protactinium), all the other elements are present in coal (Orem and Finkelman, 2003). However, the abundance of the inorganic constituents in coal varies and these variations are influenced by the geological and the geochemical processes acting during geological time (Bouska, 1981; Swaine 1990; Orem and Finkelman, 2003).

The plant materials and the detrital influx during the diagenetic process have major influence on the type and abundance of the inorganic chemical constituents of the coal. This means that these components will vary according to the set of the plant material that gave rise to it as well as the detrital material deposited during the formation of the coal and the geological history of the basin (Orem and Finkelman, 2003).

There is also chemical and mineralogical evidence showing that some minerals can precipitate as autigenic minerals while others, such as calcium, sodium, and magnesium can be lost during the coalification process (Finkelman, 1981). In the case of coal the majority of the minerals are of epigenetic origin that precipitated in the cleat and fractures subsequent to coal formation. These minerals include sulfides, carbonates, and kaolinite (Orem and Finkelman, 2003).

2.4.1. Elements abundance

The coal Clarke values represent the average trace elements values in coals all over the world, as established by Ketris and Yudovich (2009). These average values allow comparisons and the determination if the coals are enriched or depleted in elements.

The enrichment of certain trace element can be either beneficial or harmful to the human health and environment (Orem and Finkelman, 2003). The enrichment of the coal in metals can have economic potential as, in recent years, coal deposits have been addressed as a promising source of trace elements as in many coals the concentration in these elements is similar or even higher than in conventional deposits (among others, Dai et al., 2010, 2015, 2016a, 2016b).

2.4.2. Modes of occurrence

The mineral and elements contents are very important with regards to the geochemical and technological potential behavior of trace elements in coal. The mode of occurrence of trace elements is however very difficult to determine due to the low concentration of these elements, the intermixture of organic and inorganic materials and the small grain size of the minerals. Therefore, determinations have been mostly qualitative (Orem and Finkelman, 2003).

The modes of occurrence of these elements in coal were studied by Finkelman (1981) and reviewed by Swaine (1990) and in general are associated with organic matter or inorganic matter (mineral matter) (Table 4). They can be determined using a variety of methodologies, namely, scanning electron microscopy-energy dispersive X-ray analysis (SEM-EDX).

Concerning the mode of occurrence of mercury (Hg), it occurs in low concentrations and is very volatile, making it impossible to be determined in coal ash (Swaine and Goodarzi, 1995; Yudovich and Ketris, 2005). Finkelman (1981) shows a clear association of mercury with inorganic matter and some authors have already proven their organic association (Ruch et al., 1971). Nowadays, is known that mercury can be present in coal's clays (Hg_{clay}),

organic matter (Hg_{org}), and sulfides (Hg_{sulf}). The most common mode of occurrence in solid solution of Hg in coal is as pyrite, with a higher occurrence in epigenetic than in syngenetic pyrite (Yudovich and Ketris, 2005).

Table 4 - Modes of occurrence of selected elements in coal in decreasing order of probability (modified after Orem and Finkelman, 2003).

Element	Modes of occurrence
Aluminium	Clays, feldspars, organic association, Al-oxides
Antimony	Accesory sulfide, organic association
Arsenic	Solid solution in pyrite, rare organic association
Barium	Barite, crandallite, organic association
Beryllium	Clay, organic association
Bismuth	Accessory sulfide
Boron	Organic association, illite
Bromine	Organic association
Cadmium	Sphalerite, clay, pyrite
Calcium	Calcite, sulphates, organic association, silicates, phosphates
Cesium	Clays, feldspar, mica
Chlorine	Organic association
Chromium	Clays (especially illite), organic association, spinels
Cobalt	Accessory sulfides, pyrite, clays, organic association (?)
Copper	Chalcopyrite, organic association, clays
Fluorine	Perhaps apatite, clays, mica, amphiboles (rare)
Gallium	Clays, organics, sulfides
Germanium	Organic association
Gold	Native gold, organic association
Hafnium	Zircon, clays
Indium	Probably sulfides
Iodine	Probably organic association
Iron	Pyrite, siderite, sulfates, oxides, organic association
Lead	Galena, PbSe, clays, organic association (?)
Lithium	Clays
Magnesium	Clays, organic association
Manganese	Siderite, calcite, pyrite, clays, organic association
Mercury	Solid solution with pyrite, rare organic association
Molybdenum	Clays, sulfides, organic association
Nickel	Mono-sulfides, pyrite, organic association, and clay
Niobium	Oxides
Phosphorus	Phosphates
Potassium	Clays, feldspars
Platinum	Native alloys, perhaps some organic association
Rare earths	Phosphates, some organic association
Rubidium	Probably illite
Scandium	Clays, phosphates, organic association
Selenium	Organic association, pyrite, PbSe
Silicon	Quartz, clays, silicates
Silver	Perhaps silver sulfides
Sodium	Organic association, clays, zeolites, silicates
Strontium	Carbonates, phosphates, organic association
Tantalum	Oxides, silicates
Tellurium	Unclear
Thorium	Rare-earth phosphates, clays
Tin	Tin oxides, sulfides
Titanium	Clays, oxides, organic association
Tungsten	Oxides, clays, organic association
Uranium	Organic association, zircon, phosphates
Vanadium	Clays, some organic association
Yttrium	Rare-earth phosphates
Zinc	Sphalerite
Zirconium	Zircon

Chapter 3 – Geological setting

3. Geological setting

This chapter includes a general approach of the geological setting of the Iberian Peninsula Carboniferous Basins, namely one synthetic explanation of the geodynamic evolution and stratigraphy. The geological characterization of the Douro Carboniferous Basin (DCB) (Portugal) is presented first and thereafter the Central Asturian Coal Basin (CAB) and Peñarroya-Belmez-Espiel Basin (PBEB) (both in Spain). This order will also be followed in the following chapters.

3.1. Douro Carboniferous Basin

The Douro Carboniferous Basin (DCB) is located in the Northwestern of Portugal mainland, with general orientation from NW to SE (Figure 1). This is the major Carboniferous basin present in the Douro-Beira Carboniferous Trough (*Sulco Carbonífero Dúrico-Beirão* - SCDB) occurring in the Central Iberian Zone, a narrow strip extending for 53 km with a width rarely greater than 500 m (Pinto de Jesus, 2001).

In this basin, the base of the Paleozoic record rests by an angular discordance over the *Complexo Xistograuváquico* (Schist-Greywacke Complex – CXG, lower Cambrian). The top of the basin infill is cut by an important reverse fault that placed the Lower Paleozoic formations of the reverse limb of the Valongo anticline over the Carboniferous succession. The Carboniferous sedimentary record indicates an intramontane basin with Upper Pennsylvanian (Lower Stephanian C) palustrine/lacustrine/fluvial sediments, interbedded with coal seams, dated based on paleobotanical (Wagner and Lemos de Sousa, 1983; Correia et al., 2014a), paleozoological (Eagar, 1983; Correia et al., 2013, 2014b; Loureiro et al., 2010) and palynological (Fernandes et al., 1997) data.

According to the geological evolution model proposed by Pinto de Jesus (2001, 2003), during the Upper Pennsylvanian (Lower Stephanian C) the SCDB was controlled by a strike-slip fault that delimits the SW flank of the Valongo anticline. This tectonic activity lead to the opening of pull-apart sedimentary basins, with migration of the depocentre from NW to SE. The continuing compression activity has induced the formation of a transpression system, of Variscan age, where there is a prevalence of the thrust component to SW. In this context the basin formed corresponds to a foreland basin with a foreland bulge located at the SW margin and associated with a normal fault. The uplift of the SW flank resulted in an increased subsidence from NE to SW, which translated into an asymmetric cross section.

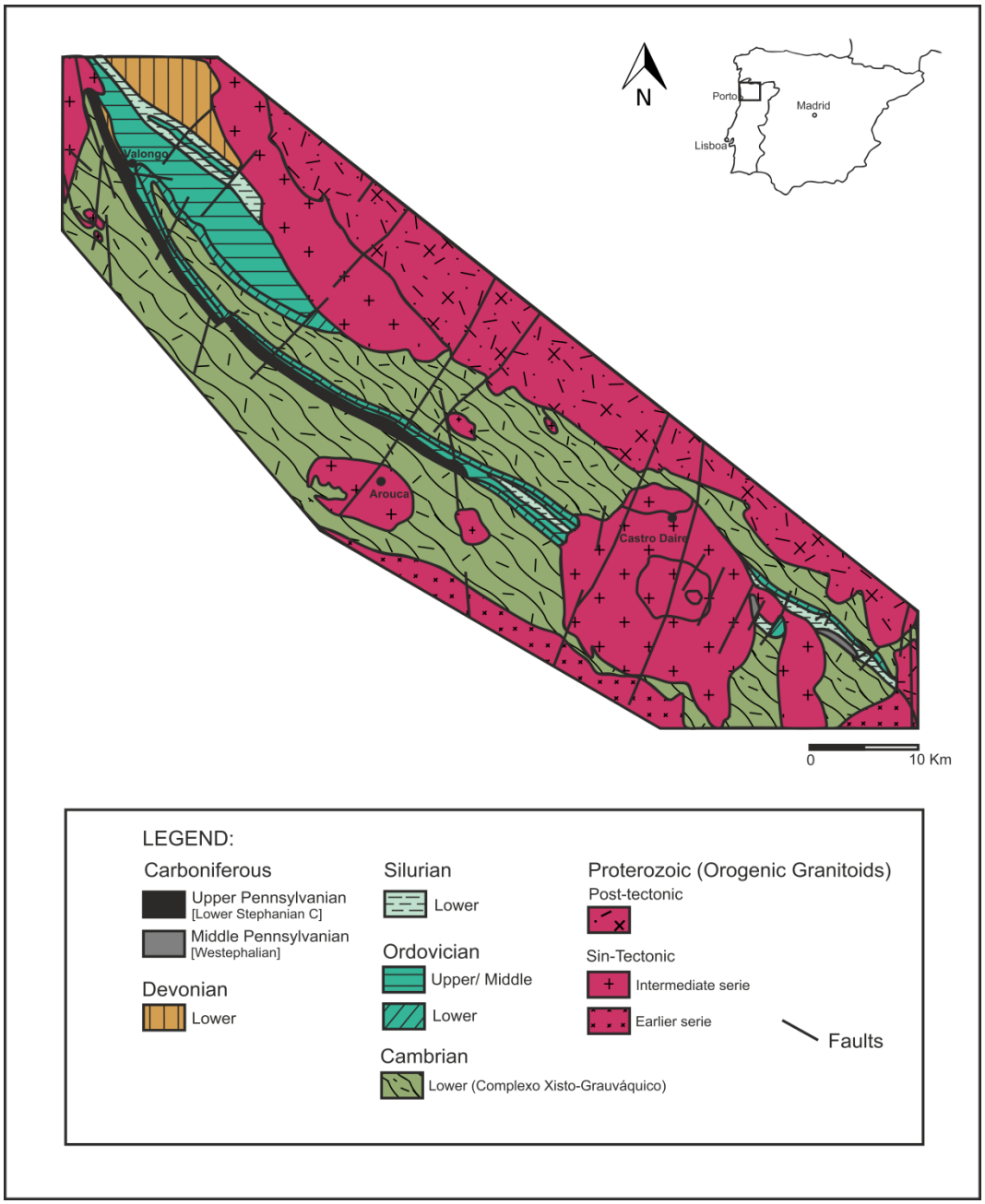

Figure 1 - Geological setting of Douro Basin, Portugal (Pinto de Jesus, 2001).

The sedimentation is related to the tectonics at both margins; there is a greater representation of clasts from the CXG in the proximal lithofacies of the basal breccia, while in the NE margin of the basal breccia there is a larger density of clasts with lithologies of the Lower Paleozoic (Figure 2). After these tectonic events there was a slowdown in the deposition and the installation of a fluvial system. The sedimentary record reveals more energetic environments progressing to sedimentary environments with less energy.

The implantation of granitoid rocks in the region and the resulting temperature increase, associated with the subsidence of the DCB, lead to the coalification of the organic matter to the meta-anthracite rank (Lemos de Sousa, 1973, 1978). At the same time, late Variscan phases acting over brittle rocks (exception of coal), with a stress torque oriented NE-SW, associated with sinistral shear activity (Ribeiro, 1974; Dias and Ribeiro, 1991), resulted in the formation of thrust faults with a “piggy-back” style (Pinto de Jesus, 2001, 2003) and the subsequent deformation forming duplex and triplex tectonic structures (Figure 2) (Pinto de Jesus, 2001). The obliqueness of the tectonic movement resulted in an asymmetrical cut of the upper series of the DCB by the major thrust fault.

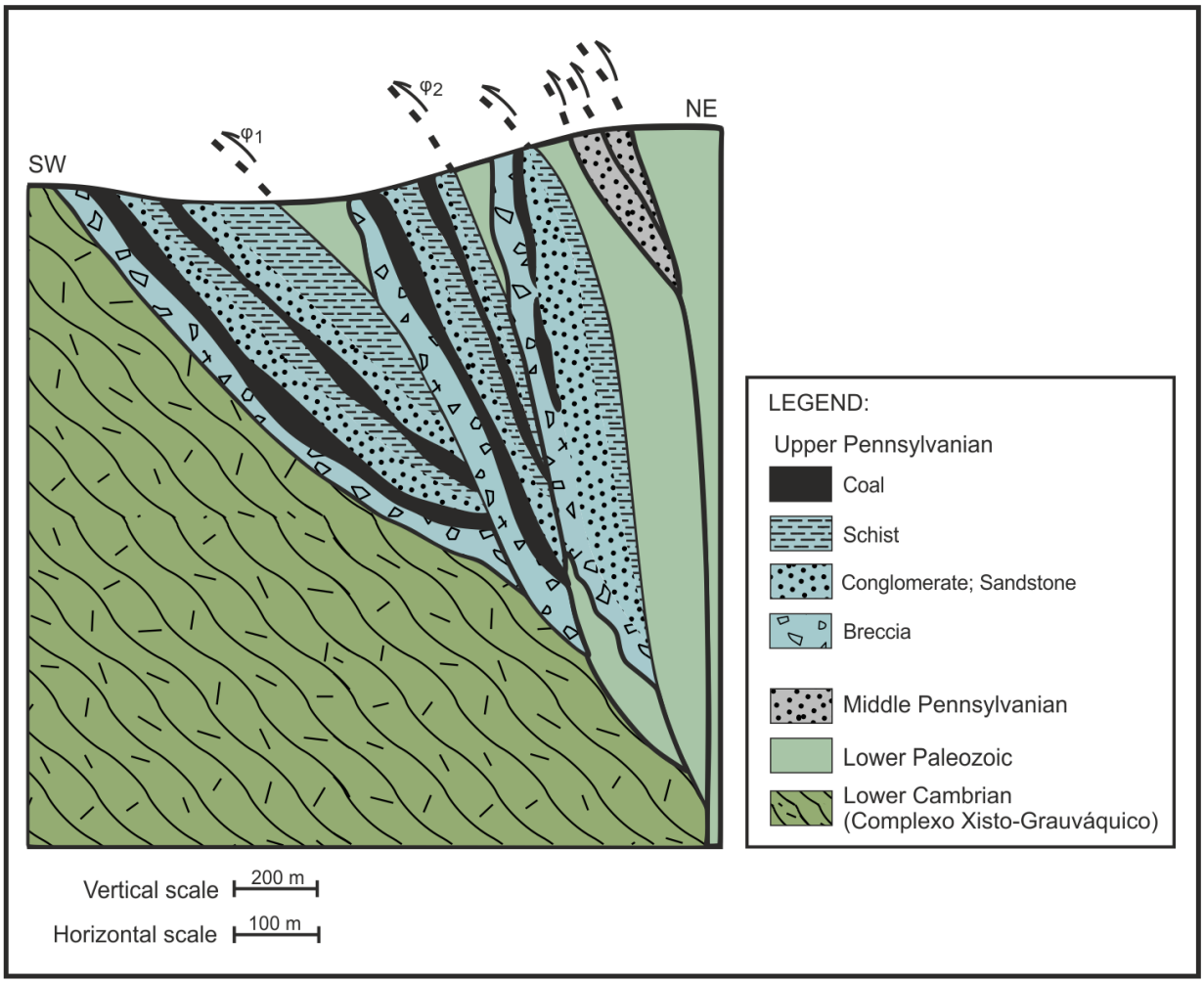

Figure 2 - Structural scheme of Douro Basin, Portugal (Pinto de Jesus, 2001).

The tectonic context caused the sectioning of the basin and consequently led to the duplication of the sedimentary series, which is particularly evident with the formation of the designated "eastern basin". Due to the tectonic compression occurred the centripetal migration of the basin depocentre, which caused the shortening of the coalfield, as well as

the rootlessness of the scaly formed by the substrate of the Lower Paleozoic in stratigraphic contact with the Carboniferous breccia (Pinto de Jesus, 2003).

Stratigraphy

The sedimentary record and the stratigraphy of the DCB are well described by Pinto de Jesus (2001, 2003) that considers the following tectono-sedimentary units [UTS] (Figure 3):

UTS A – (Complex; UTS A1 e UTS A2)

The base of the sequence includes breccias (UST A), namely the UST A1 and the UST A2. The origin of the sediments of these units is associated with the transport from the active tectonic margins of the basin.

UTS A1 is predominantly composed by high energy overlapped by lower energy very coarse alluvial fan facies, indicating a progradation of debris flow deposits.

UST A2 consists of conglomeratic alluvial fan deposits presenting clast lithologies of the Lower Paleozoic. In this unit the predominant lithofacies is interpreted as debris flow, resulting from a turbulent flow and high energy channel deposits.

UTS B – (Simple; UTS B1 e UTS B2)

This unit consists in pelitic and coal-bearing facies. Coal and carbonaceous mudstone facies overlays the UST 1 unit, that progresses to facies that consist of silt and clay, occasionally with lenticular bodies of sandstone. Both facies, pelitic and organic, were formed by vertical accretion. The sedimentary deposits present lamination, a structure typical of low energy aquatic environments.

UTS C – (Simple; UTS C1 e UTS C2)

The UTS C unit consists in a depositional system of a fluvial braided type with parallel flow to the near SW margin. The UST C1 unit is composed by alluvial fan lithofacies associations with conglomerates progressing to sandstones and upwards into siltstones. The UTS C2 is characterized by a braided fluvial system with flow SE-NW, evidenced by the lithologies and the sedimentary structures.

UTS D – (Simple; UTS D1 e UTS D2)

This unit presents lacustrine deltaic lithofacies at the base resulting in a pelitic and coal-bearing sedimentation, due to a reduction of the tectonic activity, and consequently a loss of energy in the sedimentary processes. Therefore, the palustrine sedimentation takes place on the entire basin, progressing into a lacustrine sedimentation as a result of the increasing water depth.

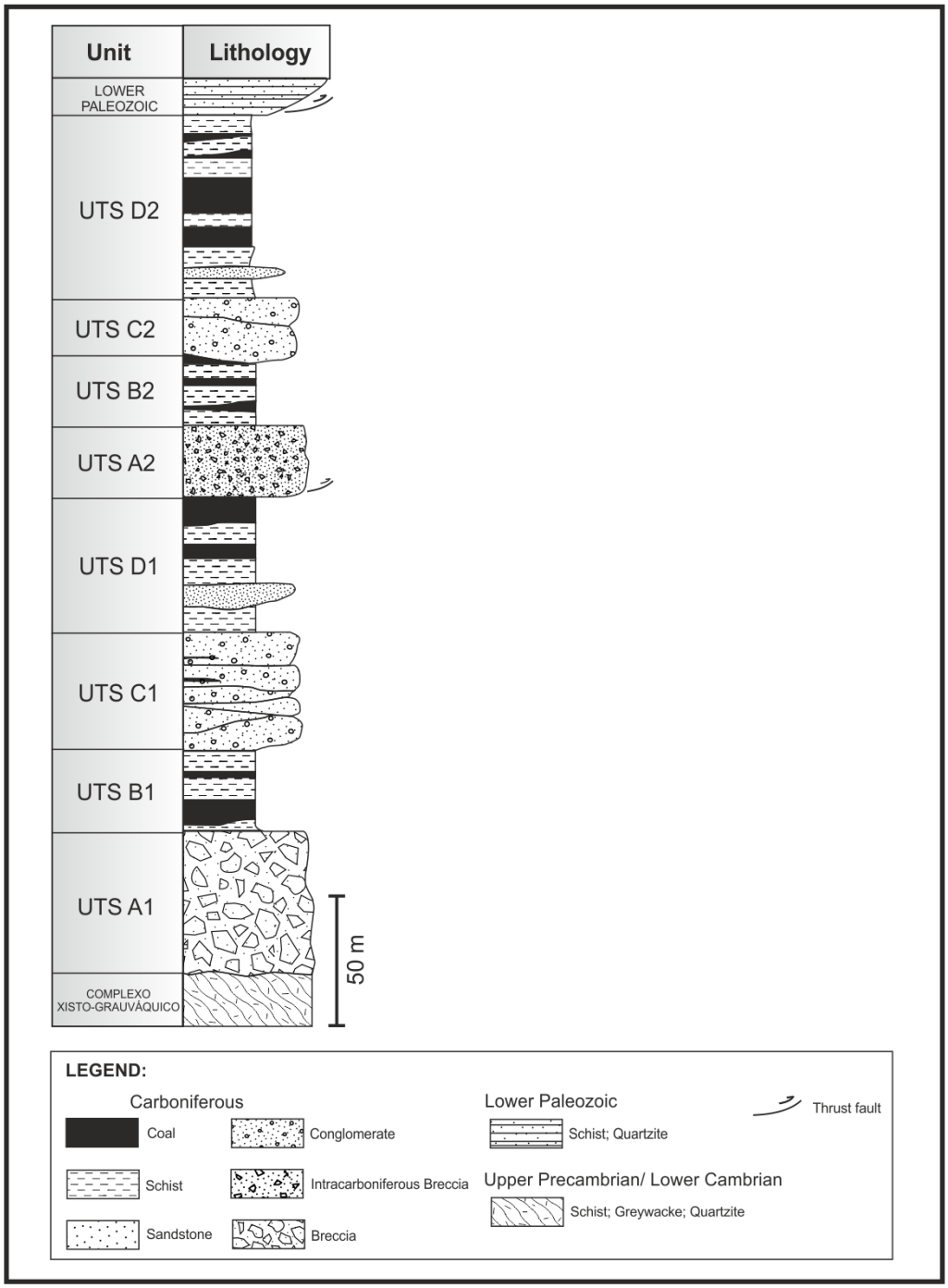

Figure 3 - Simplified column of the Douro Basin Carboniferous sedimentary succession (Pinto de Jesus, 2001).

3.2. Central Asturian Coal Basin

The Central Asturian Coal Basin (Figure 4) is located in northern Spain, specifically in the central part of the Cantabrian Zone (Julivert, 1967; Julivert et al., 1972; Gutiérrez-Claverol and Luque-Cabal, 1995). The coalfield has a general direction NE-SW in the northern sector; however, gradually evolves into N-S in the central sector, and in the most southern sector of the basin has a NW-SE direction (Gutiérrez-Claverol and Luque-Cabal, 1995; Fuente-Alonso and Sáenz de Santa María Benedet, 1999).

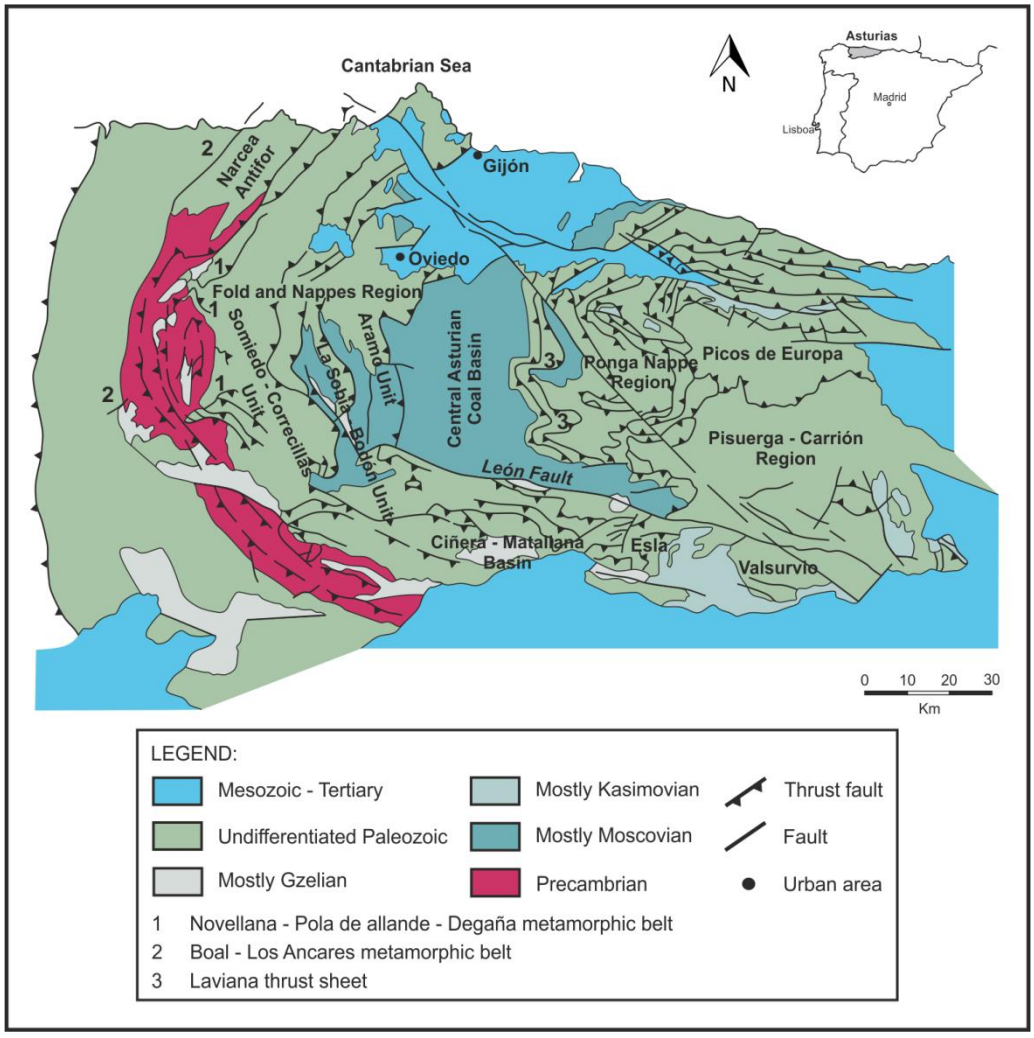

Figure 4 - Structural sketch of the Cantabrian Zone according to Julivert (1967), Pérez-Estaún et al. (1988) and Piedad-Sánchez et al. (2004a, 2004b).

It is an intramontane basin bounded in the N side by Permian, Mesozoic and Cenozoic sediments; in the S margin is cut by the Leon fault, which separates the basin from the older Paleozoic sediments; and, the E and W basin margins are bounded by sediments also dated from the older Paleozoic, namely by the Ponga Nappe Region and by the Sierra de L'Amaro in the Folds and Nappe Region, respectively (Fuente-Alonso and Sáenz de

Santa María Benedet, 1999). The sediments in the coal region are dated Late Moscovian (Westphalian D) and Kasimovian (Stephanian) (Julivert et al., 1971; Marcos and Pulgar, 1982; Aller and Gallastegui, 1995; Alonso and Pulgar, 1995; Bastida and Aller, 1995; Fuente-Alonso and Sáenz de Santa María Benedet, 1999).

During the Carboniferous the coal basin suffered a strong tectonic activity, corresponding to the Variscan Orogeny, which progressed from the west side (Sánchez de la Torre et al., 1983; Truyols-Santonja, 1983; Dallmeyer and Martínez-García, 1990; Férnandez, 1995). The input of sediments into the sedimentary basin came from the young reliefs at W created from the tectonic activity. This tectonic activity has produced a change in the basin system, from an extensional to a compressional regime. This change of the tectonic scheme increased the subsidence of the basin and its sedimentary rate (Marcos and Pulgar, 1982; Águeda et al., 1991; Colmenero et al., 1993; Fernández, 1995).

The basin developed in a foreland style in a transitional and continental sedimentary environment (Águeda et al., 1991; Piedad-Sánchez et al., 2004a, 2004b; Colmenero et al., 2008). This sequence is divided into two sets, synorogenic and tardi-orogenic, registered in both successions (Fernández, 1995).

The synorogenic succession comprises sediments from the Tournaisian to Moscovian, presenting internal deformation of coal seams, parasitic flexural folds and faults. The tardi-orogenic succession of Kasimovian age, located in the already deformed and outcropping areas in the W part of the basin, presents the strike-slip faults, subhorizontal fractures and gravitational microtectonics (Fuente-Alonso and Sáenz Santa María Benedet, 1999).

An episode of incipient metamorphism was reported to these two sequences by Aller and Brime (1985) in the S sector of the basin. However, the extent of the tectonic structures is probably related to an episode of the initial Alpine extension (Fuente-Alonso and Sáenz de Santa María Benedet, 1999) where the reactivation of faults were responsible for modifying the previous structures (Colmenero et al., 1988; Fuente-Alonso and Sáenz de Santa María Benedet, 1999).

The Central Asturian Coal Basin presents very distinct structural and lithological features and two units were recognized, from W to E: the "Riosa-Olloniego Unit" and "La Justa-Aramil and Caudally Nalón Unit" (Figure 5) (Truyols-Santonja, 1983; Luque-Cabal and Sáenz de Santa-María, 1984; Gutiérrez-Claverol and Luque-Cabal, 1995; Fuente-Alonso and Sáenz de Santa María Benedet, 1999), separated by two thrust faults, La Carrera and La Peña faults.

The sedimentary infill of the Central Asturian Coal Basin overlays the Barcaliente Formation and is divided into two groups. The "Lena Group" coal seams are thin and the lithologies are mainly represented by limestones. The "Sama Group", which overlays the above mentioned group, shows more exploitable coal seams and comprises large amounts of sandstone and occasional limestone (Fernandez, 1995). These two groups are divided lithologically into packs. The studied samples belong to the Maria Luisa and Sotón packs, from the Sama Group.

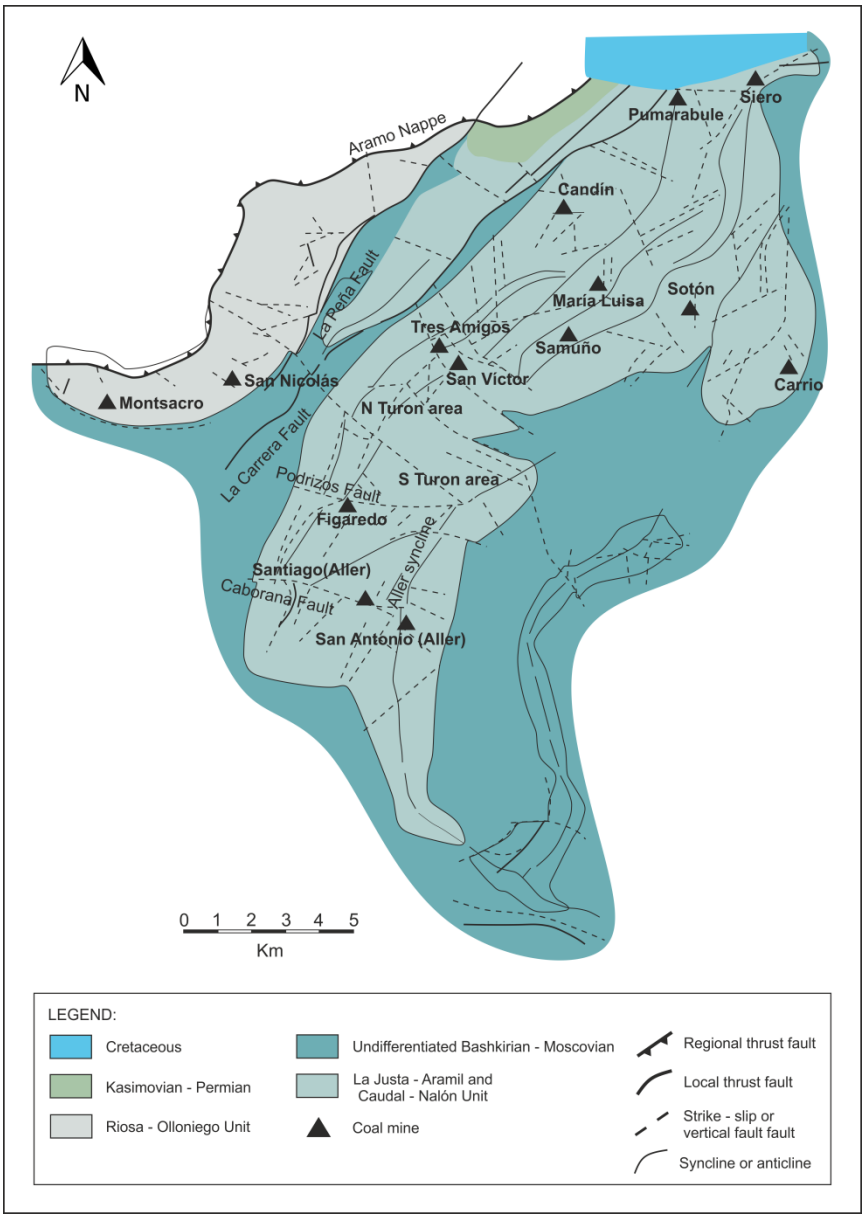

Figure 5 - Structural map of the Central Asturian Coal Basin according to data of Fuente-Alonso and Sáenz de Santa María Benedet (1999) (modified after Piedad-Sanchez et. al, 2004a, 2004b).

Stratigraphy

The facies and paleoenvironments of the Lena and Sama groups (Figure 6) have been described by Colmenero et al. (1988) and Águeda et al. (1991). An evolution of the facies from a continental to a marine environment was reported. In the NW of the basin the sequence starts with conglomerates and sandstones, which corresponds to a delta fan. This is overlapped by a delta lobate tectonic (Colmenero and Barba, 1985) or a river delta-dominated (Bowman, 1985), consisting of sandstones and mudstones. Upwards is followed by a deltaic sequence, with mudstones and limestones, topped by bioclastic and algal-bound limestones facies interbedded with mudstones. A detailed description of the lithology and stratigraphy has been reported by Piedad-Sánchez et al. (2004a, 2004b), including the description of the Maria Luisa and Sotón packs, which are the packs under study.

Maria Luisa Pack

The Maria Luisa Pack (Sama Group - Productive Series) shows a predominance of the continental influence in the basin. This pack has a thickness of 300 m and the higher number of explotable coal seams (from six to nine). Above the "Grès La Voz" is represented a continental sequence with many coal seams, corresponding to lacustrine and lagune facies about x m-thick, overlapped by a marine succession of approximately 40 m of thickness that corresponds to platform facies and then covered by a continental unit with 7 to 10 coal seams 85 to 120 m-thick. To the topis a level corresponding to marine platform facies of about 30 m-thick followed by a few coal deposits, with similar thickness. This package shows a cyclical sedimentation.

Sotón Pack

The Sotón Pack (Sama Group - Productive Series) is the thickest pack, about 40 m, with more coal seams (13 to 19). The base of this pack presents a continental succession, corresponding to lacustrine facies, about 80 m of thickness, with coal seams. This succession is overlapped by two thick marine series followed by continental strata with coal seams. There is an increasing in the sedimentary oscillations at the top of the sequence, and in the last level of continental influence there is a volcanic ash layer, the "Tonstein Lozanita", approximately 2 m thick and representation in all the basin, which is being used as a guide level.

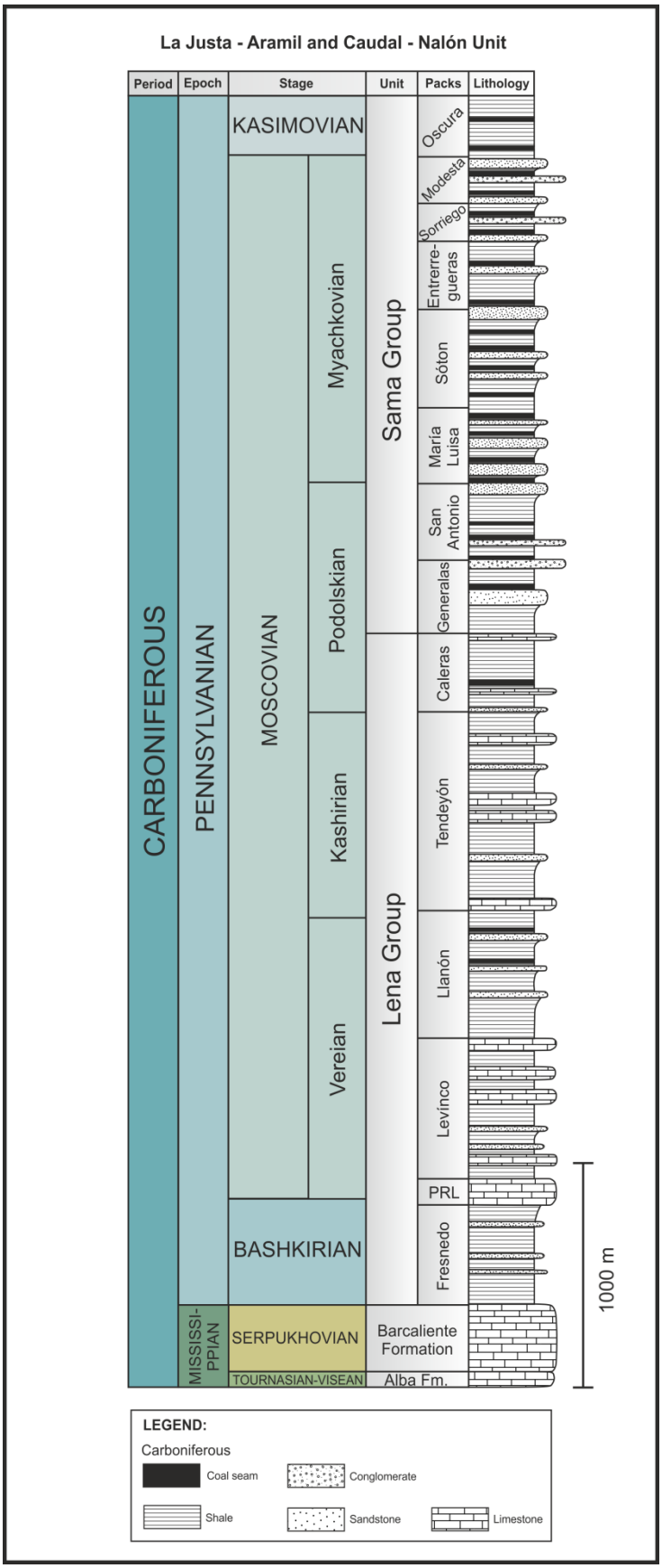

Figure 6 - General lithostratigraphic column of the La Justa - Aramil and Caudal - Nalón Unit in the Central Asturian Coal Basin (NW Spain) (after Sáenz de Santa - María et al., 1985; Sánchez de la Torre et al., 1985; Águeda et al., 1991; Fernández, 1995; Piedade-Sánchez et al., 2004a, 2004b).

3.3. Peñarroya-Belmez-Espiel Basin

The Peñarroya-Belmez-Espiel Basin is located in the South of Spain, province of Cordoba (Andalusia) (Figure 7). This coal basin consists of a narrow, elongated strip, 50 km long and 1 km wide, which strikes approximately NW-SE and is parallel to the NNW-SSE Precambrian and Lower Paleozoic structures of the Central Iberian and Ossa Morena tectonostratigraphic zones (Julivert et al., 1974). Corresponding to an intramontane basin, it is filled with Lower Pennsylvanian (Lower Westphalian) terrestrial sediments interbedded with several coal bearing units (Wagner, 1999).

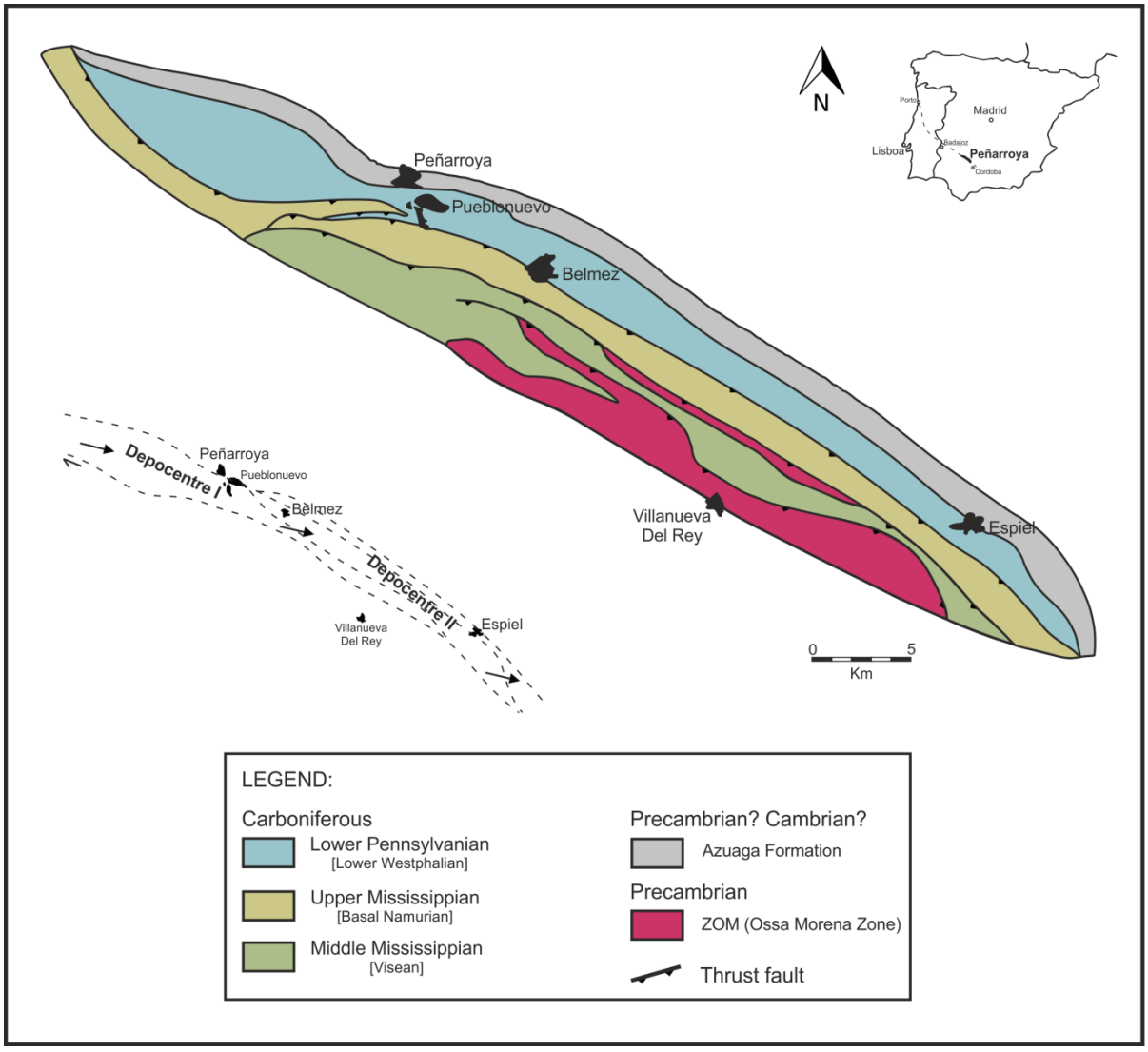

Figure 7 - Geological setting of the Peñarroya-Belmez-Espiel Basin, Spain (Marques, 1993).

The geologic profile of the coalfield is asymmetrical, with increasing dips to SW (Figure 8). To W, prior to the onset of a fault, it appears that the layers had been reversed as part of a synclinal structure, which is in accordance with basinal sag (Wagner, 2004),

controlled by a strike-slip fault. It can be assumed that the fault in question separates the NE and SW flanks of the coalfield structure and that this is a minor transcurrent fault parallel to the main fault (*Principal Displacement Zone* – PDZ - in the sense of Christie-Blick and Biddle, 1985) on the SSW edge (Wagner, 2004).

According to Wagner (1999), the sequence of events that took place in the Peñarroya-Belmez-Espiel Basin allowed the recognition of different depocentres that expanded from NW to SE along the strike of the basin. At least two successive basin zones, one located in the Peñarroya region (Depocentre I) and the other in the Belmez-Espiel region (Depocentre II) (Figure 7).

These two depocentres were formed half-million-years apart, meaning that the tectonic deformation of Depocentre I (San Rafael, Santa Rosa, Mellizo, Pardo, Maria, and Cervantes Units) occurred prior to the development of Depocentre II (Aurora and Cabeza de Vaca Units). This structural pattern is consistent with the coal rank and the tectonic structure of the natural coke occurring in the eastern part of Depocentre I (Marques, 1993), as well as the paleobotanical data (Álvarez-Vásquez, 1995).

Stratigraphically the depocentres are different and present no correlation. Through bore logs and surface mapping is possible to infer that the sedimentary facies are consistent in both depocentres. This similar distribution of sedimentary facies is a reflect of the SSW border, which is considered coincident to the transform fault responsible for controlling the basin subsidence and the changes in the depocentres. The NNE border of the basin, despite having a less permanent site, coincides with subparallel synthetic faulting originated by stresses provoked by continual movement on the PDZ (Wagner, 2004).

Hence, the existence of tectonic control throughout the sedimentation basin appears to be evidenced by the distribution of sediments from NE to SW. Indeed, at all stages of sedimentation, basin sediments located NE are represented by alluvial fan deposits that pass laterally into fluvial sediments that progressively grade into alluvial plain and lacustrine sediments towards the SW margin (Wagner, 1999).

After the sedimentary deformation occurred a reversal of the movement along the plans of normal synthetic faults in the NE border, which would then function as inverse faults, as well as the fault located in the SW edge of the basin. Afterward this phase of structuring, the sediments of the Lower Namurian would be displaced from SW to NE, overlaying the already structured Westphalian sediments, as a result of thrusting occurrence (Wagner, 1999).

There is wide variation in terms of the coals rank range from bituminous to anthracites, the coalification of the anthracites was conditioned by fluid circulation resulting

from magmatic activity (Marques, 2002; Suárez-Ruiz et al., 2006). The coals analyzed in this study belonged to San Rafael Unit (Depocentre I) and to Cabeza de Vaca and Aurora Units (Depocentre II).

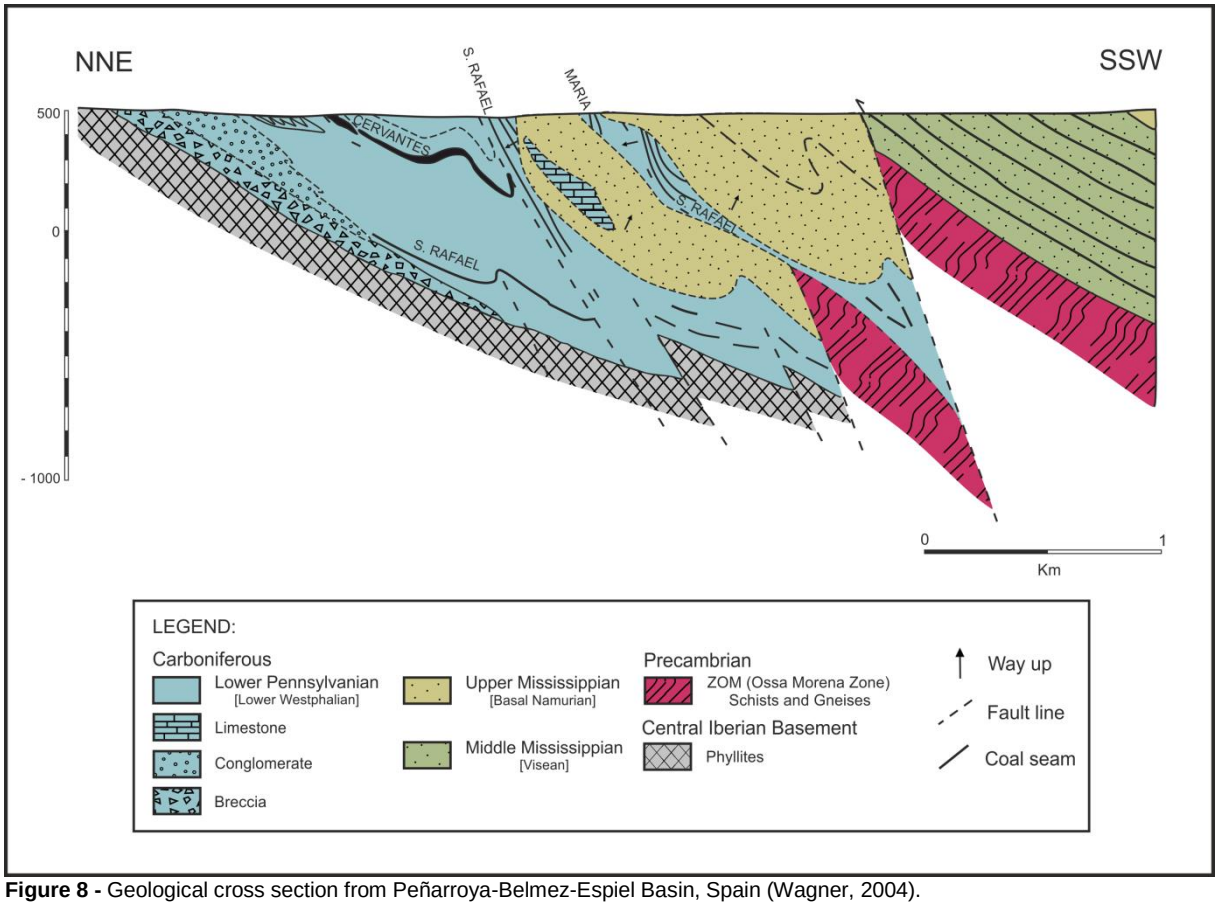

Figure 8 - Geological cross section from Peñarroya-Belmez-Espiel Basin, Spain (Wagner, 2004).

Stratigraphy

The stratigraphy of the basin was studied by Andreis and Wagner (1983), Álvarez-Vázquez (1995), R. Coquel (unpublished) and all the information was summarized by Wagner (1999). A detailed description regarding to the stratigraphy and lithology (Figure 9) is also presented by Marques (1993, 2002).

San Rafael Unit

This unit is represented in the western sector of the basin, occurring wherefore in association with the SW flank of the structure, which is inverted. This unit consists of about 150 m of fluvial deposits that contain coal levels. This set, as a whole, constitutes the Suelos Seam. The sequence gradually evolves into floodplain sediments, which relate with the coals of the Techo Seam, evolving afterward to more lacustrine sequences.

Among the Techo and San Rafael Seams the sequences consist of shales, whereas on the top of the San Rafael Seam the sequence, corresponding to a lacustrine facies, consists of gray shales and, occasionally, of levels of siltstones and fine sandstones, with a total thickness of about 110 m, indicating therefore the presence of a very deep and large lake. On the top of the stratigraphic succession for the Rampa 3W Mine is possible to recognize a similar sequence, although displaying a proximity to the source, specifically in the N edge of the basin, once it presents higher sandstone levels.

Aurora Unit

The Aurora Unit is located in the Central and Eastern Sectors of the basin, between Belmez and Espiel, and corresponds to a total of about 650-700 m sediments. The sediments begin to be deposits of alluvial fans followed upwards by sediments of fluvial and floodplain facies, forming thick mesosequences, globally characterized by the dominant presence of alluvial fan breccias and sandstones at the base and grading into siltstones and mudstones at the top.

The major mesosequences can be identified along the strike and are related with coal zones 3 and 6. The first mesosequence is characterized by fluvial conglomerates and sandstones at the base evolving to siltstones and shales that include several lenticular coal seams. The second mesosequence is represented by conglomerates and sandstones at the base, which underlie a dirty coal seam (Seam 6), followed by shales and siltstones.

Still regarding to the Aurora Unit, particularly in the Espiel area, two subunits have been identified here, the Candelaria and Sucia subunits. The first is well represented in the Candelaria Seam, where it is visible that it corresponds to lacustrine deposits, having representation for several kilometers and has been intensely explored. The Sucia subunit corresponds to fluvial conglomerate deposits followed by alluvial plain deposits with coal beds and carbonaceous shales. One mineral-rich coal seam exists in this unit, the Sucia Seam.

Cabeza de Vaca Unit

The Cabeza de Vaca Unit is located on the SW flank of the structure, E of Belmez, and corresponds to the overturned strata. The unit is represented by a total of about 400 m of sediments, which includes six major coal seams named seams 1, 2, 3, 3 bis, 4 and 5.

The sedimentary succession begins by conglomerates and breccias which are overlapped by sequences of fluvial facies and floodplain at the base of the coal Seam 1. The

first lacustrine interval known in the basin is developed among the Seam 1 and Seam 2, this is constituted by a succession of finely laminated siltstone and shales. Above this interval are located the coal seams 2, 3, 3 bis, 4 and 5, that are represented by lacustrine shales. Upper to the Seam 5 the deposits consist in fluvial and alluvial plain deposits.

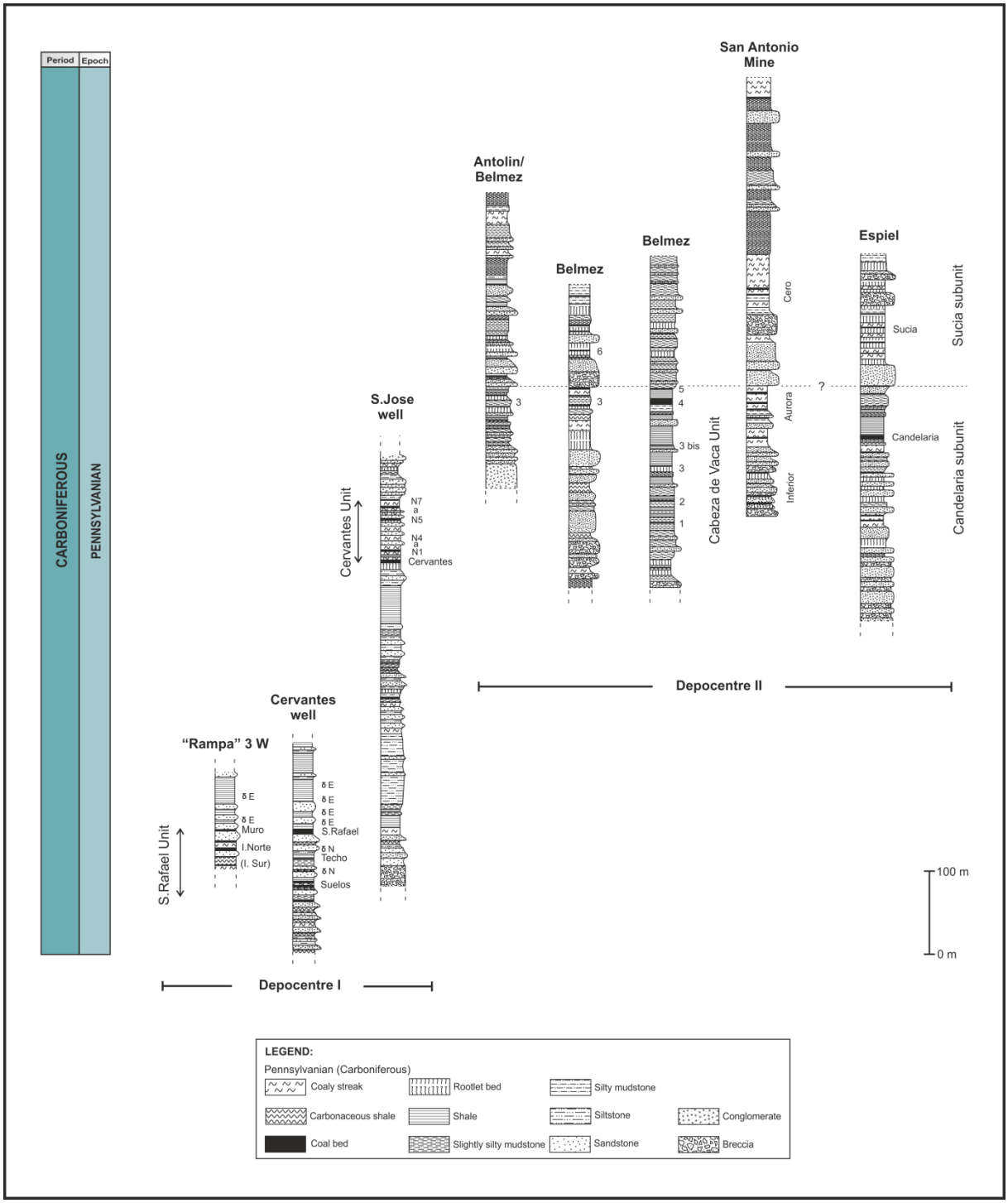

Figure 9 - Generic stratigraphic columns for the Peñarroya-Belmez-Espiel Basin (Marques, 1993).

Chapter 4 – Materials and methodologies

4. Materials and Methodologies

The study of organic matter, in particular of coals, uses analytical procedures taking into account the objectives to be achieved. The main objective of the present study is, as we saw previously, to perform an integrated study of the organic and inorganic fractions as well as the geochemical affinity of trace elements, including mercury, in bituminous and anthracite coals of Carboniferous basins from the Iberian Peninsula: Douro Carboniferous Basin (DCB), Central Asturian Coal Basin (CAB) and Peñarroya-Belmez-Espiel Basin (PBEB) through the detailed petrographic and geochemical characterization of organic and inorganic fractions; and, the definition of organic/inorganic affinities of the mercury and trace elements. Thus, a concise description of the methodologies performed in this research is presented below.

4.1. Samples selection and preparation

Considering the study purpose a set of 42 samples were used: 5 from DCB, 19 from PBEB and 18 from the CAB. The sampling was already done from previous studies (Lemos de Sousa, 1973, 1978; Marques, 1993; Colmenero et al., 2008) and were selected on the basis of rank differences and representativeness of the main units identified in each basin.

For the petrographic study some sample blocks were already prepared (10 from PBEB and 4 from DCB). The petrographic and proximate and ultimate analysis data of the samples from the CAB were available as well. Thus, for this study were prepared, according to the ISO 7404-2 (2009) standard, 9 samples from PBEB and 1 sample from DCB. The existing blocks were polished following the specifications of the same standard (Figure 10).

Figure 10 - Manual polishing of the samples.

Geochemical analysis included proximate and ultimate analysis and the determination of chemical composition in major and trace elements. For the analysis all samples were ground to pass the 212µm sieve (Figure 11).

Figure 11 - Grinding of the samples in an agate mill.

4.2. Analytical procedures

4.2.1. Petrographic composition

The **petrographic composition** was conducted using optical microscopy techniques on polished blocks, namely maceral composition and vitrinite random reflectance.

The microscope observations were performed using a Leica DM4000 microscope (Figure 12), equipped with the software “Discus-Fossil” from Technisches Büro Hilgers. This microscope has LED lightning (white and blue), color and black and white cameras, motorized stage and software to carry out reflectance, maceral analysis, acquisition of photos (software "Discus") and observation in white light and fluorescence. The polished surfaces were observed through a 20x oil (with a refractive index of 1,518 (23ºC) - ISO 8036/1 DIN 58884) immersion objective with cross hairs.

The **maceral analysis** was performed in accordance with the ISO 7404-3 (2009) standard. A minimum of 500 points were counted on each polished block. The number of points counted was converted to proportions by volume and expressed to the nearest tenth of a percent. The nomenclature used was the 1994 ICCP system (International Committee for Coal and Organic Petrology) (ICCP 1998, 2001; Pickel et al., 2015) (see Table 1).

The **vitrinite reflectance** is a physical rank parameter that increasing with coalification, which was conducted following the ISO 7405-5 (2009) standard procedure. Since the optical properties of the vitrinite particles can differ slightly, at least 100 measures were carried out aiming to obtain representative results. The mean random reflectance (Rr%) was measured on collotelinite maceral. Measurements were acquired using white light with a 560 nm filter, specific software and a YAG (Yttrium Aluminum Garnet) or Strontium-Titanat standards for calibration (0.905% and 5.3%R_r, respectively).

Figure 12 - Leica DM4000 microscope, equipped with the software "Discus-Fossil" from Technisches Büro Hilgers.

4.2.2. Geochemical characterization

The **geochemical characterization** of this study was obtained by performing various chemical analyses: proximate and ultimate analyses and the composition on major and trace elements, including the mercury content.

Proximate analysis is a routine analysis conducted in the study of coals, allowing its preliminary characterization. It includes moisture, volatile matter and ash contents in standardized conditions (ISO 589, 2008; ISO 562, 2010; ISO 1171, 2010; respectively). The

moisture content was determined by drying samples at 105 °C. With regard to the volatile matter content, the same was obtained by the pyrolysis of samples for seven minutes at 900 °C. The ash yield was determined by weight loss after the samples were burned in air at 815 °C. Fixed carbon is the difference of these three values summed and subtracted from 100.

Ultimate analysis (carbon, hydrogen, total sulfur and nitrogen) was performed using a LECO S-2000 for C, H, N and a LECO S-632 for total sulfur. The oxygen content was obtained by difference. The results from these chemical analyses were obtained in a dry basis (%, db) and then volatile matter, carbon, hydrogen, and nitrogen were calculated to a dry ash free basis (%, daf) according to the ISO 1170 (2013) standard procedure.

In the present study, the chemical composition of samples on major and trace elements and the mercury concentration was determined by inductively coupled plasma-optical emission spectrometry (ICP-OES) and by inductively coupled plasma-mass spectrometry (ICP-MS).

4.2.3. Mineralogical characterization

Aiming a **mineralogical characterization** SEM-EDS analysis were performed in four samples from PBEB (two bituminous and two anthracites coals), in order to better understand the geochemical affinities. The analysis were conducted using a high resolution (Schottky) environmental scanning electron microscope (ESEM) with X-Ray microanalysis and electron backscattered diffraction analysis: Quanta 400 FEG ESEM / EDAX Genesis X4M. These analysis were carried out in polished blocks coated with a C thin film, by vapour deposition, using the JEOL JEE – 4X Vacuum Evaporator equipment.

Chapter 5 – Results

5. Results

In this chapter is presented the petrographic data and the geochemical study of the coals of the three carboniferous basins. The petrographic study consists mainly in the characterization of the organic and inorganic fractions, including the vitrinite random reflectance and the detailed maceral composition. Simultaneously with the maceral analysis, the mineral matter was identified.

The geochemical study includes proximate and ultimate analysis, being determined the ash content (ash%), volatile matter content (VM%), carbon content (C%), hydrogen content (H%), nitrogen content (N%) and total sulfur content (St%). The fixed carbon as the oxygen contents were calculated takin into account the proximate and ultimate analysis respectively.

The geochemical study also aimed to determine the major and trace elements content. These values were compared with the world hard coals contents established by Ketris and Yudovich (2009) in order to evaluate the enrichment/depletion of the elements in the studied basins.

5.1. Douro Carboniferous Basin

5.1.1. Petrographic characterization

The vitrinite random reflectance was always performed in the collotelinite maceral and ranges from 4.89% to 5.35%, indicating that according to the ISO 11760 (2005) these coals are high rank A (anthracite A) (Table 5). Some petrographic aspects of the coal samples are shown in figure 13. The detailed petrography (Table 5) shows that the organic fraction of the studied samples from the DCB is mostly composed by macerals of the vitrinite group (89 to 98, vol %, mmf). The vitrinite occurs predominantly as telovitrinite (38% to 76%, mmf) and detrovitrinite (17% to 51%, mmf) whereas the gelovitrinite subgroup has practically no representation (< 0.2%, mmf). The inertinite group occur in small percentages ranging from 2% to 11% (vol, mmf), wherein the dominant maceral is the semifusinite (2% to 10%, mmf), followed by fusinite (< 3%, mmf). It is also present inertodetrinite (< 1%, mmf). Regarding the liptinite maceral group, as expected, is not observed due to the rank of these coals. The relationship between the three maceral groups can be analyzed in the figure 14, where it can be observed that the petrographic composition of the studied samples is identical. The relashionship between the three vitrinite maceral subgroups is also available (Figure 15).

Table 5 - Petrographic composition (maceral analysis) and random reflectance (Rr %) of the studied coals from DCB.

Douro Carboniferous Basin	Seam	Mine	Sample	Rr (%)	Mineral matter (vol. %)	Macerals (vol.%, mmf)																
						Telo-vitrinite	Detro-vitrinite	Gelo-vitrinite	Total vitrinite	Fusinite	Semifu-sinite	Fungini-te	Secreti-nite	Macrini-te	Micrini-te	Inerto-detrinite	Total inertinite	Sporinite	Cutinite	Resini-te	Liptode-trinite	Total liptinite
	UTS B1	São Pedro da Cova	15	4.89	0.2	76	22	<1	98	0	2	0	0	0	0	0	2	0	0	0	0	0
	UTS B1	Pejão	274	5.71	12.0	75	17	0	92	3	5	0	0	0	0	0	8	0	0	0	0	0
	UTS D2	São Pedro da Cova	108/116	4.80	0.4	72	21	0	94	1	5	0	0	0	0	0	6	0	0	0	0	0
	UTS D2	Pejão	721	5.35	2.7	47	43	0	90	1	8	0	0	0	0	<1	10	0	0	0	0	0
	Eastern basin	São Pedro da Cova	77	4.96	0.0	38	51	0	89	1	10	0	0	0	0	1	11	0	0	0	0	0

Rr: vitrinite random reflectance.

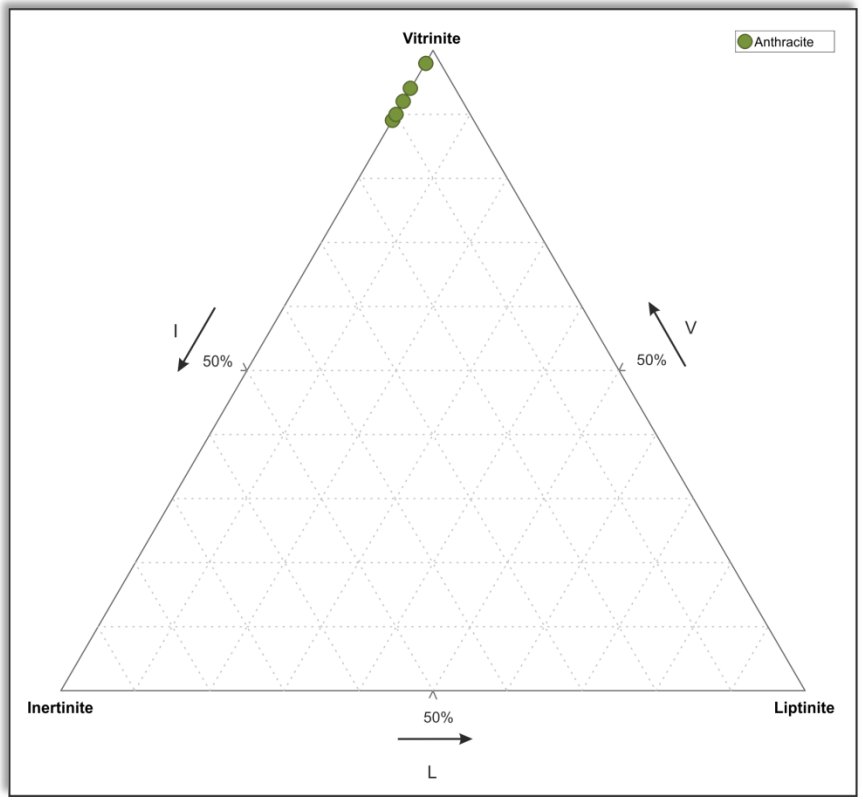

Figure 14 - Petrographic composition diagram for the three vitrinite maceral subgroups based on maceral analysis for studied coals from DCB.

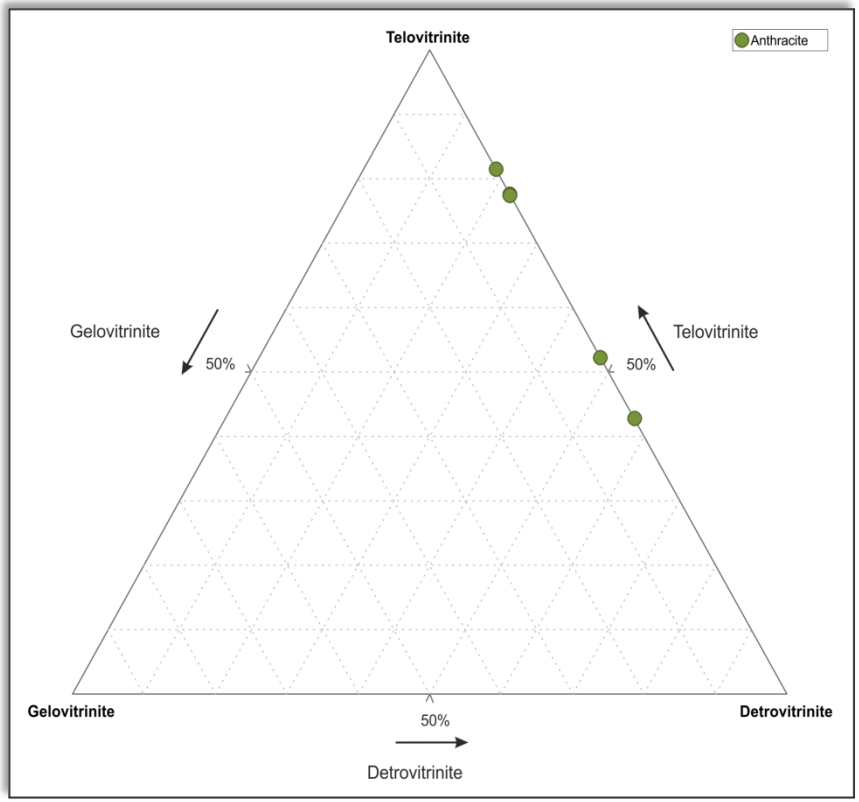

Figure 15 - Petrographic composition diagram for the tree maceral groups based on maceral analysis for studied coals from DCB.

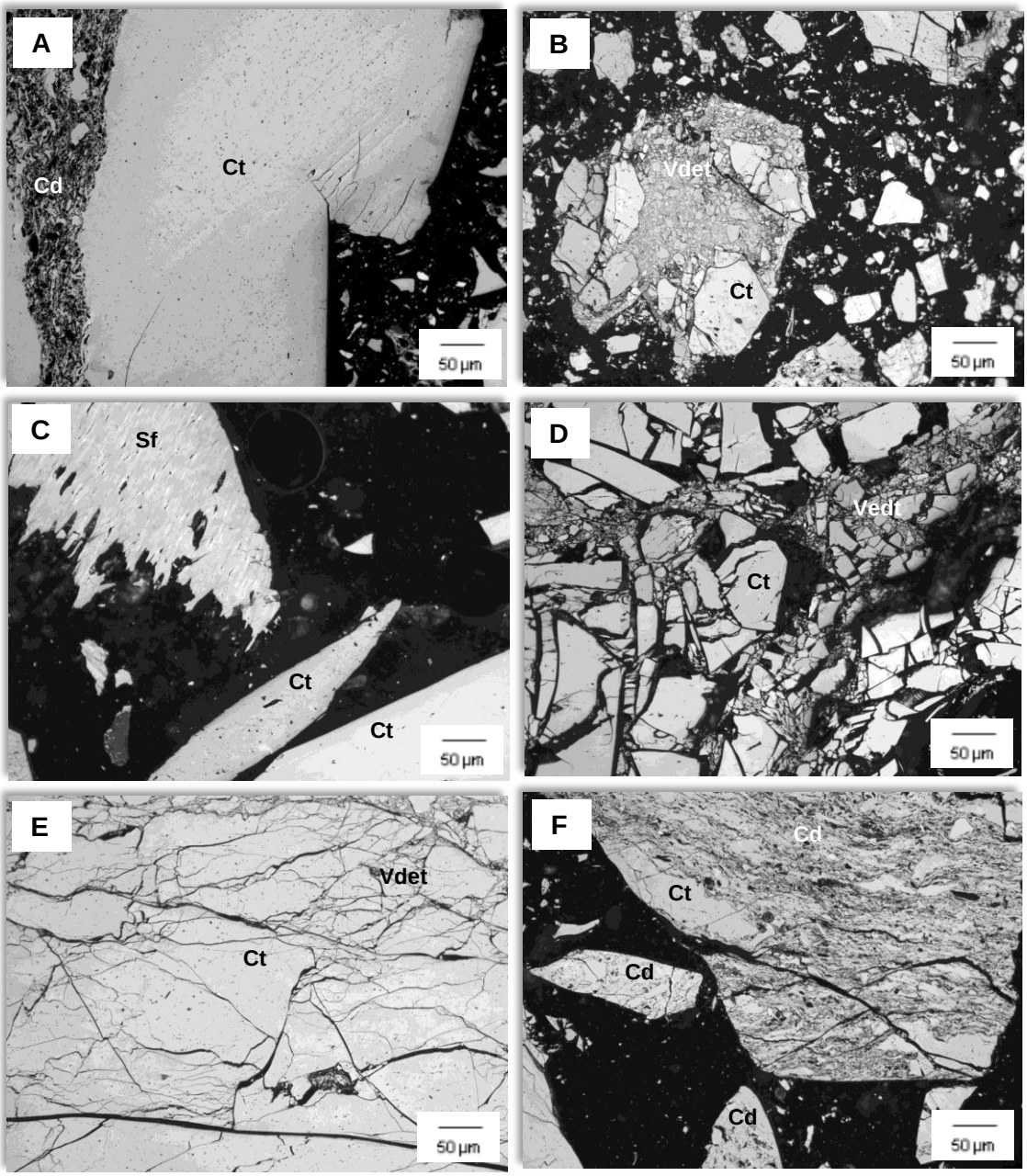

Figure 13 - Photomicrographs of the studied coal samples from DCB (all imagens were taken in reflected white light). A) collotelinite (Ct) and collodetrinite (Ct) (sample 15); B) vitrodetrinite (Vdet) and collotelinite (Ct) (sample 77); C) organic particles with semifusinite (Sf) and collotellinite (Ct) (sample 108/116); D) collotelinite (Ct) and vitrodetrinite (Vdet) (sample 274); E) collotelinite (Ct), vitrodetrinite (Vdet) and cracks (sample 721); F) collotelinite (Ct) and collodetrinite (Cd) (sample 721).

The mineral matter present in the studied samples from this basin ranges from 0% to 12% (vol.), and is mainly represented by carbonates, siderite and calcite, as well as sulphides. In the last case, pyrite occurs as framboidal indicating a syngenetic origin but most often filling fractures denoting an epigenetic origin (Figure 16). In the studied samples other petrographic aspects, including fractures and thermal effect, were often identified.

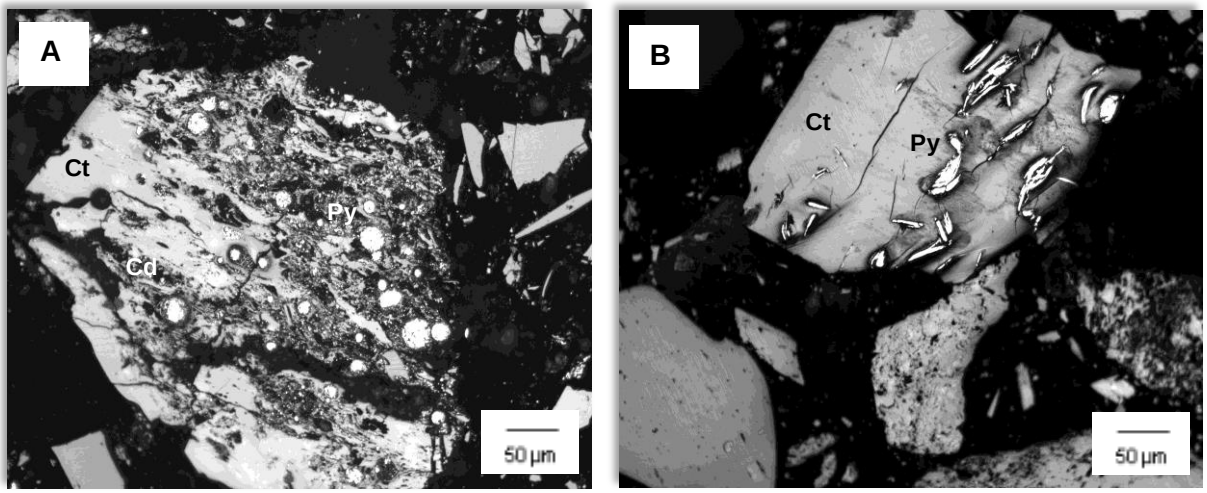

Figure 16 - Photomicrographs of the studied coal samples from DCB (imagens were taken in reflected white light). A) collotelinite (Ct) and collodetrinite (Ct) associated with framboidal pyrite (Py) (sample 274); B) collotelinite (Ct) and epigenetic pyrite (Py) filling cracks (sample 77).

5.1.2. Proximate and ultimate analysis

The results of the proximate analysis were reported in the table 6. Coals from the DCB reveals a medium to high ash content (9.98% to 43.24%, weight, db), which is consistent with the range of the mineral matter content of the same samples obtained in the maceral analysis. The VM content is low (from 3.99% to 14.90%, daf), which is in accordance with the rank of the samples analyzed.

The ultimate analysis displays high C content (83.92% to 94.28%, daf) and very low H (1.30% to 1.99%, daf), N (0.88% to 1.01%, dab) and O (2.74% to 9.35%, daf) contents, which is in agreement with the rank. Regarding the sulfur content, the values vary slightly (0.69% to 3.36%, db), having samples 15 and 274 higher values, namely 3.36% and 3.31%.

The atomic H/C and O/C ratios were calculated for each sample, and the projection in the Van Krevelen diagram was carried out (Figure 17). As expected the samples are a kerogen type III (terrestrial origin) and the rank is in accordance with the petrographic data, mainly the vitrinite reflectance previously reported.

Table 6 - Chemical analysis and H/C – O/C atomic ratios of the studied coals from DCB.

Douro Carboniferous Basin	Seam	Mine	Sample	M	Ash	MV		C		H		N		St	O		H/C	O/C
				(%, ad)	(%, db)	(%, db)	(%, daf)	(%, db)	(%, daf)	(%, db)	(%, daf)	(%, db)	(%, daf)	(%, db)	(%, db)	(%, daf)		
	UTS B1	São Pedro da Cova	15	5.97	17.58	12.28	14.90	68.92	83.62	1.64	1.99	0.79	0.96	3.36	7.71	9.35	0.28	0.08
	UTS B1	Pejão	274	4.04	43.24	6.92	12.19	48.81	85.99	0.97	1.71	0.50	0.88	3.31	3.17	5.58	0.24	0.05
	UTS D2	São Pedro da Cova	108/116	*	*	*	*	*	*	*	*	*	*	*	*	*	*	*
	UTS D2	Pejão	721	4.24	16.40	4.24	5.07	78.82	94.28	1.09	1.30	0.71	0.85	0.69	2.29	2.74	0.16	0.02
	Eastern basin	São Pedro da Cova	77	3.88	9.88	3.60	3.99	84.35	93.60	1.72	1.91	0.91	1.01	0.76	2.38	2.64	0.24	0.02

M = moisture; VM = volatile matter; St = total sulphur ; ad = as determined; db = dry basis; daf = dry ash-free basis. *data not available

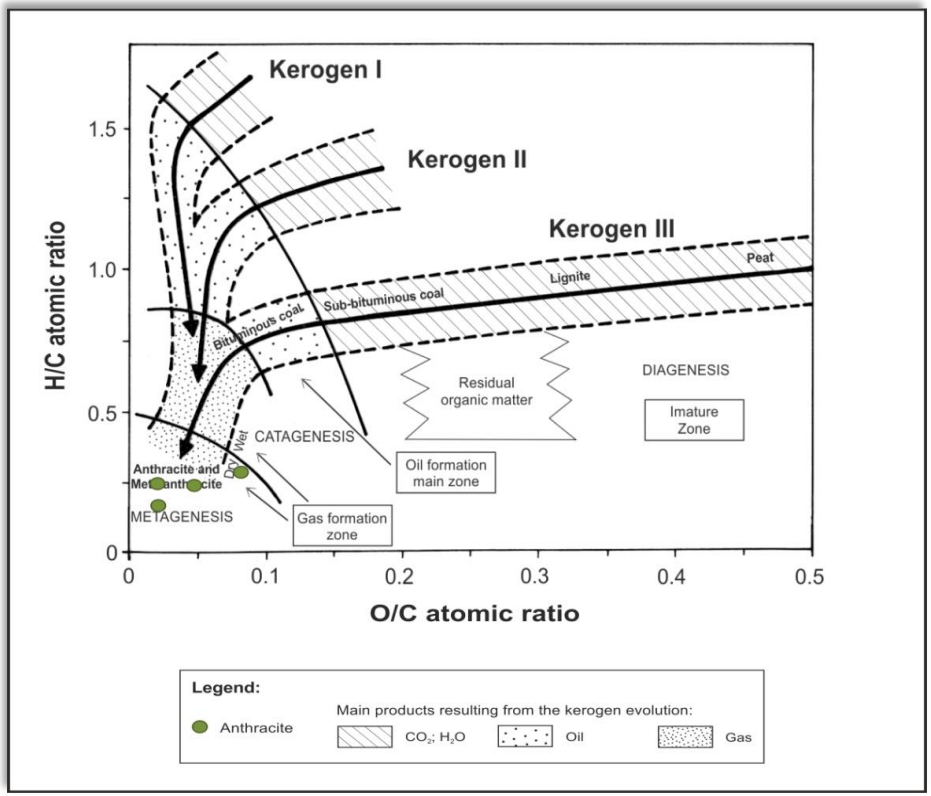

Figure 17 - Projection of the H/C – O/C atomic ratios of the studied coals from DCB in the Van Krevelen diagram.

5.1.3. Major and trace elements

The abundance on major and trace elements of the studied coal samples is reported in table 7. When compared with the average values in the world hard coals (Ketris and Yudovich, 2009), the DCB samples show that some of them are enriched in some elements. Through the observation of the table 7 is perceived that the abundance of enriched elements occurs in a greater number of elements in three samples, namely samples 15, 274 and 721, while the other two samples, 77 and 108/116, exhibit a lower number of elements enriched.

Regarding to the major elements, the studied samples display a high content of Al in the samples 15, 274 and 721 pointing out the presence of clay minerals. A high content of Fe and St is also observed in the samples 15 and 274 indicating the presence of pyrite. In sample 15 pyrite occurred filling fractures, suggesting an epigenetic origin. In sample 274 pyrite occurs mainly as framboids pointing out a syngenetic origin. Regarding the Ca content, it is generally low in all samples, although carbonate minerals were identified, except in sample 15.

Concerning the trace elements, generically, the basin under study is enriched in the following: Ag, As, Co, Cr, Cs, Cu, Ga, Hg, Mo, Ni, Pb, Rb, Sb, Sc, Se, Sn, Sr, Th V, W, Y, Zn, Zr, La, Ce, Pr, Nd, Sm, Eu, Gd, Tb, Dy, Er and Yb. Within the enriched trace elements it is important to note the contents of Ag, As and Co for the samples 15 and 274, because they present much higher values than those considered for the average of world hard coals reported by Ketris and Yudovich (2009). The same is valid for the contents of Hg in the samples 15, 274 e 721. The Cs and Sb contents are also very high in the samples 15 and 274, respectively.

Table 7 - Ash yield, total Sulphur (%, d) and elemental concentrations in the studied coals from DCB (trace elements in µg/g; major elements in %).

Douro Carboniferous Basin							
Mine		UTS B1	UTS B1	UTS D2	UTS D2	Eastern basin	Hard Coals
Seam		São Pedro da Cova	Pejão	São Pedro da Cova	Pejão	São Pedro da Cova	
Sample		15	274	108/116	721	77	
Elements	Ash	17.58	43.24	3.90	16.40	9.88	
	Al	2.22	2.88	0.78	2.29	0.69	
	Si	0.05	0.08	0.02	0.05	0.03	
	Ca	0.01	0.03	0.03	0.26	0.04	
	Mg	0.07	0.54	0.02	0.23	0.14	
	Fe	2.35	5.51	0.51	1.64	0.99	
	K	0.31	0.35	0.14	0.39	0.05	
	Mn	0.00	0.02	0.00	0.02	0.00	
	Na	0.14	0.09	0.10	0.04	0.00	
	P	0.00	0.01	0.01	0.08	0.00	0.3
	St	3.36	3.31	*	0.69	0.76	
	Ti	0.07	0.10	0.02	0.06	0.04	0.9
	Ag	**0.40**	**0.40**	0.05	0.05	0.05	0.1
	As	**71.60**	**70.30**	8.10	**23.30**	**12.60**	9
	Au	0.25	0.60	0.25	0.25	0.60	
	Ba	94.00	77.00	83.00	86.00	18.00	150
	Be	0.05	0.05	0.05	0.05	0.05	2
	Bi	0.40	0.30	0.50	0.20	0.50	1.1
	Cd	0.50	0.60	0.05	0.05	0.05	0.2
	Co	**26.00**	**23.70**	**7.80**	**7.00**	**6.10**	6
	Cr	**41.05**	**34.21**	6.84	**20.53**	**27.37**	17
	Cs	**14.10**	**3.30**	**8.50**	**5.30**	0.80	1.1
	Cu	**42.90**	**37.50**	9.80	8.70	8.60	16
	Ga	5.70	**8.20**	2.00	5.70	2.10	6
	Hf	0.70	1.10	0.30	0.60	0.50	1.2
	Hg	**44.02**	**1.07**	**0.73**	**1.09**	0.10	0.1
	Mo	**4.10**	**4.10**	**2.20**	**3.00**	0.50	2.1
	Nb	2.30	3.00	0.90	1.90	1.10	4
	Ni	**61.80**	**94.20**	4.90	**22.50**	6.20	17
	Pb	**29.50**	**41.70**	2.20	**9.80**	1.20	9
	Rb	**29.20**	**23.70**	13.70	**29.60**	3.30	18
	Sb	0.60	**12.60**	0.20	**1.10**	0.10	1
	Sc	**5.00**	**7.00**	1.00	**4.00**	1.00	3.7
	Se	1.40	**2.80**	0.25	0.25	0.25	1.6
	Sn	1.00	1.00	0.50	**2.00**	1.00	1.4
	Sr	47.00	31.80	24.80	37.40	13.90	100
	Ta	0.10	0.20	0.05	0.20	0.05	0.3
	Th	**5.30**	**4.70**	1.10	**4.10**	1.40	3.2
	Tl	0.05	0.05	0.05	0.05	0.05	0.6
	U	1.60	1.30	0.80	1.30	0.50	1.9
	V	**49.00**	**52.00**	20.00	**36.00**	16.00	28
	W	**1.40**	**1.20**	0.25	0.60	**1.90**	1
	Y	**10.90**	**12.50**	2.80	**9.30**	3.90	8.2
	Zn	**35.00**	**140.00**	14.00	16.00	7.00	28
	Zr	22.30	**36.50**	9.70	19.40	16.90	36
	La	**20.60**	**14.70**	4.50	**16.60**	5.30	11
	Ce	**44.00**	**36.10**	10.50	**37.50**	12.50	23
	Pr	**5.27**	**3.88**	1.31	**4.35**	1.43	3.4
	Nd	**20.70**	**14.40**	5.30	**17.70**	5.90	12
	Sm	**4.42**	**2.95**	0.97	**3.67**	1.01	2.2
	Eu	**0.78**	**0.63**	0.21	**0.78**	0.20	0.4
	Gd	**3.65**	**2.83**	0.83	**3.09**	0.91	2.7
	Tb	**0.48**	**0.43**	0.11	**0.38**	0.13	0.3
	Dy	**2.37**	**2.45**	0.57	1.95	0.66	2.1
	Ho	0.44	0.45	0.11	0.33	0.14	0.6
	Er	**1.08**	**1.20**	0.32	0.96	0.41	1
	Tm	0.17	0.19	0.04	0.12	0.06	0.3
	Yb	**1.08**	**1.24**	0.26	0.78	0.35	1
	Lu	0.16	0.18	0.04	0.11	0.05	0.2

Values in boldface are higher than concentration for worldwide hard coals by Ketris and Yudovich (2009).

5.2. Central Asturian Coal Basin

5.2.1. Petrographic characterization

The vitrinite random reflectance of the Central Asturian Coal Basin samples ranges from 0.7% to 2.5% (Table 8). Based on these data all samples are classified as medium rank C to A (bituminous C to A; 0.7% to 1.5%) coals according to the ISO 11760 (2005) standard, with the exception of the sample 40776 (Rr = 2.5%) that is classified as high rank C (anthracite C) coal, considering the same standard.

The petrographic analysis performed in the samples (Table 8) evidences a predominance of the vitrinite maceral group (60% to 94%, mmf), thereby in some of the samples this maceral group covers almost the entire sample. No data on the percentages of the subgroups of this maceral group is available.

Table 8 - Petrographic composition (maceral analysis) and random reflectance (Rr %) of the studied coals from CAB.

	Pack	Mine	Sample	Rr (%)	Mineral mater (vol. %)	Macerals (vol.%, mmf)		
						Total vitrinite	Total inertinite	Total liptinite
Central Asturian Coal Basin	Sotón	Sóton	40634	0.8	3.0	77.1	13.2	9.7
			40642	0.9	4.4	71.8	19.2	9.0
		Maria Luisa	40398	0.9	2.8	79.4	12.3	8.2
			40370	1.0	7.6	72.7	20.8	6.5
		Samuño	40361	0.9	1.3	68.3	23.1	8.6
			40366	1.0	10.2	60.2	29.4	10.4
		Candin	39755	0.7	1.2	70.6	13.6	15.8
			39759	0.9	5.4	72.1	12.1	15.9
		San Victor	39152	0.6	32.0	90.3	1.2	8.5
		Pumarabule	39311	0.8	6.8	83.7	9.0	7.3
		Figaredo	39169	1.2	1.6	90.2	8.0	1.8
	Maria Luisa	Pumarabule	39313	0.8	5.6	94.1	3.2	2.8
		Tres amigos	39768	1.0	1.6	62.6	32.1	5.3
			39772	0.9	8.0	83.9	10.4	5.7
		Candin	39733	0.9	4.2	79.6	16.4	3.9
		Sóton	40616	1.0	1.8	85.9	9.4	4.6
		Figaredo	39162	1.5	14.7	80.4	19.6	0.0
		Aller (San Antonio)	40776	2.5	1.6	76.0	24.0	0.0

Rr: vitrinite random reflectance.

Regarding these samples there is no data related to the macerals of the inertinite and liptinite group. The liptinite group vary between 0% and 19%, mmf. For the inertinite maceral group values vary widely depending on the sample, the lowest value displayed is 1%, mmf and the higher 32%, mmf. The relationship between the three maceral groups can be

analyzed in the triangular diagram (Figure 18), where variations in the petrographic composition of the samples can be observed.

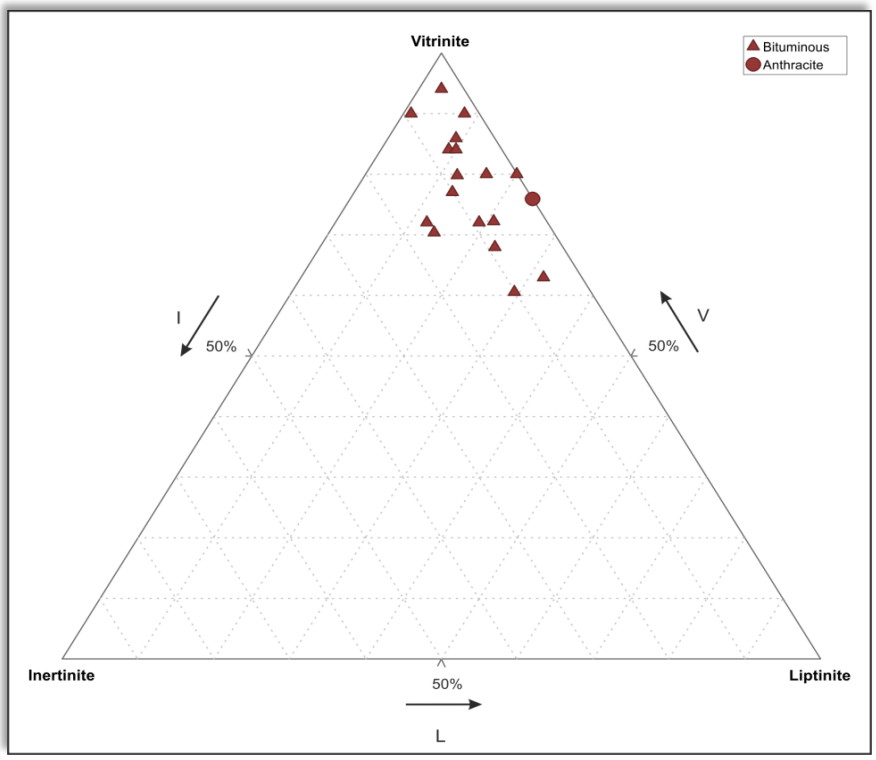

Figure 18 - Petrographic composition diagram for the three maceral groups based on maceral analysis for studied coals from CAB.

The content of mineral matter also varies in these samples within a wide range values from sample to sample, with the lowest value being 2% and the higher 32%, there is however no information about the type of mineral matter.

5.2.2. Proximate and ultimate analysis

The results of the proximate analysis (Table 9) of the samples from the Central Asturian Coal Basin express an ash content ranging from a large set of values (2.83% to 34.22%, db), which indicates that the content varies from very low to moderately high, which is in accordan ce with the content of the inorganic fraction reported for the maceral analysis. Relating to the VM content, they vary greatly (8.40% to 43.35%, daf) and are within the standard values.

With regard to the ultimate analysis, the coal samples show C contents ranging between 71.40% and 91.89%, daf. The H (3.03% to 5.63%, daf), N (1.39% to 2.17%, daf) and O (3.04% to 21.13%, daf) contents are in accordance with the rank of the samples. The total S values vary slightly (0.35% to 3.18%, db) and the samples that display higher values are 39759 and 40634, with values of 3.18% and 2.29%, respectively.

Table 9 - Chemical analysis and H/C – O/C atomic ratios of the studied coals from CAB.

	Pack	Mine	Sample	M	Ash	MV		C		H		N		St	O		H/C	O/C
				(%, ad)	(%, db)	(%, db)	(%, daf)	(%, db)	(%, daf)	(%, db)	(%, daf)	(%, db)	(%, daf)	(%, db)	(%, db)	(%, daf)		
Central Asturian Coal Basin	Sotón	Sóton	40634	1.65	7.67	36.23	39.24	76.42	82.77	5.06	5.48	1.49	1.61	2.29	7.07	7.66	0.79	0.07
			40642	1.90	9.38	34.17	37.71	74.76	82.50	4.52	4.99	1.59	1.75	0.48	9.27	10.23	0.72	0.09
		Maria Luisa	40398	1.66	6.22	32.33	34.47	80.05	85.36	4.85	5.17	1.80	1.92	1.06	6.02	6.42	0.72	0.06
			40370	1.24	10.15	30.29	33.71	77.45	86.20	4.85	5.40	1.72	1.91	1.51	4.32	4.81	0.75	0.04
		Samuño	40361	1.39	2.83	34.81	35.82	84.29	86.74	5.25	5.40	1.81	1.86	0.40	5.42	5.58	0.74	0.05
			40366	1.24	21.65	28.55	36.44	67.68	86.38	4.35	5.55	1.41	1.80	0.35	4.56	5.82	0.77	0.05
		Candin	39755	1.50	3.31	36.64	37.89	80.57	83.33	5.04	5.21	1.61	1.67	0.71	8.76	9.06	0.75	0.08
			39759	1.58	6.26	40.64	43.35	76.06	81.14	5.28	5.63	1.53	1.63	3.18	7.69	8.20	0.83	0.08
		San Victor	39152	6.88	34.22	26.07	39.63	46.97	71.40	2.78	4.23	1.27	1.93	0.86	13.90	21.13	0.71	0.22
		Pumarabule	39311	1.84	15.83	38.55	45.80	69.20	82.21	4.44	5.28	1.55	1.84	0.46	8.52	10.12	0.76	0.09
		Figaredo	39169	1.14	6.41	28.57	30.53	82.49	88.14	4.86	5.19	2.03	2.17	0.97	3.24	3.46	0.70	0.03
	Maria Luisa	Pumarabule	39313	2.14	12.79	35.07	40.21	71.93	82.48	4.55	5.22	1.73	1.98	0.80	8.20	9.40	0.75	0.09
		Tres amigos	39768	1.38	4.60	29.37	30.79	81.59	85.52	4.75	4.98	1.33	1.39	0.51	7.22	7.57	0.69	0.07
			39772	1.33	18.63	29.06	35.71	68.74	84.48	3.82	4.69	1.33	1.63	0.73	6.75	8.30	0.66	0.07
		Candin	39733	1.72	8.14	28.69	31.23	77.61	84.49	4.15	4.52	1.57	1.71	0.74	7.79	8.48	0.64	0.08
		Sóton	40616	1.29	6.35	33.27	35.53	79.86	85.27	4.56	4.87	1.66	1.77	1.57	6.00	6.41	0.68	0.06
		Figaredo	39162	0.86	18.36	17.92	21.95	72.05	88.25	3.41	4.18	1.29	1.58	0.42	4.47	5.48	0.56	0.05
		Aller (San Antonio)	40776	1.30	4.09	8.06	8.40	88.13	91.89	2.91	3.03	1.47	1.53	0.48	2.92	3.04	0.39	0.02

M = moisture; VM = volatile matter; St = total sulphur ; ad = as determined; db = dry basis; daf = dry ash-free basis.

The projection of the atomic H/C and O/C ratios in the Van Krevelen diagram was performed for each sample (Figure 19). As predicted the samples are a kerogen type III (terrestrial origin) and the rank is in accordance with the petrographic data, except for sample 39152. This sample, which refers to a medium rank C (bituminous C) according to the vitrinite reflectance, is designed as residual organic matter when projected in the Van Krevelen diagram, which can be explained by the high ash yield (34%) and mineral matter content (32%).

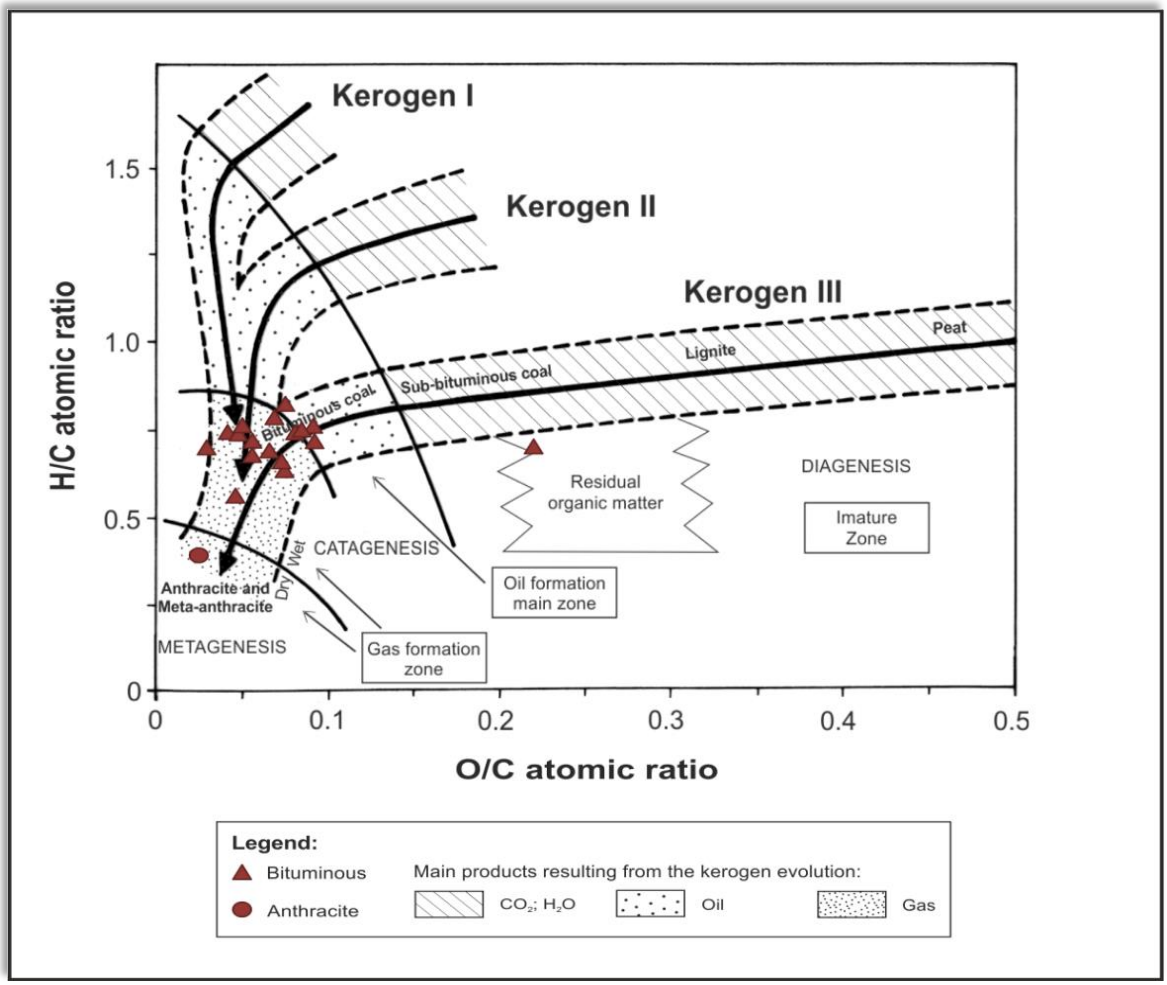

Figure.19- Projection of the H/C – O/C atomic ratios of the studied coals from CAB in the Van Krevelen diagram.

5.2.3. Major and trace elements

The study of the abundance of elements in the Central Asturian Coal Basin (Table 10) revealed that globally the samples do not present a great enrichment of the elements analyzed when compared to the average values of the world hard coals reported by Ketris and Yudovich (2009). There are, however, three samples that differ from the others having a larger number of elements enriched, namely the samples 40366, 39152 and 39162. The

opposite occurs for the samples 39755, 39733, 40398, 40361, 39313, 39768, 40776 and 40616, that have few elements enriched. The sample 39169 presents all element bellow the Clarke values for world hard coals defined by Ketris and Yudovich (2009).

Regarding the major elements, Al and Si stands out in the samples 40366 and 39152. A high content for Ca is observed for the samples 40642, 39759, 39768, 39772 and 39162. With respect to the Fe content high values are observed in the samples 40642, 40370, 39579, 39152, 39311, 39169 and 39313 and for total S samples 40634, 40398, 40370, 39759 and 40616 displayed also high contents.

Concerning to the trace elements, the studied samples reveal an enrichment in As, Ba, Be, Co, Cr, Cs, Cu, Ga, Hg, Mo, Pb, Rb, Sb, Sc, Se, Sr, Th, U, V, W, Y, Zn, La , Ce, Pr, Nd, Sm, Eu, Gd, Tb, Dy, Er and Yb when compared to the average values of the world hard coals. It is clear that Ag, Cu, Pb and Zn possess higher evidence because these elements are in abundance in a greater number of the studied coal samples. It is important to highlight the As content of the samples 40370 and 39152, since they are well above the established for the Clarke values established by Ketris and Yudovich (2009). The same happens with the Cu and Pb elements, although in the first case the enrichment is observed in samples 40634 and 39755, for the Pb the enriched samples are 39759 and 39152. One element that has a great abundance in two of the coals is Zn, namely in samples 40634 and 39755. The Sb also shows very high values in the sample 39152.

Table 10 - Ash yield, total Sulphur (%, d) and elemental concentrations in the studied coals from CAB (trace elements in µg/g; major elements in %).

Central Asturian Coal Basin																			
Pack		Sotón										Maria Luisa							Hard Coals
Mine		Sóton		Maria Luisa		Samuño		Candin		San Victor	Pumarabule	Figaredo	Pumarabule	Tres amigos		Candin	Sóton	Figaredo	Aller (San Antonio)	
Sample		40634	40642	40398	40370	40361	40366	39755	39759	39152	39311	39169	39313	39768	39772	39733	40616	39162	40776	
	Ash	7.67	9.38	6.22	10.15	2.83	21.65	3.31	6.26	34.22	15.83	6.41	12.79	4.60	18.63	8.14	6.35	18.36	4.09	
	Al	1.15	0.16	0.50	1.23	0.20	3.36	0.29	0.24	3.79	0.29	0.29	0.85	0.20	2.19	0.96	0.40	1.95	0.14	
	Si	1.57	0.33	0.91	1.73	0.18	5.26	0.45	0.16	5.94	0.30	0.48	1.11	0.23	3.10	1.12	0.64	2.78	0.17	
	Ca	0.59	2.32	0.71	0.34	0.77	0.41	0.57	1.10	0.01	0.87	0.81	0.99	1.03	1.18	0.91	0.76	2.69	0.98	
	Mg	0.11	0.54	0.08	0.14	0.14	0.24	0.16	0.21	0.10	0.25	0.26	0.40	0.31	0.19	0.15	0.13	0.19	0.17	
	Fe	0.85	1.43	0.70	1.33	0.36	0.79	0.39	1.96	2.21	3.62	3.07	1.76	0.73	0.73	0.47	1.18	0.40	0.48	
	K	0.25	0.02	0.11	0.32	0.02	0.81	0.05	0.02	0.90	0.04	0.07	0.19	0.03	0.52	0.21	0.06	0.39	0.02	
	Mn	0.00	0.05	0.00	0.00	0.00	0.00	0.00	0.01	0.00	0.05	0.03	0.02	0.02	0.00	0.00	0.01	0.00	0.00	
	Na	0.03	0.00	0.02	0.04	0.01	0.08	0.01	0.00	0.10	0.01	0.04	0.03	0.02	0.06	0.04	0.01	0.07	0.01	
	P	0.00	0.00	0.00	0.00	0.00	0.01	0.00	0.00	0.02	0.00	0.01	0.00	0.00	0.02	0.00	0.00	0.03	0.00	0.3
	St	2.29	0.48	1.06	1.51	0.40	0.35	0.71	3.18	0.86	0.46	0.97	0.80	0.51	0.73	0.74	1.57	0.42	0.48	
	Ti	0.04	0.01	0.02	0.04	0.01	0.13	0.01	0.01	0.09	0.01	0.01	0.03	0.01	0.08	0.03	0.01	0.07	0.01	0.9
	Ag	0.05	0.05	0.05	0.05	0.05	0.05	0.05	0.05	0.20	0.05	0.05	0.05	0.05	0.05	0.05	0.05	0.05	0.05	0.1
	As	**13.00**	3.10	**13.90**	**81.40**	0.90	2.10	2.70	**23.60**	**123.80**	3.30	5.60	5.50	0.25	8.20	**9.20**	**27.20**	0.25	0.25	9
	Au	0.25	0.25	0.25	0.25	0.90	0.25	0.25	0.25	0.25	0.25	0.25	0.25	0.25	0.25	0.25	0.25	0.25	0.25	
	Ba	81.00	37.00	47.00	98.00	70.00	**217.00**	61.00	98.00	**175.00**	47.00	38.00	68.00	37.00	**189.00**	74.00	58.00	**182.00**	107.00	150
	Be	0.50	0.50	0.50	2.00	0.50	1.00	0.50	0.50	2.00	0.50	0.50	**3.00**	**3.00**	1.00	0.50	0.50	0.50	0.50	2
	Bi	0.05	0.05	0.05	0.10	0.05	0.10	0.05	0.05	0.50	0.05	0.05	0.05	0.05	0.10	0.05	0.05	0.10	0.05	1.1
	Cd	0.05	0.05	0.05	0.05	0.05	0.05	0.05	0.05	0.05	0.60	0.05	0.05	0.05	0.10	0.05	0.05	0.05	0.05	0.2
	Co	1.00	1.80	1.40	3.70	1.00	4.40	1.20	2.30	1.50	**23.80**	0.60	1.90	2.10	5.70	2.20	1.00	3.10	1.40	6
	Cr	6.84	6.84	6.84	**20.53**	6.84	**27.37**	6.84	6.84	**34.21**	6.84	6.84	6.84	6.84	**27.37**	6.84	6.84	6.84	6.84	17
	Cs	**1.60**	0.05	0.40	**2.20**	0.30	**4.10**	0.20	0.10	**5.50**	0.30	0.30	1.00	0.20	**2.10**	1.10	0.10	**2.10**	0.20	1.1
	Cu	**511.90**	**69.00**	13.50	**18.70**	**17.70**	**21.50**	**365.50**	**30.10**	**30.50**	9.40	6.20	9.90	3.20	10.60	12.60	10.20	8.60	**20.40**	16
	Ga	1.90	0.25	2.00	4.20	1.80	**6.40**	0.25	1.90	**9.90**	3.00	0.25	1.20	1.90	6.00	4.00	2.10	**7.60**	1.10	6
	Hf	0.20	0.05	0.30	0.30	0.05	0.70	0.05	0.05	0.80	0.05	0.10	0.20	0.20	0.40	0.10	0.05	0.50	0.05	1.2
	Hg	**0.44**	0.04	0.10	**0.18**	0.02	0.03	0.04	**0.55**	**0.78**	0.05	0.04	0.05	0.02	0.08	0.08	**0.19**	0.03	0.08	0.1
	Mo	0.80	0.20	1.00	1.70	0.60	0.70	0.80	0.50	**14.30**	1.00	0.70	1.30	0.50	1.10	1.40	1.40	0.70	0.50	2.1
	Nb	0.80	0.05	0.50	2.20	0.90	3.10	0.05	0.90	3.60	0.05	0.05	0.80	0.80	2.20	1.20	0.30	2.20	1.00	4
	Ni	8.30	3.30	3.60	9.50	1.70	10.60	2.70	8.30	7.80	7.30	1.50	6.30	2.90	10.40	5.10	3.90	1.60	1.00	17
	Pb	**31.20**	8.90	9.00	**23.60**	3.20	**31.90**	**21.20**	**45.00**	**91.20**	7.70	2.20	8.80	0.70	**22.20**	**14.10**	3.60	**11.90**	2.90	9
	Rb	14.10	1.20	4.60	**18.40**	2.30	**41.60**	2.30	2.30	**49.20**	2.10	3.10	11.40	2.20	**26.10**	11.90	2.80	**20.80**	1.90	18
	Sb	0.60	0.70	0.70	**1.20**	0.05	0.10	0.20	0.60	**11.50**	0.20	0.70	0.20	0.10	0.50	0.30	0.80	0.05	0.05	1
	Sc	2.00	2.00	1.00	3.00	0.50	**6.00**	2.00	1.00	**9.00**	3.00	0.50	3.00	0.50	3.00	2.00	2.00	**6.00**	0.50	3.7
	Se	1.10	0.25	0.60	0.90	0.25	0.25	0.25	1.50	**2.50**	0.25	0.25	0.25	0.25	0.80	0.25	1.00	0.25	0.25	1.6
	Sn	0.50	0.50	0.50	2.00	1.00	0.50	0.50	1.00	0.50	0.50	0.50	0.50	3.00	0.50	2.00	0.50	0.50	1.00	1.4
	Sr	42.20	19.70	48.10	31.30	36.00	76.80	30.80	36.80	54.30	22.00	26.20	29.70	17.80	97.10	35.90	31.60	**128.40**	**110.50**	100
	Ta	0.05	0.05	0.05	0.10	0.05	0.20	0.05	0.10	0.20	0.05	0.05	0.05	0.05	0.30	0.10	0.10	0.20	0.20	0.3
	Th	1.60	0.20	0.60	1.90	0.20	**3.80**	0.40	0.40	**6.30**	0.40	0.40	1.20	0.40	**3.70**	1.40	0.60	2.40	0.20	3.2
	Tl	0.05	0.05	0.05	0.05	0.05	0.05	0.05	0.05	0.05	0.05	0.05	0.05	0.05	0.05	0.05	0.05	0.05	0.05	0.6
	U	0.50	0.10	0.10	0.60	0.05	1.00	0.10	0.10	**5.90**	0.40	0.40	0.30	0.05	0.90	0.70	0.40	0.90	0.05	1.9
	V	23.00	4.00	4.00	19.00	4.00	**50.00**	4.00	4.00	**94.00**	11.00	16.00	17.00	4.00	**39.00**	19.00	4.00	**37.00**	4.00	28
	W	0.25	0.25	0.25	0.90	0.50	0.25	0.25	0.25	**1.80**	0.50	0.25	0.25	0.25	0.70	0.60	0.25	0.80	0.70	1
	Y	3.50	**8.40**	3.60	4.00	2.20	**9.40**	5.30	4.30	**12.00**	**10.00**	1.10	5.00	1.70	5.70	3.20	3.70	**10.10**	0.60	8.2
	Zn	**275.00**	**103.00**	**31.00**	21.00	20.00	**44.00**	**316.00**	**87.00**	22.00	**141.00**	7.00	**45.00**	26.00	**75.00**	**75.00**	12.00	25.00	21.00	28
	Zr	8.50	3.20	7.10	10.70	1.90	24.40	3.20	2.00	29.00	2.50	2.70	6.20	4.10	17.70	8.10	4.40	16.30	3.20	36
	La	5.30	1.00	3.10	5.50	1.30	**14.40**	2.00	1.20	**17.20**	2.30	2.00	4.40	1.40	9.20	4.90	2.10	10.80	1.20	11
	Ce	10.10	2.70	5.30	9.60	2.30	**27.10**	3.70	2.30	**29.70**	4.30	3.20	7.80	2.10	17.50	9.20	4.70	21.10	1.40	23
	Pr	1.11	0.44	0.66	1.15	0.29	3.23	0.49	0.35	**3.52**	0.73	0.35	1.00	0.26	2.09	1.05	0.50	2.43	0.19	3.4
	Nd	4.20	2.70	2.90	3.80	1.00	11.90	2.20	1.80	**13.90**	4.10	1.10	4.30	1.10	7.50	4.00	2.20	9.10	0.70	12
	Sm	0.91	1.52	0.68	0.68	0.46	**2.34**	0.57	0.68	**2.87**	1.32	0.23	1.18	0.32	1.62	0.75	0.53	1.68	0.20	2.2
	Eu	0.21	**0.48**	0.18	0.20	0.12	**0.56**	0.19	0.16	**0.69**	**0.41**	0.06	0.25	0.08	0.35	0.18	0.13	**0.44**	0.03	0.4
	Gd	0.83	2.42	0.75	0.88	0.52	2.17	1.03	0.94	**2.80**	2.10	0.24	1.26	0.53	1.37	0.83	0.65	2.01	0.20	2.7
	Tb	0.08	**0.34**	0.11	0.12	0.08	**0.31**	0.14	0.14	**0.43**	**0.33**	0.03	0.20	0.08	0.19	0.12	0.11	0.29	0.02	0.3
	Dy	0.59	1.89	0.73	0.69	0.34	1.88	0.88	0.71	**2.51**	1.60	0.14	1.05	0.31	1.05	0.58	0.60	1.81	0.10	2.1
	Ho	0.12	0.30	0.13	0.13	0.09	0.32	0.16	0.15	0.56	0.30	0.04	0.18	0.08	0.20	0.10	0.10	0.35	0.03	0.6
	Er	0.37	0.62	0.30	0.40	0.14	0.93	0.41	0.36	**1.48**	0.77	0.06	0.49	0.18	0.57	0.28	0.35	**1.01**	0.08	1
	Tm	0.05	0.07	0.05	0.06	0.03	0.13	0.05	0.05	0.22	0.10	0.01	0.06	0.02	0.09	0.06	0.04	0.14	0.02	0.3
	Yb	0.26	0.39	0.23	0.39	0.21	0.89	0.27	0.37	**1.40**	0.53	0.08	0.42	0.18	0.65	0.33	0.27	0.89	0.06	1
	Lu	0.05	0.04	0.03	0.05	0.02	0.12	0.04	0.05	0.19	0.09	0.01	0.06	0.02	0.09	0.04	0.04	0.13	0.01	0.2
Elements																				

Values in boldface are higher than concentration for worldwide hard coals by Ketris and Yudovich (2009).

5.3. Peñarroya-Belmez-Espiel Basin

5.3.1. Petrographic characterization

The results of the detailed petrographic study of the Peñarroya-Belmez-Espiel Basin selected samples (Table 11) are presented separately, according to the rank. For the E sector of the basin, the vitrinite reflectance was always performed in the collotelinite ranging between 0.57% and 0.71%. According to this parameter the samples are classified (ISO 11760, 2005) as medium rank D to C (bituminous D to C) coals. Figures 20 and 21 shows some petrographic aspects of the coal samples from the E and W sector of the basin, respectively. The maceral composition (Table 11) revealed that vitrinite is the main component of the organic fraction of the samples, presenting very high values (80% to 97%, mmf). Regarding this maceral group a subgroup analysis was performed, being telovitrinite the dominant subgroup (50% to 63%, mmf) followed by the detrovitrinite subgroup, whose values vary between 22% and 38%, mmf, while the occurrence of gelovitrinite has very low percentages (< 2%, mmf).

The inertinite maceral group (1% to 13%, mmf) occurs as fusinite (1% to 6%, mmf) as major maceral, followed by inertodetrinite (< 3.2%, mmf), semifusinite (0.3% to 2%, mmf), funginite (< 0.3%, mmf) and secretinite (< 0.2%, mmf). The liptinite maceral group has a lower representation, ranging between 0% and 12% mmf, with sporinite (< 12%, mmf) as the main maceral and traces of resinite (< 0.5%, mmf) and liptodetrinite (< 0.5%, mmf).

In the W sector of the basin vitrinite random reflectance, performed on collotelinite, varies between 2.34% and 3.16%, being these coals classified (ISO 11760, 2005) as high rank C to B (anthracite C to B). Vitrinite is the major organic component for these samples (84% to 98%, mmf), comprising telovitrinite (58% to 73%, mmf) and detrovitrinite (13% to 52%, mmf) subgroups. These coals also have inertinite content from 2% to 16%, mmf, having fusinite as the main maceral (1% to 9%, mmf) followed by semifusinite (1% to 7%, mmf) and traces of inertodetrinite (< 1%, mmf), micrinite (< 1%, mmf), macrinite (< 0.3%, mmf) and funginite (< 0.3%, mmf).

The relations between the vitrinite maceral subgroups of the samples from both sectors of the basin are presented in the triangular diagram (Figure 22), where it can be observed the variations described above. It is also presented the triangular diagram for the three maceral groups (Figure 23), where a slight difference between the bituminous and anthracites coals can be recognizable, but overall the petrographic composition is homogeneous in all the samples.

Table 11 - Petrographic composition (maceral analysis) and random reflectance (Rr %) of the studied coals from PBEB.

							Macerals (vol.%, mmf)															
	Unit	Seam	Mines	Samples	Rr (%)	Mineral matter (vol. %)	Telo-vitrinite	Detro-vitrinite	Gelo-vitrinite	Total vitrinite	Fusinite	Semifu-sinite	Fungini-te	Secreti-nite	Macrini-te	Micrini-te	Inerto-detrinite	Total inertinite	Sporinite	Cutinite	Resini-te	Liptode-trinite	Total liptinite
Peñarroya-Belmez-Espiel Basin	Aurora Unit	Candelaria	P250	2230	0.75	14.2	51	35	<1	86	5	1	0	0	0	0	3	9	4	0	<1	<1	5
			SEP-4bis	2085	0.66	16.7	56	32	0	88	6	<1	<1	0	0	0	1	8	4	0	<1	0	4
			P325	2229	0.71	8.0	58	22	<1	80	8	2	0	0	0	0	3	13	7	0	<1	0	7
	Cabeza de Vaca Unit	C4	SB18	1377/1379	0.63	17.2	63	22	2	87	2	2	0	0	0	0	2	5	8	0	0	0	8
			SB28	1501/1502	0.57	37.6	54	38	1	93	1	<1	0	0	0	0	1	2	5	0	0	0	5
		C3bis	SB6	1358	0.69	32.6	60	36	0	97	1	1	0	0	0	0	0	1	1	0	<1	0	2
			SB25	1476	0.7	8.8	59	28	1	88	6	1	0	0	0	0	1	8	4	0	<1	0	5
		C1	SB26	1509	0.66	3.0	50	29	0	79	5	2	0	<1	0	0	2	9	12	0	0	0	12
			SB13	1511/1513	0.67	24.0	52	38	0	90	4	1	0	0	0	0	<1	6	4	0	0	0	4
	S. Rafael Unit (Minas Maria e Cervantes)	S. Rafael	SM-18	214/275	3.16	6.6	67	30	0	97	2	1	0	0	0	0	0	3	0	0	0	0	0
			SM-2	48/63	2.61	6.0	64	31	0	95	2	2	0	0	0	0	1	5	0	0	0	0	0
		Techo	SM-27	712/715	3.12	21.4	73	22	0	95	1	3	<1	0	<1	0	1	5	0	0	0	0	0
		Suelos	SM-27	705/708	3.01	23.4	58	34	0	92	4	3	0	0	0	<1	1	8	0	0	0	0	0
	S. Rafael Unit (Mina Rampa 3W)	Muro	SRE-1	746/751	2.46	18.6	66	30	0	96	1	3	0	0	0	0	0	4	0	0	0	0	0
			P160	894/896	2.44	12.4	69	29	0	98	1	1	0	0	0	0	0	2	0	0	0	0	0
		I. Norte	SER-1	752/754	2.42	27.8	63	32	0	94	3	2	0	0	0	0	<1	6	0	0	0	0	0
			P160	891/893	2.45	1.8	34	52	0	86	9	5	<1	0	0	0	<1	14	0	0	0	0	0
		I. Sur	SRI-4	1078	2.49	19.6	71	13	0	84	7	7	0	0	0	1	<1	16	0	0	0	0	0
			SRI-14	1102	2.34	40.1	68	27	0	96	2	2	0	0	0	0	<1	4	0	0	0	0	0

Rr: vitrinite random reflectance.

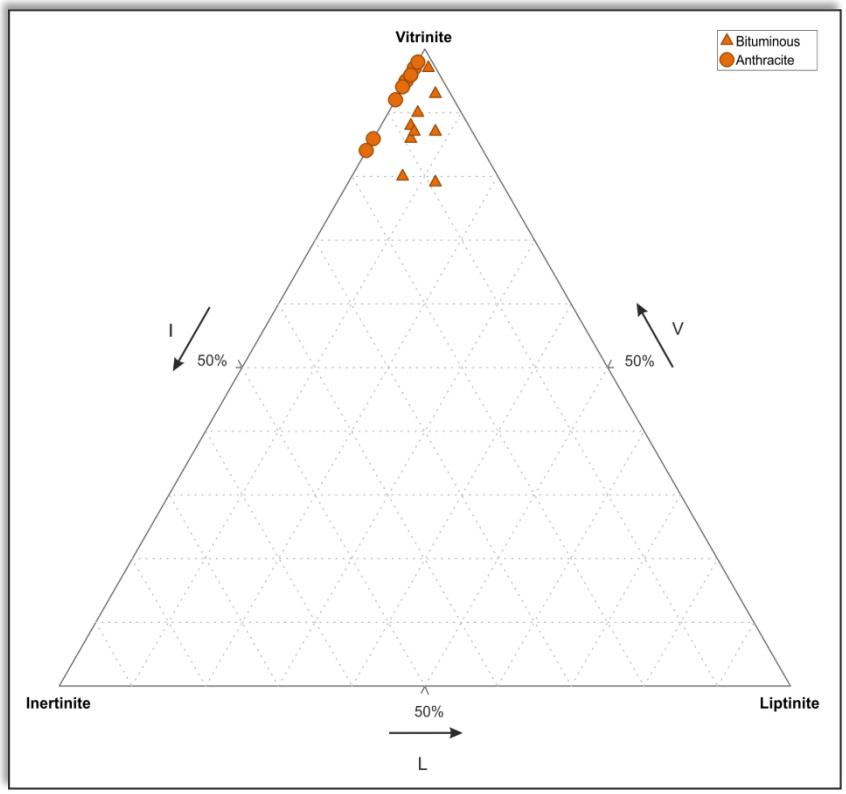

Figure 22 - Petrographic composition diagram for the three maceral groups based on maceral analysis for studied coals from PBEB.

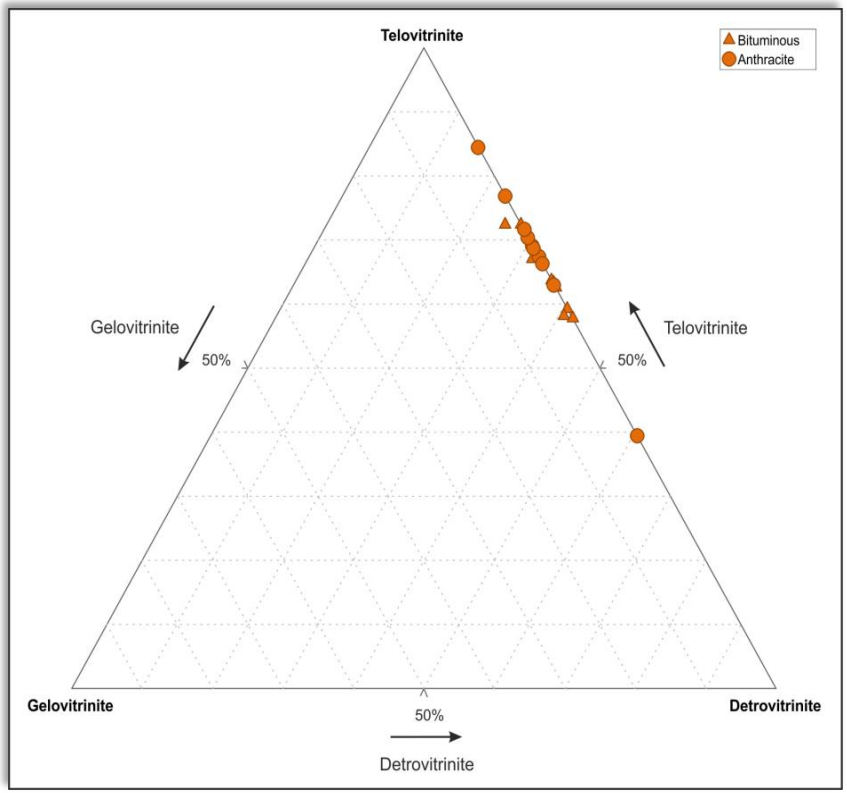

Figure 23 - Petrographic composition diagram for the three vitrinite maceral subgroups based on maceral analysis for studied coals from PBEB.

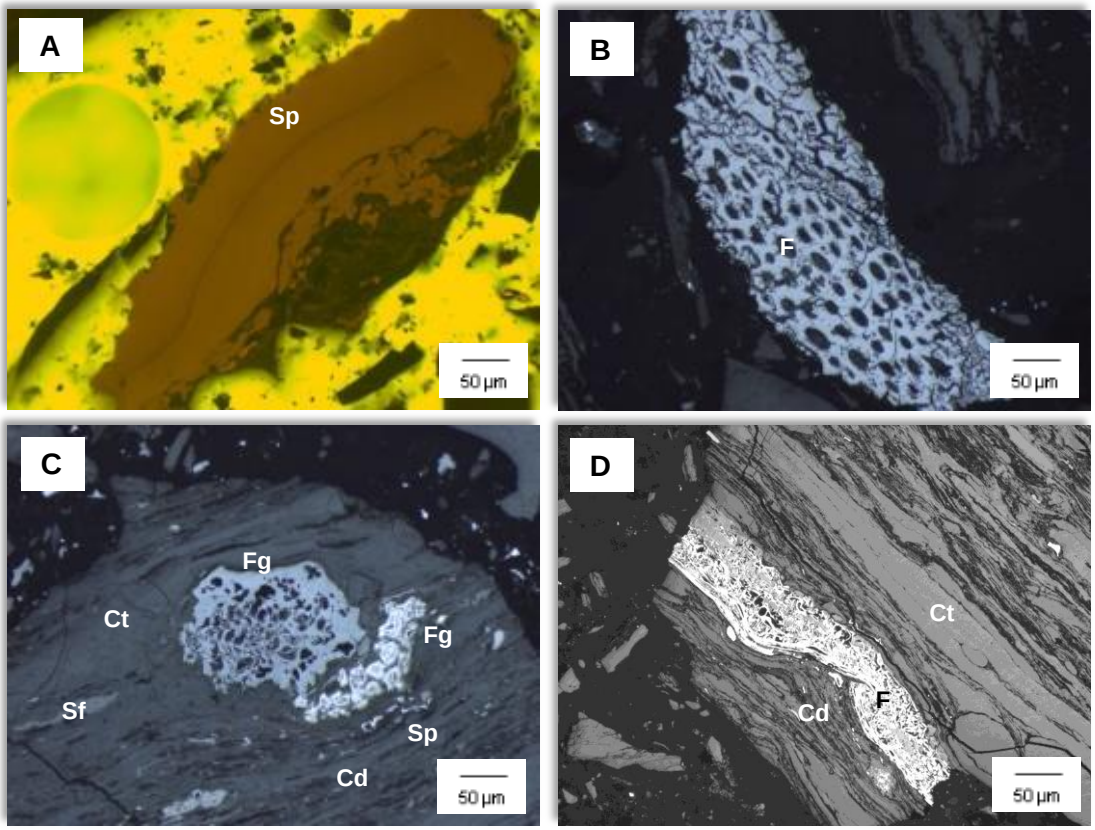

Figure 20 - Photomicrographs of the studied coal samples from the E sector of PBEB (all imagens were taken in reflected white light, except image A that was taken with fluorescence light). A) sporinite (Sp) in sample (2230); B) fusinite (F) (sample 2085); C) semifusinite (Sf), funginite (Fg), sporinite (Sp), collodetrinite (Cd) and collotellinite (Ct) (sample 2229); D) fusinite (F), collotelinite (Ct) and collodetrinite (Cd) (sample 1358).

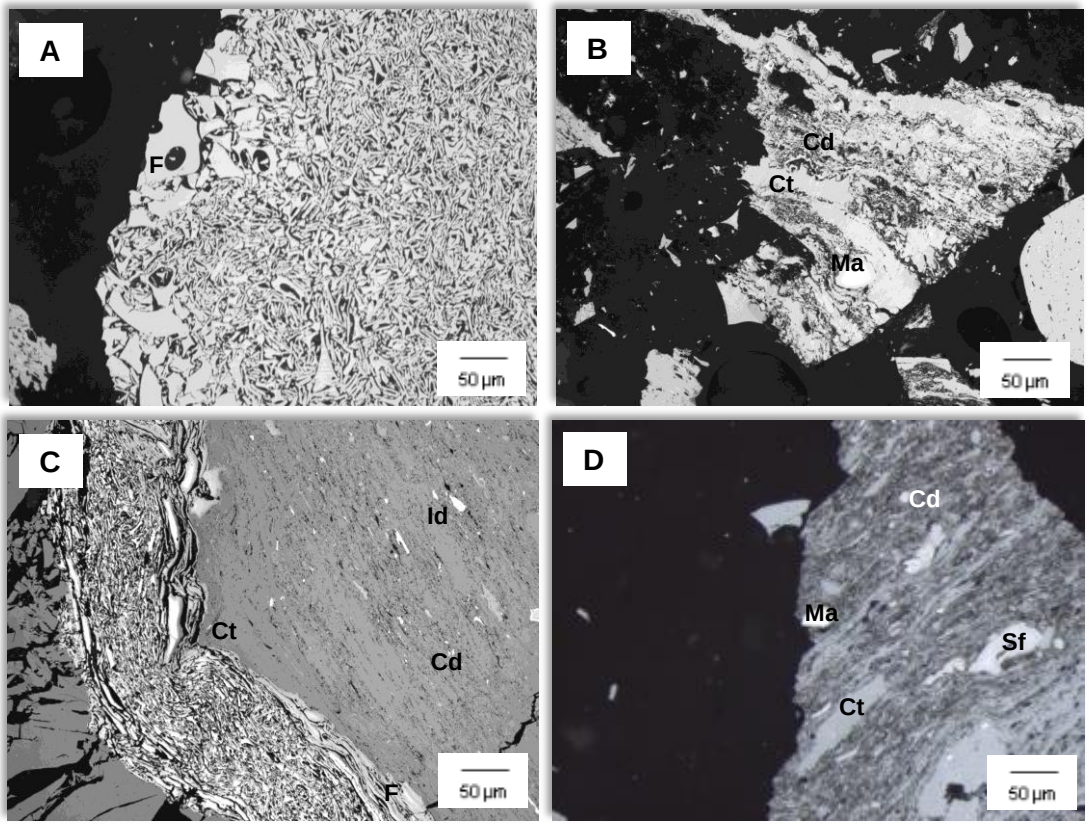

Figure 21 - Photomicrographs of the studied coal samples from the W sector of PBEB (all imagens were taken in reflected white light). A) fusinite (F) (sample 43/68); B) collotelinite (Ct), collodetrinite (Cd) and macrinite (Ma) (sample 712/715); C) fusinite (F), inertodetrinite (Id), collodetrinite (Cd) and collotellinite (Ct) (sample 891/893); D) macrinite (Ma), semifusinite (Sf), collotelinite (Ct) and collodetrinite (Cd) (sample 1102).

The inorganic fraction varies greatly, the percentages range from 3% to 37.6% in the E sector of the basin. On the other hand, the coals from the W sector the mineral matter content range from 1.8% to 40.1%. This mineral matter (Figure 24) consists mainly of clay minerals, carbonates (calcite, siderite and ankerite) and also sulphides, particularly pyrite. The ankerite is often associated with oligonite (a manganiferous variety of siderite) and kutnohorite (a calcium manganese carbonate mineral). Pyrite has syngenetic origin, with framboidal aspect, and also epigenetic origin, although this is rare, mainly filling fractures. The samples also have other petrographic aspects, including oxidation and fracturing signs as well as thermal and folding effects.

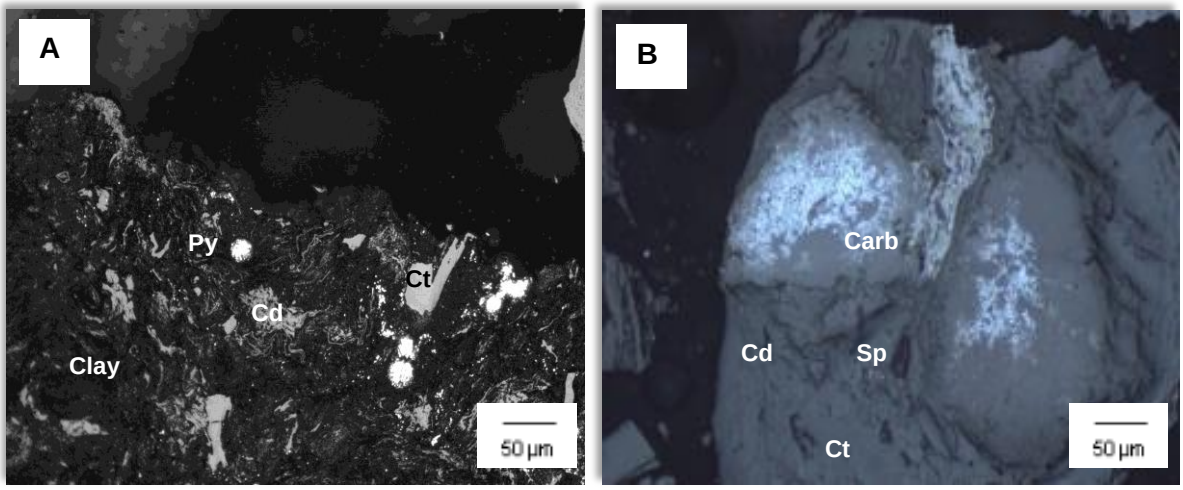

Figure 24 - Photomicrographs of the studied coal samples from PBEB (imagens were taken in reflected white light). A) collotelinite (Ct) and collodetrinite (Cd) associated with framboidal pyrite (Py) and clay minerals (Clay) (sample 746/751); B) collotelinite (Ct) and collodetrinite (Cd) associated with carbonates (Carb), namely ankerite associated with kutnohorite (sample 1051/1502).

5.3.2. Proximate and ultimate analysis

The results determined in the proximate and ultimate analysis related to the Peñarroya-Belmez-Espiel Basin coals samples are also presented in accordance with their rank (Table 12). Concerning the coals of the E sector the results obtained by the proximate analysis reveal an ash content varying between values considered low to values exceeding those established as very high (8.99% to 57.43%, db). Thus, the sample with the highest ash content (57.43%) should be considered as a carbonaceous rock. The VM content is according with the rank (35.14% to 46.39%, daf).

Regarding the ultimate analysis data show a C (67.14% to 80.68%, daf), H (4.74% to 5.82%, daf), N (1.46% to 2.24%, daf) and O (12.14% to 21.49%, daf) contents re in accordance with the rank of the studied samples. The total S contents are low (0.32% to 1.71%, db).

Table 12 - Chemical analysis and H/C – O/C atomic ratios of the studied coals from PBEB.

	Unit	Seam	Mine	Sample	M	Ash	MV		C		H		N		St	O		H/C	O/C
					(%, ad)	(%, db)	(%, db)	(%, daf)	(%, db)	(%, daf)	(%, db)	(%, daf)	(%, db)	(%, daf)	(%, db)	(%, db)	(%, daf)		
Peñarroya-Belmez-Espiel Basin	Aurora Unit	Candelaria	P250	2230	3.19	21.94	27.43	35.14	62.94	80.63	4.03	5.16	1.14	1.46	0.41	9.54	12.22	0.76	0.11
			SEP-4bis	2085	3.16	28.60	25.42	35.60	57.33	80.29	3.64	5.10	1.07	1.50	0.55	8.81	12.34	0.76	0.12
			P325	2229	2.97	19.34	28.98	35.93	65.08	80.68	4.17	5.17	1.21	1.50	0.41	9.79	12.14	0.76	0.11
	Cabeza de Vaca Unit	C4	SB18	1377/1379	3.53	23.24	29.71	38.71	60.76	79.16	4.12	5.37	1.27	1.65	0.47	10.14	13.21	0.81	0.13
			SB28	1501/1502	3.55	48.14	22.68	43.73	37.90	73.08	3.02	5.82	1.16	2.24	0.40	9.38	18.09	0.95	0.19
		C3bis	SB6	1358	3.21	12.62	36.86	42.18	68.90	78.85	4.42	5.06	1.61	1.84	0.32	12.13	13.88	0.76	0.13
			SB25	1476	6.26	16.53	29.45	35.28	64.56	77.35	3.96	4.74	1.75	2.10	0.47	12.73	15.25	0.73	0.15
		C1	SB26	1509	3.56	8.99	35.54	39.05	73.51	80.77	4.89	5.37	1.37	1.51	0.41	10.83	11.90	0.79	0.11
			SB13	1511/1513	3.91	57.43	19.75	46.39	28.58	67.14	2.38	5.59	0.75	1.76	1.71	9.15	21.49	0.99	0.24
	S. Rafael Unit (Minas Maria e Cervantes)	S. Rafael	SM-18	214/275	5.30	21.76	7.70	9.84	71.16	90.95	2.24	2.86	1.30	1.66	0.80	2.74	3.50	0.38	0.03
			SM-2	48/63	4.24	17.01	7.33	8.83	75.40	90.85	2.57	3.10	1.37	1.65	0.82	2.83	3.41	0.41	0.03
		Techo	SM-27	712/715	4.10	40.35	6.38	10.70	51.78	86.81	1.88	3.15	0.87	1.46	0.75	4.37	7.33	0.43	0.06
		Suelos	SM-27	705/708	3.86	39.18	6.20	10.19	53.41	87.82	1.98	3.26	0.76	1.25	0.71	3.96	6.51	0.44	0.06
	S. Rafael Unit (Mina Rampa 3W)	Muro	SRE-1	746/751	2.94	37.86	10.50	16.90	53.78	86.55	2.21	3.56	0.98	1.58	0.94	4.23	6.81	0.49	0.06
			P160	894/896	3.01	37.66	10.76	17.26	50.65	81.25	2.18	3.50	1.05	1.68	1.11	7.35	11.79	0.51	0.11
		I. Norte	SER-1	752/754	2.50	38.89	9.82	16.07	51.62	84.47	2.20	3.60	0.85	1.39	0.70	5.74	9.39	0.51	0.08
			P160	891/893	2.58	25.22	10.10	13.51	67.22	89.89	2.50	3.34	0.99	1.32	0.61	3.46	4.63	0.44	0.04
		I. Sur	SRI-4	1078	2.96	20.32	15.50	19.45	68.00	85.34	2.43	3.05	0.90	1.13	1.62	6.73	8.45	0.43	0.07
			SRI-14	1102	2.54	41.93	8.56	14.74	49.46	85.17	2.20	3.79	0.98	1.69	0.66	4.77	8.21	0.53	0.07

M = moisture; VM = volatile matter; St = total sulphur ; ad = as determined; db = dry basis; daf = dry ash-free basis.

For the coals of the W sector of the basin presented an ash content ranging from 17.01% to 41.93%, db, values considered as moderate to high, which is in accordance with the variations of the mineral matter content of the maceral analysis. The VM vary widely (8.83% to 19.45%, daf), the anomalous values for the samples 894/896, 752/754 and 1708 can be explained for the presence of carbonate minerals.

The ultimate analysis data show a high C content (81.25% to 90.95%, daf). The H (2.86% to 3.79%, daf), N (1.13% to 1.68%, daf) and O (3.41% to 11.79%, daf) are all in accordance with the rank of these samples. Regarding the total S content (0.71% to 1.62%, db), they are considered low.

The H/C and O/C atomic ratios projected on the Van Krevelen diagram (Figure 25) indicate that samples are a kerogen type III (terrestrial origin) and for some of the samples the rank does not match with the petrographic data. The samples belonging to the western basinal sector (samples 894/896, 752/754, 1102, 746/751, 712/715, 705/708 and 1780) do not follow the rank indicated by the vitrinite reflectance (anthracite C to B), which can be explained by their high ash yield that lowers the C content and consequently increases the O/C atomic ratio. Only samples 214/275, 891/893 and 48/63 are in accordance with the rank inferred by the vitrinite reflectance, these are the samples that present the lowest ash yield of the entire sector. In the first case, the most reliable rank parameter is the petrographic data (Rr %) as it is determined in a specific maceral (collotelinite).

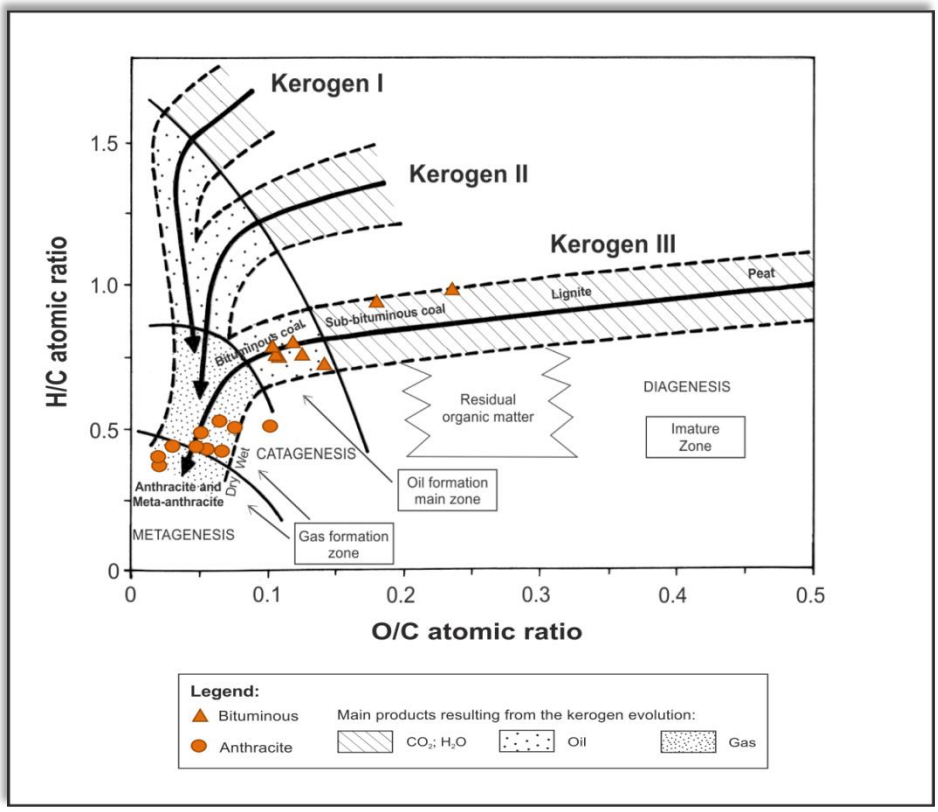

Figure 25 - Projection of the H/C – O/C atomic ratios of the studied coals from PBEB in the Van Krevelen diagram.

5.3.3. Major and trace elements

The Peñarroya-Belmez-Espiel Basin reveals an enrichments of a large set of elements when compared to the average values in the world hard coals (Ketris and Yudovich, 2009), for both bituminous and anthracite coals (Table 13). In a set of 19 samples there are ten that show a strong enrichment, namely 2085, 1377/1379, 1501/1502, 1511/1513, 712/715, 705/708, 746/751, 894/896, 752/754 and 1102. Regarding to the samples 2230, 2229, 1476, 1511/1513, 48/63, 891/893 and 1078, despite possessing a lower set of elements enriched when compared with the previous samples, they still have few elements enriched. The only samples that did not follow the enrichment trend in the basin are samples 1358 and 1509, when compared to the other sampled coals.

As regards to the major elements, a high Ca content is observed in samples 1358, 214/275, 746/751, 894/896 and 1078. Three of such samples, in particular samples 1358, 746/751 and 1078, present a high content of Mg. Fe also presents high values, namely for samples 1501/1502, 1358, 1511/1513, 214/275, 712/715, 746/751, 894/896, 752/754, 891/893 and 1078. The same applies to K for samples 2085, 1501/1502, 1511/1513, 712/715, 705/708, 894/896 and 1102.

Concerning the trace elements a high enrichment content in comparison to the average values in the world hard coals is observed, particularly in As, Ba, Be Cd, Co, Cr, Cs, Cu, Ga, Hf, Hg, Mo, Nb, Ni, Pb , Rb, Sb, Sc, Sn, Sr, Ta, Th, U, V, W, Y, Zn, Zr, La, Ce, Pr, Nd, Sm, Eu, Gd, Th, Dy, Ho, Er, Tm , Yb and Lu. Among those elements the Pb, Rb, Sc, Sr, V, Y, Zn, Zr and all the REEs (excluding Dy, Ho and Tm) are highlighted, because they exhibit contents higher than the Clarke values (Ketris and Yudovich, 2009) in almost all the samples. The Sb is particularly depleted in all bituminous coals however some anthracite samples present an higher content in this element.

It should be noted that in some samples exhibit much higher values compared to the average values in the world hard coals. This occurs with the As in sample 1078 and Cs in samples 2085, 712/715, 705/708, 746/751, 894/896, 752/754 and 1102. Regarding the Rb, it also present high contents in some samples, namely 1501/1502 and 705/708, as well as V in samples 1501/1502 and 1511/1513. Sc reveals a great abundance in almost all the samples and Zn also expresses great enrichment in a significant number of samples, including 1377/1379, 48/63, 746/751 and 1078. Finally, it can also be observed a high Pb content in the samples 1377/1379, 746/751 and 1708.

Table 13 - Ash yield, total Sulphur (%, d) and elemental concentrations in the studied coals from PBEB (trace elements in µg/g; major elements in %).

Peñarroya-Belmez-Espiel Basin																			
Unit	Aurora Unit			Cabeza de Vaca Unit						S. Rafael Unit (Minas Maria e Cervantes)				S. Rafael Unit (Mina Rampa 3W)						Hard Coals
Seam	Candelaria			C4		C3bis		C1		S. Rafael		Techo	Suelos	Muro		I. Norte		I. Sur		
Mine	P250	SEP-4bis	P325	SB18	SB28	SB6	SB25	SB26	SB13	SM-18	SM-2	SM-27	SM-27	SRE-1	P160	SER-1	P160	SRI-4	SRI-14	
Sample	2230	2085	2229	1377/1379	1501/1502	1358	1476	1509	1511/1513	214/275	48/63	712/715	705/708	746/751	894/896	752/754	891/893	1078	1102	
Ash	21.94	28.60	19.34	23.24	48.14	12.62	16.53	8.99	57.43	21.76	17.01	40.35	39.18	37.86	37.66	38.89	25.22	20.32	41.93	
Al	3.87	4.72	3.21	3.90	7.38	0.95	2.58	1.63	7.59	2.87	2.71	6.86	7.44	5.20	6.06	6.21	3.27	1.09	7.48	
Si	5.28	6.75	4.24	5.62	11.82	1.10	3.50	1.60	14.27	3.20	3.10	9.16	8.86	6.77	7.51	8.38	4.34	1.42	9.99	
Ca	0.09	0.24	0.53	0.10	0.14	2.77	0.28	0.29	0.56	2.21	0.86	0.06	0.26	2.03	2.39	1.47	1.70	3.96	0.99	
Mg	0.14	0.24	0.29	0.21	0.50	1.00	0.22	0.12	0.52	0.47	0.25	0.45	0.35	0.74	0.60	0.65	0.66	1.33	0.46	
Fe	0.33	0.72	0.66	0.89	1.92	1.17	0.53	0.20	4.13	1.05	0.66	2.08	0.78	1.80	1.50	1.31	2.22	3.52	1.08	
K	0.78	1.12	0.65	0.81	1.69	0.10	0.52	0.22	1.67	0.44	0.53	1.62	1.93	0.98	1.08	0.99	0.47	0.16	1.49	
Mn	0.00	0.00	0.00	0.01	0.03	0.03	0.00	0.00	0.05	0.02	0.01	0.02	0.01	0.02	0.02	0.02	0.02	0.04	0.00	
Na	0.05	0.08	0.07	0.08	0.16	0.01	0.08	0.01	0.16	0.07	0.07	0.22	0.25	0.13	0.13	0.15	0.08	0.03	0.18	
P	0.03	0.02	0.01	0.03	0.04	0.00	0.13	0.10	0.07	**0.53**	0.22	0.01	0.03	0.15	0.24	0.05	0.26	0.00	0.09	0.3
St	0.41	0.55	0.41	0.47	0.40	0.32	0.47	0.41	1.71	0.80	0.82	0.75	0.71	0.94	1.11	0.70	0.61	1.62	0.66	
Ti	0.12	0.16	0.10	0.13	0.31	0.02	0.08	0.06	0.36	0.07	0.07	0.17	0.23	0.14	0.16	0.21	0.10	0.02	0.28	0.9
Ag	0.05	0.05	0.05	0.05	0.05	0.05	0.05	0.05	0.05	0.05	0.05	0.05	0.10	0.05	0.05	0.05	0.05	0.30	0.05	0.1
As	0.25	6.60	0.25	**12.00**	1.00	0.25	8.00	0.90	4.50	7.60	3.80	**11.20**	**13.20**	**12.00**	**11.30**	**11.40**	3.50	**140.60**	**12.90**	9
Au	0.25	0.25	0.25	0.25	1.10	0.25	0.80	0.25	1.30	0.25	0.90	1.70	1.30	0.25	0.25	0.25	0.25	0.25	0.25	
Ba	**172.00**	**198.00**	106.00	**237.00**	**443.00**	34.00	**341.00**	**412.00**	**503.00**	**155.00**	140.00	**352.00**	**432.00**	**237.00**	**230.00**	**255.00**	142.00	75.00	**345.00**	150
Be	0.50	**3.00**	0.50	0.50	**3.00**	0.50	2.00	1.00	2.00	2.00	0.50	**6.00**	**3.00**	0.50	1.00	2.00	**3.00**	2.00	**5.00**	2
Bi	0.20	0.30	0.30	0.20	0.50	0.05	0.20	0.20	0.30	0.90	0.05	0.20	0.40	0.20	0.10	0.30	0.10	0.05	0.20	1.1
Cd	0.05	0.10	0.05	**0.90**	**0.30**	0.10	0.05	0.05	0.05	0.20	**0.60**	0.05	0.05	**0.90**	**0.30**	**0.30**	0.05	**1.20**	0.05	0.2
Co	**6.90**	**11.80**	**8.40**	**17.50**	**28.70**	**9.10**	4.00	3.60	**14.50**	**6.60**	4.10	**14.70**	**13.50**	**17.50**	**16.90**	**17.50**	**9.80**	**44.90**	**13.40**	6
Cr	**61.58**	**61.58**	**54.74**	**54.74**	**102.63**	13.68	**41.05**	6.84	**82.10**	**41.05**	**27.37**	**68.42**	**61.58**	**61.58**	**61.58**	**61.58**	**27.37**	13.68	**82.10**	17
Cs	**8.20**	**9.30**	**6.00**	**7.60**	**9.10**	0.05	**3.40**	1.00	**7.10**	**2.80**	**5.40**	**17.70**	**23.60**	**7.60**	**8.50**	**9.90**	**3.30**	0.90	**10.60**	1.1
Cu	**22.50**	**35.50**	**21.20**	**67.90**	**31.50**	11.90	**17.90**	**18.10**	**39.40**	**47.40**	**18.60**	14.80	**29.80**	**67.90**	**39.30**	**38.60**	**17.80**	**40.50**	**38.00**	16
Ga	**9.90**	**11.90**	**8.00**	**11.80**	**17.80**	1.60	**7.10**	4.40	**17.70**	6.00	**6.60**	**15.50**	**17.40**	**11.80**	**13.50**	**13.80**	**6.90**	2.10	**17.20**	6
Hf	1.20	**1.50**	0.90	**1.30**	**2.40**	0.40	0.80	0.50	**3.20**	0.60	0.70	**1.70**	**2.10**	**1.30**	**1.30**	**1.80**	0.80	0.20	**2.10**	1.2
Hg	0.08	**0.33**	0.08	**0.25**	**0.25**	**0.23**	**0.11**	0.09	**0.18**	0.05	0.07	0.05	0.07	**0.25**	**0.17**	**0.18**	0.09	**0.37**	**0.13**	0.1
Mo	0.90	2.00	1.70	1.90	1.30	0.50	0.60	0.40	1.50	0.40	0.70	1.00	1.50	1.90	1.70	2.10	0.90	**5.60**	1.40	2.1
Nb	3.40	3.90	2.70	3.70	**8.40**	0.20	2.80	1.60	**9.90**	1.70	1.80	**5.80**	**6.60**	3.70	3.90	**6.40**	2.50	0.90	**6.70**	4
Ni	11.20	**17.10**	9.20	**21.20**	**32.30**	6.80	8.50	5.00	**34.50**	4.60	3.90	**20.70**	10.30	**21.20**	13.10	13.90	8.20	**22.40**	12.80	17
Pb	7.50	**15.50**	**13.50**	**69.50**	**13.80**	4.10	**11.10**	**9.10**	**19.60**	**23.30**	**27.60**	**9.80**	**36.70**	**69.50**	**65.30**	**28.60**	**23.10**	**110.30**	**21.60**	9
Rb	**50.20**	**72.50**	**41.90**	**58.40**	**110.60**	4.70	**41.20**	13.00	**98.80**	**26.60**	**30.60**	**95.50**	**107.70**	**58.40**	**65.00**	**57.60**	**26.60**	8.90	**89.10**	18
Sb	0.30	0.50	0.20	0.30	0.40	0.60	0.20	0.05	0.20	1.00	**9.60**	**2.60**	0.50	0.30	0.40	0.20	0.10	**1.40**	0.10	1
Sc	**6.00**	**9.00**	**7.00**	**10.00**	**13.00**	3.00	**5.00**	3.00	**14.00**	**4.00**	**4.00**	**10.00**	**12.00**	**10.00**	**9.00**	**10.00**	**7.00**	**12.00**	**13.00**	3.7
Se	0.60	0.70	1.50	1.40	0.25	0.25	0.25	0.25	0.50	0.60	0.25	0.25	0.25	1.40	0.70	0.70	0.80	1.40	0.70	1.6
Sn	**2.00**	**2.00**	**2.00**	**2.00**	**4.00**	0.50	1.00	1.00	**4.00**	**2.00**	**2.00**	**3.00**	**3.00**	**2.00**	**2.00**	**4.00**	**2.00**	0.50	**3.00**	1.4
Sr	**125.80**	**106.20**	44.60	77.40	**133.90**	17.50	**222.60**	**594.10**	**193.70**	**188.30**	65.30	58.10	76.20	77.40	98.00	66.60	74.70	30.00	99.60	100
Ta	0.20	0.20	0.20	0.30	**0.40**	0.05	0.10	0.20	**0.70**	**0.40**	0.20	0.20	0.30	0.30	0.30	**0.40**	0.10	0.05	0.20	0.3
Th	**6.90**	**8.30**	**5.70**	**7.40**	**12.60**	1.40	**4.60**	**4.20**	**13.20**	**4.90**	**7.00**	**16.80**	**17.40**	**7.40**	**8.60**	**8.20**	**4.70**	1.10	**12.50**	3.2
Tl	0.05	0.05	0.05	0.05	0.05	0.05	0.05	0.05	0.05	0.05	0.05	0.05	0.05	0.05	0.05	0.05	0.05	0.05	0.05	0.6
U	1.20	1.70	1.10	1.10	**2.70**	0.30	0.80	0.80	**2.60**	1.00	1.00	**2.50**	**3.30**	1.10	1.10	**2.00**	0.90	0.10	1.70	1.9
V	**63.00**	**81.00**	**56.00**	**75.00**	**116.00**	23.00	**44.00**	**31.00**	**114.00**	**40.00**	**34.00**	**75.00**	**83.00**	**75.00**	**79.00**	**78.00**	**49.00**	**52.00**	**107.00**	28
W	0.60	0.60	0.25	0.60	**1.70**	0.25	0.60	0.25	**1.70**	0.80	0.60	0.80	1.00	0.60	0.60	**1.60**	0.60	0.70	0.90	1
Y	**10.10**	**12.30**	**10.20**	**16.90**	**20.70**	5.70	7.10	5.60	**21.80**	**10.40**	**8.80**	**20.40**	**19.20**	**16.90**	**14.80**	**15.10**	**14.30**	**20.70**	**18.90**	8.2
Zn	**31.00**	**36.00**	**47.00**	**210.00**	**101.00**	**65.00**	**31.00**	10.00	**65.00**	**71.00**	**250.00**	**51.00**	13.00	**210.00**	**75.00**	**114.00**	**29.00**	**408.00**	17.00	28
Zr	**41.20**	**49.60**	32.00	**40.80**	**80.30**	10.10	27.00	19.40	**120.20**	25.50	29.30	**60.30**	**77.10**	**40.80**	**43.00**	**66.40**	27.40	12.40	**67.50**	36
La	**17.80**	**21.90**	**13.70**	**22.30**	**37.20**	5.10	**12.30**	10.80	**36.80**	**12.80**	**14.80**	**33.60**	**28.20**	**22.30**	**25.40**	**23.40**	**15.90**	9.70	**34.60**	11
Ce	**37.30**	**45.80**	**30.20**	**50.10**	**77.30**	9.50	**26.40**	22.60	**79.90**	**24.40**	**30.50**	**75.20**	**59.60**	**50.10**	**54.70**	**52.90**	**36.00**	16.10	**75.30**	23
Pr	**4.09**	**4.81**	3.24	**5.48**	**8.44**	1.02	2.87	2.31	**8.40**	2.74	3.20	**7.83**	**6.25**	**5.48**	**5.69**	**5.57**	**4.16**	1.78	**8.00**	3.4
Nd	**15.00**	**18.20**	**12.30**	**22.20**	**31.10**	4.80	10.80	8.90	**31.90**	11.00	12.00	**28.20**	**23.20**	**22.20**	**21.10**	**20.70**	**17.20**	7.80	**29.20**	12
Sm	**2.91**	**3.48**	**2.61**	**4.42**	**6.22**	0.91	2.04	1.80	**5.61**	**2.43**	**2.28**	**5.62**	**4.65**	**4.42**	**4.27**	**3.81**	**4.32**	**2.58**	**5.59**	2.2
Eu	**0.61**	**0.73**	**0.53**	**1.00**	**1.31**	0.26	0.40	0.36	**1.22**	**0.60**	**0.52**	**1.02**	**0.88**	**1.00**	**0.93**	**0.81**	**1.01**	**0.65**	**1.24**	0.4
Gd	2.45	**2.98**	2.49	**4.56**	**5.44**	1.19	1.88	1.48	**5.12**	**2.85**	2.21	**4.97**	**3.84**	**4.56**	**4.44**	**3.68**	**4.70**	**4.01**	**5.02**	2.7
Tb	**0.35**	**0.42**	**0.35**	**0.69**	**0.78**	0.18	0.28	0.21	**0.75**	**0.45**	**0.32**	**0.76**	**0.63**	**0.69**	**0.65**	**0.56**	**0.70**	**0.72**	**0.79**	0.3
Dy	1.77	**2.53**	1.92	**3.54**	**4.18**	1.12	1.49	1.13	**4.06**	**2.33**	1.72	**4.10**	**3.78**	**3.54**	**3.44**	**2.98**	**3.51**	**3.77**	**4.08**	2.1
Ho	0.37	0.49	0.37	**0.67**	**0.80**	0.18	0.29	0.20	**0.84**	0.44	0.29	**0.79**	**0.79**	**0.67**	0.59	0.57	0.59	**0.64**	**0.80**	0.6
Er	**1.10**	**1.49**	**1.13**	**1.59**	**2.40**	0.53	0.76	0.66	**2.37**	0.93	0.87	**2.40**	**2.11**	**1.59**	**1.64**	**1.65**	**1.41**	**1.98**	**2.23**	1
Tm	0.17	0.23	0.16	0.23	**0.34**	0.07	0.11	0.09	**0.34**	0.12	0.12	**0.32**	0.29	0.23	0.23	0.23	0.19	0.28	**0.31**	0.3
Yb	**1.07**	**1.46**	**1.09**	**1.49**	**2.30**	0.40	0.72	0.59	**2.26**	0.79	0.78	**1.92**	**1.99**	**1.49**	**1.44**	**1.63**	**1.15**	**1.75**	**1.96**	1
Lu	0.16	**0.22**	0.16	**0.22**	**0.34**	0.05	0.11	0.10	**0.32**	0.10	0.12	**0.28**	**0.30**	**0.22**	**0.23**	**0.25**	0.16	**0.40**	**0.32**	0.2

Elements

Values in boldface are higher than concentration for worldwide hard coals by Ketris and Yudovich (2009).

Chapter 6 – Discussion of the results

6. Discussion of the results

In this chapter the results obtained for each of the coal basins are analyzed. The enrichment/depletion of the trace elements was investigated and discussed, and the concentration coefficients (CC) were calculated. The CC is the ratio of trace element concentration in coal samples studied *versus* the respective values established for the worldwide coals by Ketris and Yudovich (2009). Regarding the concentrations of trace elements in coal, Dai et al. (2015) considered six categories: unusually enriched (CC> 100), significantly enriched (10 <CC <100), enriched (5 <CC <10), slightly enriched (2 <CC <5), normal (0.5 <CC <2) and depleted (CC <0.5). The CC calculated were then projected in diagrams considering the origin at 1 so that the elements with CC above 1 (enriched) are projected on top of the graphic and the depleted elements (CC<1) in the lower part.

The geochemical affinities of the major and trace elements were also investigated. A statistical study using the correlation matrix was used to establish geochemical affinities for trace elements, meaning the association of the different elements with the organic and/or inorganic matter of coals. Pearson's correlation coefficients of element concentrations with ash yield provide preliminary information for their organic or inorganic affinities. Three groups of elements have been considered according to their correlation coefficients with ash yield: Group 1: elements with r_{ash} <−0.50 have mainly organic affinity; Group 2: elements with $-0.50<r_{ash}<+0.50$ have intermediate (organic and/or inorganic) affinity; and Group 3: elements $r_{ash}>+0.50$ have inorganic affinity (Suárez-Ruiz et al., 2006). The aluminum–silicate, sulfur and carbonate affinities were also identified.

Finally, a relationship between the enrichment and its origin was established, namely the genesis of the coal in each of the basins. A relationship between the three studied basins was also performed.

In addition, for the CAB and PBEB an analysis of the major elements content and the mineralogy of the studied samples were also included in this chapter.

6.1. Douro Carboniferous Basin

6.1.1. Concentration coefficients

Compared to the average for world hard coals (Ketris and Yudovich, 2009) the coals from the DCB can be considered as enriched in trace elements, although this enrichment is not detected in all studied coals, and were classified according to the CC (Figure 26).

Mercury exhibits an unusual enrichment (CC> 100) in sample 15. In the other samples this element, as well as Cs and Sb, has CC considered as significantly enriched (CC> 10). The trace elements considered enriched are Ni and Zn (5 <CC <10). With lower CC (2 <CC <5), and therefore only slightly enriched, are Ag, Cd, Co, Cr, Cu and Pb. Among the elements with CC values considered as average for world hard coals (0.5 <CC <2) are Ga, Mo, Rb, Sc, Se, Sn, Th, V, W and Y. A depletion (CC <0.5) is observed for the other elements, including Ti, Ba, Be, Bi, Hf, Sr, Ta, Tl and U.

Concerning the REEs (Figure 27), only the CC of Sm reveals a slightly enrichment (2 <CC <5). The remaining REEs exhibit concentration values within the average for world hard coals (0.5 <CC <2). The Ho, Tm and Lu are depleted (CC <0.5) in these coals.

In summary, in samples 15 and 274 some of the elements are enriched comparing with the Clarke values established for hard coals and, in opposition, samples 77 and 108/116 present depletion on the majority of the elements.

6.1.2. Geochemical affinities

Table 14 shows the geochemical affinities of the elements with the ash yield, obtained through the correlation coefficients of trace elements in order to gather information about the mode of occurrence of the elements. Pearson correlation coefficients of the elements relating to Al and Ca were used, with the aim of representing the carbonate and aluminum-silicate affinities. The figure 28 summarizes the results obtained using the intercorrelation analysis of major and trace elements.

In the coals from the DCB some elements have an organic (Bi) or intermediate affinity (Ca, Mn, Na, P, Ba, Cs, Hg, Rb, Sn, Sr, W, Nd and Sm). On the other hand, several present an inorganic affinity, including Al, Si, Mg, Fe, K, St, Ti, Ag, As, Au, Cd, Co, Cr, Cu, Ga, Hf, Mo, Nb, Ni, Pb, Sb, Sc, Se, Ta, Th, U, V, Y, Zn, Zr, La, Ce, Pr, Eu, Gd, Tb, Dy, Ho, Er, Tm, Yb and Lu. Most of them also have an aluminum-silicate affinity, which is in agreement with the high clay minerals content in the mineral matter of the coals from this basin.

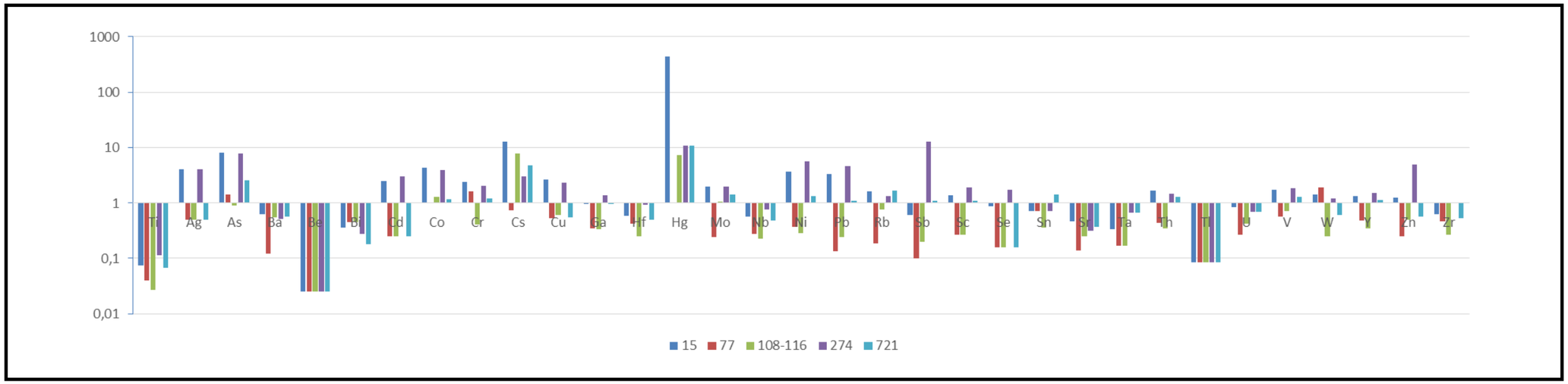

Figure 26 - Concentration coefficients (CC) of trace elements of the studied coals from DCB, normalized by average trace element concentrations in the world hard coals (Ketris and Yudovich, 2009).

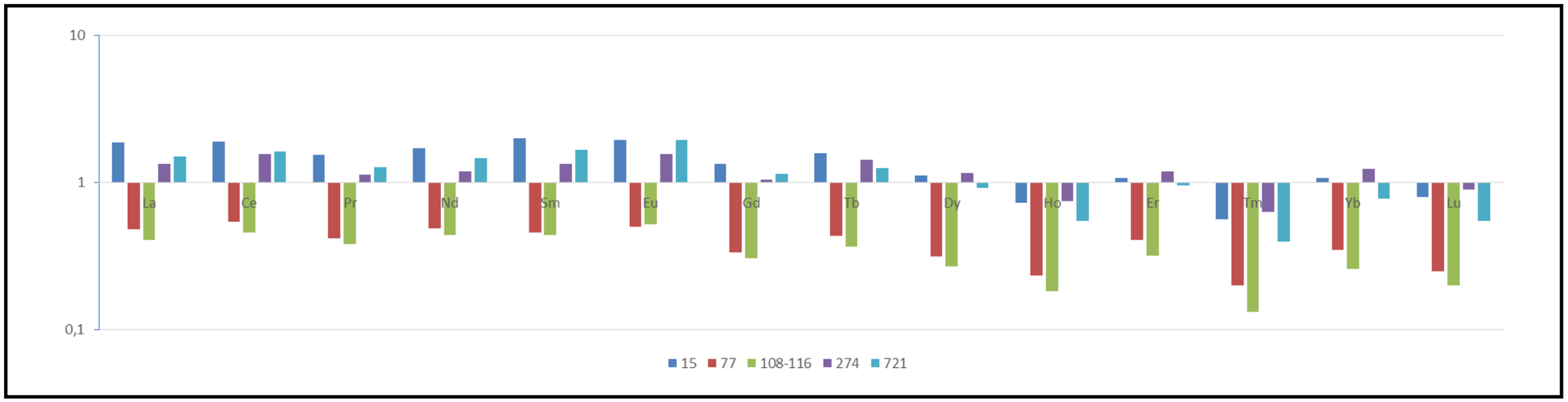

Figure 27 - Concentration coefficients (CC) of REEs of the studied coals from DCB, normalized by average trace element concentrations in the world hard coals (Ketris and Yudovich, 2009).

A carbonate affinity can be observed for Mn, K and Ta; however, only the Mn has a high affinity value (r_{Ca-Mn}= 0.83) and is the only to which a mode of occurrence in carbonates is attributed (Orem and Finkelman, 2003, see Table 4).

Table 14 - Trace and major element affinities deduced from the calculation of Pearson's correlation coefficients between the content of each element in the coal and ash yield or selected elements for the studied coals from DCB.

Douro Carboniferous Basin		
Correlation with ash content	Group 1: rash= −0.50 to −1.00 – Mainly organic affinity	Bi
	Group 2: rash= −0.50 to +0.50 – Intermediate (organic and inorganic) affinity	Ca, Mn, Na, P, Ba, Cs, Hg, Rb, Sn, Sr, W, Nd, Sm
	Group 3: rash= +0.50 to +1.0 – Inorganic affinity	Al, Si, Mg, Fe, K, S total, Ti, Ag, As, Au, Cd, Co, Cr, Cu, Ga, Hf, Mo, Nb, Ni, Pb, Sb, Sc, Se, Ta, Th, U, V, Y, Zn, Zr, La, Ce, Pr, Eu, Gd, Tb, Dy, Ho, Er, Tm, Yb, Lu
Aluminum-silicate affinity – $r_{Al–Si}$ > 0.70:		Mg, Fe, K, Ti, Ag, As, Cd, Co, Cu, Ga, Hf, Mo, Nb, Ni, Pb, Sc, Se, Ta, Th, V, Y, Zn, Zr, Ce, Pr, Eu, Gd, Tb, Dy, Ho, Er, Tm, Yb, Lu
Carbonate affinity – $r_{Ca–Mg}$>0.50:		K, Mn, Ta
Sulphur affinity – rSt>0.70:		Si, Fe, Na, Ti, Ag, As, Cd, Co, Cr, Cu, Hf, Mo, Nb, Ni, Pb, Sc, Se, Th, V, Y, Zn, Zr, Tb, Dy, Ho, Er, Tm, Yb, Lu

A sulfur affinity is observed in a large number of elements including Si, Fe, Na, Ti, Ag, As, Cd, Co, Cr, Cu, Hf, Mo, Nb, Ni, Pb, Sc, Se, Th, V Y, Zn, Zr, Tb, Dy, Ho, Er, Tm, Yb and Lu. Although a sulfide occurrence will not be conferred to some of these elements, such as Na, Cr, Sc, among others, these may present this geochemical affinity because the minerals in which they occur may be associated with sulfides.

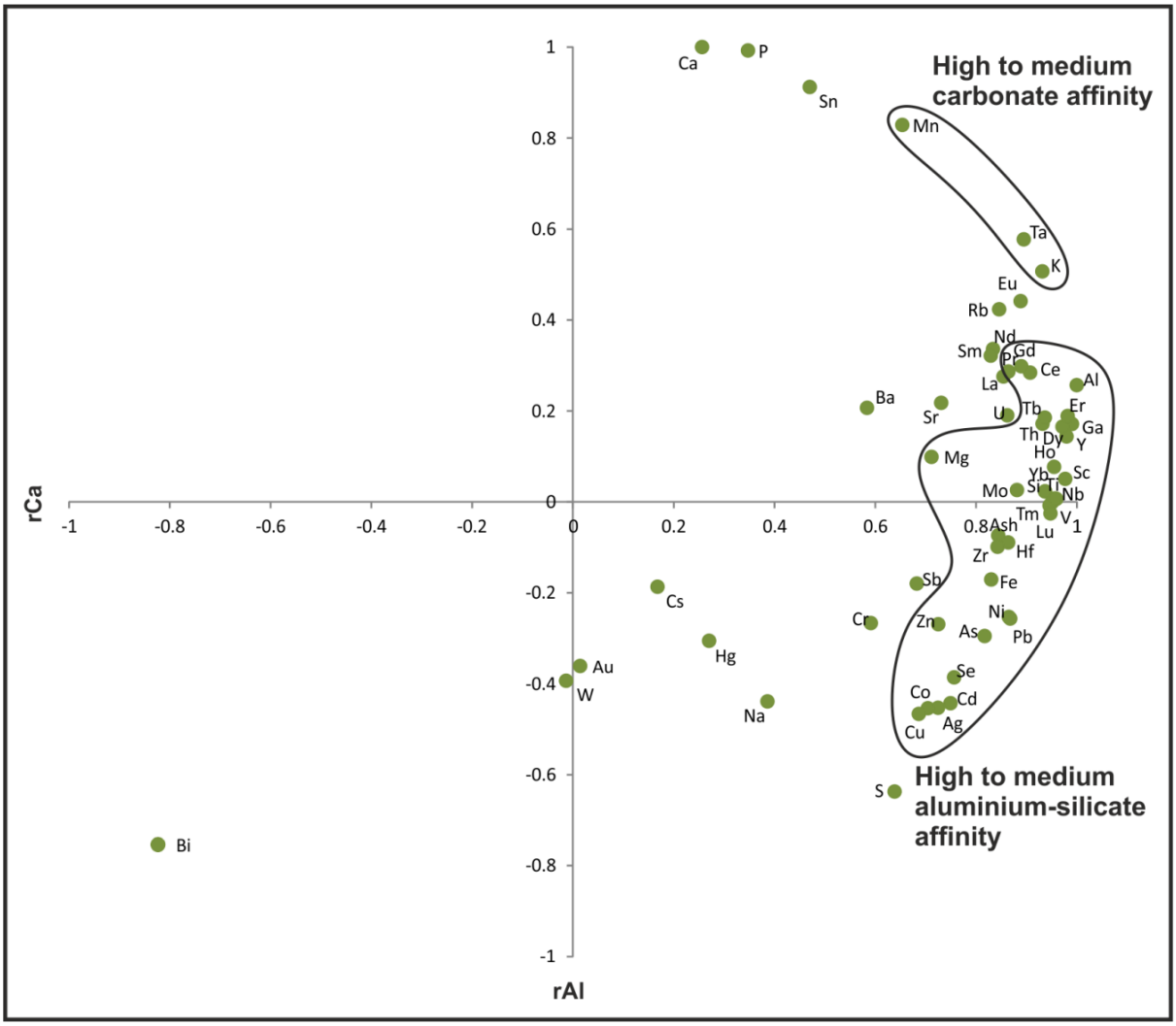

Figure 28 - Cross-plot correlation of the Pearson's correlation coefficients of the major and trace elements versus calcium and aluminium contents for the studied coals from DCB.

Mercury, which revealed an unusually enrichment, is referred by Orem and Finkelman (2003) as occurring in pyrite, mineral identified in these samples. However, this element does not have a good relation with Fe and does not exhibit a correlation coefficient high enough to be considered as having a sulfur affinity ($r_{St\text{-}Hg}$=0.60). The silicate-bound Hg in coals influenced by a magmatic intrusion may be mainly absorbed by clay minerals (Zheng et al., 2007a), which in this case it can also be one of the causes of the enrichment and mode of occurrence; however, Hg does not display an aluminum-silicate affinity. Thus an occurrence with an organic association is more likely since an intermediate affinity is presented and this is another of the modes of occurrence attributed to Hg by the same authors.

Cesium is another element that is enriched and displays an intermediate affinity ($r_{Ash\text{-}Cs}$= -0.21). Orem and Finkelman (2003) assigned a mode of occurrence in clay minerals, feldspar and mica, but the occurrence as clay minerals in this case is unlikely since it does not provide an aluminum-silicate affinity. An occurrence in plagioclase is the most plausible

explanation, given the good relationship with Na and Ba (r_{Cs-Na}=0.86 and r_{Cs-Ba}=0.74, respectively).

The enrichment of Sb is also observed and, although Orem and Finkelman (2003) suggested an occurrence as an accessory sulfide and an organic association, this element does not show a sulfur affinity, displaying an inorganic (r_{Ash-Sb}= 0.98) affinity. Therefore to infer about this element's mode of occurrence is complex.

Although REEs do not show relevant CC, a higher enrichment is displayed for the light rare earth elements (LREEs), since they are less correlated with the ash yield than HREEs, this may mean that their enrichment is a result of their absorption by the organic matter.

6.1.3. Abundance and genetic consequences

The DCB, as previously reported, presents a different enrichment depending on the sample. The samples 15 and 274 (São Pedro da Cova and Pejão mines, respectively) have a higher enrichment and both belong to the UTS B1 coal seam. These samples exhibit the same geochemical markers, since they have higher content of Fe and St, and the contents of some of the trace elements are almost identical, including Ag, As, Cd, Co and Cu.

The remaining samples (108/116, 721 and 77) are not as enriched but in this case only the samples 108/116 and 721 (São Pedro da Cova and Pejão mine, respectively) belong to the same seam, namely to the UTS D2 (the duplication of the seam UST D1) seam. The sample 77 belongs to São Pedro da Cova mine and occurs stratigraphically between UTS D2 and the sequences of the Lower Paleozoic, the so called "Eastern Basin". As this is a fault contact the coal seams of this package are very mylonitized, as it can be observed in some of the petrographic images of this sample (see Figures in chapter 8).

It is noticed that there is a more obvious enrichment in the lower coal seams, namely seam UST B1 and probably also in the duplicated seam UST B2. This enrichment is probably due to magmatic fluids and percolating waters enriched in these elements resulting from the implantation of granitoid rocks in the region, that lead to the coalification of the coal to the anthracite A rank. In addition to the higher enrichment in seam UST B1, some elements displays very high contents, in particular Hg in sample 15, showing also the higher REEs contents. This factor can be an indicator that the crustal stretching may have been greater than initially thought (Pinto de Jesus, personal communication). Wang et al. (1999) reported enrichment for some trace elements as a result of a granite intrusion for the Late Permian anthracites in the Coalfield Meitian, Hunan Province, southern China. It is therefore

concluded that the igneous minerals from the hydrothermal fluids were the main responsible for the enrichment of trace elements in the coals from the DCB.

6.2. Central Asturian Coal Basin

6.2.1. Major elements and mineralogy

An analysis concerning the concentration of major elements related to the content of mineral matter is difficult to perform in this basin, since there is no data available on the mineral matter present in the samples under study. However, minerals such as cinnabar, metacinnabar, native mercury, As-rich pyrite, melnikovite, sphalerite, marcasite, chalcopyrite, galena, stibnite, realgar, native gold, pyrrhotite, and other sulfides are reported in the Central Asturian Coal Basin (Loredo et al., 1999). This mineralization is considered to be an epigenetic type and is thought to have occurred as a result of the circulation of low-temperature hydrothermal solutions during the Permian period (Martínez-García, 1981; Loredo et al., 1988, 1999). According to Piedad-Sánchez et al. (2004a), the mineral matter content in these coals is extremely variable and characterized by a low pyrite content. Thus, and based on this information, an analysis of the major elements content can be carried out.

The Al and Si contents are indicative of aluminum-silicate minerals such as clay minerals. There are some samples that have higher contents of these elements, including 40634, 40366, 40370, 39313, 39772, 39733 and 3962, which may be an indication of a more continental input. The levels that stand out are those of the samples 40366 and 39152, they share a geographical relation and greater mineral matter content than the remaining samples. Therefore, high levels can be explained by a fluvial input into the center of the basin.

With respect to the samples 40642, 39759, 39768, 39772 and 39162, they show higher contents in Ca, reflecting a possibly higher content of carbonates in these samples. The Fe content is high in the samples 40642, 40370, 39579, 39152, 39311, 39169 and 39313, element that is present in many sulfide minerals as arsenopyrite, marcasite and chalcopyrite. These minerals are all described above as reported in this coal basin and thus this may be one of the explanations for these high Fe concentrations.

The sulfides previously mentioned may also be the explanation for the high St content of samples 40634, 40398, 40370, 39759 and 40616. The samples 40634 and 39759 are those with a more relevant content and share a geographical correlation, thereby the source of enrichment of the samples in total sulfur may have had more influence in this location.

6.2.2. Concentration coefficients

The enrichment in the CAB coals does not appear to be very relevant when compared to the average for world hard coals (Ketris and Yudovich, 2009). Considering the higher value content for each of the trace elements, the coals were classified according to their enrichment through the projection of their CC. As almost all the coals are bituminous coals (except sample 40776 that is an anthracite C) the CC of the trace elements was projected in the same figure (Figure 29).

The elements As, Cu, Pb, Sb and Zn displays CC considered as significantly enriched (CC> 10). About the Hg and Mo trace elements, they are considered enriched since their CC are between 5 and 10. A slight enrichment (2 <CC <5) is observed for the elements Cd, Co, Cr, Cs, Rb, Sc, Sn, U and V. The trace elements Ag, Ba, Be, Ga, Se, Sr, Th, W and Y have CC within the average for the world hard coals (0.5 <CC <2). The other elements, particularly Ti, Bi, Hf, Nb, Ni, Tl and Zr, are depleted (CC <0.5).

It is important to emphasize that although some elements are significantly enriched, the basin is not considered to be enriched based on the studied samples. This is because the enrichment is only punctual in some samples, especially in the samples 39152, 40634 and 39755, which is not representative of a total of 18 samples.

The REEs do not demonstrate enrichment (Figure 30) and most of their CC are close to the average for world hard coals (0.5 <CC <2), specifically La, Ce, Nd, Sm, Eu, Gd, Tb, Dy, Er and Yb, in the sample 39152. In the remaining samples the REEs are depleted, as the CC is lower than 0.5.

The depletion in the studied samples is supported by the diagram that compares the average contents of each of the elements for bituminous and anthracite samples with the average content for the world hard coals (Figure 31 and 32).

6.2.3. Geochemical affinities

The Pearson correlation coefficients between the concentration of the elements and ash yield to the coals from the basin resulted in the geochemical affinities are shown in table 15. The geochemical affinities were firstly calculated for all studied coals and then only for bituminous coals and, as it can be seen, the affinities do not differ from those obtained for all the studied coals. The projection of the intercorrelation results of major and trace elements was performed for all coals and can be observed in figure 33. The Pearson correlation coefficients of the elements of Al and Ca were used in order to represent the carbonate and aluminum-silicate.

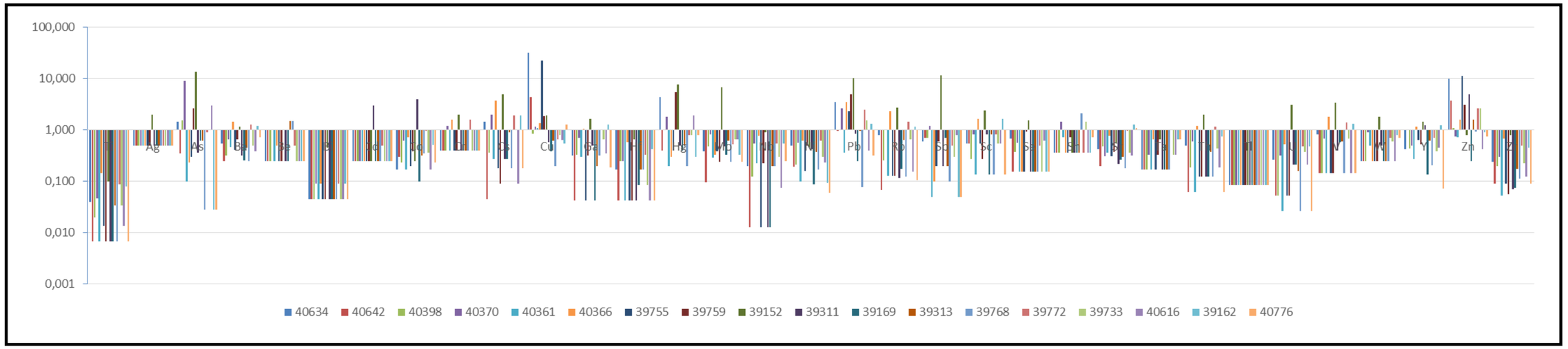

Figure 29 - Concentration coefficients (CC) of trace elements of the studied coals from CAB, normalized by average trace element concentrations in the world hard coals (Ketris and Yudovich, 2009).

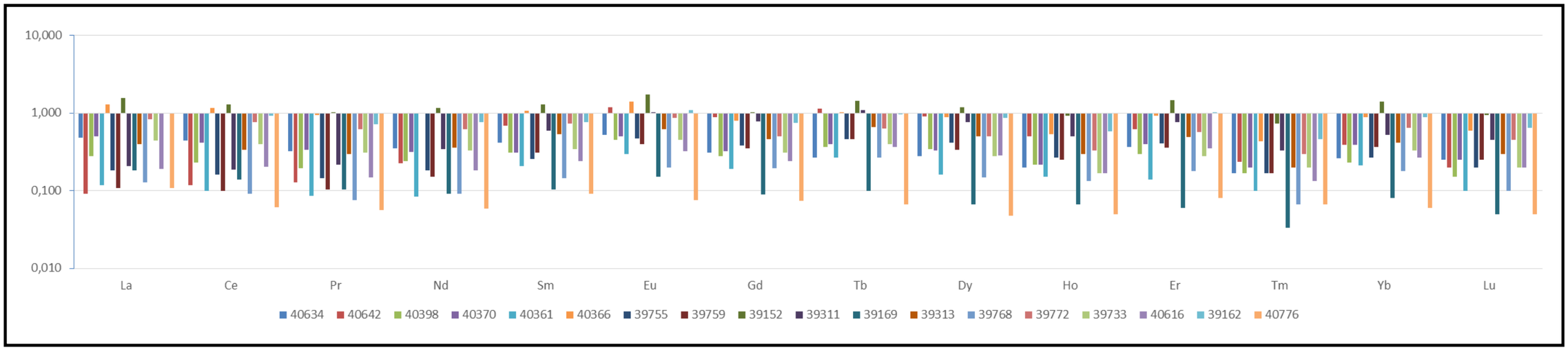

Figure 30 - Concentration coefficients (CC) of REEs of the studied coals from CAB, normalized by average trace element concentrations in the world hard coals (Ketris and Yudovich, 2009).

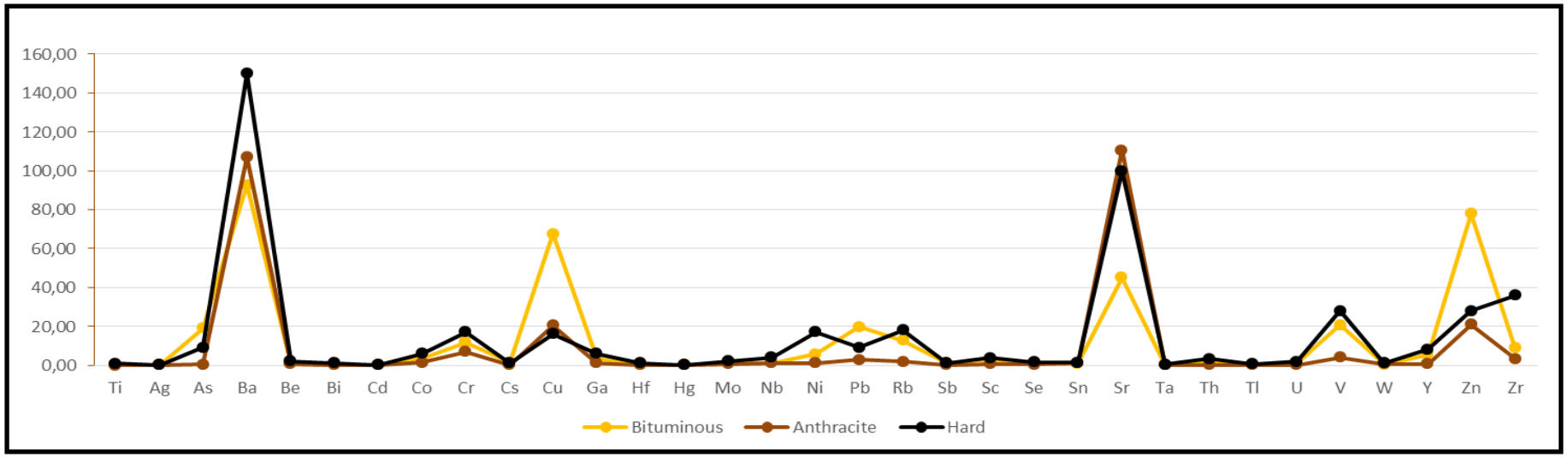

Figure 31 - Comparative diagram of the average contents of trace elements for bituminous and anthracite samples from CAB with the average content for the world hard coals (Ketris and Yudovich, 2009).

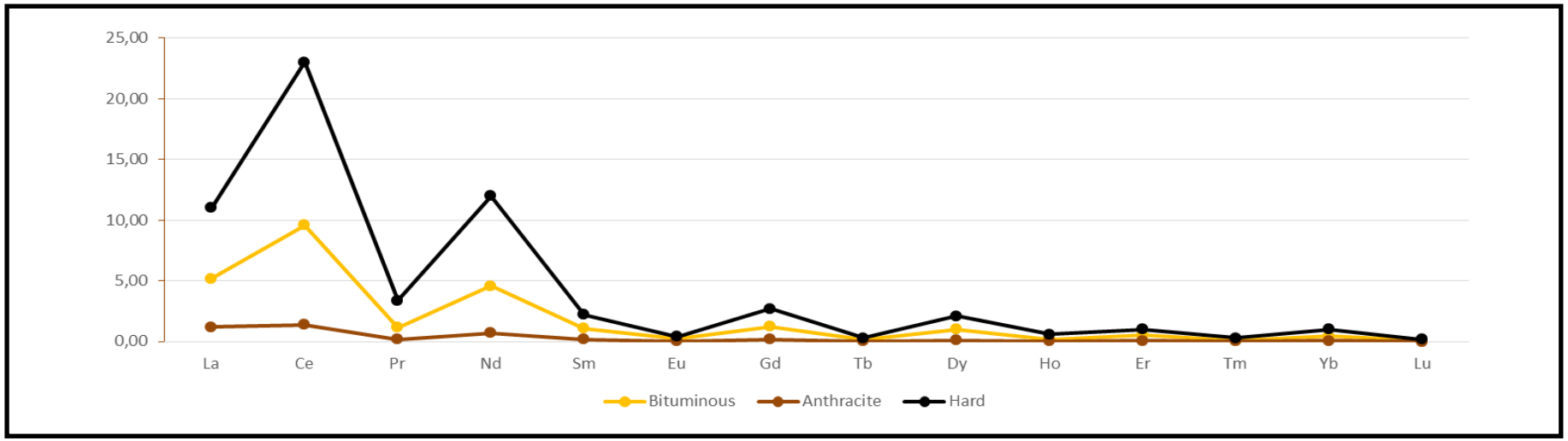

Figure 32 - Comparative diagram of the average contents of trace elements for bituminous and anthracite samples from CAB with the average content for the world hard coals (Ketris and Yudovich, 2009).

Table 15 - Trace and major element affinities deduced from the calculation of Pearson's correlation coefficients between the content of each element in the coal and ash yield or selected elements for all the studied coals and bituminous coals from CAB.

Central Asturian Coal Basin			
		All coal samples	Bituminous coals
Correlation with ash content	Group 1: rash= −0.50 to −1.00 – Mainly organic affinity	–	–
	Group 2: rash= −0.50 to +0.50 – Intermediate (organic and inorganic) affinity	Ca, Mg, Fe, Mn, Stotal, Au, Be, Cd, Co, Cu, Hg, Sn, Sr, Tl, Zn	Ca, Mg, Fe, Mn, Stotal, Au, Be, Cd, Co, Cu, Hg, Se, Sn, Tl, Zn
	Group 3: rash= +0.50 to +1.0 – Inorganic affinity	Al, Si, K, Na, P, Ti, Ag, As, Ba, Bi, Cr, Cs, Ga, Hf, Mo, Nb, Ni, Pb, Rb, Sb, Sc, Se, Ta, Th, U, V, W, Y, Zr, La, Ce, Pr, Nd, Sm, Eu, Gd, Tb, Dy, Ho, Er, Tm, Yb, Lu	Al, Si, K, Na, P, Ti, Ag, As, Ba, Bi, Cr, Cs, Ga, Hf, Mo, Nb, Ni, Pb, Rb, Sb, Sc, Sr, Ta, Th, U, V, W, Y, Zr, La, Ce, Pr, Nd, Sm, Eu, Gd, Tb, Dy, Ho, Er, Tm, Yb, Lu
Aluminum-silicate affinity – rAl–Si > 0.70:		K, Na, Ti, Ba, Bi, Cr, Cs, Ga, Hf, Nb Pb, Rb, Sc, Th, U, V, Zr, La, Ce, Pr, Nd, Sm, Eu, Ho, Er, Tm, Yb, Lu	K, Na, Ti, Ba, Bi, Cr, Cs, Ga, Hf, Nb, Pb, Rb, Sc,Ta, Th, U, V, Zr, La, Ce, Pr, Nd, Sm, Eu, Ho, Er, Tm, Yb, Lu
Carbonate affinity – rCa–Mg>0.50:		–	–
Sulphur affinity – rSt>0.70:		–	–

The majority of the elements presented in the coals from the basin possess an inorganic affinity (Al, Si, K, Na, P, Ti, Ag, As, Ba, Bi, Cr, Cs, Ga, Hf, Mo, Nb, Ni, Pb, Rb, Sb, Sc, Se, Ta, Th, U, V, W, Y, Zr, La, Ce, Pr, Nd, Sm, Eu, Gd, Tb, Dy, Ho, Er, Tm, Yb, and Lu. Most of these elements, in particular K, Na, Ti, Ba, Bi, Cr, Cs, Ga, Hf, Nb, Pb, Rb, Sc, Th, U, V, Zr, La, Ce, Pr, Nd, Sm, Eu, Ho, Er, Tm, Yb, Lu, also exhibit an aluminum-silicate affinity and occur in clay minerals. However none of the elements presents a carbonate or sulfur affinity although the Mg/Mn ratio is 0.79, which may indicate the presence of siderite.

It is important to try to understand the mode of occurrence of As, Cu, Pb, Sb and Zn, because, as mentioned previously, the CC shows a significant enrichment. In the case of As, it reveals an inorganic affinity ($r_{ash\text{-}As}$= 0.56), which is indicative of an occurrence associated to the mineral matter, namely in solid solution in pyrite (Orem and Finkelman, 2003), since is described for the basin As pyrite and realgar (Loredo et al., 1999).

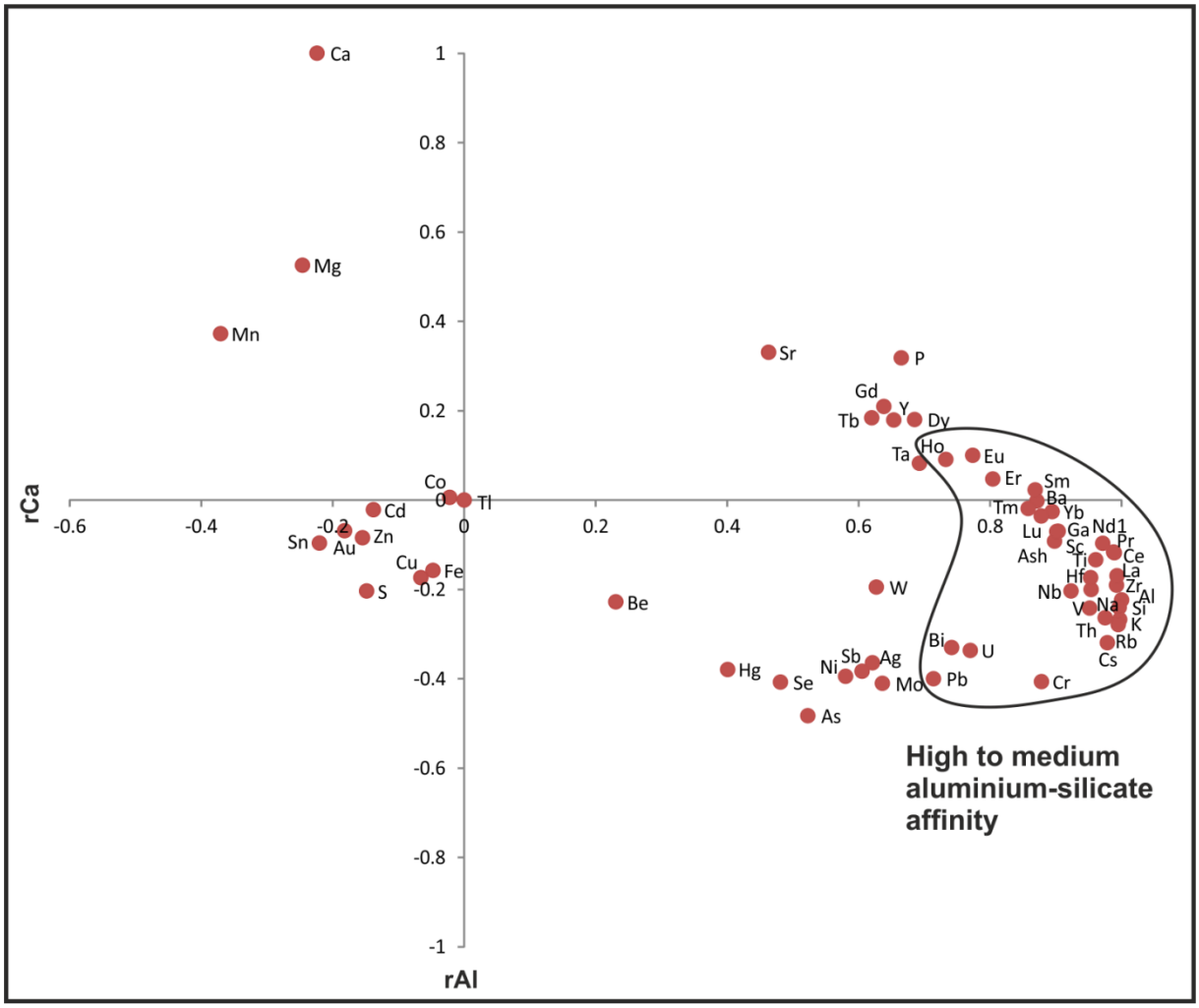

Figure 33 - Cross-plot correlation of the Pearson's correlation coefficients of the major and trace elements versus calcium and aluminium contents for the studied coals from CAB.

Cu reveals an intermediate affinity ($r_{ash\text{-}Cu}$= -0.21) and is referenced by Orem and Finkelman (2003) as occurring in chalcopyrite as well as in clay minerals and organic association. Firstly an occurrence in chalcopyrite appears to be the most likely explanation since this mineral is reported for the basin. However, the Cu and Fe correlation coefficient is low, thus an organic association is possible given the intermediate affinity presented for Cu.

Pb features an aluminum-silicate affinity ($r_{Al\text{-}Pb}$= 0.71; $r_{Si\text{-}Pb}$= 0.71) and also a good correlation coefficient with Se ($r_{Pb\text{-}Se}$= 0.86), which is in agreement with two of the occurrence modes attributed to this element by Orem and Finkleman (2003), including clay minerals and PbSe.

In the case of Sb, Orem and Finkelman (2003) mention accessory sulfide and organic association as modes of occurrence. Thus, since there is evidence of an intermediate affinity ($r_{ash\text{-}Sb}$= 0.70) and that stibnite is a mineral identified in the basin, both occurrences appear to be valid explanations for the enrichment.

Regarding Zn, it has an intermediate affinity (r_{ash-Zn}= -0,19) and the only mode of occurrence which is assigned by Orem and Finkelman (2003) is spharelite, a mineral mentioned as belonging to the mineral matter content of CAB.

Hg, although only enriched, is relevant in this study and therefore its mode of occurrence should be investigated. It displays an intermediate affinity (r_{ash-Hg}= 0.42) and is the element that presents a best relation with St (r_{Hg-St}= 0.64). However, given the low Hg/Fe ratio, an occurrence in pyrite seems to not be possible, making more sense an occurrence as cinnabar, a mineral described as present in this basin and which is in accordance with the occurrence mode attributed to it (Orem and Finkelman, 2003).

Still regarding the geochemical affinities, trace elements as Hg, Se, Ni, As, Sb, Ag, Mo, Pb, Bi, U and Cr appear to have a specific geochemical affinity, having correlation coefficients with Al close to -0.40 (Figure 33). The most probable explanation for this geochemical affinity concerns to a marine influence on the genesis of these coals, since they were formed in a transitional and continental paleosedimentary environment (Colmenero et al., 2008; Águeda et al., 1991; Piedad-Sánchez et al., 2004a, 2004b). According to Dai et al. (2012), a high enrichment in B, V, Cr, Ni, Mo, and U is the result of coals deposited in tidal flat environments of restricted carbonate platforms (Dai et al., 2008; Shao et al., 2003; Zeng et al., 2005). Although only sample 39152 presents relevant CC for these elements, this may be the explanation for this affinity. Considering that, according to Fertl (1979) a ratio Th/U <7 reveals a marine influence on the sediments, in the case of sample 39152 it is in the threshold (Th/U=7.03). Other samples also show a marine influence according to the Th/U ratio (Figure 34).

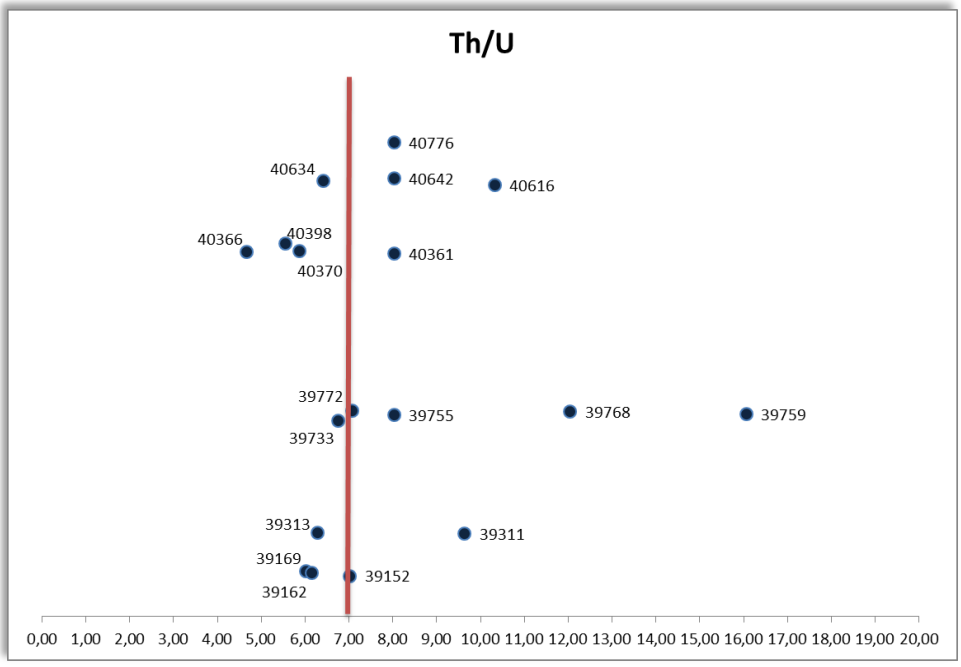

Figure 34 - Th/U ratios of the studied coals from CAB.

The major determinant in this geochemical affinity is possibly the pH and Eh, as these environments often had algae growing and a low Eh value. Biogenetic pyrites, an assemblage of pyritized monosporaphyte of red algae, have been found in other marine-influenced coals of southwestern China (Dai et. al, 2003), and since most of the elements that display this geochemical affinity have an occurrence in pyrite, this can also be one of the explanations for it. However, samples 40366 and 39152 that have a high content of Al and Si which is explained by a fluvial input into the center of the basin, are two of the samples that appear to have been marine influenced. Therefore evidences that can be somewhat contradictory arise and this explanation of a marine influence as the responsible for the geochemical affinity of these elements is not strongly supported. It would require further studies in order to achieve more conclusions as here is only performed a preliminary analysis.

6.2.3. Abundance and genetic consequences

The enrichment of certain elements in this basin is due to the mode of occurrence and therefore is closely related to the mineral content. Mineralization at CAB was due to the circulation of low-temperature hydrothermal solutions during the Permian (Martínez-García, 1981; Loredo et al., 1988, 1999).

According to Dai et al. (2012) the major carriers of some trace elements in coals of southwestern China are the epigenetic minerals derived from hydrothermal fluids, including sulfides (pyrite, chalcopyrite, alabandite, sphalerite, galena, selenio-galena, getchellite, realgar, orpiment, cinnabar, and stibnite), carbonates (calcite, dolomite, ankerite, and strontianite), clay minerals (kaolinite and chamosite), oxides (quartz), fluorides (fluorite) (Dai et al., 2004a, 2005, 2006; Dai and Chou, 2007; Zhang, 1999; Yang, 2006; Zhang et al., 1999, 2002, 2004). An enrichment in As, Hg, Se and Zn in the Late Permian coals in western Guizhou are due to pyrite infilling veins (Zhang, 1999; Zhang et al., 1999). Enrichment in Cu and U is observed in coal No. 30 because of an alteration by a siliceous low-temperature hydrothermal fluid (Dai et al., 2004).

Given the similarities, in particular the geological time and the mineral matter content (including cinnabar, pyrite, sphalerite, chalcopyrite, galena, stibnite, realgar) as well as an enrichment of some of the same trace elements (As, Hg, Cu and Zn), the most probable explanation is that the enrichment of these elements is due to an epigenetic mineralization originated in a low-temperature hydrothermal fluid source.

As mentioned before, the evidences on the geochemical affinities of the sensitive elements that are associated to the marine influence in the deposition of the biomass of

these coals require further investigation, mainly the study of more samples as well as the mineralogy of the same samples.

6.3. Peñarroya-Belmez-Espiel Basin

6.3.1. Major elements and mineralogy

The major elements content for this basin is in agreement with the mineralogical composition. Figures 35 and 36 show some of the minerals identified through the SEM analysis, carried out on samples 1358, 1501/1502, 891/893 and 1708. The Si contents are always higher than the Al contents, due to the high content of quartz and clay minerals (as kaolinite and chlorite) in these samples. Figure 35-A shows authigenic kaolinite.

Regarding the high Ca contents in the samples 1358, 214/275, 746/751, 894/896 and 1078, these are explained by the high content of carbonates, especially calcite (Figure 36-D) and siderite. Similarly high concentrations of Mg are also related to the presence of carbonates, particularly ankerite (Figure 36A) and dolomite, for samples 1358 and 1078.

The samples 1501/1502, 1358, 1511/1513, 214/275, 712/715, 746/751, 894/896, 752/754, 891/893 and 1078 reveal high Fe contents, due to the presence of sulfides, namely pyrite, chalcopyrite and spharelite (Figure 36-B), and others as kutnohorite and oligonite (Figure 35-C and 36-A, respectively). The sample 1511/1513 exhibits a Fe content that stands out, and that is a result of the high content of syngenetic pyrite (framboids) and Fe oxides.

The high K content in the samples 2085, 1501/1502, 1511/1513, 712/715, 705/708, 894/896 and 1102, is due to the detrital clay minerals content as well as the presence of authigenic minerals. The epigenetic events are associated to magmatic events, which are thought to be responsible for the anthracite rank of these coals as well as the occurrence of natural cokes and the enrichment of the surrounding fluids in this element (Suárez-Ruiz et al., 2006). The high P content, mainly in the sample 214/275, is associated with the presence of apatite, which is also thought to be a result of the same magmatic activity (Suárez-Ruiz et al., 2006).

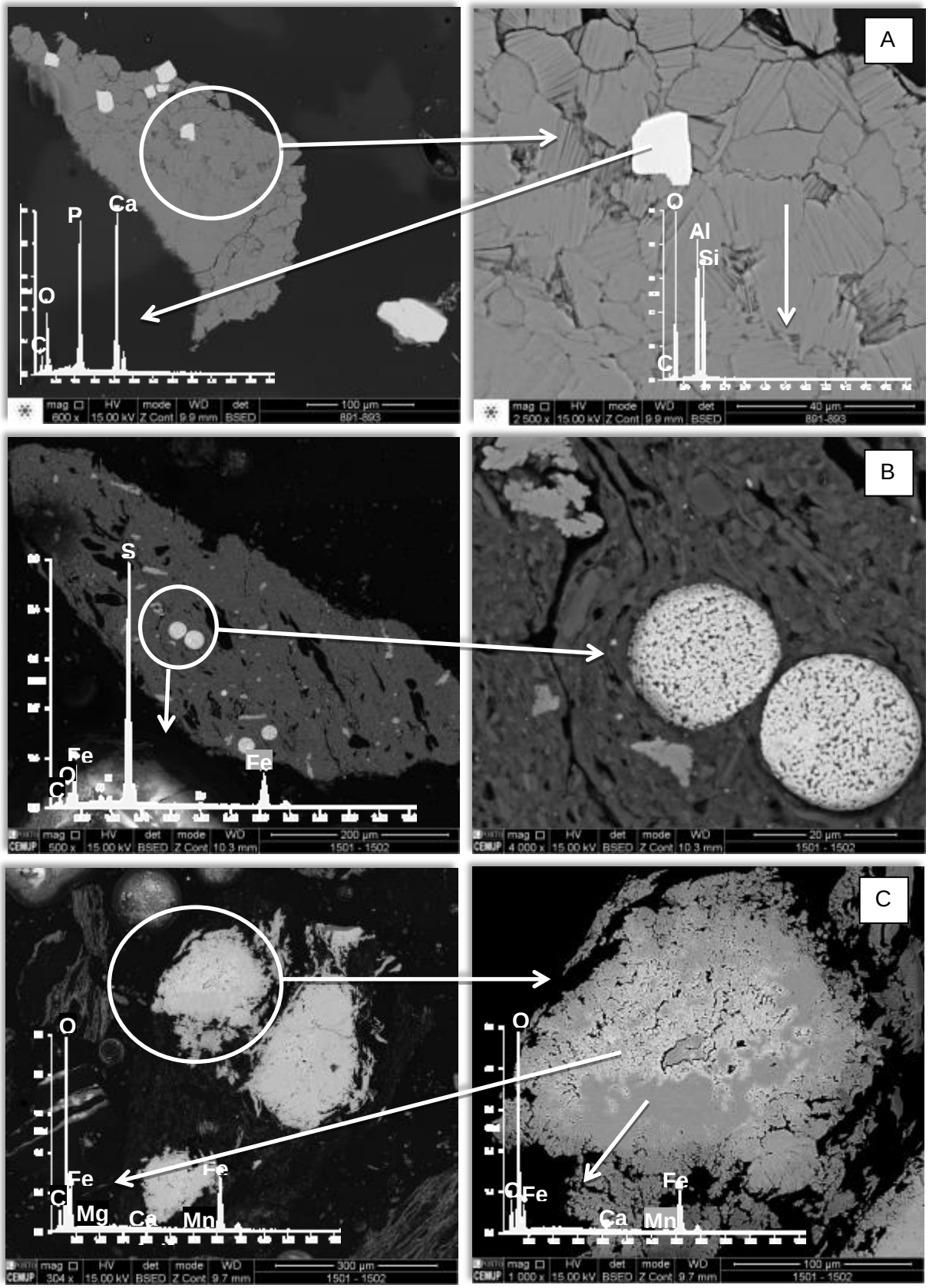

Figure35 - SEM (BSE images) and EDS spectrum of the mineral phases found in the coal samples: A) apatite (EDS spectrum in the left) and authigenic kaolinite (EDS spectrum in the right) (sample 891/893); B) pyrite (sample 1501/1502); C) kutnohorite (EDS spectrum in the right associated with ankerite (EDS spectrum in the left) (sample 1501/1502).

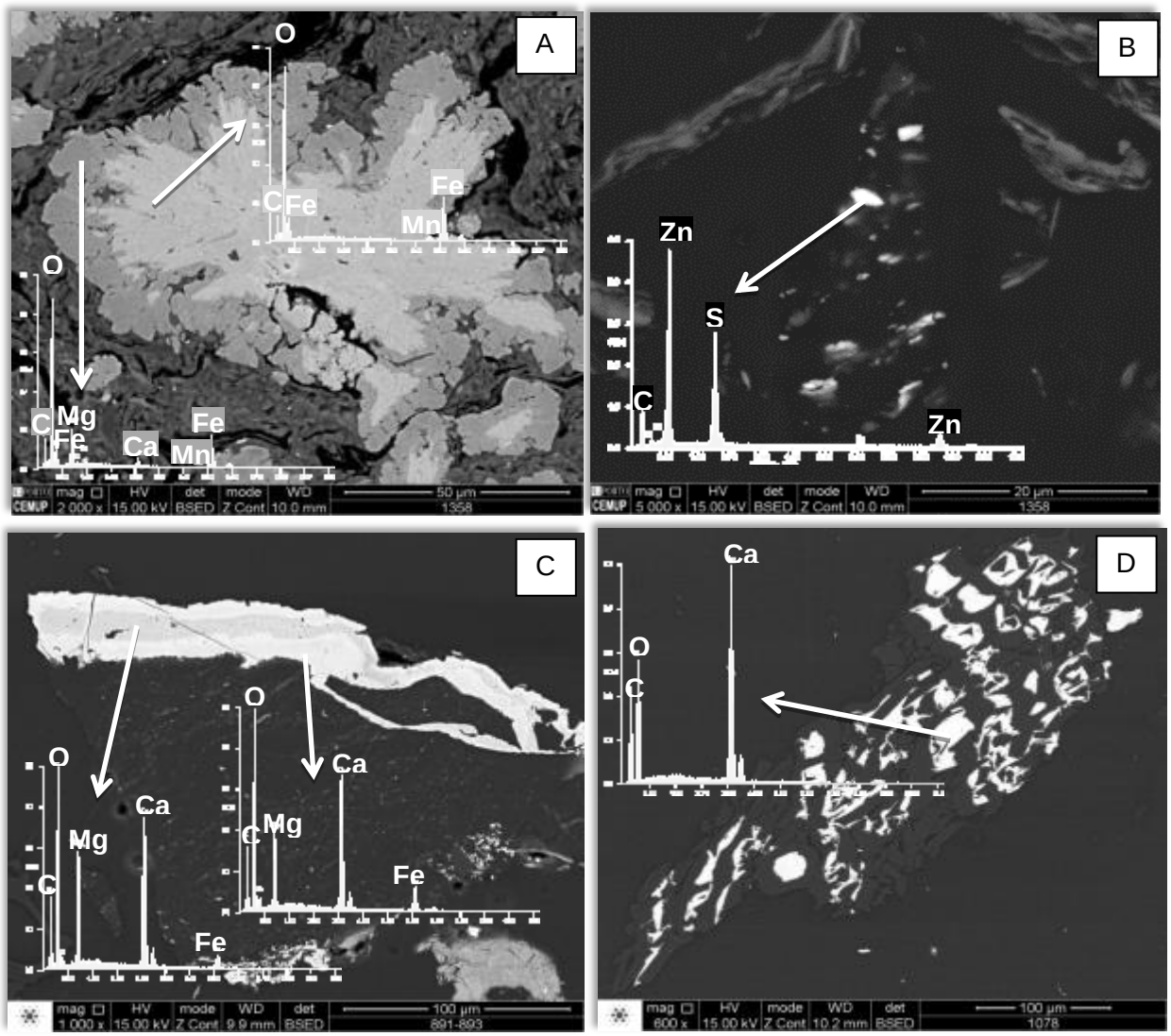

Figure 36 - SEM (BSE images) and EDS spectrum of the mineral phases found in the coal samples: A) ankerite (EDS spectrum in the bottom left) associated with oligonite (EDS spectrum in the top right) (sample 1358); B) sphalerite (sample 1358); C) dolomite (sample 891/893); D) calcite filling cellular lumens (sample 1078).

6.3.2. Concentration coefficients

The coals from the PBEB carboniferous basin, as noted before, are enriched when compared to the average for the world hard coals (Ketris and Yudovich, 2009). The coals from the east and west sector correspond to bituminous coals and anthracites, respectively; thus the CC were calculated, projected and discussed separately.

Bituminous coals

For the bituminous coals (Figure 37) no trace element presents a significant enrichment (CC > 10). The trace elements that present a 5 <CC <10 are Cr, Cs, Pb, Rb, Sr

and Zn and are considered enriched. The elements with a CC between 2 and 5 are Ba, Cd, Co, Cu, Ga, Hg, Hf, Nb, Ni, Sc, Sn, Ta, Th, V, Y and Zr, thereby considered as slightly enriched elements. The As, Be, U and W are close to the average for the world hard coals (0.5 <CC <2). The elements Ti, Ag, Bi, Mo, Sb, Se and Tl are depleted in all the studied coals (CC <0.5). It can be emphasized the global depletion of the samples 1358, 1476 and 1509, contrasting with a strong enrichment of the samples 1501/1502 and 1511/1513.

The REEs (Figure 38) are slightly enriched in La, Ce, Pr, Nd, Sm, Eu, Gd, Tb, Er and Yb, as the CC are between 2 and 5. The remaining REEs, in particular Dy, Ho, Tm and Lu, present CC within the average for the world hard coals (0.5 <CC <2). As for the other trace elements, a global depletion of the REEs occurs in the samples 1358, 1476 and 1509, and an enrichment is observed for samples 1501/1502 and 1511/1513.

Anthracite coals

As regards to the anthracite coals (Figure 39), Cs, Pb and Zn, are the elements with CC above 10 and therefore are significantly enriched. Enriched trace elements (5 <CC <10) include Cd, Co, Rb, Sb and Sc. On the other hand the elements with CC between 2 and 5 comprise Ag, Ba, Be, Cu, Ga, Hg, Mo, Sn, V, Y and Zn, corresponding to elements slightly enriched. Elements such as Hf, Nb, Sr, Ta, U and W are within that considered as a normal concentration (0.5 <CC <2). However, elements such as Ti, Bi, Se and Tl are depleted in the studied coals. Still concerning the enrichment, this depends on the element and not necessarily on the sample as there is no general trend.

The REEs slightly enriched (2 <CC <5) are La, Ce, Pr, Sm, Eu, Tb, Er and Lu (Figure 40). The others REEs, including Gd, Dy, Ho, Tm and Yb, are within the normal standards (0.5 <CC <2). There is an enrichment tendency for samples 1102 and 712/715 and a general depletion of the samples 1078, 214/275 and 48/63.

Based on a comparison of the CC from the two sectors of the basin, it is noticed that the samples from the W sector possess a larger and more global enrichment in trace elements than the E sector samples, this global enrichment is more notorious for the REEs.

The diagrams of the figures 41 and 42 show the tendencies described above. It can be observed that the average values of the elements are generally higher in anthracites than in the bituminous coals.

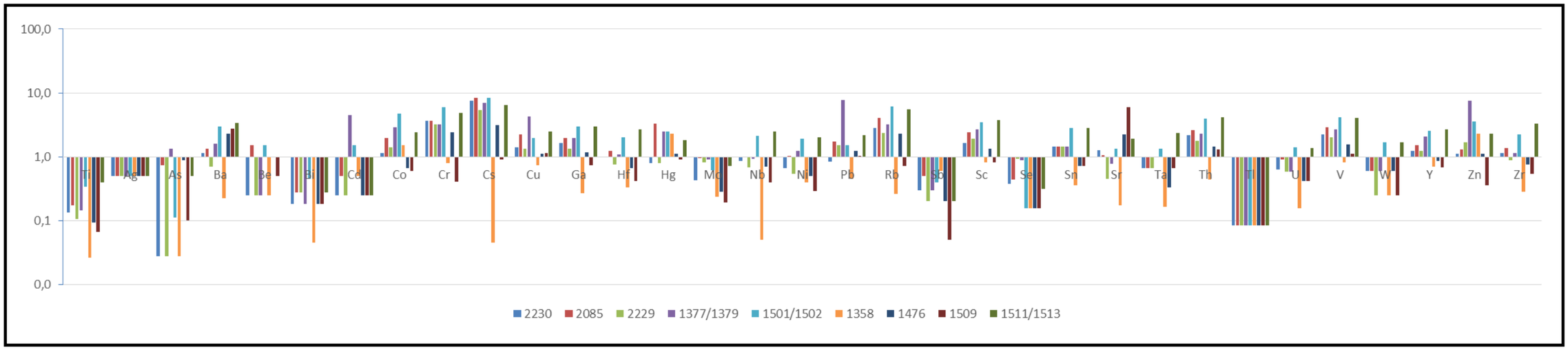

Figure 37 - Concentration coefficients (CC) of trace elements for the bituminous coal samples from PBEB, normalized by average trace element concentrations in the world hard coals (Ketris and Yudovich, 2009).

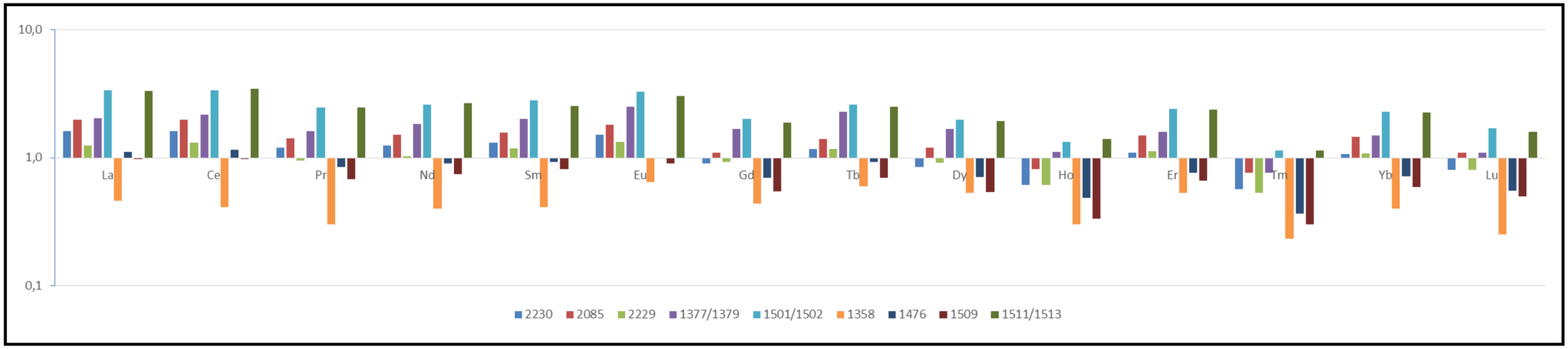

Figure 38 - Concentration coefficients (CC) of REEs for the bituminous coal samples from PBEB, normalized by average trace element concentrations in the world hard coals (Ketris and Yudovich, 2009).

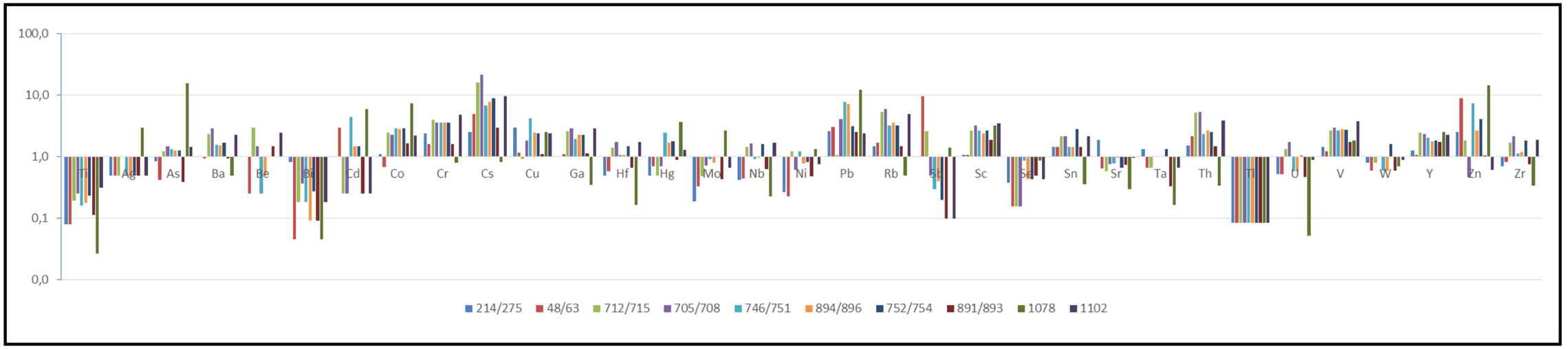

Figure 39 - Concentration coefficients (CC) of trace elements for the anthracites samples from PBEB, normalized by average trace element concentrations in the world hard coals (Ketris and Yudovich, 2009).

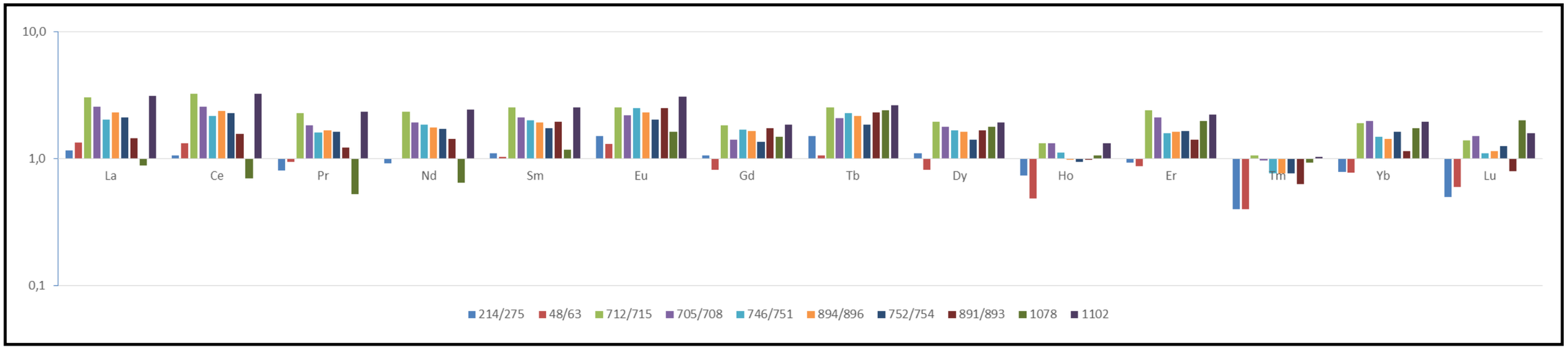

Figure 40 - Concentration coefficients (CC) of REEs for the anthracites samples from PBEB, normalized by average trace element concentrations in the world hard coals (Ketris and Yudovich, 2009).

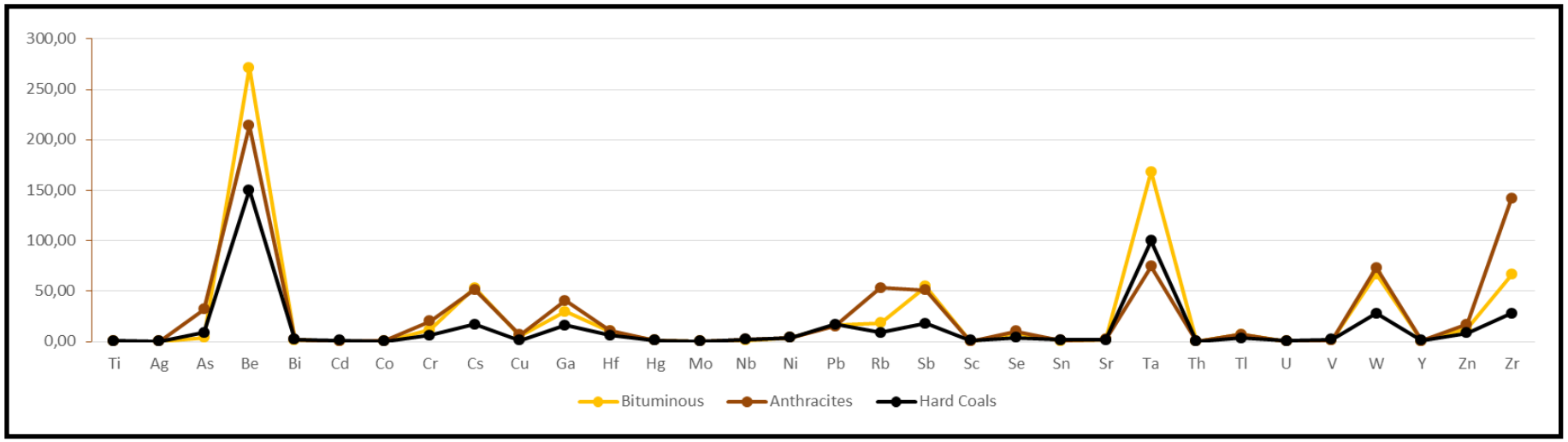

Figure 41 - Comparative diagram of the average contents of trace elements for bituminous and anthracite samples from PBEB with the average content for the world hard coals (Ketris and Yudovich, 2009).

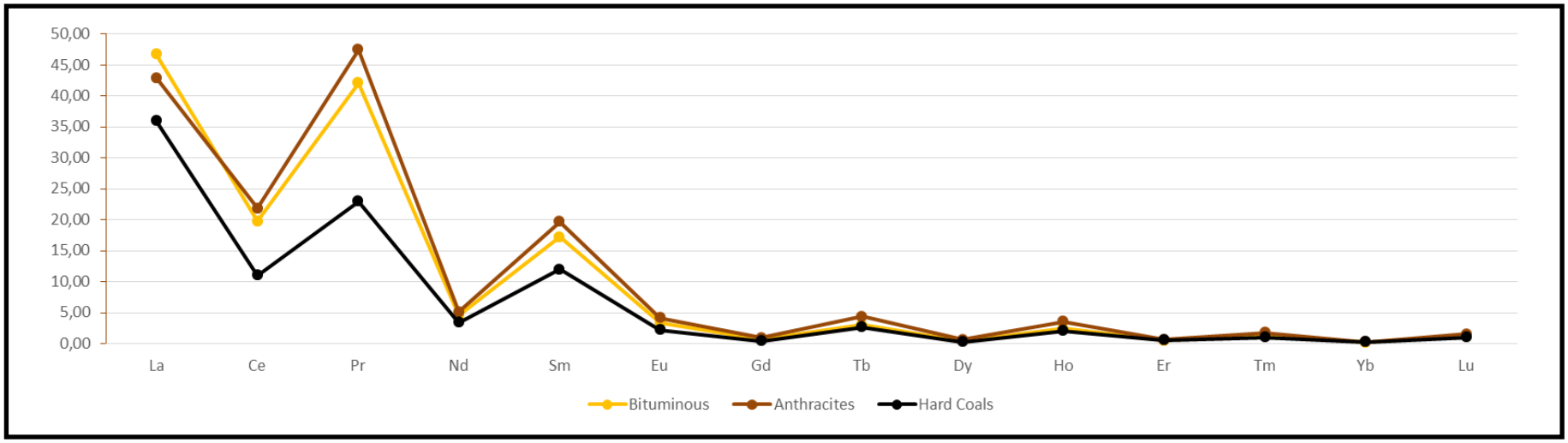

Figure 42 - Comparative diagram of the average contents of REEs for bituminous and anthracite samples from PBEB with the average content for the world hard coals (Ketris and Yudovich, 2009).

6.3.3. Geochemical affinities

The geochemical affinities of elements with ash yield were calculated trough the correlation coefficients of the elements that were made separately for the bituminous coals and anthracites as shown in Table 16.

The figures 43 and 44 summarize the results obtained for the intercorrelation analysis of major and trace elements in the bituminous coals and anthracites from the PBEB, respectively. In order to represent the carbonate and aluminum-silicate affinities Pearson correlation coefficients of the elements as well as the levels of calcium and aluminum were used for both rank coals.

Table 16 - Trace and major element affinities deduced from the calculation of Pearson's correlation coefficients between the content of each element in the coal and ash yield or selected elements for the studied bituminous and anthracite coals from PBEB.

Peñarroya-Belmez-Espiel Basin			
		Bituminous coals	Anthracites
Correlation with ash content	Group 1: rash= −0.50 to −1.00 – Mainly organic affinity	-	Sb, Zn
	Group 2: rash= −0.50 to +0.50 – Intermediate (organic and inorganic) affinity	Ca, Mg, P, Ag, As, Cd, Cu, Hg, Mo, Pb, Sb, Se, Sr, Tl, Zn	Ca, Mg, Fe, Mn, P, S total, Ag, As, Au, Be, Bi, Cd, Co, Cu, Hg, Mo, Ni, Pb, Se, Sr, Ta, Tl, W, Lu
	Group 3: rash= +0.50 to +1.0 – Inorganic affinity	Al, Si, Fe, K, Mn, Na, Stotal, Ti, Au, Ba, Be, Bi, Co, Cr, Cs, Ga, Hf, Nb, Ni, Rb, Sc, Sn, Ta, Th, U, V, W, Y, Zr, La, Ce, Pr, Nd, Sm, Eu, Gd, Tb, Dy, Ho, Er, Tm, Yb, Lu	Al, Si, K, Na, Ti, Ba, Cr, Cs, Ga, Hf, Nb, Rb, Sc, Sn, Th, U, V, Y, Zr, La, Ce, Pr, Nd, Sm, Eu, Gd, Tb, Dy, Ho, Er, Tm, Yb
Aluminum-silicate affinity – rAl–Si > 0.70:		Fe, K, Na, Ti, Au, Bi, Co, Cr, Cs, Ga, Hf, Nb, Ni, Rb, Sc, Sn, Ta, Th, U, V, W, Y, Zr, La, Ce, Pr, Nd, Sm, Eu, Gd, Tb, Dy, Ho, Er, Tm, Yb, Lu	K, Na, Ti, Ba, Cr, Cs, Ga, Hf, Rb, Nb, Sn, Th, U, V, Zr, La, Ce, Pr, Nd, Sm, Eu
Carbonate affinity – rCa–Mg>0.50:		Sb	Fe, Mn, Stotal, Ag, As, Cd, Co, Hg, Mo, Pb, Se, Zn
Sulphur affinity – rSt>0.70:		Si, Fe, Ti, Hf, Nb, Ta, Zr	Ca, Mg, Mn, Ag, As, Cd, Co, Hg, Mo, Pb, Zn

Bituminous coals

The bituminous coals belonging to E sector, present elements that have an inorganic affinity (Fe, K, Mn, Na, St, Ti, Au, Ba, Be, Bi, Co, Cr, Cs, Ga, Hf, Nb, Ni, Rb, Sc, Sn, Ta, Th,

U, V, W, Y, Zr, La, Ce, Pr, Nd, Sm, Eu, Gd, Tb, Dy, Ho, Er, Tm, Yb and Lu) as well as an aluminum-silicate affinity, so there is an agreement with the clay mineral content in these coals. It should be noted that the CC of some of these elements such as Cr, Cs and Rb are considered enriched. Thus enrichment in these trace elements together with its aluminum-silicate affinity can be an indicator of a siliciclastic detrital material supply into the basin. This is coincident with information already reported in previous studies (Suárez-Ruiz et al., 2006).

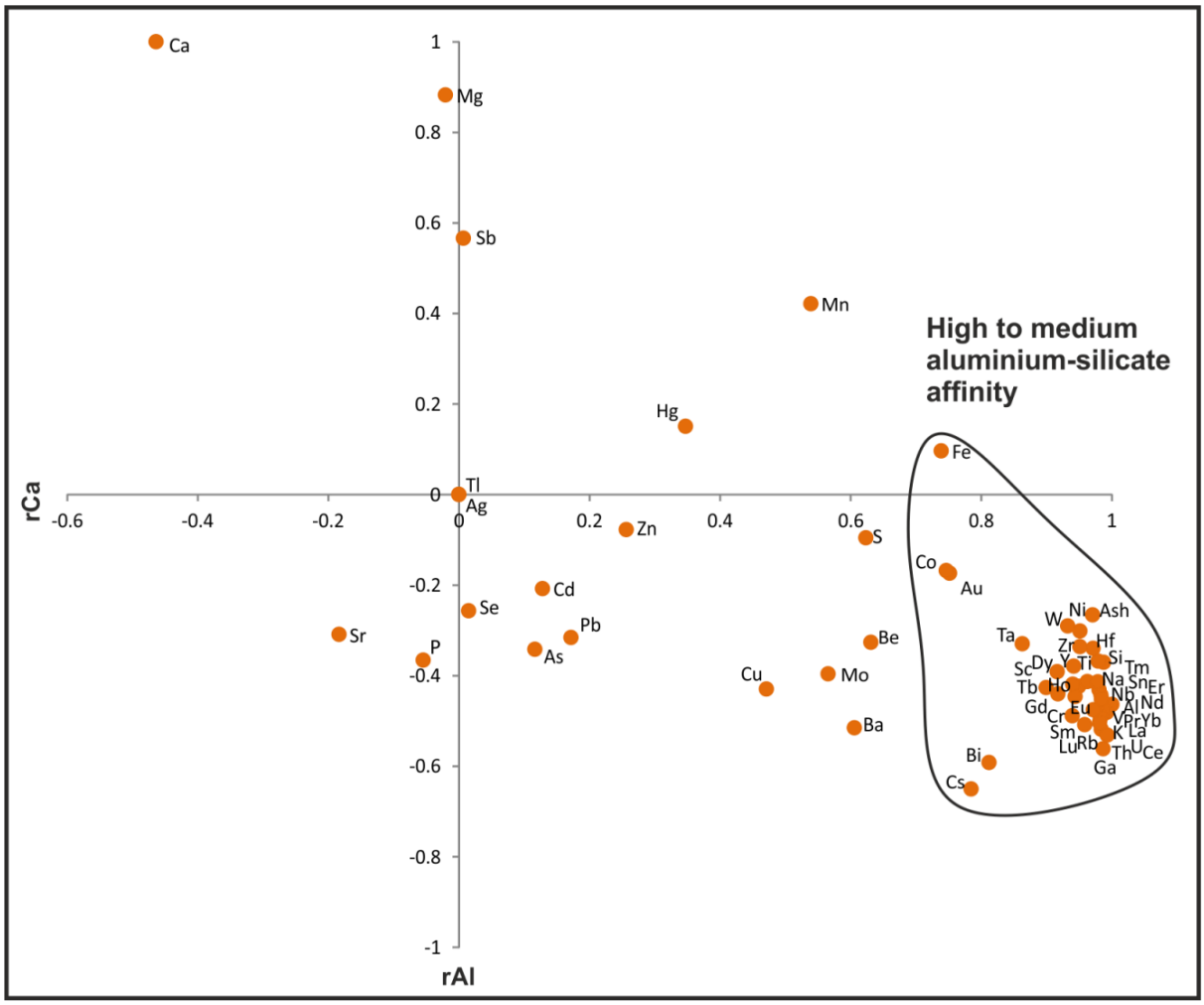

Figure 43 - Cross-plot correlation of the Pearson's correlation coefficients of the major and trace elements versus calcium and aluminium contents for bituminous coals from PBEB.

The carbonate minerals content is also high in these samples however, despite the good Mn/Mg correlation coefficient, only Ca, Mg and Sb show a carbonated affinity. Antimony (r_{Ca-Sb}= 0.57; r_{Mg-Sb}=0.64) is usually not referred with an occurrence in carbonates but as an accessory sulfide and an organic association (Orem and Finkelman, 2003). The Sb occurs as stibnite in hydrothermal deposits associated with minerals such as calcite and ankerite, this may be the explanation for the carbonate affinity of Sb. The igneous events that took place near this sector could have led to the enrichment of these elements in hydrothermal waters and consequently in this coals.

The elements that exhibit a major sulfur affinity include Si, Fe, Ti, Hf, Nb, Ta and Zr. Some of these elements in particular Hf, Nb, Ta and Zr are referred by Dai et al. (2015) as enriched as a result of coals being affected by hydrothermal solutions. In this particular case, even though these elements are found only slightly enriched and that some of them are not associated with sulfides, such as Hf and Zr, the percolation of enriched waters in these elements as a result of the magmatic events from W may explain its sulfur affinity and the transport to bituminous coals. The relationship between the Fe and St is 0.88, which indicates that iron sulfides occur in relevant amounts.

Anthracite coals

In the anthracite coals, a major number of elements has an organic (Sb and Zn) and intermediate (Ca, Mg, Fe, Mn, P, total S, Ag, As, Au, Be, Bi, Cd, Co, Cu, Hg, Mo, Ni, Pb, Se, Sr, Ta, Tl, W, and Lu) affinities and therefore in these coals a greater part of the elements may be associated with the organic matter. As in the bituminous coals, the elements with inorganic and aluminum-silicate affinities are mostly coincident (K, Na, Ti, Ba, Be, Cr, Cs, Ga, Hf, Nb, Rb, Sc, Sn , Th, U, V, Y, Zr, La, Ce, Pr, Nd, Sm, Eu, Gd, Dy, Ho, Er, Tm and Yb), reflecting the clay minerals content.

Regarding the elements presenting a carbonate affinity (Fe, Mn, St, Ag, As, Cd, Co, Hg, Mo, Pb, Se and Zn), Fe and Mn indicate an occurrence of carbonates, such as ankerite or siderite. The same applies to the elements that show a sulfur affinity (Ca, Mg, Mn, Ag, As, Cd, Co, Hg, Mo, Pb and Zn) where As may be associated to the pyrite. However, some elements, such as Ag, As, Cd, Co, Hg, Mo, Pb and Zn, present both affinities which could be explained by the association of some carbonate and sulfide minerals. The association of these type of mineral matter may also explain why some elements to which is not attributed an occurrence in carbonates, such as Ag, Cd, Co, Hg, Mo, Pb and Zn, exhibit a carbonate affinity.

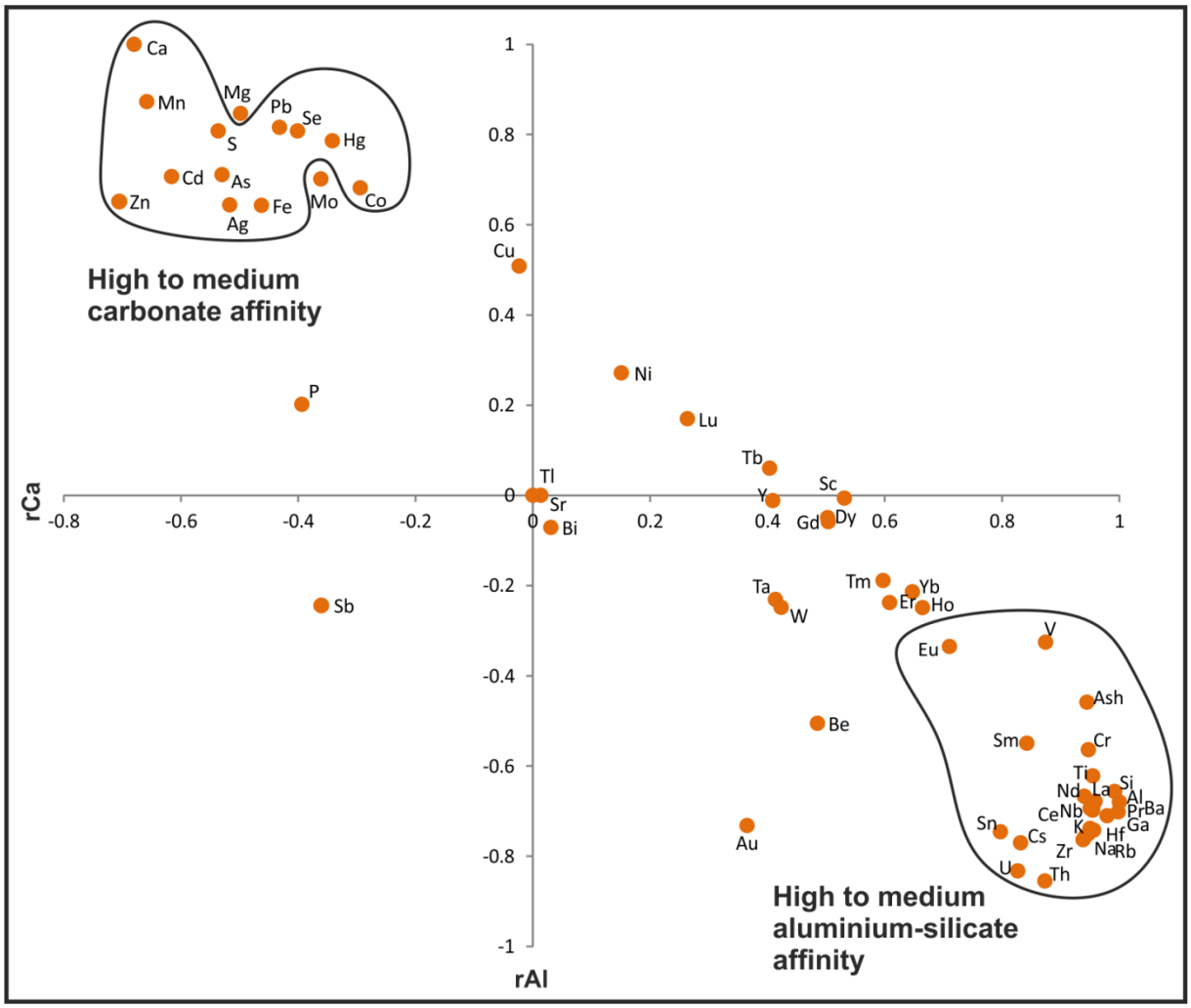

Figure 44 - Cross-plot correlation of the Pearson's correlation coefficients of the major and trace elements versus calcium and aluminium contents for anthracite coals from PBEB.

Regarding the elements presenting a carbonate affinity (Fe, Mn, St, Ag, As, Cd, Co, Hg, Mo, Pb, Se and Zn), Fe and Mn indicate an occurrence of carbonates, such as ankerite or siderite. The same applies to the elements that show a sulfur affinity (Ca, Mg, Mn, Ag, As, Cd, Co, Hg, Mo, Pb and Zn) where As may be associated to the pyrite. However, some elements, such as Ag, As, Cd, Co, Hg, Mo, Pb and Zn, present both affinities which could be explained by the association of some carbonate and sulfide minerals. The association of these type of mineral matter may also explain why some elements to which is not attributed an occurrence in carbonates, such as Ag, Cd, Co, Hg, Mo, Pb and Zn, exhibit a carbonate affinity.

In this sector of the basin As, Cs, Zn and Pb are significantly enriched. The As in coal is associated to the pyrite (Orem and Finkelman, 2003), the enrichment of this element is due to the high content of pyrite in the studied coals (r_{As-Fe} = 0.78 and r_{As-St} = 0.87) (Figure

45). Cs presents an aluminum-silicate affinity (r_{Al-Cs}= 0.83; r_{Si-Cs}=0.78), which is in accordance with one of the modes of occurrence indicated by Orem and Finkelman (2003). The enrichment in Pb and Zn is typically justified by the presence of galena and sphalerite, respectively, which is in accordance with the sulfur affinity. Pb shows a strong relationship with the total S (r_{Pb-St}= 0.92) and Se (r_{Pb-Se}= 0.71) thus it can possibly occur in galena or as PbSe (Orem and Finkelman, 2003). However, in the SEM-EDS analysis only an occurrence of PbSe and Pb was identified (Figure 45). Zn has a good correlation with total S (r_{Zn-St}= 0.81) and Fe (r_{Zn-Fe}= 0.54), confirming perhaps the occurrence as sphalerite (Orem and Finkelman, 2003). Moreover the occurrence of sphalerite in SEM-EDS analysis was identified (Figure 36-B).

In the Jianou anthracites, minerals such as galena and sphalerite were observed due to a magmatic intrusion, resulting in an enrichment of Pb and Zn (Ren et al., 2006). Therefore, given the similarities, the magmatic events which thermally affected the coals in this sector of the basin may also be responsible for the enrichment of these elements. Zn is often replaced by Ga in sphalerite (Swaine, 1990; Sun et al., 2007) which may explain a slight enrichment in this element.

Sc and V have an aluminum-silicate affinity (r_{Al-V}= 0.87; r_{Si-V}=0.80 and r_{Al-Sc}= 0.53; r_{Si-Sc}=0.56, respectively). Thus, although the CC is not high, the affinity is in accordance to the clay minerals association attributed by Orem and Finkelman (2003).

Rare earth element and yttrium (REY) exhibit higher CC in a larger number of samples in the coals from this sector. Yttrium may display enrichment as result of a phosphate-rich sedimentation source as well as the presence of TiO_2 minerals (Johnston et al., 2015). The Y enrichment as a result of TiO_2 minerals is confirmed since the coal samples that display higher contents of Ti also present higher CC for Y. Moreover Y and Ti show the same affinities, including inorganic and aluminum-silicate affinities for both sectors.

Therefore, the Y enrichment in the bituminous coals is probably a result of a phosphate-rich sedimentation source and possibly of enriched waters in these elements that leached from the W sector. On the other hand the enrichment in the anthracites is probably the result of a phosphate-rich sedimentation source and of the presence of TiO_2, presumably originated from the sedimentation influx (Figure 46) as well as of the magmatic events. As Ti is one of the elements that presents one of the higher percentages in the chemical constitution of dolerites (Zheng et al., 2007b), the magmatic rocks that resulted from the magmatic events, Y enrichment is not the result of a single geochemical process.

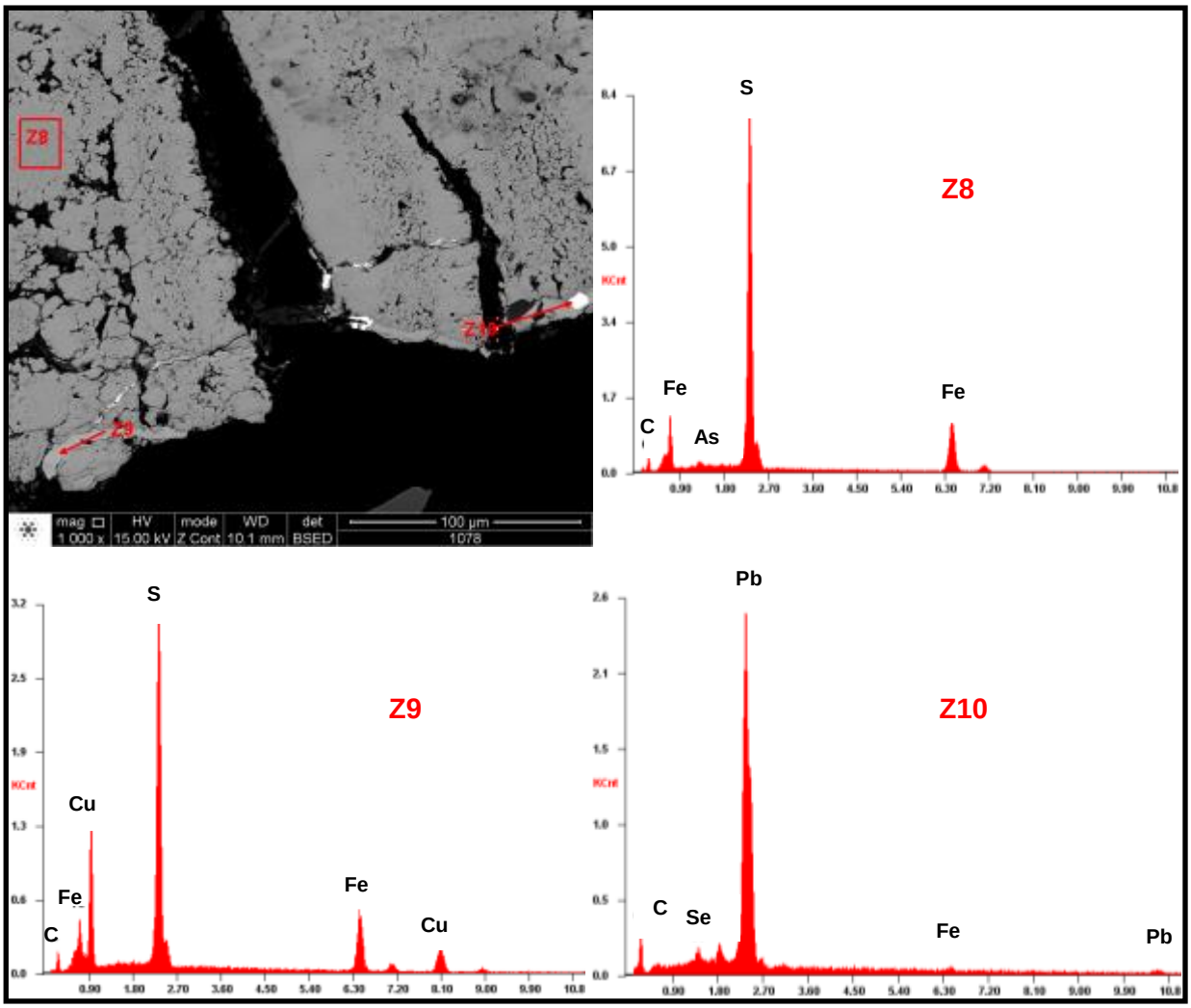

Figure 45 - SEM (BSE images) and EDS spectrum of pyrite (Z8), chalcopyrite (Z9) and PbSe (Z10) in sample 1078.

In the specific case of REEs they are strongly associated with the ash yield and the clay minerals, which is in agreement with the studies of Finkelman (1995) and Chou (1997). However, REEs shows a more inorganic affinity for the bituminous coals than for anthracites. The anthracites presents REEs with lower ash correlation coefficients, specifically the HREEs, moreover Lu displays an intermediate affinity. The REEs with organic affinity for anthracites may be the explanation for a more global enrichment than in the bituminous coals. This is in accordance with the information reported by Orem and Finkelman (2003) that the REEs may also present an organic association in coal.

In the anthracites only LREEs present an aluminum-silicate affinity, which is also in agreement with a more organic affinity in these coals, namely for HREEs. However this aluminum-silicate affinity also appears to reflect into a slight enrichment of the LREES compared to the HREEs. Therefore, the abundant REEs in the W sector appear to have two sources: one is due to the presence of clay minerals, resulting from the sedimentation source

and from authigenic origin (since authigenic kaolinite was observed in the anthracites (Figure 35-A) and it lead to an enrichment mainly of LREEs. This explanation is supported by Wang (2009) which reported that authigenic rhabdophane and kaolinite in the K8 Coal in the Changhe Mine of Sichuan Basin are the main carriers of the elevated REEs. The other source is a REEs absorption by organic matter resulting from the magmatic events, particularly for HREEs. Whereas in the bituminous coals the enrichment is probably a result of a phosphate-rich sedimentation source (Orem and Finkelman, 2003) and possibly of enriched waters in REEs that leached from the W sector.

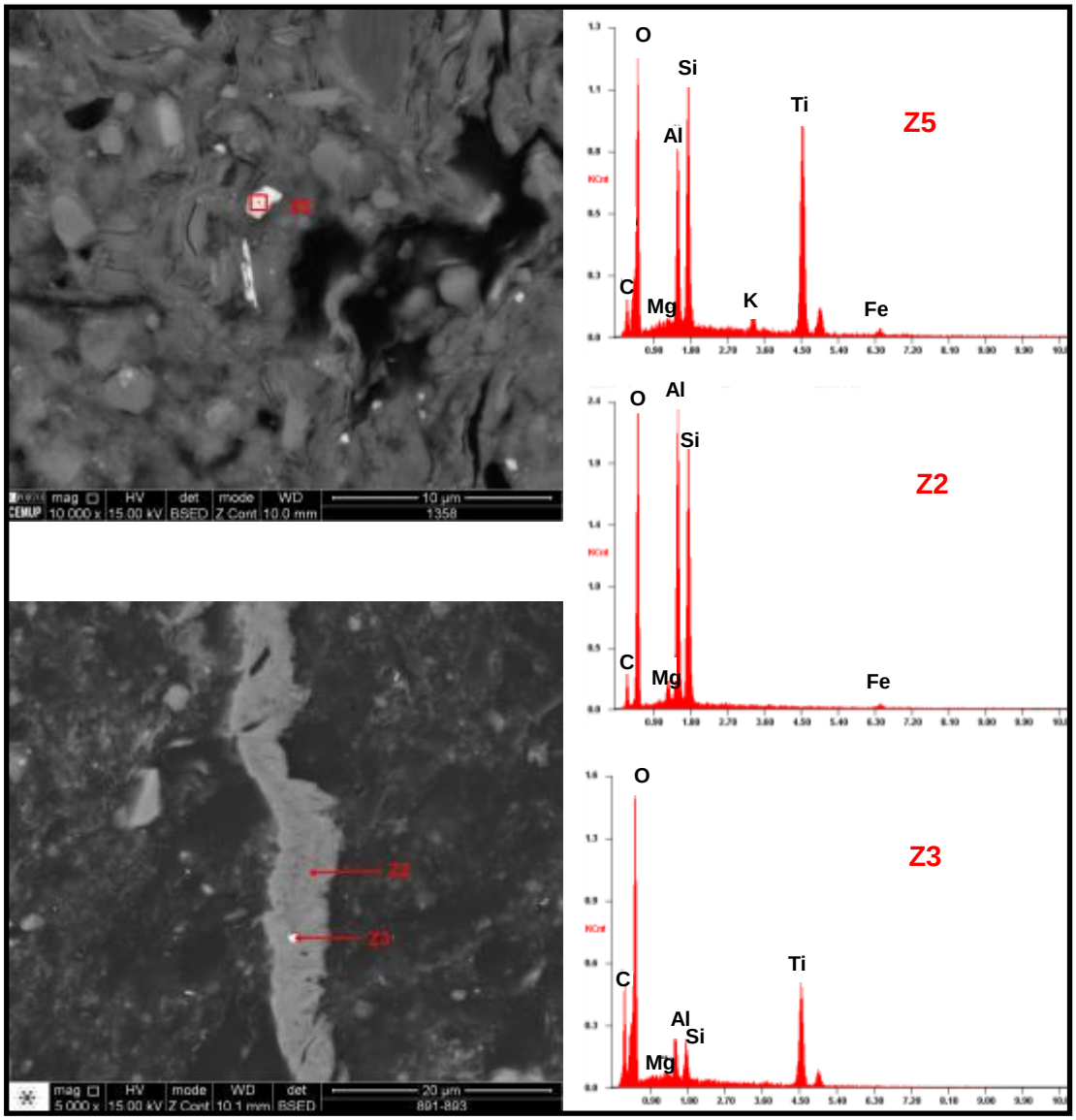

Figure 46 - SEM (BSE images) and EDS spectrum of Ti (Z5) associated with aluminum-silicate minerals in sample 1358 and kaolinite (Z2) associated with Ti (Z3) in sample 891/893.

Finally, with regards to the Hg element, which is given significance in this study, it has in both sectors an intermediate affinity and, in the case of the anthracites, it has a good relationship with Fe (0.69) and St (0.81), which may be an indicator of an occurrence in the pyrite (Orem and Finkelman, 2003).

6.3.3. Abundance and genetic consequences

The coals from the Peñarroya-Belmez-Espiel Basin display a considerable enrichment in all studied samples. However, through the intercorrelation diagrams designed for the two sectors, the enrichment appears to be higher and more global in anthracites. This conclusion seems to be supported by the projection of the elements average contents in the coals from each sector. With respect to geochemical affinities of elements with ash yield, they show that elements have a higher organic affinity for the anthracites, suggesting that a different genesis for these coals is responsible for the differences found between them, since the geological context was identical.

The rank of anthracites (Depocentre I) seems to have originated in the burial, as well as a magmatic activity that thermally affected the coals and also led to the formation of natural coke. This magmatic event appears to be the explanation for the enrichment of some elements in anthracites. They possibly have retained elements from the magmatic fluids and percolating waters enriched in them. This would also explain the fact that a large number of elements possess an organic affinity. Bituminous coals, of posterior origin (Depocentre II), also present some enrichment which may be the result of the leaching of some elements of the anthracites and subsequent transport by percolating waters to the coals deposited in the Depocentre II.

The enrichment can also be caused by the sedimentation source in both depocentres, as well as an event of post-tectonic origin probably associated with the implantation of an igneous body in depth (Marques, 1993). Hence, the enrichment has different genetic origins, being the result of several geochemical processes, but some show more evidence than others, as is the case of magmatic events.

6.4. Iberian Peninsula Carboniferous Basins

The three carboniferous basins studied (DCB, CAB and PEB) located in the Iberian Peninsula, although they all belong to the Carboniferous and share a geographical relationship, each of them has specific peculiarities. The characteristics exhibited by each of the basins are mainly determined by the different geological events that took place in each of

them. Enrichment of trace elements in these basins is mainly the result of mineralization by fluids circulation, whether it is by magmatic fluids or by low-temperature hydrothermal fluid source. DCB and PEB present a mineralization resultant from magmatic events, on the other hand CAB mineralization is due to a low-temperature hydrothermal fluid source.

Enrichment in REEs can occur, as can be observed in the CC in the coals from PEB, however this enrichment is not necessarily across all coalfields, as it is noticeable on the DCB and CAB. The enrichment of REEs is mainly related to the clay minerals, particularly by sedimentation processes and precipitation of authigenic minerals, but also to an organic association. The Y content seems somehow track the contents of the REEs, since in the three basins the Y enrichment occurred only where the REEs enrichment is also present, perhaps as a result of a phosphate-rich sedimentation source. The mercury enrichment turns out to be more global in all the basins, especially in DCB, and is strongly associated with the pyrite, but also has an organic association. Other elements such as As, also hazardous in the coal utilization processes, presents considerable concentration in all basins. The enrichment of Zn, Pb, Sb and Cs is more or less transversal to all basins as a result of hydrothermal fluids circulation.

Depending on the basin the conclusions differ, not only because their typology is different, but also because the data that was available was not absolutely similar. In CAB there is no data regarding the mineral matter content which difficult the geochemical affinities analysis. In the DCB the mineral matter content data was determined; however, mineralogical data is needed to support the interpretations. The SEM-EDS analysis performed in the PBEB proved to be a good methodology in order to identify the mineralogy and the mode of occurrence of the trace elements of the coals. However, given the large set of samples this technique was used only in some samples. To support all the interpretations mentioned above it is necessary further studies, mainly the mineralogical composition by using XRD and SEM-EDS.

Chapter 7 – Conclusions

7. Conclusions

The characterization of coals is relevant for geological, technological and industrial purposes, and, more recently, as unconventional deposits for REEs and other traces elements. Despite the economic importance of some elements in coals, some may also be harmful and hence an environmental hazard is associated with them. Considering the above, an integrated study of the organic and inorganic fractions, the definition of the geochemical affinities and the assessment of the enrichment/depletion and modes of occurrence of mercury and other trace elements in coals from the Carboniferous Basins of Iberian Peninsula were the main goals of this study. For this purpose, a set of 42 samples (5 from DCB, 19 from PBEB and 18 from the CAB) was selected, covering a wide range of bituminous and anthracite coals. The three Carboniferous Basins were characterized from a petrographic (maceral composition and vitrinite reflectance) and geochemical (proximate and ultimate analysis and composition in major and trace elements) point of view. Furthermore, the enrichment/depletion of trace elements was discussed as well as the geochemical affinities of the elements. The establishment of the relationship between the enrichment of elements present in coals and its mode of occurrence was also investigated.

Based on vitrinite reflectance the coals from DCB are classified as high rank A (anthracite A), whereas the coals from CAB range from medium rank C to A (bituminous C to A), with one sample being classified as high rank C coal (anthracite C). The coals from PBEB are grouped as medium rank D to C (bituminous D to C) and as high rank C to B coals (anthracite C to B). The petrographic analysis revealed that vitrinite is the major constituent of the organic fraction in all the studied coals, occurring mainly as telovitrinite in DCB and PBEB. Regarding the mineral matter, carbonates, specifically siderite and calcite, and sulfiides were identified for DCB. In the PBEB, the mineral matter comprises clay minerals, sulfiides and carbonates (calcite, siderite and ankerite), being ankerite often associated with oligonite and kutnohorite. Fractures and thermal effects were also identified in both basins, but more often in DCB.

The proximate and ultimate analysis data is in agreement with the coals rank. The ash yield of the samples is also in accordance with the content of the mineral matter determined in the maceral analysis. The atomic H/C and O/C ratios of the coal samples in the Van Krevelen diagram is not always in accordance with the petrographic data for CAB and PBE.

The study of the geochemical composition revealed that some coals from the DCB can be considered as enriched in trace elements according to their concentration coefficient (CC), especially mercury in sample 15, which exhibit an unusual enrichment (CC> 100).

Some coal samples from CAB present CC considered as significantly enriched for As, Cu, Pb, Sb and Zn; however, considering that the enrichment is only punctual, the basin is not considered enriched. The higher CC is displayed in the PBE basin, particularly for the anthracite coals, where economic viable elements as REEs and Y are slightly enriched. Mercury and As, both hazardous elements, present considerable CC in all basins. The enrichment of trace elements in these basins is mainly the result of mineralization by fluids circulation.

Regarding the geochemical affinities, Bi reveals an organic affinity in DCB, whereas in the anthracites PBEB an organic affinity is presented for Sb, Zn, and REEs. A geochemical association of the Hg, Se, Ni, As, Sb, Ag, Mo, Pb, Bi, U and Cr in CAB is thought to be related with a marine influence in some of the samples. For all the basins, the elements with an inorganic affinity appear to be in accordance with the elements that reveal an aluminium silicate affinity.

The study of the mineral matter together with the geochemical affinities allowed the identification of the mode of occurrence of some elements. Mercury seems to have a different mode of occurrence for each basin, revealing an organic association in the DCB, an association with cinnabar in the CAB and an association with pyrite in the PBEB. In the W sector of PBEB, the REEs occur in clay minerals and also in association with the organic fraction. The study of the mineralogical composition through SEM-EDS analysis was done to support and accurate the conclusions mentioned above.

From a geological point of view, it would be interesting to investigate a higher number of samples from DCB, in order to prove and identify the existence of different geochemical markers in each seam, and therefore to support the duplication of the sedimentary series.

Chapter 8 – Atlas

8. Atlas

This chapter aims to present some of the microscopic aspects of the studied samples from DCB and PBEB.

The petrographic composition of the coals was conducted, as mentioned previously, following standard procedures and the International Committee for Coal and Organic Petrology (ICCP) nomenclature and recommendations (ISO 7404-5, 2009; ICCP, 1998, 2001; Pickel et al., 2015). The petrographic photomicrographs presented were taken in reflected white and fluorescent lights using an oil objective and a Leica DM4000 microscope equipped with a Discus software from Technisches Büro Hilgers at the Department of Geosciences, Environment and Spatial Planning, Faculty of Sciences, University of Porto.

The SEM images and respective EDS spectrum of the mineral phases were performed using an FEI Quanta 400FEG environmental scanning electron microscope (ESEM), equipped with a EDAX Genesis X4M energy dispersive spectroscopy (EDS) at the Materials Centre of the University of Porto (CEMUP).

Nomenclatures:

- Incident blue light (fluorescence mode) – FM;
- Reflect light – RL;
- Collotelinite (Ct);
- Collodetrinite (Cd);
- Vitrodetrinite (Vdet);
- Fusinite (F);
- Semifusinite (Sf);
- Inertodetrinite (Id);
- Funginite (Fg);
- Macrinite (Ma);
- Micrinite (Mi);
- Sporinite (Sp);
- Cutinite (Cut);
- Resinite (R);
- Carbonates (Carb);
- Clays (Clay);
- Pyrite (Py).

8.1. Atlas of Optical Microscopy

8.1.1. Douro Carboniferous Basin

8.1.1.1. Sample 15 – Seam UTS B1

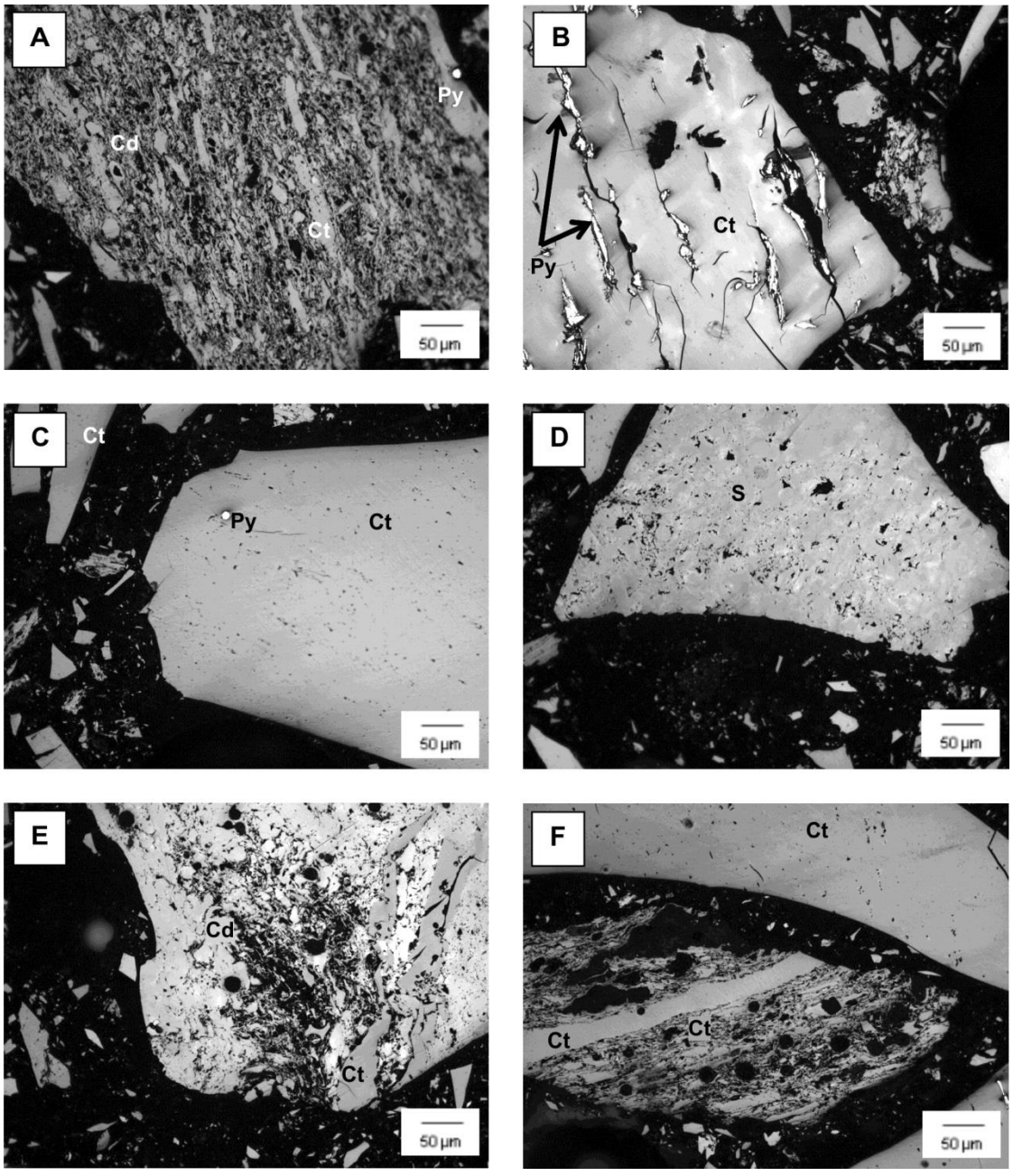

A – Collodetrinite (Cd), collotelinite (Ct) and pyrite (Py) - RL.

B – Collotelinite (Ct) and pyrite (Py) filling the cracks - RL.

C – Collotelinite (Ct) and pyrite (Py) in the right and organic particles with collotelinite (Ct) in the top - RL.

D – Semifusinite (Sf) - RL.

E – Collodetrinite (Cd), collotelinite (Ct) and devolatilization vacuoles - RL.

F – Collotelinite (Ct) in the top and organic particle with collotelinite (Ct), collodetrinite (Cd) and devolatilization vacuoles in the bottom - RL.

8.1.1.2. Sample 274 – Seam UTS B1

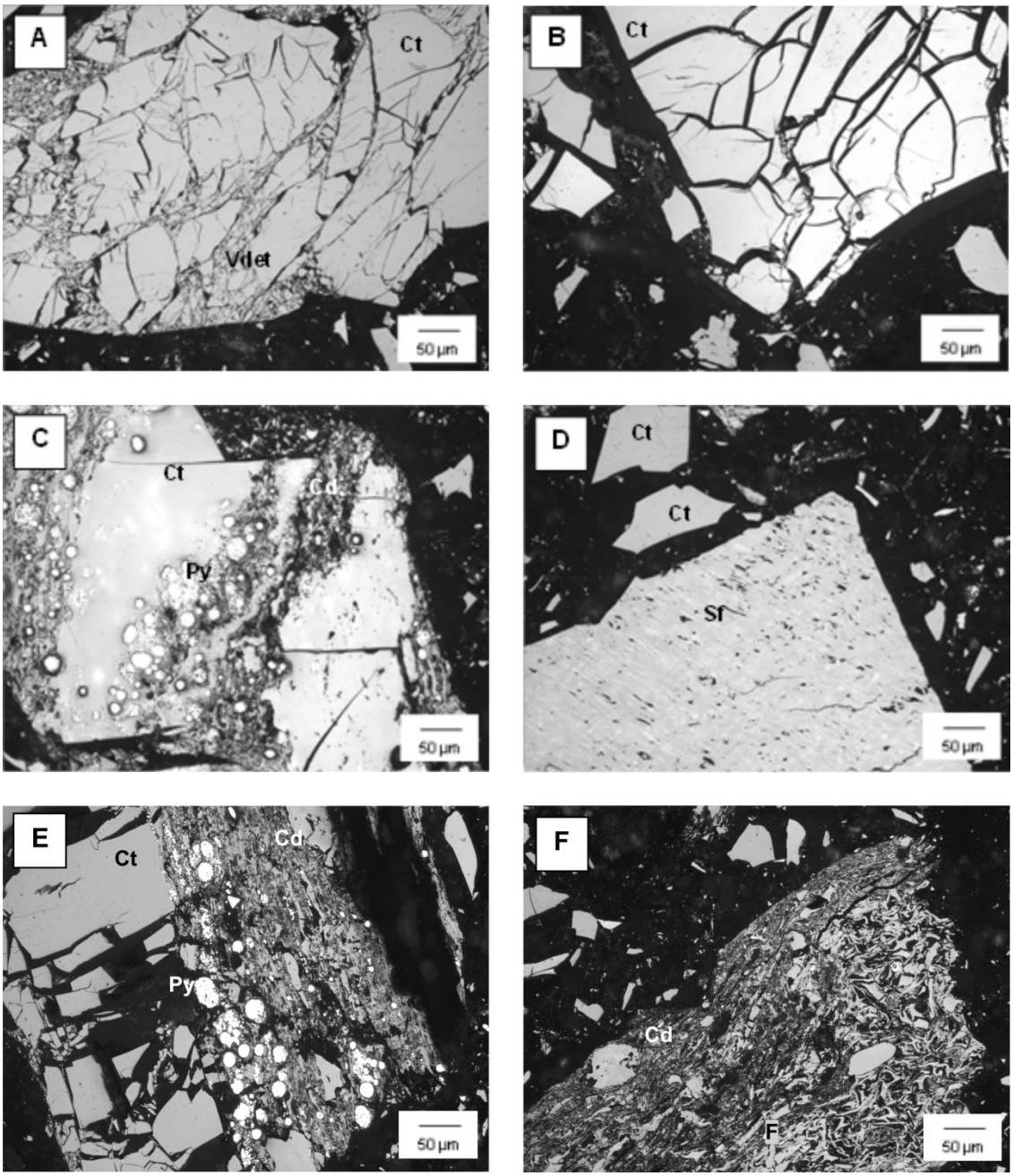

A – Collotelinite (Ct) and vitrodetrinite (Vdet) - RL.

B – Collotelinite (Ct) and cracks - RL.

C – Collotelinite (Ct) collodetrinite (Cd) and framboidal pyrite (Py) - RL.

D – Collotelinite (Ct) and semifusinite (Sf) - RL.

E – Collotelinite (Ct) and cracks in the left and framboidal pyrite (Py) and collodetrinite (Cd) in the right - RL.

F – Collodetrinite (Cd) and fusinite (F) - RL.

8.1.1.3. Sample 108/116 – Seam UTS D2

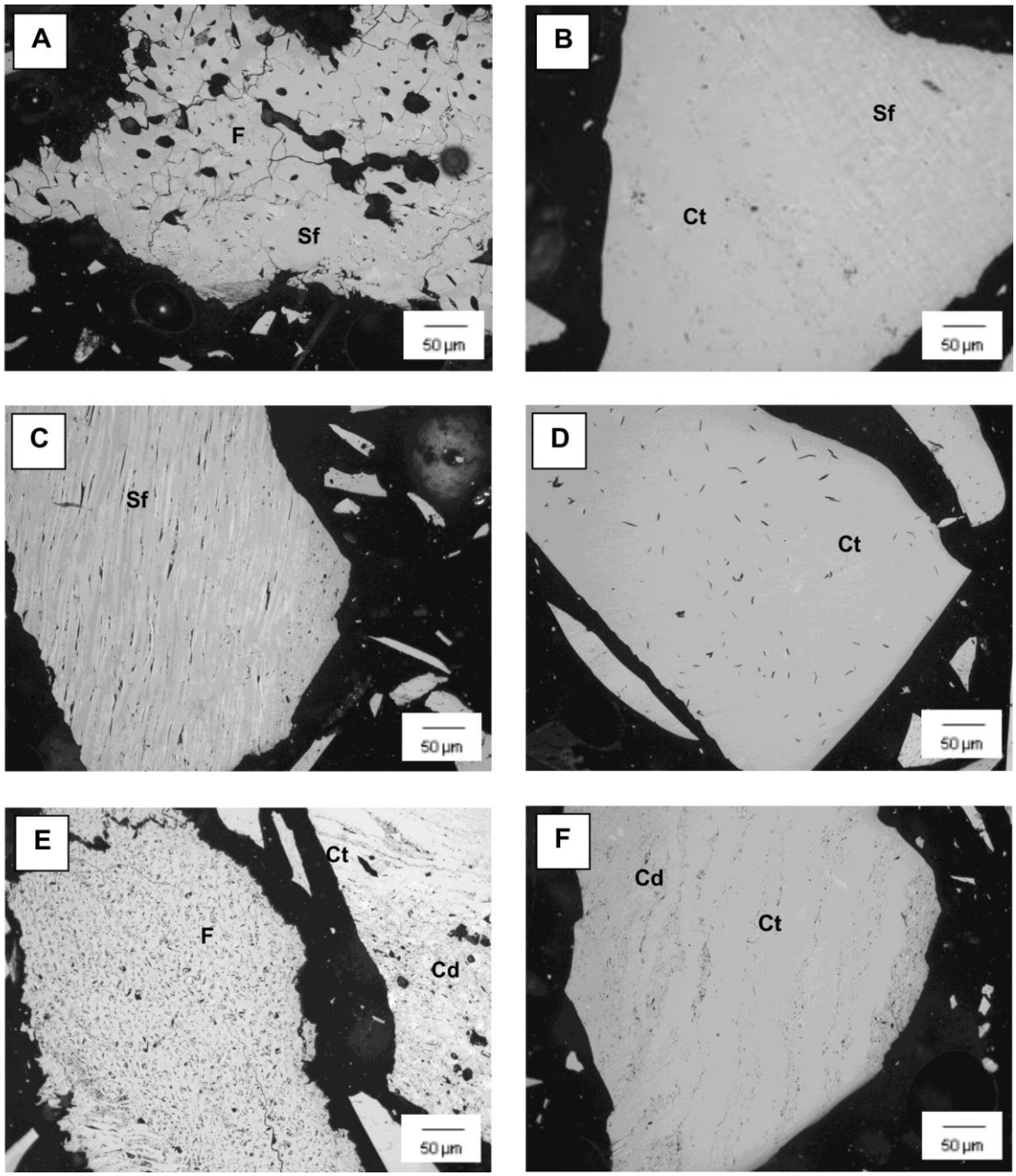

A – Fusinite (F) and semifusinite (Sf) - RL.

B – Collotelinite (Ct) and semifusinite (Sf) - RL.

C – Semifusinite (Sf) - RL.

D – Collotelinite (Ct) - RL.

E – Fusinite (F) in the left and collotelinite (Ct) and collodetrinite (Cd) in the right - RL.

F – Collotelinite (Ct) and collodetrinite (Cd) - RL.

8.1.1.4. Sample 721 – Seam UTS D2

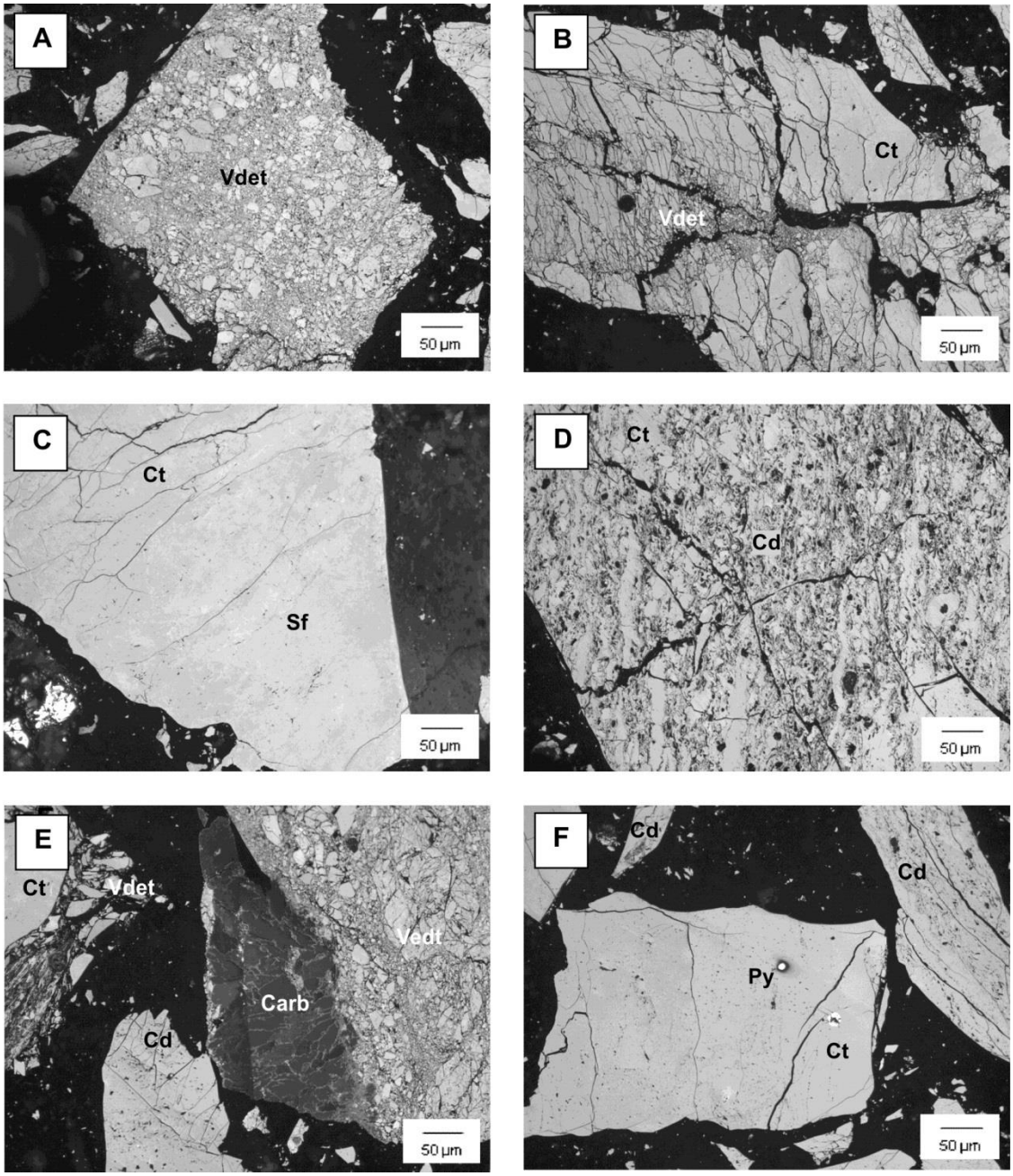

A – Vitrodetrinite (Vdet) - RL.

B – Collotelinite (Ct) and vitrodetrinite (Vdet) - RL.

C – Collotelinite (Ct) and semifusinite (Sf) - RL.

D – Collodetrinite (Cd), collotelinite (Ct) and devolatilization vacuoles - RL.

E – Collotelinite (Ct), vitrodetrinite (Vdet), collodetrinite (Cd) and carbonates (Carb) - RL.

F – Pyrite (Py), collotelinite (Ct) and collodetrinite (Cd) - RL.

8.1.1.5. Sample 77 – Seam Eastern Basin

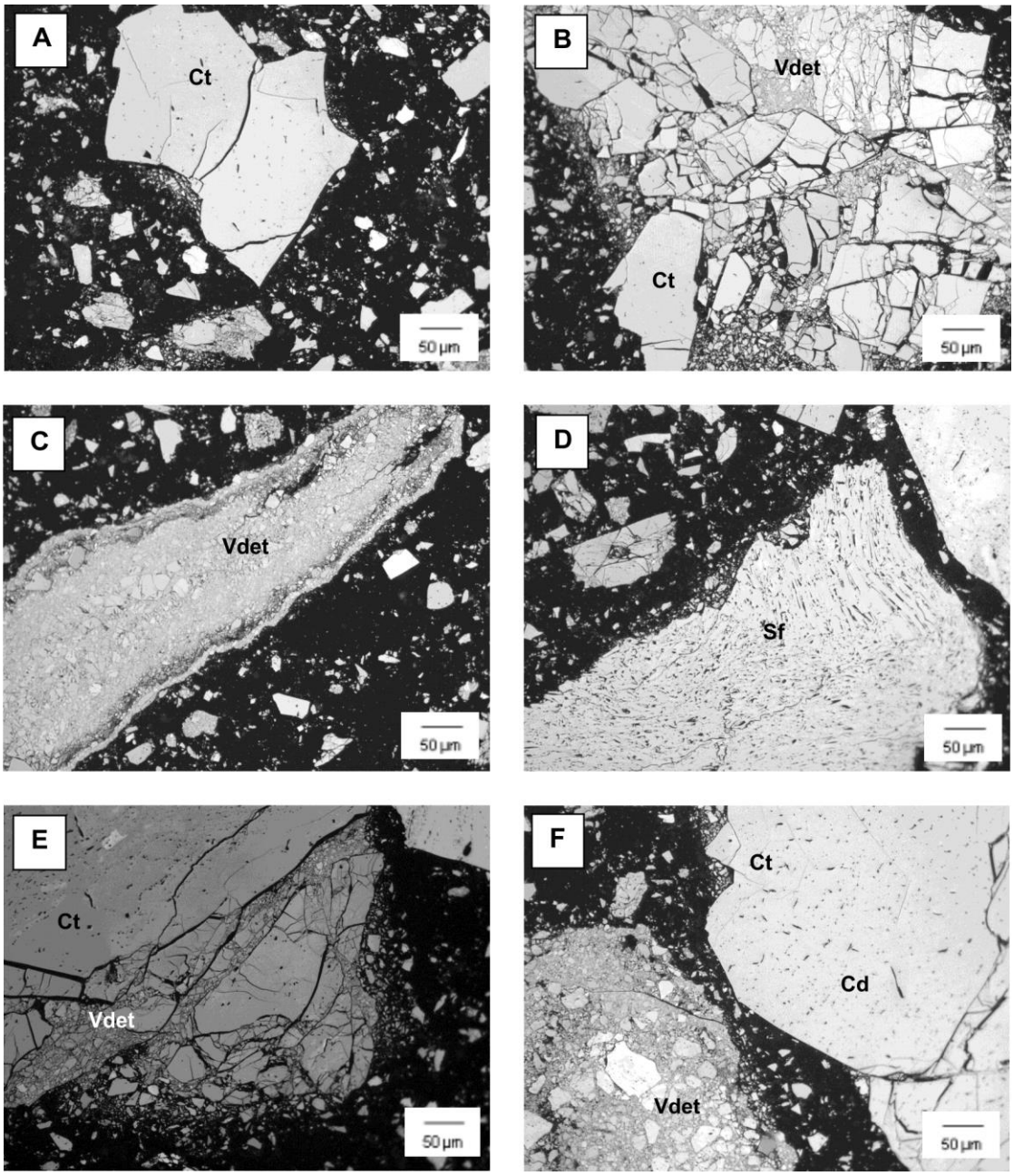

A – Collotelinite (Ct) and cracks - RL.

B – Organic particle of collotelinite (Ct) showing cracks (vitrodetrinite - Vdet) produced by tectonic. Note that the particles bounded by the cracks were not displaced relatively to each other - RL.

C – Vitrodetrinite (Vdet) - RL.

D – Semifusinite (Sf) - RL.

E – Organic particle of collotelinite (Ct) showing cracks (vitrodetrinite - Vdet) produced by tectonic. Note that the particles bounded by the cracks were not displaced relatively to each other - RL.

F – Vitrodetrinite (Vdet), collotelinite (Ct), collodetrinite (Cd) and cracks - RL.

8.1.2. Peñarroya-Belmez-Espiel Basin

8.1.2.1. Sample 2230 – Seam Candelaria

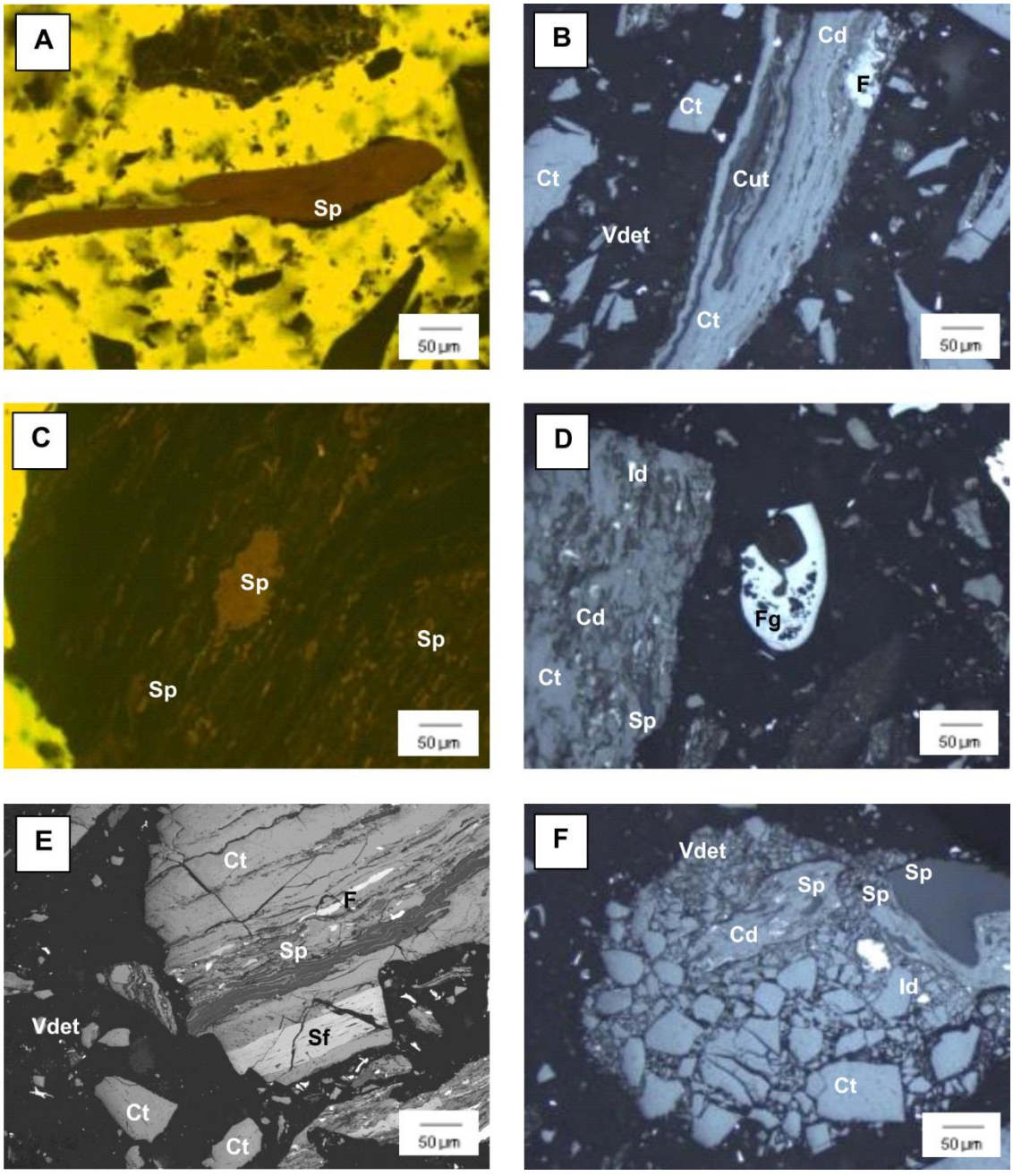

A – Sporinite (Sp) - FM.

B – Cutinite (Cut), fusinite (F), collodetrinite (Cd), collotelinite (Ct) and vitrodetrinite (Vdet) - RL.

C – Sporinite (Sp) - FM.

D – Fragment of funginite (Fg) and collodetrinite (Cd), collotelinite (Ct), sporinite (Sp) and inertodetrinite (Id) in the left - RL.

E – Semifusinite (Sf), fusinite (F), sporinite (Sp), collotelinite (Ct) and vitrodetrinite (Vdet) - RL.

F – Sporinite (Sp), collotelinite (Ct), colldetrinite (Cd), vitrodetrinite (Vdet) and inertodetrinite (Id) - RL.

8.1.2.2. Sample 2085 – Seam Candelaria

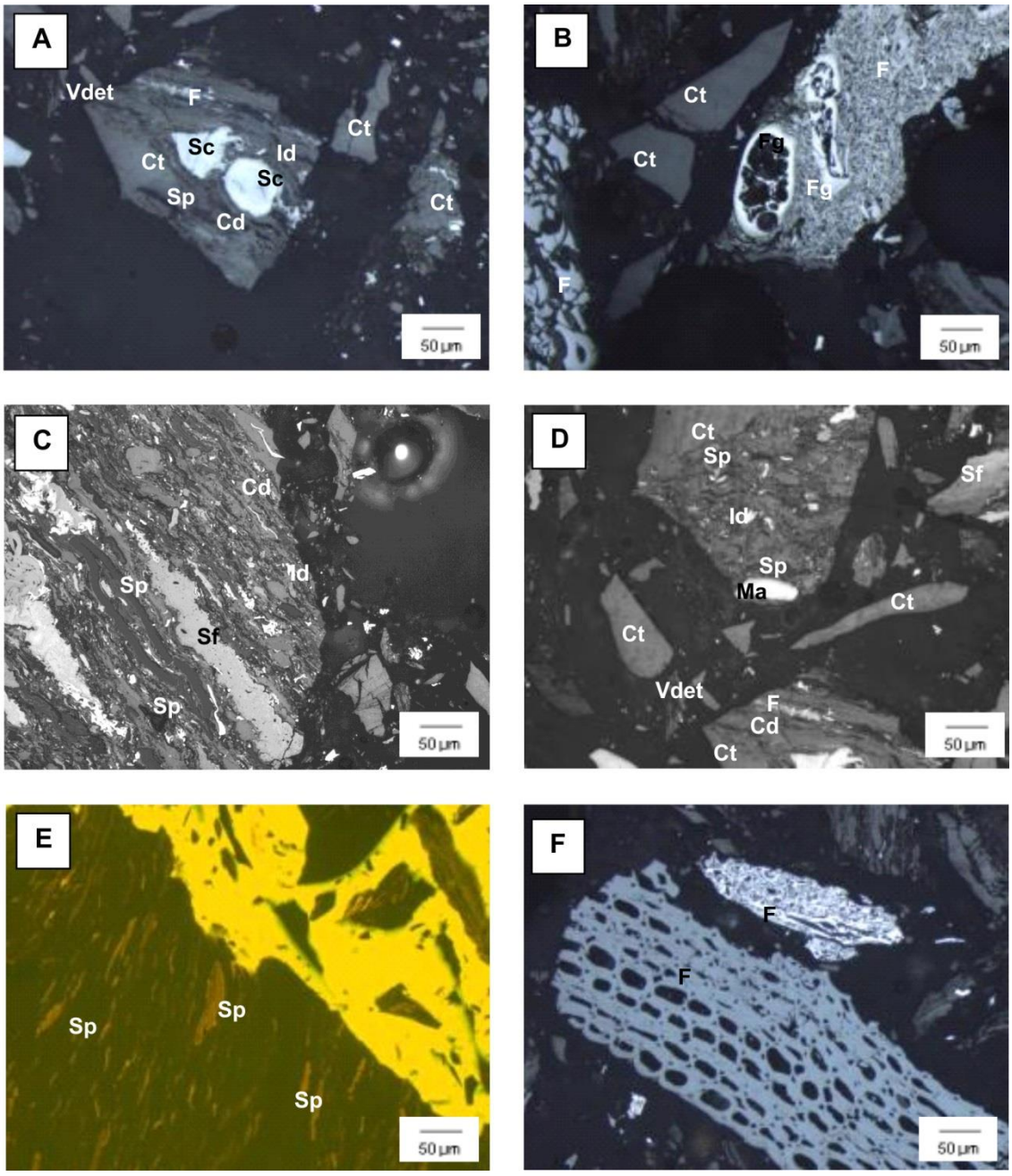

A – Sporinite (Sp), collodetrinite (Cd), collotelinite (Ct), fusinite (F), secretinite (Sc), inertodetrinite (Id) and vitrodetrinite (Vdet) - RL.

B – Funginite (Fg), fusinite (F) and collotelinite (Ct) - RL.

C – Sporinite (Sp), semifusinite (Sf), inertodetrinite (Id) and collodetrinite (Cd) - RL.

D – Vitrodetrinite (Vdet), collotelinite (Ct),collodetrinite (Cd) sporinite (Sp), semifusinite (Sf), fusinite (F), macrinite (Ma) and inertodetrinite (Id) - RL.

E – Sporinite (Sp) - FM.

F – Fusinite (F) - RL.

8.1.2.3. Sample 2229 – Seam Candelaria

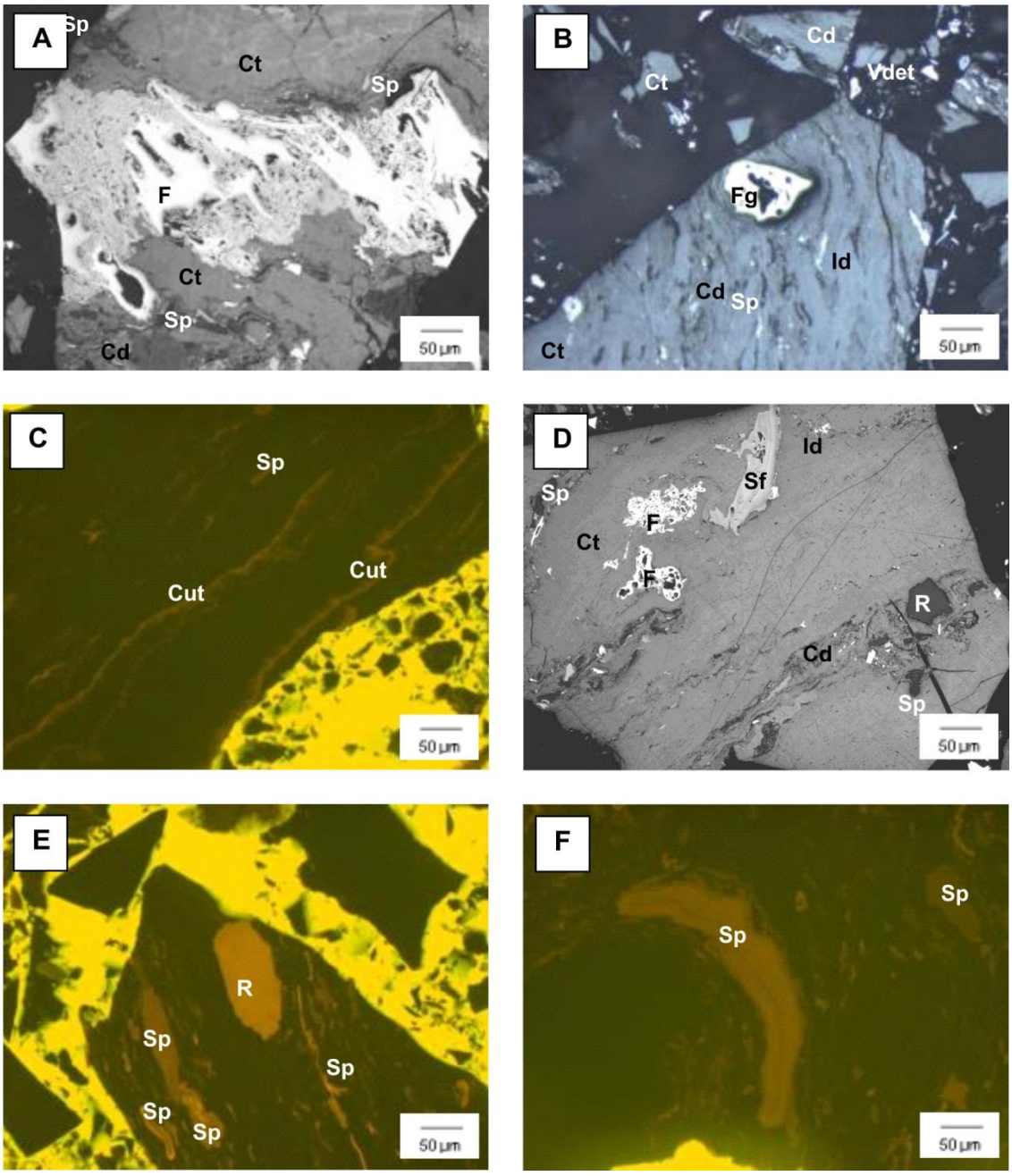

A – Sporinite (Sp), collodetrinite (Cd), collotelinite (Ct) and fusinite (F) - RL.

B – Funginite (Fg), inertodetrinite (Id), sporinite (Sp), collotelinite (Ct) and collodetrinite (Cd) and vitrodetrinite (Vdet) - RL.

C – Sporinite (Sp) and cutinite (Cut) - FM.

D – Resinite (R), sporinite (Sp), fusinite (F), semifusinite (Sf), collodetrinite (Cd), collotelinite (Ct) and inertodetrinite (Id) - RL.

E – Resinite (R) and sporinite (Sp) - FM.

F – Sporinite (Sp) - FM.

8.1.2.4. Sample 1377/1379 – Seam C4

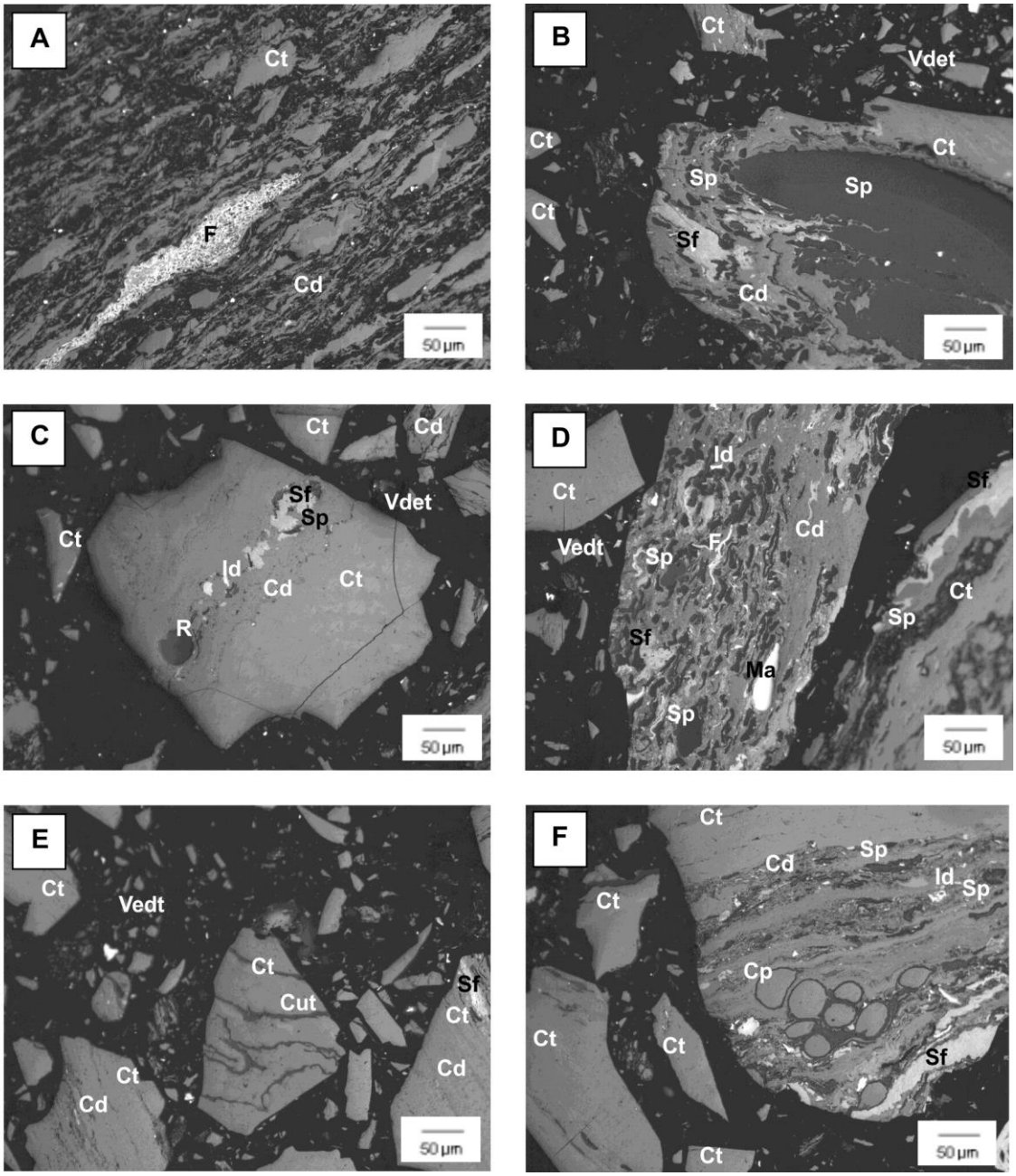

A – Collodetrinite (Cd), collotelinite (Ct) and fusinite (F) - RL.

B – Semifusinite (Sf), sporinite (Sp), collotelinite (Ct) and collodetrinite (Cd) and vitrodetrinite (Vdet) - RL.

C – Sporinite (Sp), semifusinite (Sf), collotelinite (Ct), inertodetrinite (Id), resinite (R) and collodetrinite (Cd) and vitrodetrinite (Vdet) - RL.

D – Macrinite (Ma), sporinite (Sp), fusinite (F), semifusinite (Sf), collodetrinite (Cd), collotelinite (Ct) and inertodetrinite (Id) and vitrodetrinite (Vdet) - RL.

E – Cutinite (Cut), c semifusinite (Sf), collotelinite (Ct), vitrodetrinite (Vdet) and collodetrinite (Cd) - RL.

F – Sporinite (Sp), corpogelinite (Cp), semifusinite (Sf), collodetrinite (Cd) and collotelinite (Ct) with collotelinite (Ct) and sporinite (Sp) in the left - RL.

8.1.2.5. Sample 1501/1502 – Seam C4

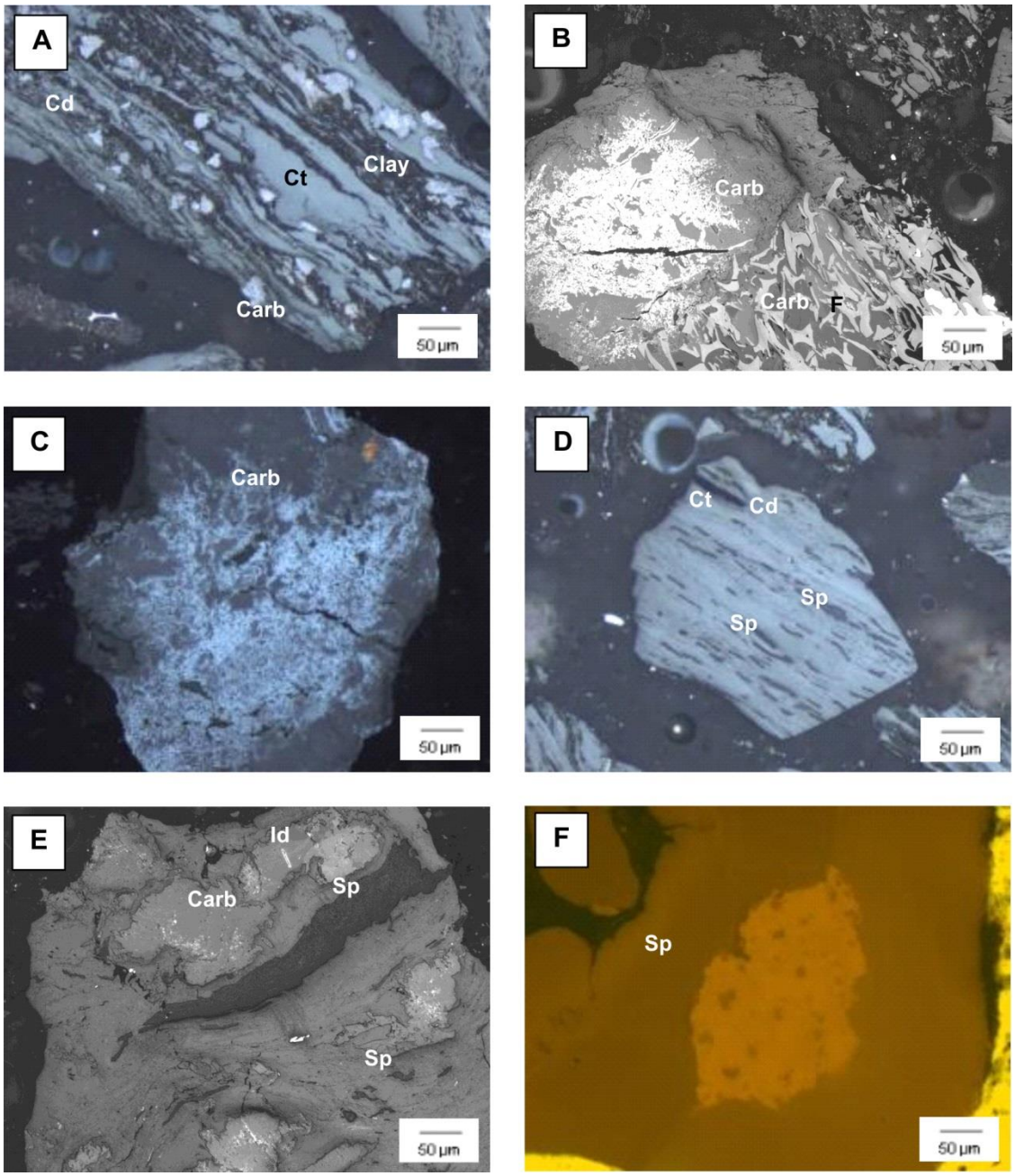

A – Collodetrinite (Cd), collotelinite (Ct), clay minerals (Clay) and carbonates (Carb), namely ankerite and oligonite - RL.

B – Carbonates (Carb), namely ankerite associated with kutnohorite, and gragment of fusinite (F) associated with carbonates (Carb) as well - RL.

C – Carbonate (Carb) particle and ankerite associated with kutnohorite - RL.

D – Sporinite (Sp), collodetrinite (Cd) and collotelinite (Ct) - RL.

E – Sporinite (Sp), inertodetrinite (Id) and carbonates (Carb), namely ankerite and oligonite - RL.

F – Sporinite (Sp) - FM.

8.1.2.6. Sample 1358 – Seam C3bis

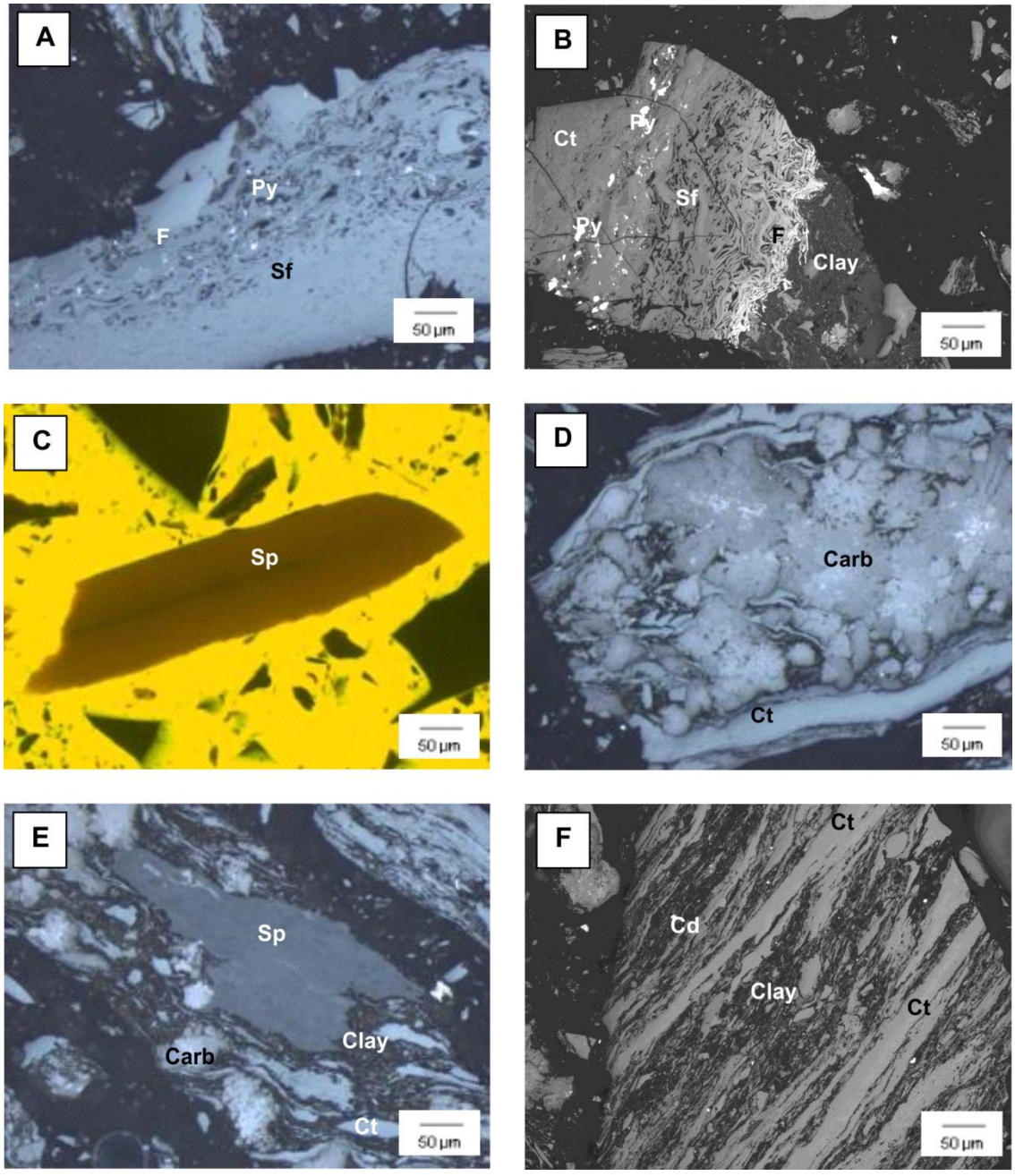

A – Fusinite (F), semifusinite (Sf) and pyrite (Py) - RL.

B – Transition between fusinite (F) and semifusinite (Sf), collotelinite (Ct), pyrite (Py) and clay minerals (Clay) - RL.

C – Sporinite (Sp) - FM.

D – Carbonates (Carb), namely ankerite and oligonite, and collotelinite (Ct) - RL.

E – Sporinite (Sp), forming a sporangium, clay minerals (Clay), carbonates (Carb), namely ankerite and oligonite, and collotelinite (Ct) – RL.

F – Clay minerals (Clay), collodetrinite (Cd) and collotelinite (Ct) - RL.

8.1.2.7. Sample 1476 – Seam C3bis

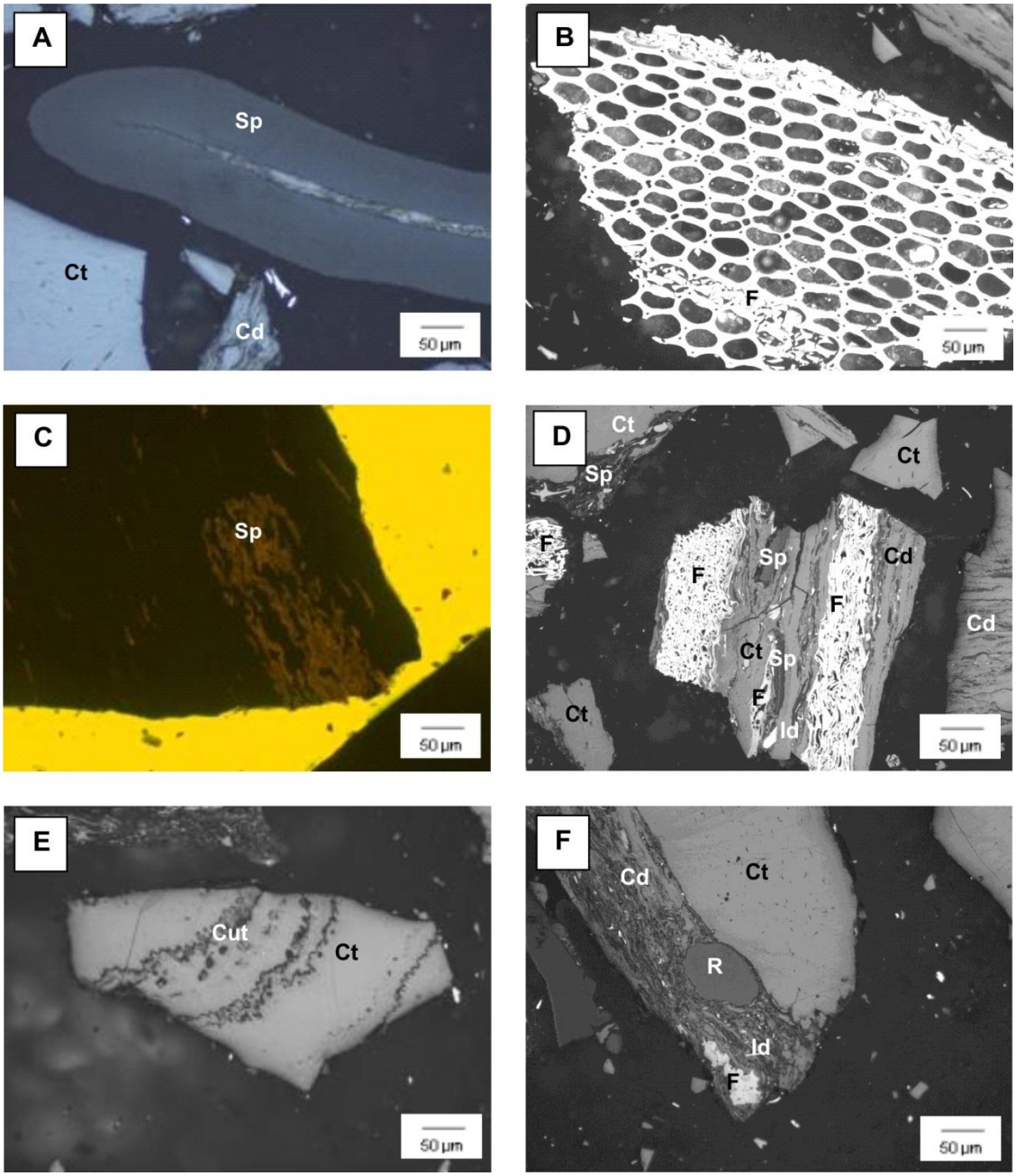

A – Sporinite (Sp), colotelinite (Ct) and collodetrinite (Cd) - RL.

B – Fusinite (F) - RL.

C – Sporinite (Sp), forming a sporangium - FM.

D – Sporinite (Sp), fusinite (F), inertodetrinite (Id), collotelinite (Ct) and collodetrinite (Cd) - RL.

E – Cutinite (Cut) and collotelinite (Ct) - RL.

F – Resinite (R), fusinite (F), inertodetrinite (Id), collodetrinite (Cd) and collotelinite (Ct) - RL.

8.1.2.8. Sample 1509 – Seam C1

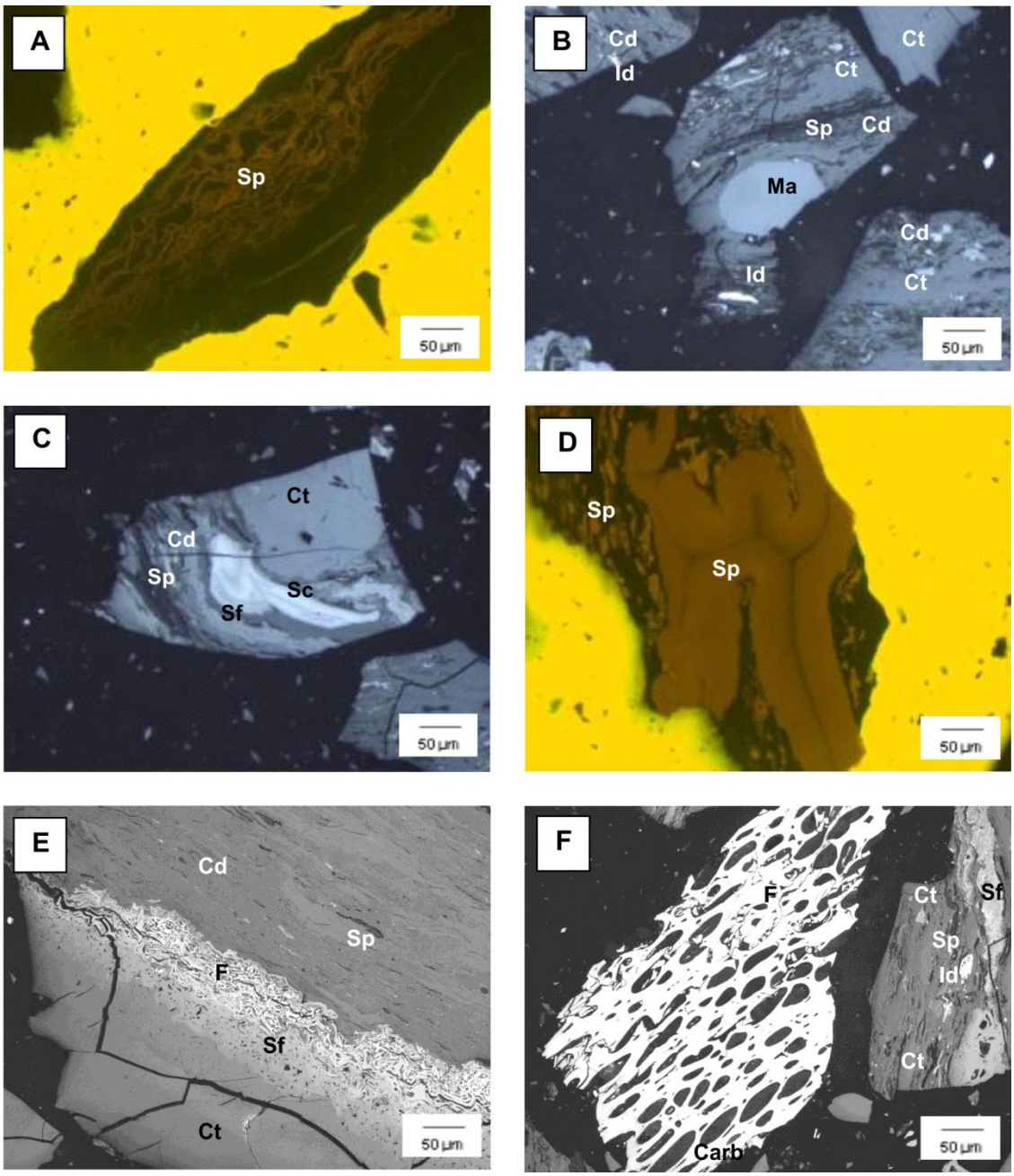

A – Sporinite (Sp) - FM.

B – Macrinite (Ma), inertodetrinite (Id), sporinite (Sp), collotelinite (Ct), collodetrinite (Cd) - RL.

C – Sporinite (Sp), secretinite (Sc), semifusinite (Sf), collodetrinite (Cd) and collotelinite (Ct) - RL.

D – Sporinite (Sp) - FM.

E – Transition between collodetrinite (Cd), semifusinite (Sf) and fusinite (F). Collodetrinite (Cd) and sporinite (Sp) - RL.

F – Fusinite (F) filled with carbonates (Carb) in the left and semifusinite (Sf), sporinite (Sp), collodetrinite (Cd), inertodetrinite (Id) and collotelinite (Ct) in the right - RL.

8.1.2.9. Sample 1511/1513 – Seam C1

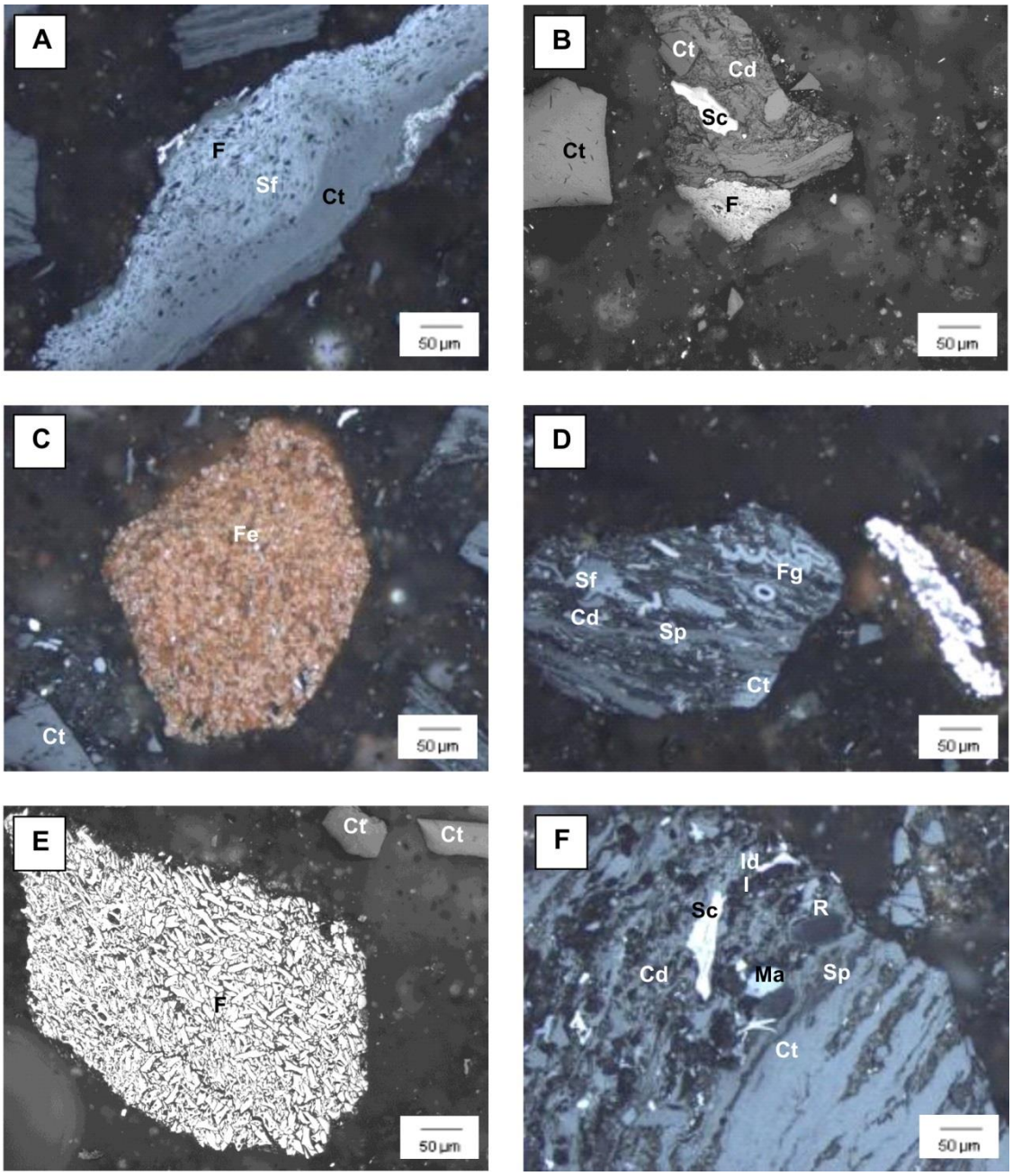

A – Fusinite (F), semifusinite (Sf) and collotelinite (Ct) - RL.

B – Fusinite (F), secretinite (Sc), collotelinite (Ct) and collodetrinite (Cd) - RL.

C – Iron oxides (Fe) and collotelinite (Ct) - RL.

D – Sporinite (Sp), semifusinite (Sf), funginite (Fg), collotelinite (Ct) and collodetrinite (Cd) - RL.

E – Fusinite (F) and collotelinite (Ct) - RL.

F – Sporinite (Sp), resinite (R), secretinite (Sc), macrinite (Ma), inertodetrinite (Id), collodetrinite (Cd) and collotelinite (Ct) - RL.

8.1.2.10. Sample 214/275 – Seam S. Rafael

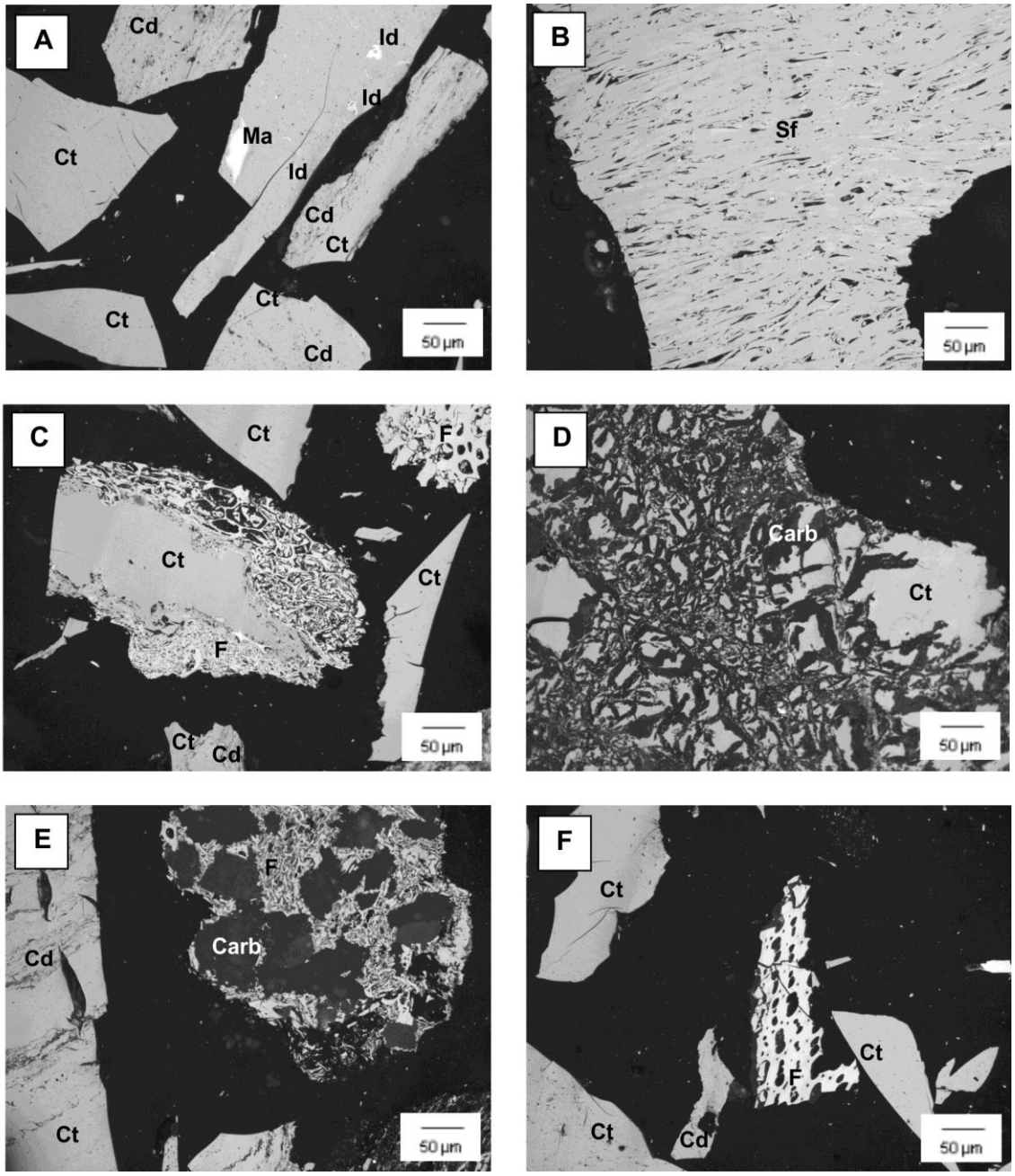

A – Collotelitine (Ct), collodetrinite (Cd), macrinite (Ma) and inertodetrinite (Id) - RL.

B – Semifusinite (Sf) - RL.

C – Fusinite (F), collotelinite (Ct) and collodetrinite (Cd) - RL.

D – Carbonates (Carb) and collotelinite (Ct) - RL.

E – Collotelinite (Ct) and collodetrinite (Cd) in the left and carbonates (Carb) and fusinite (F) in the center - RL.

F – Collotelinite (Ct), collodetrinite (Cd) and fusinite (F) - RL.

8.1.2.11. Sample 48/63 – Seam S. Rafael

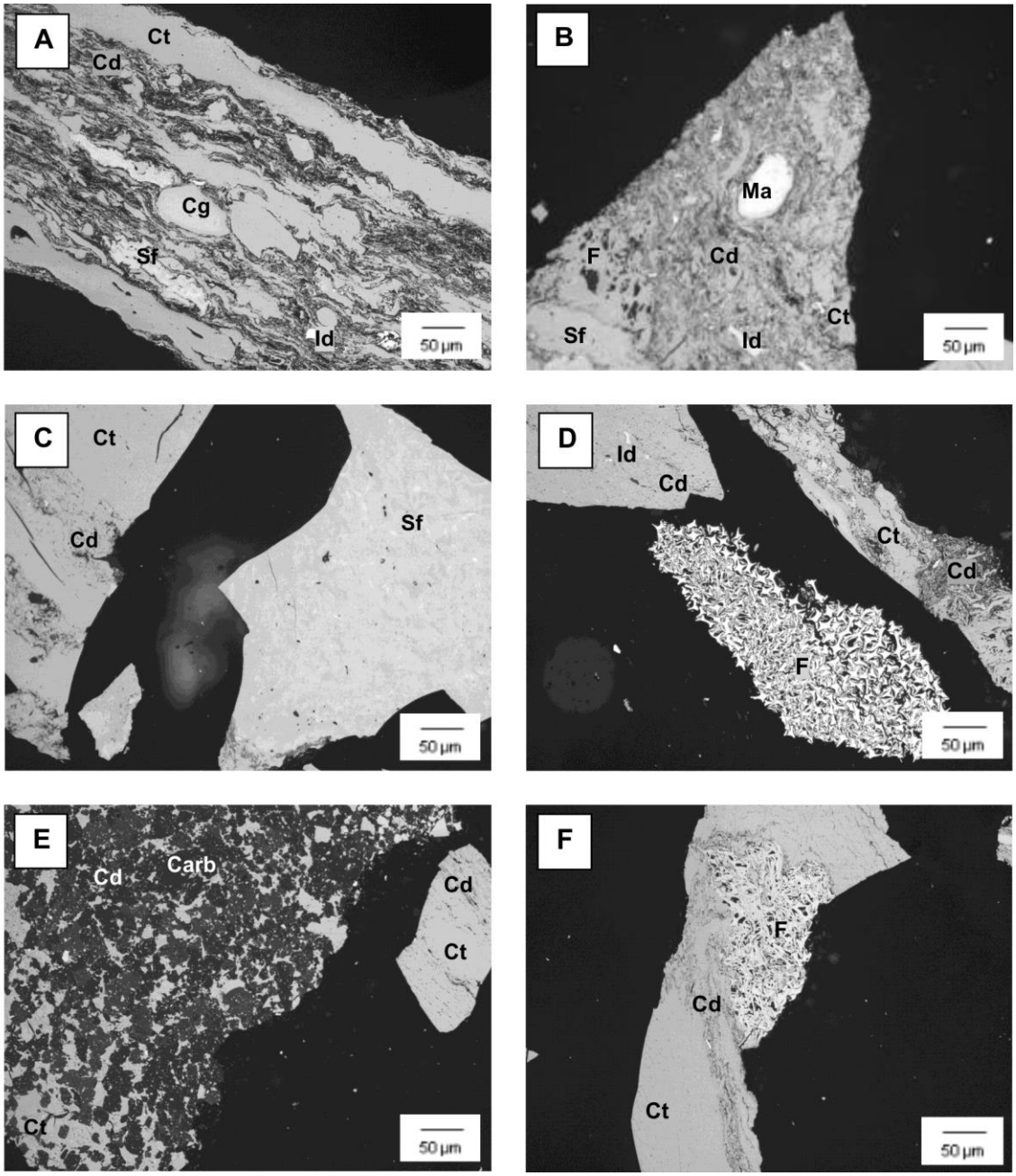

A – Collotelitine (Ct), collodetrinite (Cd), corpogelinite (Cg), semifusinite (Sf) and inertodetrinite (Id) - RL.

B – Collotelitine (Ct), collodetrinite (Cd), fusinite (F), semifusinite (Sf), macrinite (Ma) and inertodetrinite (Id) - RL.

C – Collotelinite (Ct) and collodetrinite (Cd) in the left and semifusinite (Sf) in the right - RL.

D – Collodetrinite (Cd), collotelinite (Ct), inertodetrinite (Id) and fusinite (F) - RL.

E – Collodetrinite (Cd) and mineral matter, namely carbonates (Carb), in the left and collodetrinite (Cd) and collotelinite (Ct) in the right - RL.

F – Collotelinite (Ct), collodetrinite (Cd) and fusinite (F) - RL.

8.1.2.12. Sample 712/715 – Seam Techo

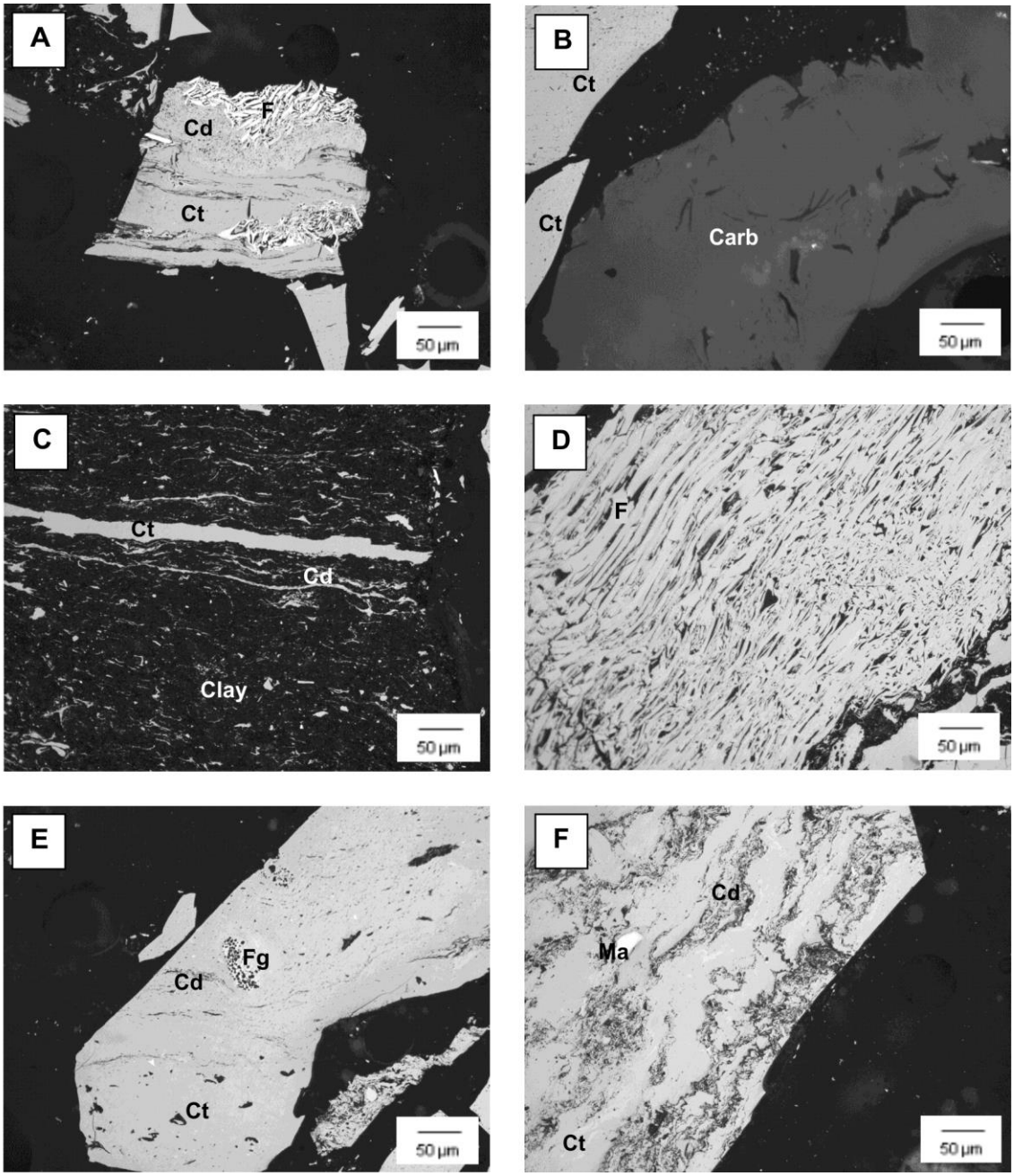

A – Collotelitine (Ct), collodetrinite (Cd) and fusinite (F) - RL.

B – Mineral matter, namely a carbonate (Carb), in the right and collotelitine (Ct) in the left - RL.

C – Collotelinite (Ct), collodetrinite (Cd) and mineral matter, namely clays (Clay) - RL.

D – Fusinite (F) - RL.

E – Collodetrinite (Cd), collotelinite (Ct) and funginite (Fg) - RL.

F – Collotelinite (Ct), collodetrinite (Cd) and macrinite (Ma) - RL.

8.1.2.13. Sample 705/708 – Seam Suelos

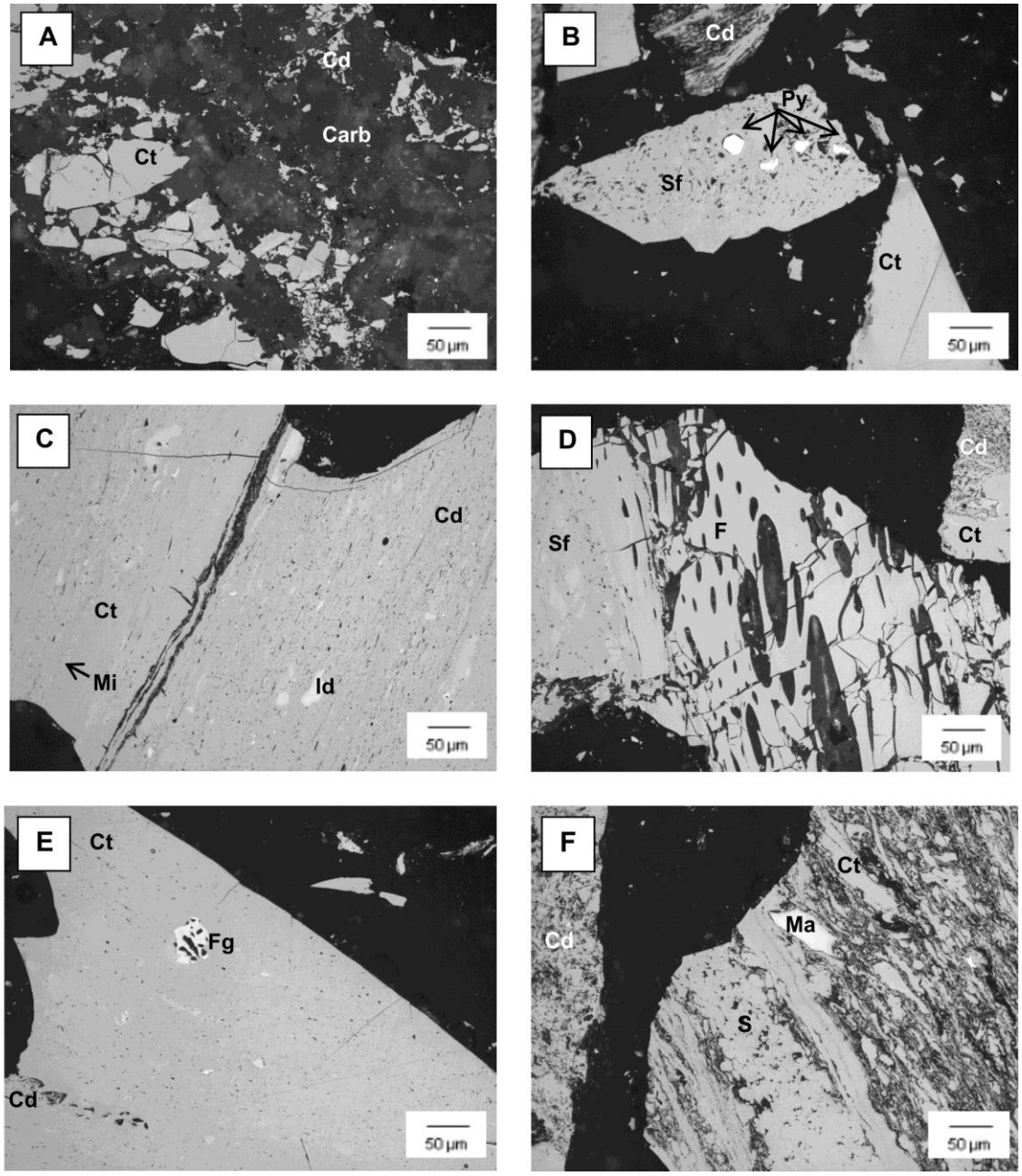

A – Epigenetic carbonates (Carb) agglomerating organic particles of collotelinite (Ct) and collodetrinite (Cd) - RL.

B – Semifusinite (Sf) particle with pyrite in the center and organic particles with collotelinite (Ct) and collodetrinite (Cd) - RL.

C – Collotelinite (Ct), collodetrinite (Cd), micrinite (Mi) and inertodetrinite (Id) - RL.

D – Transition between semifusinite (Sf) and fusinite (F) with the the celular lumens filled with carbonates (Carb). Collodetrinite (Cd) and collotelinite (Ct) in the right - RL.

E – Collodetrinite (Cd), collotelinite (Ct) and funginite (Fg) - RL.

F – Collotelinite (Ct), semifusinite (Sf), macrinite (Ma) and collodetrinite (Cd) - RL.

8.1.2.14. Sample 746/751 – Seam Muro

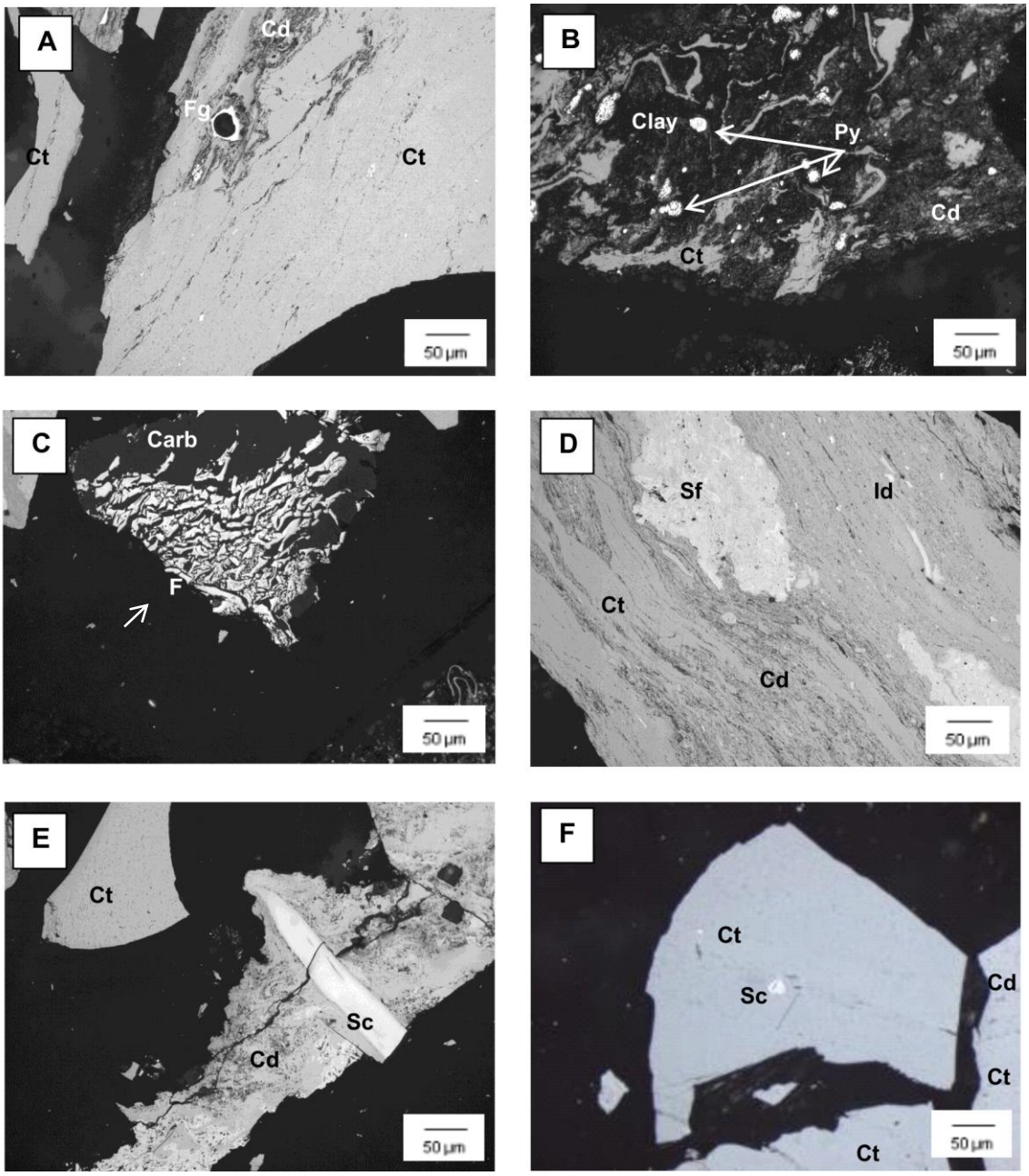

A – Collotelinite (Ct), collodetrinite (Cd) and funginite (Fg) and collotelinite (Ct) in the left - RL.

B – Pyrite (Py), clay minerals (Clay), collotelinite (Ct) and collodetrinite (Cd) - RL.

C – Mineral mater, namely carbonates (Carb), and fusinite (F) - RL.

D – Collotelinite (Ct), collodetrinite (Cd) semifusinite (Sf) and inertodetrinite (Id) - RL.

E – Collodetrinite (Cd), secretinite (Sc) and collotelinite (Ct) in the left - RL.

F – Collotelinite (Ct), secretinite (Sc) and collodetrinite (Cd) - RL.

8.1.2.15. Sample 894/896 – Seam Muro

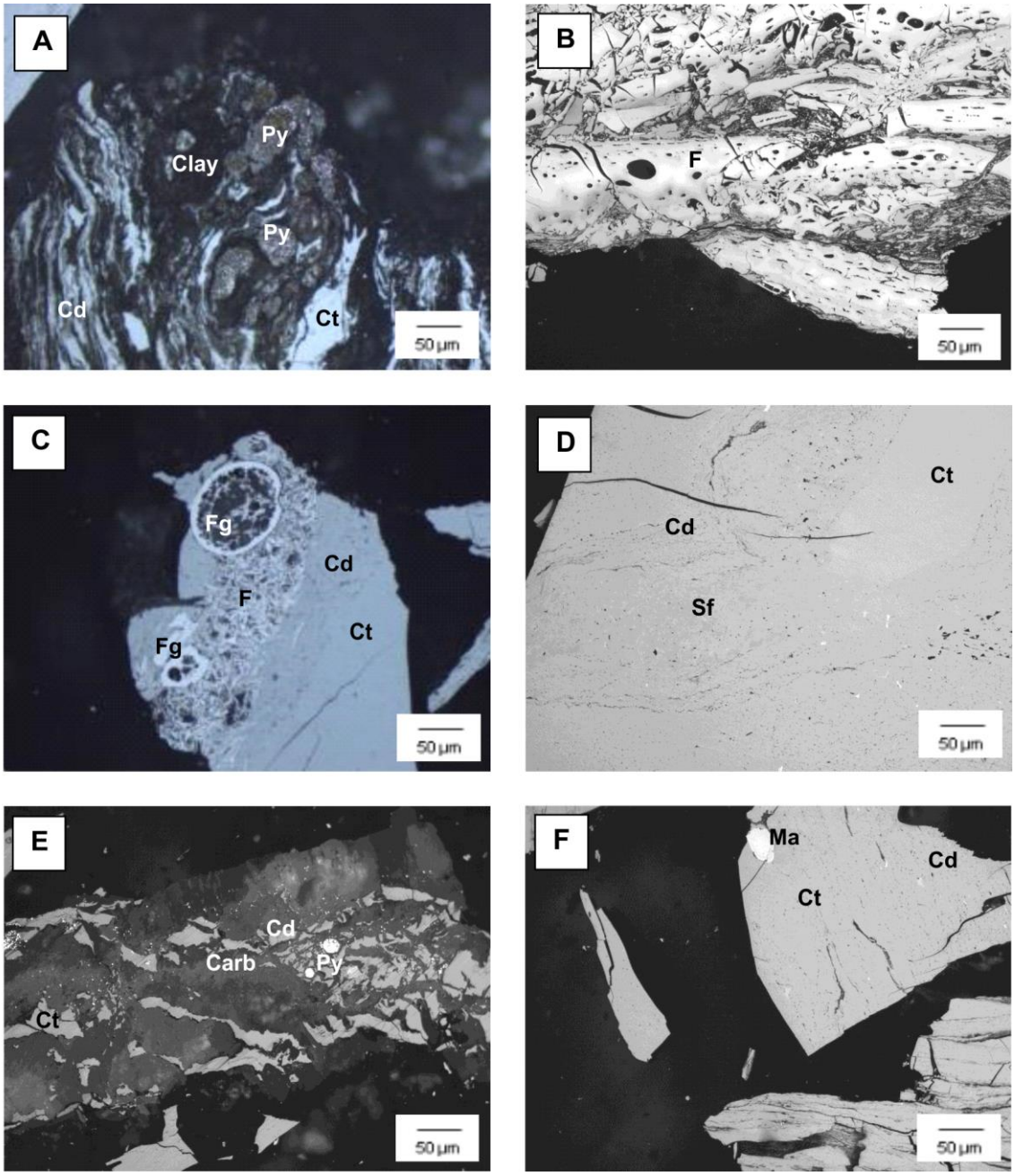

A – Collotelinite (Ct), collodetrinite (Cd), framboidal pyrite (Py) and clay minerals (Clay) - RL.

B – Fusinite (F) - RL.

C – Collotelinite (Ct), collodetrinite (Cd) fusinite (F) and funginite (Fg) - RL.

D – Collotelinite (Ct), collodetrinite (Cd) and semifusinite (Sf) - RL.

E – Framboidal pyrite (Py) and epigenetic carbonates agglomerating organic particles of collotelinite (Ct) and collodetrinite (Cd) - RL.

F – Collotelinite (Ct), collodetrinite (Cd) and macrinite (Ma) - RL.

8.1.2.16. Sample 752/754 – Seam I. Norte

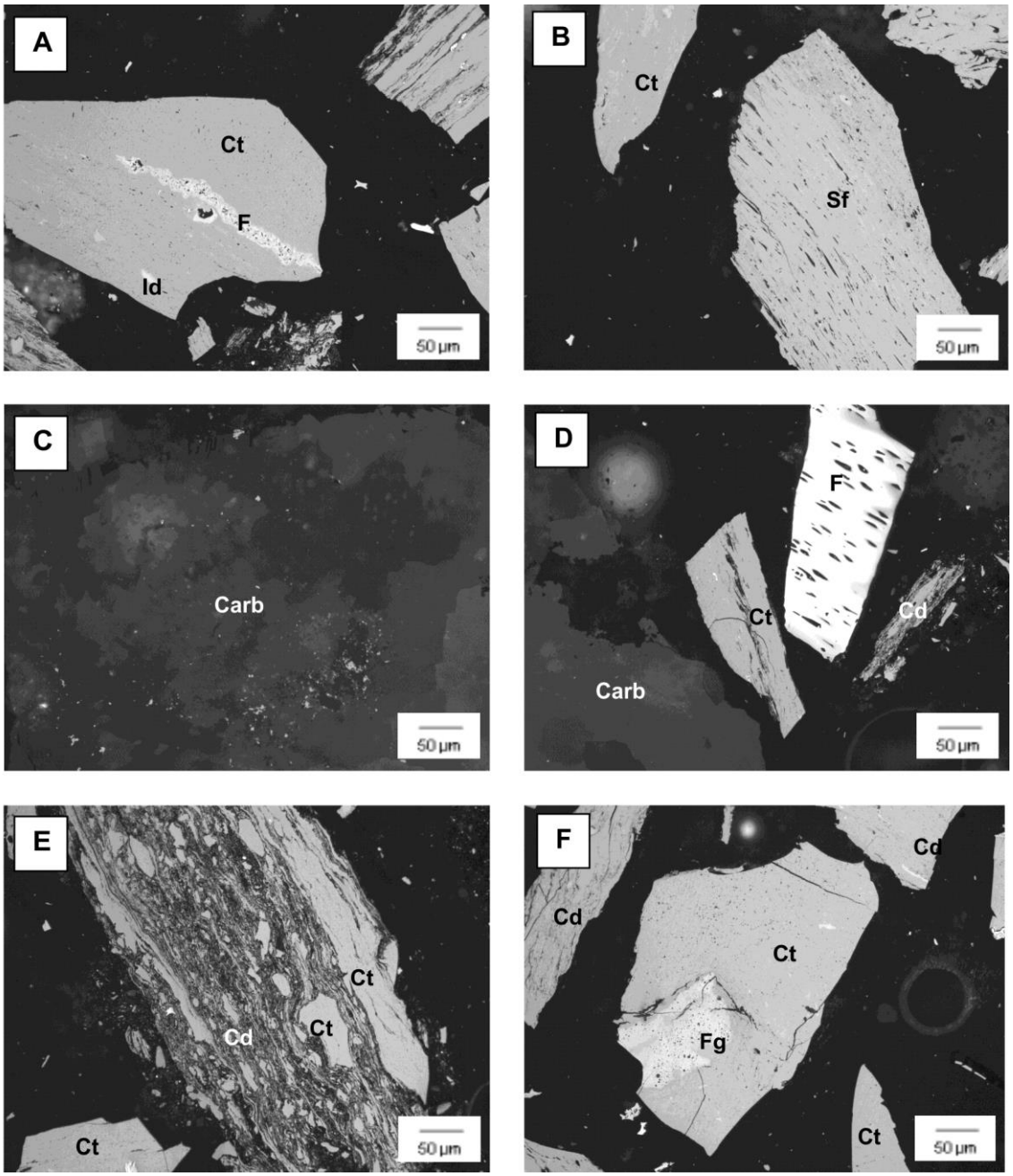

A – Collotelinite (Ct), fusinite (F) and inertodetrinite (Id) - RL.

B – Semifusinite (Sf) and collotelinite (Ct) - RL.

C – Mineral matter particle, minerals corresponds to carbonates (Carb) - RL.

D – Carbonates (Carb), collotelinite (Ct), fusinite (F) and collodetrinite (Cd) - RL.

E – Collotelinite (Ct) and collodetrinite (Cd) - RL.

F – Collotelinite (Ct), collodetrinite (Cd) and funginite (Fg) - RL.

8.1.2.17. Sample 891/893 – Seam I. Norte

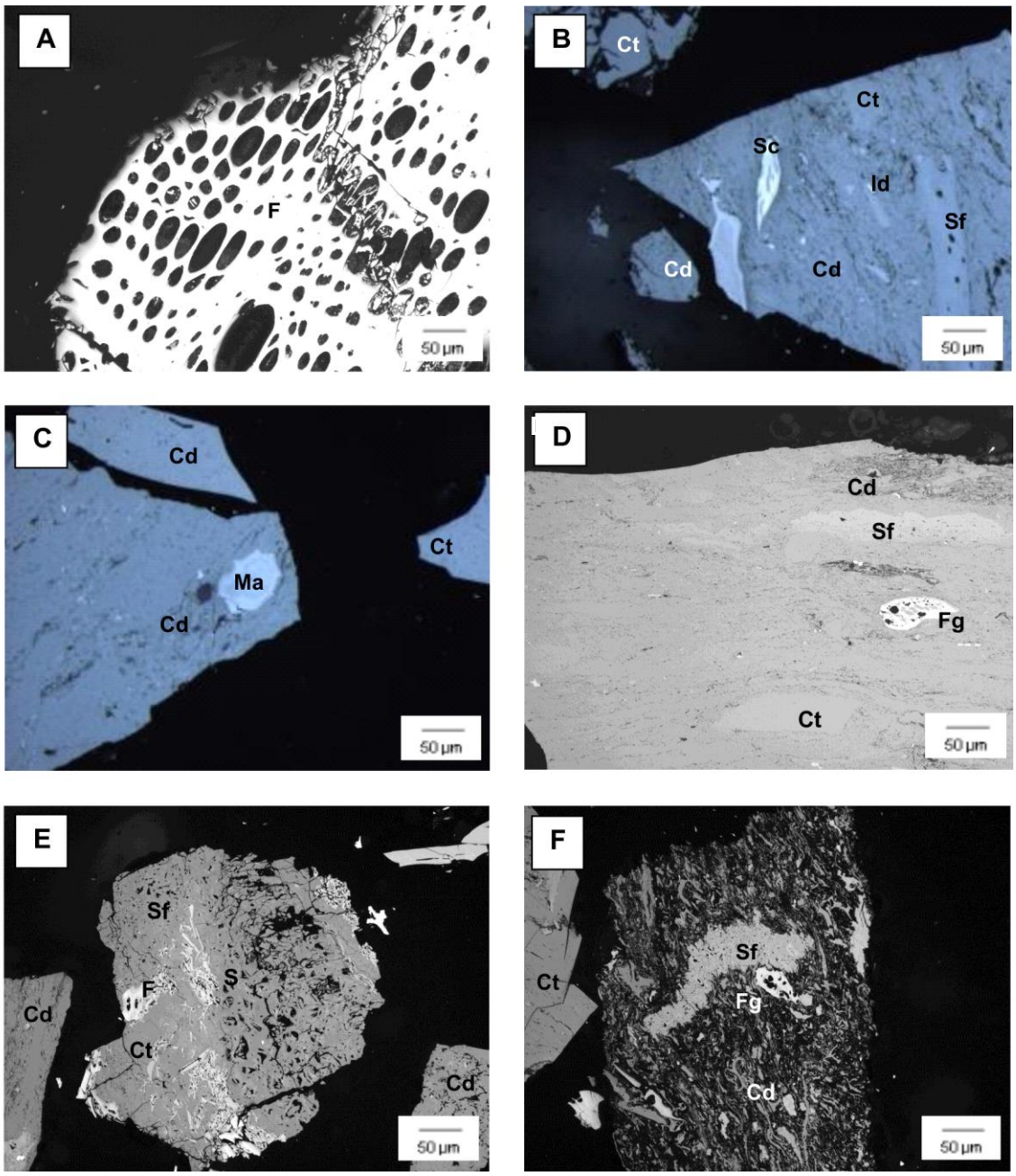

A – Fusinite (F) - RL.

B – Collotelinite (Ct), collodetrinite (Cd), semifusinite (Sf), inertodetrinite (Id) and secretinite (Sc) - RL.

C – Collodetrinite (Cd), macrinite (Ma) and collotelinite (Ct) - RL.

D – Collotelinite (Ct), collodetrinite (Cd), semifusinite (Sf) and funginite (Fg) - RL.

E – Collotelinite (Ct, collodetrinite (Cd), semifusinite (Sf) and fusinite (F) - RL.

F – Collotelinite (Ct), collodetrinite (Cd) semifusinite (Sf) and funginite (Fg) - RL.

8.1.2.18. Sample 1078 – Seam I. Sur

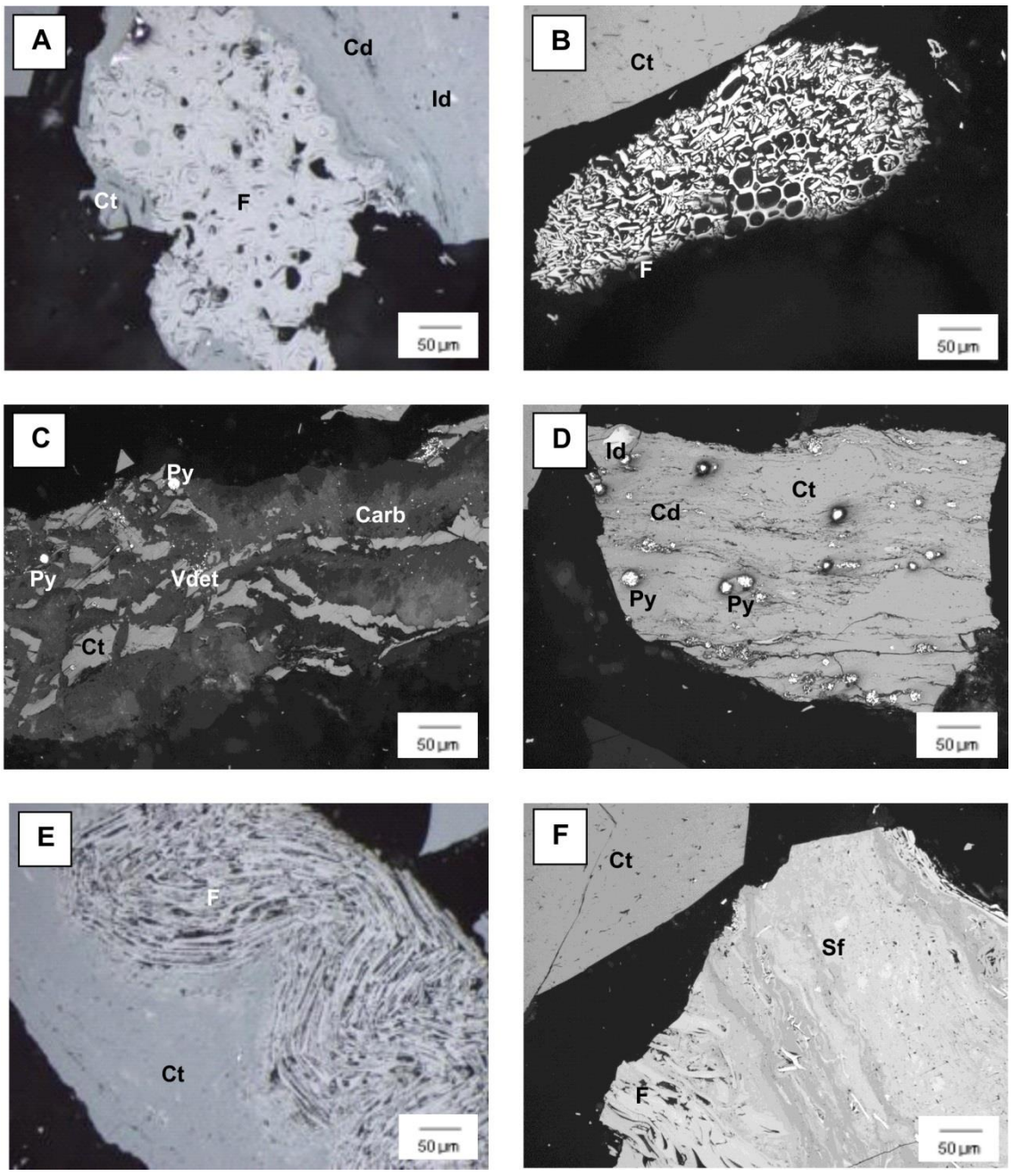

A – Fusinite (F), collodetrinite (Cd), collotelinite (Ct) and inertodetrinite (Id) - RL.

B – Fusinite (F) and collotelinite (Ct) - RL.

C – Framnoidal pyrite (Py) and epigenetic carbonates agglomerating organic particles of collotelinite (Ct) and vitrodetrinite (Vdet)) - RL.

D – Collotelinite (Ct), collodetrinite (Cd), inertodetrinite (Id) and framboidal pyrite (Py) - RL.

E – Collotelinite (Ct) and fusinite (F) - RL.

F – Collotelinite (Ct) in the left and fusinite (F) and semifusinite (Sf) in the right - RL.

8.1.2.19. Sample 1102 – Seam I. Sur

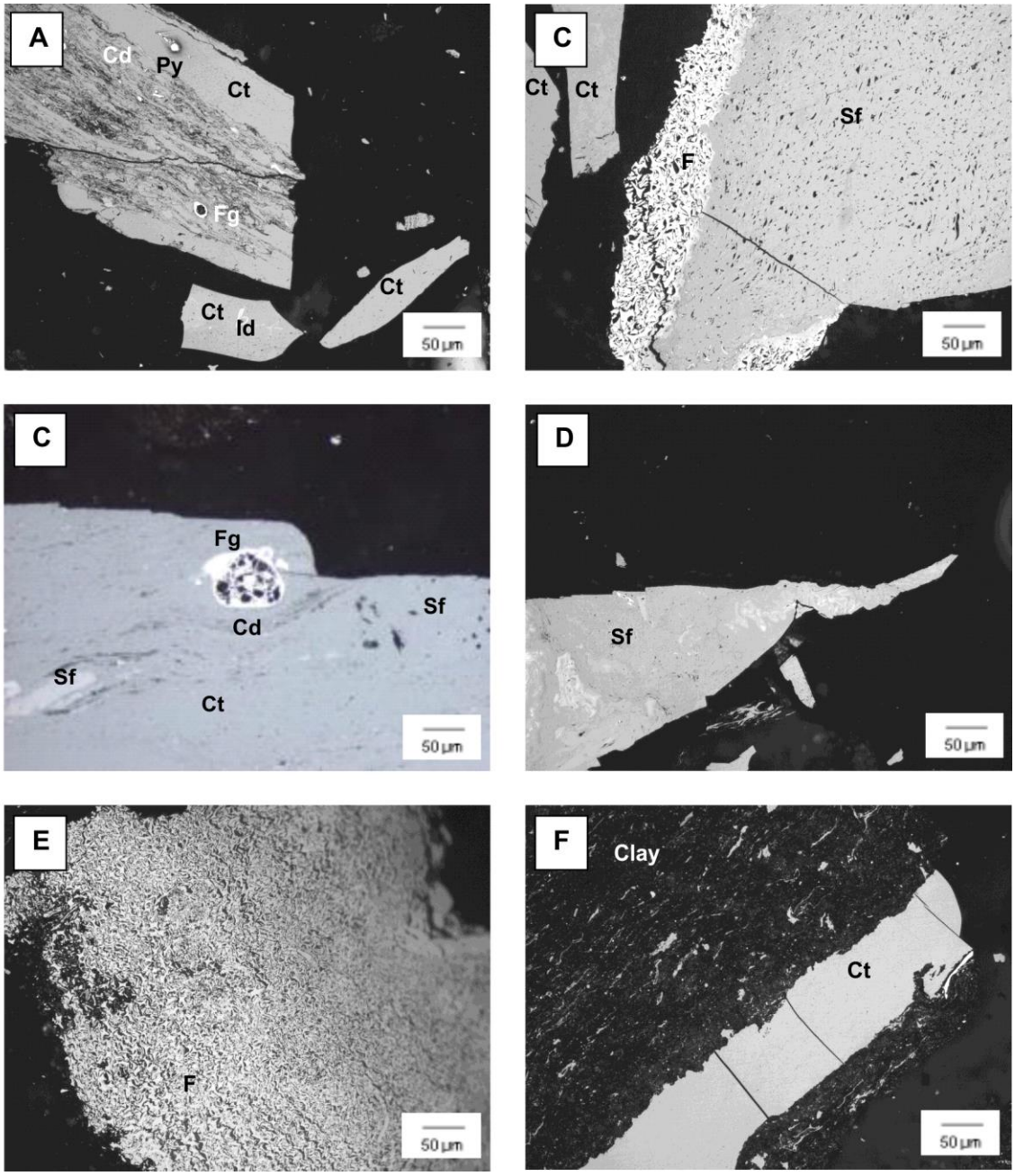

A – Funginite (Fg), collodetrinite (Cd), collotelinite (Ct), pyrite (Py) and inertodetrinite (Id) - RL.

B – Semifusinite (Sf), fusinite (F) and collotelinite (Ct) - RL.

C – Funginite (Fg), semifusinite (Sf) collodetrinite (Cd) and collotelinite (Ct) - RL.

D – Semifusinite (Sf) - RL.

E – Fusinite (F) - RL.

F – Layer of collotelinite (Ct) in clay minerals (Clay). Note the lamination materialized by vitrodetrinite (Vdet) parallel to the collotelinite layer - RL.

8.2. SEM aspects of the inorganic fraction – PBEB

8.2.1. Sample 1358 – Seam C3bis

The following images show that in this sample was observed Lead (Pb) occurring in carbonates, namely ankerite (A). Clay minerals such as chlorite (B) were also observed.

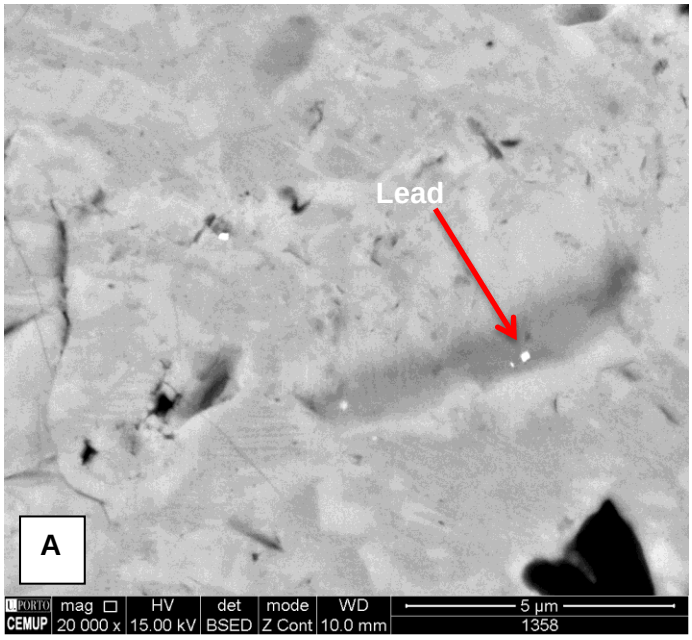

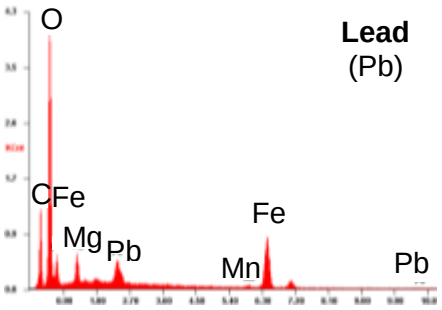

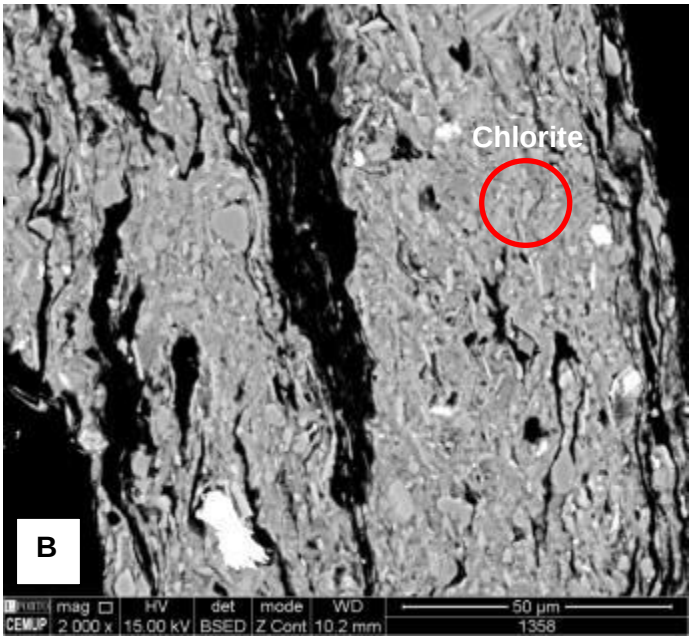

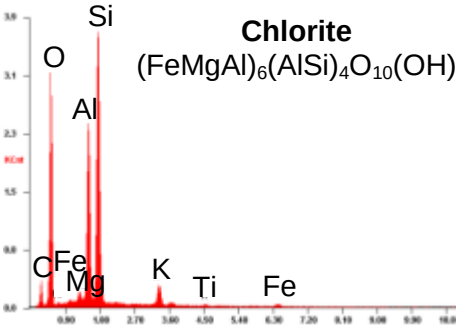

8.2.2. Sample 891/893 – Seam I. Norte

Clay minerals such as chlorite (A) and kaolinite (B, C and D) are present in sample 891/893. Apatite (A, C, D and D) occurs in a high content and calcite (C) was observed as well. In this sample kaolinite and apatite also occur filling cellular lumens (image D).

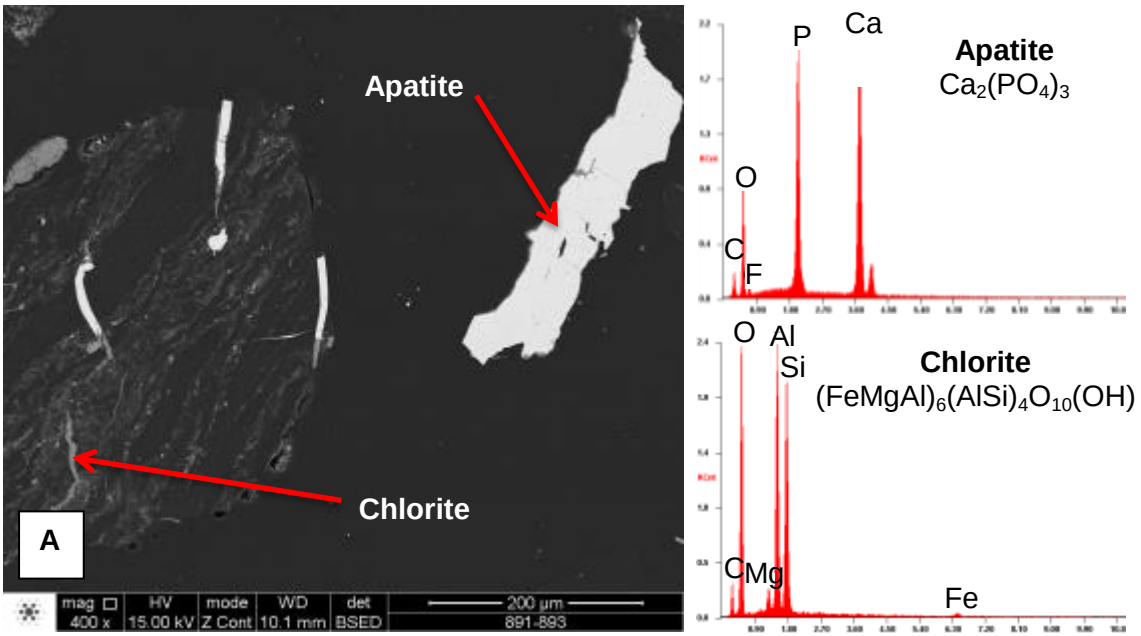

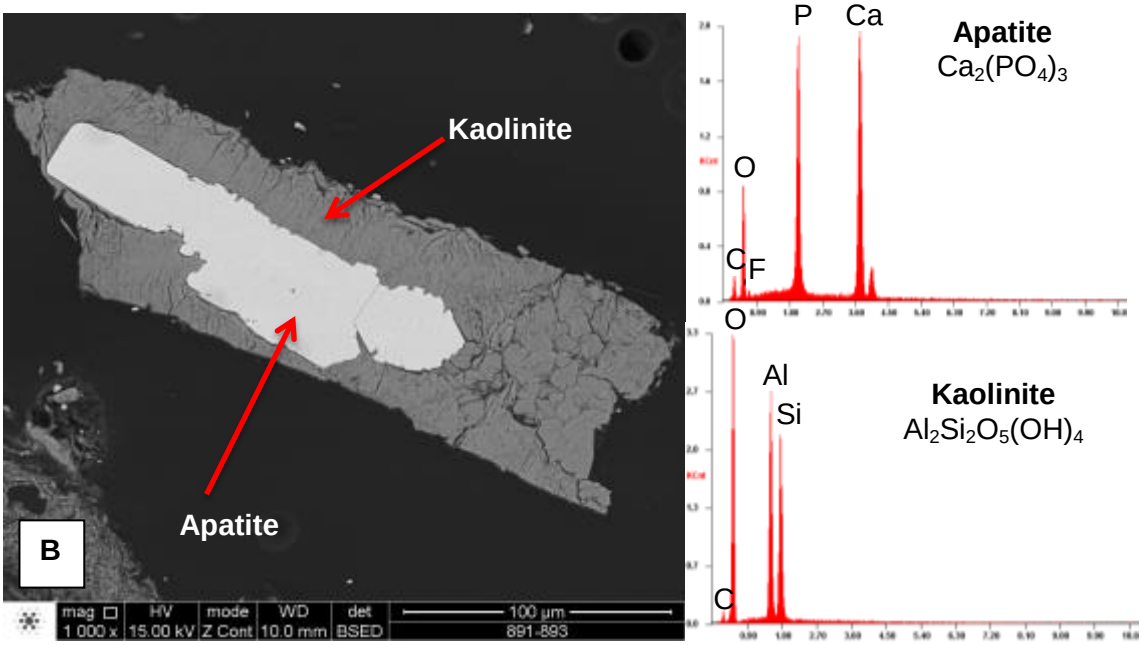

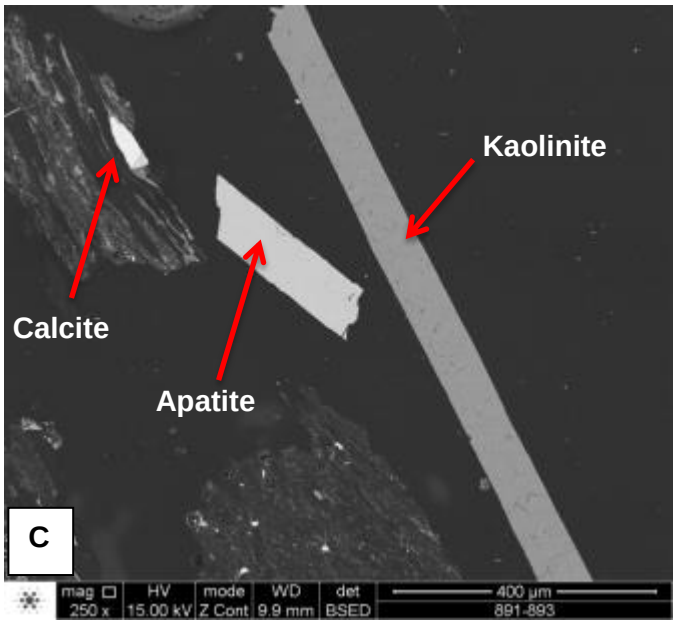

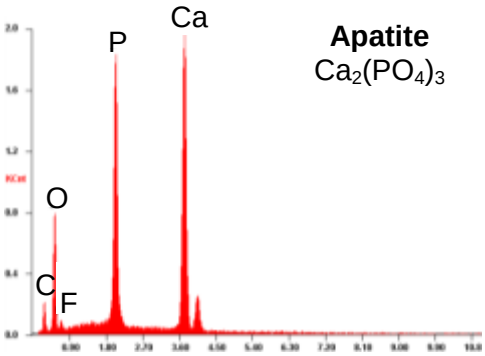

Apatite
$Ca_2(PO_4)_3$

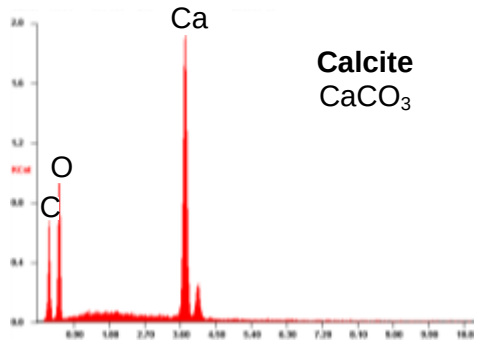

Calcite
$CaCO_3$

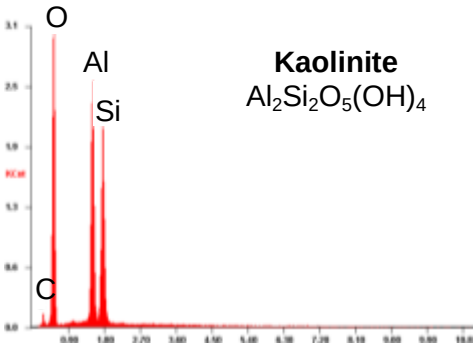

Kaolinite
$Al_2Si_2O_5(OH)_4$

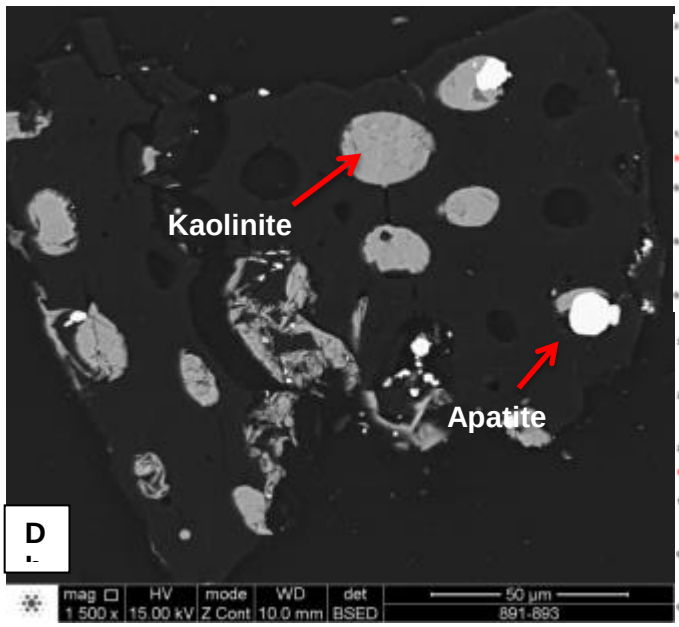

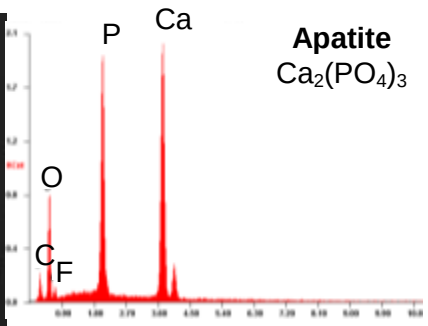

Apatite
$Ca_2(PO_4)_3$

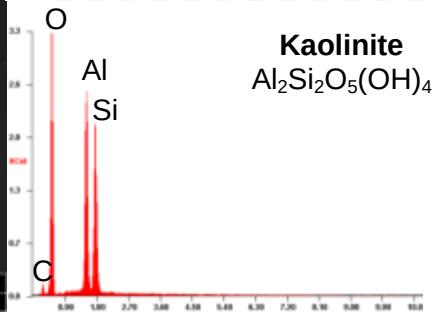

Kaolinite
$Al_2Si_2O_5(OH)_4$

8.2.3. Sample 1078 – Seam I. Sur

Sulfide phases were identified, as sphalerite (A), pyrite (B) and Pb associated with pyrite (D). Some carbonate minerals, namely dolomite (A and C) and kutnohorite were observed, as well as kaolinite (C).

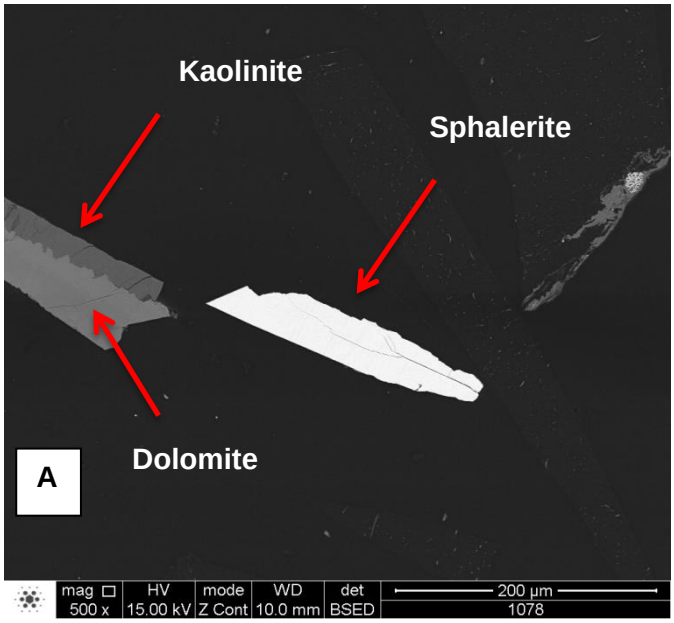

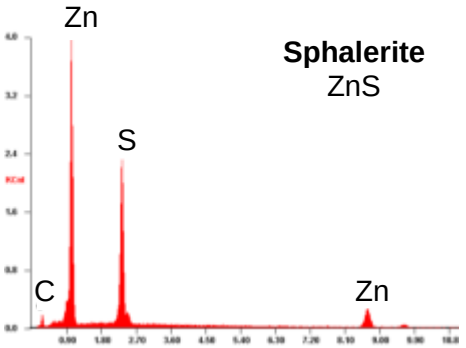

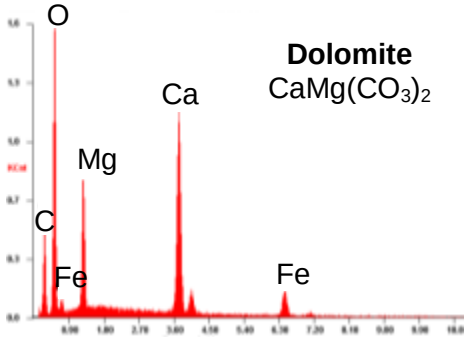

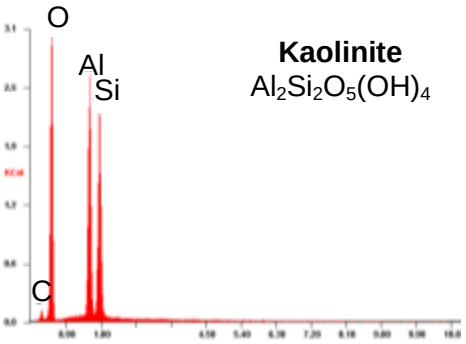

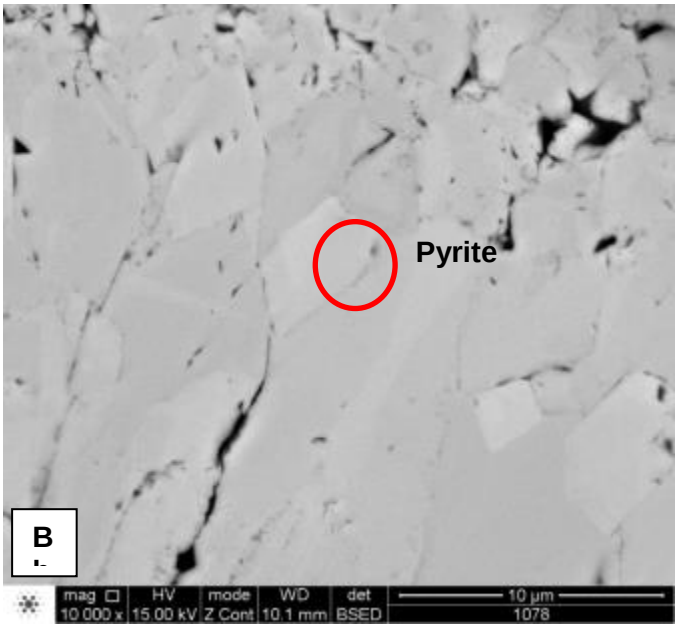

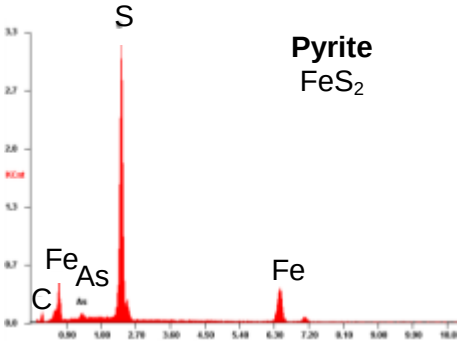

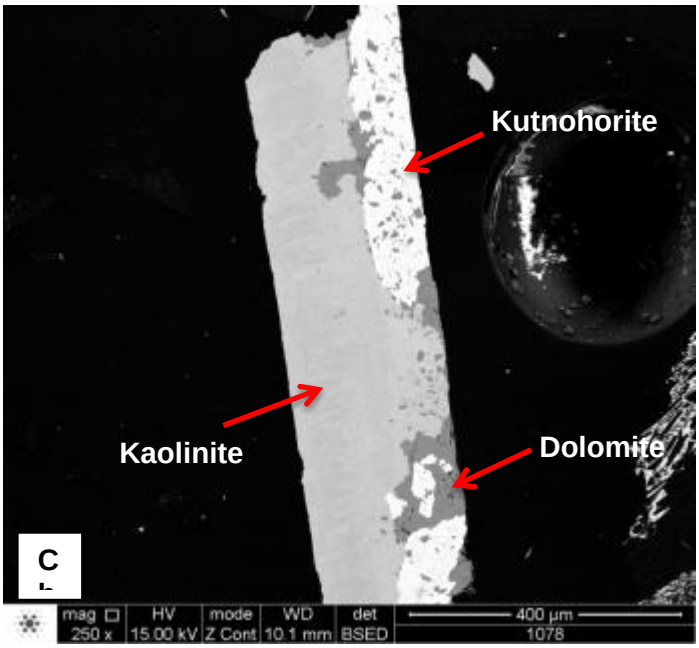
Kutnohorite
Kaolinite
Dolomite
C
mag 250 x
HV 15.00 kV
mode Z Cont
WD 10.1 mm
det BSED
400 µm
1078

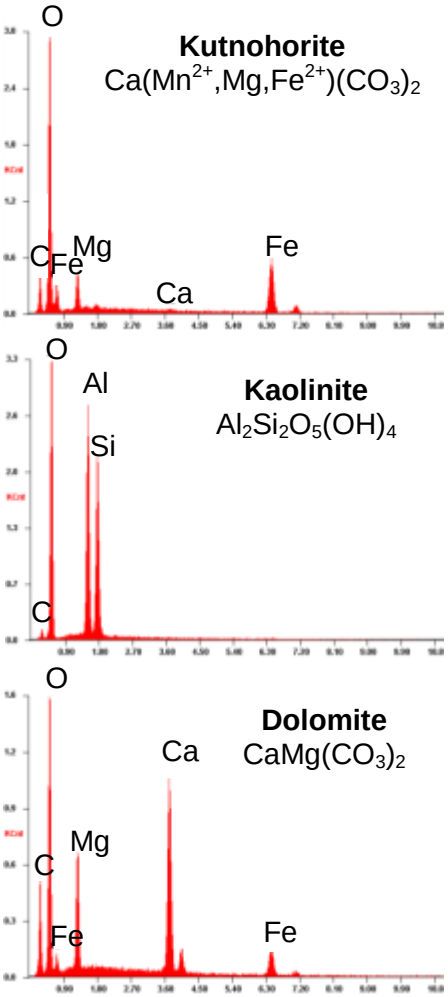
O
C
Fe
Mg
Ca
Fe
Kutnohorite
Ca(Mn2+,Mg,Fe2+)(CO3)2
O
Al
Si
C
Kaolinite
Al2Si2O5(OH)4
O
Ca
C
Mg
Fe
Fe
Dolomite
CaMg(CO3)2

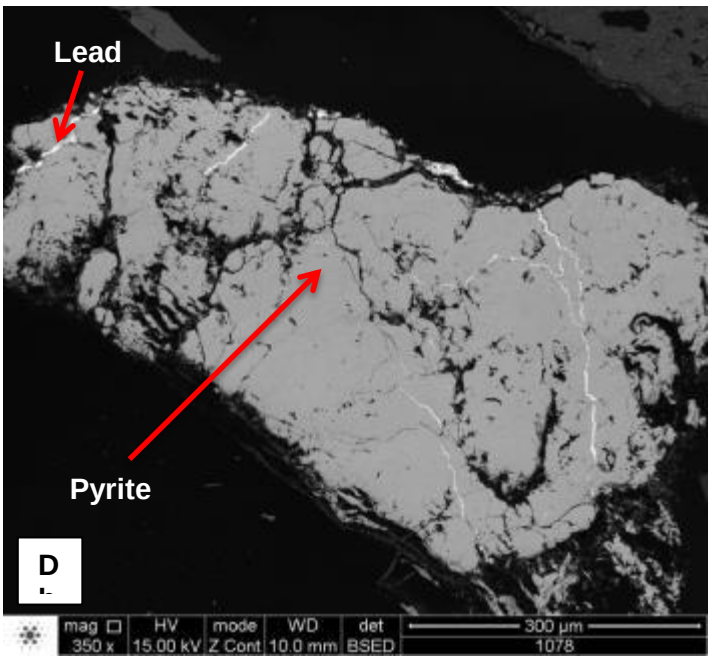
Lead
Pyrite
D
mag 350 x
HV 15.00 kV
mode Z Cont
WD 10.0 mm
det BSED
300 µm
1078

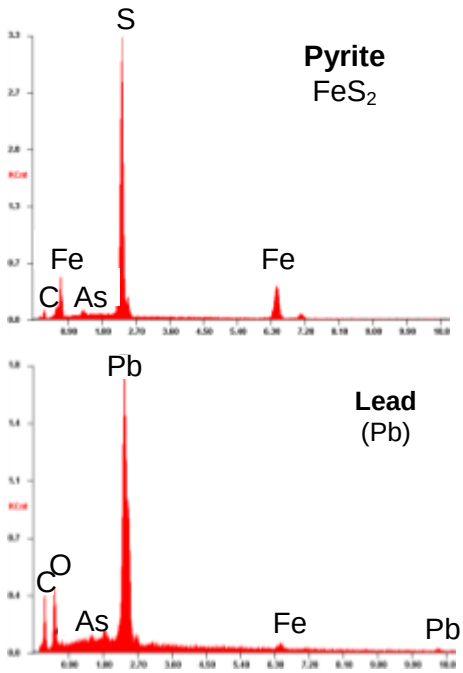
S
Fe
C
As
Fe
Pyrite
FeS2
Pb
C
O
As
Fe
Pb
Lead
(Pb)

Chapter 9 – References

9. References

Águeda, J.A., Bahamonde, J.R., Barba, F.J., Barba, P., Colmenero, J.R., Fernández, L.P., Salvador, C.I., Vera, C., 1991. Depositional environments in Westphalian coal-bearing successions of the Cantabrian Mountains, northwest Spain. Bulletin de la Société Géologique de France, 162(2), 325-337.

Aller, J., Brime, C., 1985. Deformación y metamorfismo en la parte sur de la Cuenca Carbonífera Central (NO. de España). Compte Rendu du Dixième Congrès International de Stratigraphie et de Géologie du Carbonifère 1983, Madrid, Spain, 3, 541–548.

Aller, J., Gallastegui, J., 1995. Analysis of kilometric scale superposed folding in the Central Coal Basin (Cantabrian zone NW Spain). Journal of Structural Geology, 17, 961–969.

Alonso, J.L., Pulgar, J.A., 1995. La estructura de la Zona Cantábrica. In: C. Aramburu, F. Bastida (Eds.), Geología de Asturias. Ediciones Trea, Principado de Asturias, Spain, 103–112.

Álvarez-Vázquez, C., 1995. Macroflora del Westfaliense inferior de la cuenca de Peñarroya-Belmez-Espiel (Córdoba). PhD Thesis, Universidad de Oviedo, 393 pp.

Andreis, R.R., Wagner, R.H., 1983. Estudio de abanicos aluviales en el borde Norte de la cuenca Westfaliense B de Peñarroya-Belmez (Córdoba). In: M.J. Lemos de Sousa (Ed.) Contributions to the Carboniferous Geology and Palaeontology of the Iberian Peninsula. Universidade do Porto, Faculdade de Ciências, Mineralogia e Geologia. Volume dedicated to Wenceslau de Lima, 171-227.

Benner R., Moran M.A., Hodson R.E., 1985. Effects of pH and plant source on lignocellulose biodegradation rates in two wetland ecosystems, the Okefenokee Swamp and a Georgia salt marsh. Limnology and Oceanography, 30, 489-499.

Bastida, F., Aller, J., 1995. Rasgos geológicos generales. In: C. Aramburu, F. Bastida, (Eds.), Geología de Asturias. Ediciones Trea, Principado de Asturias, Spain, 27–33.

Bouska, V., 1981. Geochemistry of coal. Elsevier Scientific Publishing Co., New York, 274 pp.

Bowman, M.B.J., 1985. The sedimentology and palaeo-geographic setting of late Namurian–Westphalian A basin-fill successions in the San Emiliano and Cármenes areas of NW León, Cantabrian Mts., NW Spain. In: M.J. Lemos de Sousa, R.H. Wagner, (Eds.), Papers on the Carboniferous of the Iberian Peninsula (Sedimentology, Stratigraphy, Palaeontology, Tectonics and Geochronology). Anais Faculdade de Ciências (Suppl. 1983), Universidade do Porto, Portugal, 64,117– 169.

Chou, C.-L., 1997. Abundances of sulfur, chlorine, and trace elements in Illinois Basin coals, USA. Proceedings of the 14th Annual International Pittsburgh Coal Conference & Workshop, Taiyuan, China, Sept. 23–27, 1997, Section 1, 76–87.

Christie-Blick, N., Biddle, K. T., 1985. Deformation and basin formation along strike-slip faults. In: K. T. Biddle, N. Christie-Blick (Eds.), Strike-slip deformation, basin formation and sedimentation. Society of Economic Paleontologists and Mineralogists, Special Publication, 37, 1-34.

Colmenero, J.R., Águeda, J.A., Fernández, L.P., Salvador, C.I., Bahamonde, J.R., Barba, P., 1988. Fan-delta systems related to the Carboniferous evolution of the Cantabrian zone, northwestern Spain. In: W. Nemec, R.J. Steel, (Eds.), Fan Delta: Sedimentology and Tectonic Setting. Blackie, Glasgow, 267–285.

Colmenero, J.R., Barba, P., 1985. Un tipo de ciclo deltaico en el Westfaliense superior de la Cuenca Carbonífera Central. Universidad de Oviedo, Trabajos de Geología, 15, 29–36.

Colmenero, J.R., Águeda, J.A., Bahamonde, J.R., Barba, F.J., Barba, P., Fernández, L.P., Salvador, C.I., 1993. Evolución de la Cuenca de antepaís namuriense y westfaliense de la Zona Cantábrica, NW de España. C.R. XII International Congress on Carboniferous and Permian, Buenos Aires, 2, 175–190.

Colmenero, J. R., Suárez-Ruiz, I., Fernández-Suárez, J., Barba, P., & Llorens, T., 2008. Genesis and rank distribution of Upper Carboniferous coal basins in the Cantabrian Mountains, Northern Spain. International Journal of Coal Geology, 76(3), 187-204.

Correia, P., Murphy, J.B., Sá, A.A., Domingos, R., Flores, D., 2013. First Palaeozoic arachnid from Portugal and implications for Carboniferous palaeobiogeography. Geological Journal, 48, 101-107.

Correia, P., Šimůnek, Z., Pšenička, J., Sá, A.A., Domingos, R., Carneiro, A., Flores, D., 2014a. New paleobotanical data on the Portuguese Pennsylvanian (Douro Carboniferous Basin, NW Portugal). Comunicações Geológicas, 101(Especial I), 409-414.

Correia, P., Nel, A., Sá, A., Domingos, R., Carneiro. A., Flores, D., 2014b. A new Palaeodictyoptera from the Late Carboniferous of Portugal. Annales de la Société Entomologique de France, (n.s.), 49(4), 398-401.

Dai, S., Chou, C.-L., 2007. Occurrence and origin of minerals in a chamosite-bearing coal of Late Permian age, Zhaotong, Yunnan, China. American Mineralogist, 92, 1253–1261.

Dai, S., Hou, X., Ren, D., Tang, Y., 2003. Surface analysis of pyrite in the No. 9 coal seam, Wuda Coalfield, Inner Mongolia, China, using high-resolution time-of-flight secondary ion mass-spectrometry. International Journal of Coal Geology, 55, 139–150.

Dai, S., Li, D., Ren, D., Tang, Y., Shao, L., Song, H., 2004. Geochemistry of the late Permian No. 30 coal seam, Zhijin Coalfield of Southwest China: influence of a siliceous low temperature hydrothermal fluid. Applied Geochemistry, 19, 1315–1330.

Dai, S., Chou, C.-L., Yue, M., Luo, K., Ren, D., 2005. Mineralogy and geochemistry of a Late Permian coal in the Dafang Coalfield, Guizhou, China: influence from siliceous and iron-rich calcic hydrothermal fluids. International Journal of Coal Geology, 61, 241–258.

Dai, S., Zeng, R., Sun, Y., 2006. Enrichment of arsenic, antimony, mercury, and thallium in a Late Permian anthracite from Xingren, Guizhou, Southwest China. International Journal of Coal Geology, 66, 217–226.

Dai, S., Ren, D., Zhou, Y., Chou, C.-L., Wang, X., Zhao, L., Zhu, X., 2008. Mineralogy and geochemistry of a superhigh-organic-sulfur coal, Yanshan Coalfield, Yunnan, China: evidence for a volcanic ash component and influence by submarine exhalation. Chemical Geology, 255, 182–194.

Dai, S., Zhou, Y., Zhang, M., Wang, X., Wang, J., Song, X., Ren, D., 2010. A new type of Nb (Ta)–Zr (Hf)–REE–Ga polymetallic deposit in the late Permian coal-bearing strata, eastern Yunnan, southwestern China: Possible economic significance and genetic implications. International Journal of Coal Geology, 83(1), 55-63.

Dai, S., Ren, D., Chou, C.-L., Finkelman, R.B., Seredin, V.V., Zhou, Y., 2012. Geochemistry of trace elements in Chinese coals: a review of abundances, genetic types, impacts on human health, and industrial utilization. International Journal of Coal Geology, 94, 3–21.

Dai, S., Liu, J., Ward, C.R., Hower, J.C., French, D., Jia, S., Hood, M.M., Garrison, T.M., 2015. Mineralogical and geochemical compositions of Late Permian coals and host rocks from the Guxu Coalfield, Sichuan Province, China, with emphasis on enrichment of rare metals. International Journal of Coal Geology. DOI http://dx.doi.org/10.1016/j.coal.2015.12.004.

Dai, S., Chekryzhov, I.Y., Seredin, V.V., Nechaev, V.P., Graham, I.T., Hower, J.C., Ward, C.R., Ren, D., Wang, X., 2016a. Metalliferous coal deposits in East Asia (Primorye of Russia and South China): a review of geodynamic controls and styles of mineralization. Gondwana Research, 29(1), 60-82.

Dai, S., Graham, I.T., Ward, C.R., 2016b. A review of anomalous rare earth elements and yttrium in coal. International Journal of Coal Geology, 159, 82-95.

Dallmeyer, R.D., Martínez García, E. (Eds.), 1990. Pre-Mesozoic Geology of Iberia. Springer-Verlag, Berlin, Germany, 416 pp.

Dias, R., Ribeiro, A., 1991. Finite strain analysis in a transpressive regime (Variscan autochthon, northeast Portugal). Tectonophysics, 191(3), 389-397.

Eagar, R.M.C., 1983. The non-marine bivalve fauna of the Stephanian C of North Portugal. In: Lemos de Sousa, M.J., Oliveira, J.T. (Eds.), The Carboniferous of Portugal. Memórias dos Serviços Geológicos de Portugal, 29, 179-185.

Fertl, W. H., 1979. Gamma Ray Spectral Data Assists in Complex Formation Evaluation. Log Analyst, 20, 5, 3–37.

Fernandes, J.P., Pinto de Jesus, A., Teixeira, F., Lemos de Sousa, M.J., 1997. Primeiros resultados palinológicos na Bacia Carbonífera do Douro (NO de Portugal). XIII Jornadas de Paleontologia “Fósiles de Galicia” y V Reunión Internacional Proyecto, 351, 176-179.

Fernández, L.P., 1995. El Carbonífero. In: Aramburu, C., Bastida, F. (Eds.), Geología de Asturias. Ediciones Trea, S.L., Oviedo, España, 63–80.

Finkelman, R.B., 1981. Modes of occurrence of trace elements in coal. US Geological Survey, Open–file Report 81–99, 312 pp.

Finkelman, R.B., 1995. Modes of occurrence of environmentally-sensitive trace elements of coal. In: D.J. Swaine, F. Goodarzi, (Eds.), Environmental Aspects of Trace Elements of Coal. Kluwer Academic Publishers, Dordrecht, 24–50.

Fuente-Alonso, P., Sáenz de Santa María Benedet, J.A., 1999. La tectónica y microtectónica de la Cuenca Carbonífera Central de Asturias. Vol. Homenaje a J. Truyols. Universidad de Oviedo, Trabajos de Geología, 21, 121-140.

Gutiérrez Claverol, M., Luque Cabal, C., 1995. Recursos geológicos. Geología de Asturias, 187-202.

International Committee for Coal and Organic Petrology (ICCP), 1963. International Handbook of Coal Petrography - 2nd ed. CNRS (Paris), 162 pp.

International Committee for Coal and Organic Petrology (ICCP), 1998. The new vitrinite classification (ICCP System 1994). Fuel 77, 349-358.

International Committee for Coal and Organic Petrology (ICCP), 2001. The new inertinite classification (ICCP system 1994). Fuel 80, 459-471.

ISO 589, 2008. Hard Coal – Determination of total moisture. International Organization for Standardization, Geneva, Switzerland, 9 pp.

ISO 7404-1, 2016. Methods for the petrographic analysis of coals - Part 1: Vocabulary. International Organization for Standardization, 6 pp.

ISO 7404-2, 2009. Methods for the petrographic analysis of coals - Part 2: Methods of preparing coal samples. International Organization for Standardization, 12 pp.

ISO 7404-3, 2009. Methods for the petrographic analysis of coals - Part 3: Method of determining maceral group composition. International Organization for Standardization, 7pp.

ISO 7404-5, 2009. Methods for the petrographic analysis of coals - Part 5: Method of determining microscopically the reflectance of vitrinite. International Organization for Standardization, 14 pp.

ISO 1171, 2010. Solid mineral fuels - Determination of ash. International Organization for Standardization, Geneva, Switzerland. 4pp.

ISO 562, 2010. Hard coal and coke - determination of volatile matter. International Organization for Standardization, Geneva, Switzerland. 7 pp.

Julivert, M., 1967. La ventana del Río Monasterio y la terminación meridional del Manto de Ponga. Universidad de Oviedo, Trabajos de Geología 1, 59 - 76.

Julivert, M., Ramírez del Pozo, J., Truyols, J., 1971. Le réseau de failles et la couverture post-hercynienne dans les Asturies. In: J. Debyser, X. Le Pichon, L. Montadert (Eds.), Histoire Structurale du Golfe de Gascogne. Collection Colloques et Séminaires, Institut Français du Pétrole, Éditions Technip, 22, 1 - 34.

Julivert, M., Fontboté, J.M., Ribeiro, A., Conde, L., 1972. Mapa Tectónico de la Península Ibérica y Baleares. Instituto Geológico y Minero de España (IGME), Madrid, Spain.

Julivert, M., Fontboté, J., Ribeiro, A., Conde, L., 1974. Memória explicativa del Mapa Tectónico de la Península Ibérica y Baleares. Escala 1/100000. Instituto Geológico y Minero de España (IGME), Madrid, Spain.

Ketris, M.P., Yudovich, Y.E., 2009. Estimations of Clarkes for Carbonaceous biolithes: World averages for trace element contents in black shales and coals. International Journal of Coal Geology, 78(2), 135-148.

van Krevelen, D.W., 1993. Coal: typology, chemistry, physics, constitution - 3rd ed. Elsevier, Amsterdam, 979 pp.

Lemos de Sousa, M.J., 1973. Contribuição para o conhecimento da Bacia Carbonífera do Douro. PhD Thesis, University of Porto, 427 pp.

Lemos de Sousa, M.J., 1978. O grau de incarbonização (rang) dos carvões durienses e as consequências genéticas, geológicas e estruturais que resultam do seu conhecimento. Comunicações dos Serviços Geológicos de Portugal, Lisboa, 63, 179-365.

Lemos de Sousa, M.J., 1999. Notas de Petrologia Orgânica 1. A Tetratologia clássica "turfa-lignite-hulha-antracite". Geólogos, 5, 105-107.

Loureiro, J.P., Correia, P., Nel, A., Pinto de Jesus, A., 2010. *Lusitaneura covensis* nov. gen. & nov. sp., first Caloneurodea from the Carboniferous of Portugal (Insecta: Pterygota: Panorthoptera). Annales de la Société Entomologique de France (n.s.), 46, 242-246.

Loredo, J., Luque, C., García-Iglesias, J., 1988. Conditions of formation of mercury deposits from the Cantabrian Zone (Spain). Bulletin de Minéralogie, 111, 393– 400.

Loredo, J., Ordóñez, A., Gallego, J.R., Baldo, C., García-Iglesias, J., 1999. Geochemical characterisation of mercury mining spoil heaps in the area of Mieres (Asturias, northern Spain). Journal of Geochemical Exploration, 67, 377–390.

Luque-Cabal, C., Sáenz de Santa-María, J.A., 1984. Los conglomerados brechoides de La Peña (Mieres, Asturias): características estratigráficas. Actas del I Congreso Español de Geología, Segovia, Spain, 1, 187–197.

Mackowsky, M.T., 1968. Mineral Matter in Coal. In: D. Murchson, T.S. Westoll (Eds.), Coal and Coal-Bearing Strata. Oliver & Boyd, Ltd., 309–321.

Marcos, A., Pulgar, J., 1982. An approach to the tectonostrastigraphic evolution of the Cantabrian foreland and thrust belt, Hercynian Cordillera of NW Spain. Neues Jahrbuch fur Geologie und Palaeontologie, Abhandlungen, 163, 256 - 260.

Marques, M., 1993. Contribuição para o conhecimento da petrologia dos carvões da Bacia de Peñarroya–Belmez–Espiel (Córdova–Espanha). PhD Thesis, University of Porto, 157 pp.

Marques, M., 2002. Coal facies and depositional environments of the Aurora and Cabeza de Vaca Units, Peñarroya–Belmez–Espiel Coalfield (Cordoba, Spain). International Journal of Coal Geology, 48, 181–195.

Martínez-García, E., 1981. Tectónica y mineralizaciones pérmicas en la Cordillera Cantábrica Oriental (Noroeste de España). Cuadernos do Laboratorio Xeolóxico de Laxe, 2, 263– 271.

Orem, W.H., Finkelman, R.B., 2003. Coal formation and geochemistry. Treatise on Geochemistry, 7, 407 pp.

Pérez-Estaún, A., Bastida, F., Alonso, J.L., Marquínez, J., Aller, J., Álvarez-Marrón, J., Marcos, A., Pulgar, J.A., 1988. A thin-skinned tectonics model for an arcuate fold and thrust belt: the Cantabrian Zone (Variscan Ibero–Armorican Arc). Tectonics, 7 (3), 517–537.

Pickel, W., Wolf, M., 1989. Kohlen petrologische und geochemische Charakterisierung von Braunkohlen aus dem Geiseltal (DDR). Erdöl Kohle, 42, 481-484.

Pickel, W., 2015. Fundamentals of organic petrology. 8th ICCP Training Course, Potsdam, Germany, 1, 303 pp.

Pickle, W., Kus, J., Flores, D., Kalaitzidi, S., 2015. Draft Classification of Liptinite – ICCP System 1994. 51 pp.

Piedad-Sánchez, N., Suárez-Ruiz, I., Martinez, L., Izart, A., Elie, M., Keravis, D., 2004a. Organic petrology and geochemistry of the Carboniferous coal seams from the Central Asturian Coal Basin (NW Spain). International Journal of Coal Geology, 57, 211–242.

Piedad-Sánchez, N., Izart, A., Martínez, L., Suárez-Ruiz, I., Elie, M., Menetrier, C., 2004b. Paleothermicity in the Central Coal Basin of the Cantabrian Mountains (Spain). International Journal of Coal Geology 58, 205–229.

Pinto de Jesus, A., 2001. Génese e evolução da Bacia Carbonífera do Douro (Estefaniano C inferior, NW de Portugal): um modelo. PhD Thesis, University of Porto, Vol. Text: 157pp., Vol. Atlas: 71 pp.

Pinto de Jesus, A., 2003. Evolução sedimentar e tectónica da Bacia Carbonífera do Douro (Estefaniano C inferior, NW de Portugal). Cuadernos do Laboratorio Xeolóxico de Laxe, 28, 107-125.

Ribeiro, A., 1974. Contribution à l'étude tectonique de Trás-os-Montes Oriental. Memórias dos Serviços Geológicos de Portugal, Lisboa, 24, 1-168.

Ruch, R.R., Harold, J., Gluskoter, H.J., Kennedy, E.J., 1971. Mercury content of Illinois coals. Environmental Geology Notes, 43, 15 pp.

Sáenz de Santa-María, J.A., Luque, C., Gervilla, M., Laveine, J.P., Loboziak, S., Brousmiche, C., Coquel, R., Martínez-Díaz, C., 1985. Aportación al conocimiento estratigráfico y sedimentológico del Carbonífero productivo de la Cuenca Central Asturiana. Compte Rendu du Dixième Congrès International de Stratigraphie et de Géologie du Carbonifère 1983, Madrid, Spain, 1, 303–326.

Sánchez de la Torre, L., Águeda, J., Colmenero, J. R., García-Ramos, J. C., & González-Lastra, J., 1983. Evolución sedimentaria y paleogeográfica del Carbonífero en la Cordillara Cantábrica. Carbonífero y Pèrmico de España. Instituto Geológico y Minero de España, Madrid, 133-150.

Shao, L., Jones, T., Gayer, R., Dai, S., Li, S., Jiang, Y., Zhang, P., 2003. Petrology and geochemistry of the high-sulphur coals from the Upper Permian carbonate coal measures in the Heshan Coalfield, southern China. International Journal of Coal Geology, 55, 1–26.

Suárez-Ruiz, I., Crelling, J.C. (Eds.), 2008. Applied coal petrology. The role of petrology in coal utilization. Elsevier, 388 pp.

Suárez-Ruiz, I., Flores, D., Marques, M.M., Martinez-Tarazona, M.R., Pis, J., Rubiera, F., 2006. Geochemistry, mineralogy and technological properties of coals from Rio Maior (Portugal) and Peñarroya (Spain) basins. International Journal of Coal Geology, 67, 171-190.

Sun, Y., Lin, M., Qin, P., Zhao, C., Jin, K., 2007. Geochemistry of the barkinite liptobiolith (Late Permian) from the Jinshan Mine, Anhui Province, China. Environmental Geochemistry and Health, 29, 33–44.

Swaine, D.J., 1990. Trace Elements in Coal. Butterworths, London, 278 pp.

Swaine, D. J., Goodarzi, F. (Eds.), 1995. Environmental aspects of trace elements in coal. Kluwer Academic Publishers, Dordrecht, 312 pp.

Sýkorová, I., Pickel, W., Christanis, K., Wolf, M., Taylor, G. H., Flores, D., 2005. Classification of huminite – ICCP System 1994. International Journal of Coal Geology, 62, 85-106.

Taylor, G.H., Teichmüller, M., Davis, A., Diessel, C.F.K., Littke, R., Robert, R., 1998. Organic Petrology. Berlin, Gebrüder Borntraeger, 704 pp.

Tissot, B.P., Welte, D.H., 1984. Petroleum formation and occurrence - 2nd ed. Springer-Verlag, Berlin, 699 pp.

Truyols-Santonja, J., 1983. La Cuenca Carbonífera Central. In: Martínez-Díaz, C. (Ed.), Carbonífero y Pérmico de España. X Congreso Internacional de Estratigrafía y Geología del Carbonífero. Instituto Geológico y Minero de España (IGME), Madrid, Spain, 60– 81.

Wagner, R.H., Lemos de Sousa, M.J., 1983. The Carboniferous Megafloras of Portugal - A revision of identifications and discussion of stratigraphic ages. In: Lemos de Sousa, M. J., Oliveira, J. T. (Eds.), The Carboniferous of Portugal. Memórias dos Serviços Geológicos de Portugal, 29, 127-152.

Wagner, R. H., 1999. Peñarroya, a strike-slip controlled basin of early Westphalian age in Southwest Spain. Bulletin of the Czech Geological Survey, 74 (2), 87-108.

Wagner, R. H., 2004. The Iberian Massif: a carboniferous assembly. Cuadernos de geología ibérica= Journal of iberian geology: an international publication of earth sciences, 30, 93-108.

Wang, X., 2009. Geochemistry of Late Triassic coals in the Changhe Mine, Sichuan Basin, southwestern China: evidence for authigenic lanthanide enrichment. International Journal of Coal Geology 80, 167–174.

Wang, Y., Mo, J., Ren, D., 1999. Distribution of minor and trace elements in magmatic hydrothermal metamorphic coal of Meitian Coal Mine, Hunan Province. Geochimica, 28, 289–296 (in Chinese with English abstract).

Ward, C.R., Suárez-Ruiz, I., 2008. Introduction to applied coal petrology. In: I. Suárez-Ruiz, J.C. Crelling, (Eds.), Applied Coal Petrology: *The* Role *of* Petrology *in* Coal Utilization. Amsterdam, Elsevier, *1–18*.

Yang, J., 2006. Concentrations and modes of occurrence of trace elements in the Late Permian coals from the Puan Coalfield, southwestern Guizhou, China. Environmental Geochemistry and Health, 28, 567–576.

Yudovich, Y.E., Ketris, M.P., 2005. Mercury in coal: A review: Part 1. Geochemistry. International Journal of Coal Geology, 62(3), 107-134.

Zhang, J., 1999. Enrichment mechanism and pollution restraining of potentially hazardous trace elements in coal. Ph.D. Thesis, China University of Mining and Technology, Beijing (in Chinese with English abstract).

Zhang, J., Ren, D., Xu, D., Liu, J., Dong, B., 1999. The distribution of mercury in major associated minerals from coal beds in southwestern Guizhou. Geological Review, 45, 539–542 (in Chinese with English abstract).

Zhang, J., Ren, D., Zheng, C., Zeng, R., Chou, C.-L., Liu, J., 2002. Trace element abundances in major minerals of Late Permian coals from southwestern Guizhou Province, China. International Journal of Coal Geology, 53, 55–64.

Zhang, J., Ren, D., Zhu, Y., Chou, C.-L., Zeng, R., Zheng, B., 2004. Mineral matter and potentially hazardous trace elements in coals from Qianxi Fault Depression Area in southwestern Guizhou, China. International Journal of Coal Geology, 57, 49–61.

Zeng, R., Zhuang, X., Koukouzas, N., Xu, W., 2005. Characterization of trace elements in sulphur-rich Late Permian coals in the Heshan coal field, Guangxi, South China. International Journal of Coal Geology 61, 87–95.

Zheng, L., Liu, G., Qi, C., Zhang, Y., Wong, M., 2007a. The use of sequential extraction to determine the distribution and modes of occurrence of mercury in Permian Huaibei coal, Anhui Province, China. International Journal of Coal Geology, 73(2), 139-155.

Zheng, L., Liu, G., Chou, C. L., 2007b. Abundance and modes of occurrence of mercury in some low-sulfur coals from China. International Journal of Coal Geology, 73(1), 19-26.